UNIVERSITY OF THE WITWATERSRAND, JOHANNESBURG

OPTIMISATION OF THE MINERAL GRADING WIND SIFTER SEPARATOR FOR COAL BENEFICIATION

A doctoral thesis submitted to the Faculty of Engineering and the Built Environment, University of the Witwatersrand, Johannesburg, South Africa, in fulfillment of the requirements for the degree of Doctor of Philosophy in Engineering

by

Jimmy Joanah Alade (1914799)

Submitted to:

The School of Chemical and Metallurgical Engineering, Faculty of Engineering and the Built Environment, University of the Witwatersrand, Johannesburg, South Africa.

Supervisor: Prof. Samson Bada

DECLARATION

I declare that this thesis is my unaided work. It is being submitted for the Doctorate in Engineering to the University of the Witwatersrand, Johannesburg, South Africa. It has not been submitted before for any degree or examination to any other University.

…………………………
(Signature of Candidate)

13th day of December 2023
(Day) / (Month) / (Year)

ABSTRACT

The concept of wind sifting for particle separation has been successfully implemented for various concentration purposes. Diverse configurations based on this concept have been fabricated over many decades. It has been used in recycling, agriculture, electronic waste sorting, furniture, food and beverages, and mineral processing industries to some extent. The approach's effectiveness stems from the capability of separating lighter particles from heavier ones. This study utilised an optimised version of the wind-sifter that was designed and fabricated by the author during his master's degree.

The drawback experienced while testing the first prototype wind-sifting separator led to this investigation. This study used a computer simulation technique (the Lagrangian particle tracking method). This resulted in observing the effectiveness of the separation process in the newly designed separator. The design of the new separator was made flexible in its mode of operation by fabricating detachable collecting bins to the separator assembly. This means the optimised separator can be operated with or without the coal collecting bins, unlike the prototype version, which could only run with its bins.

The design of the separator was done with the aid of Autodesk Inventor, and simulation was carried out using Star-CCM+^{TM} computer software. The simulation tests were performed for different particle sizes (−6.7+3.35 mm), (−3.35+1.0 mm) and (−1.0+0.2 mm) at different airstream velocities. The optimal airstream velocities from the previous study (at a cut point of 1.6 g/cm^3) were also used in this study when the separator was run with its bins. These airstream velocities were 6.0 to 4.0 m/sec, 4.2 to 2.0 m/sec and 1.7 to 1.0 m/sec for the (−6.7+3.35 mm), (−3.35+1.0 mm) and (−1.0+0.2 mm) particle sizes, respectively. A simulation was used to determine the airstream velocity ranges of the separator without collecting bins. These were 10.5 to 9.0 m/sec for the (−6.7+3.35 mm), 7.0 to 5.0 m/sec for the (−3.35+1.0 mm) and 3.5 to 2.5 m/sec for the (−1.0+0.2 mm) particles. For the –1.0 mm size faction, three particle size distributions (–1.0+0.1 mm), (–1.0+0.15 mm) and (–1.0+0.2 mm) were simulated. The best airstream velocities of 1.7 m/sec and 3.5 m/sec were achieved, respectively, for the closed and opened bins. The results of the simulation study led to the fabrication of the optimised wind sifter used in this study.

From the sink and float test conducted on two sets of feed-coal (coal A and coal B), the extent to which the separator could beneficiate coal was determined. The sink and float analysis revealed that coal A has a higher ash content than coal B. Coal A, at (−1.0+0.2 mm) size

fraction, has an ash content of 4.29% at 1.3 relative density (RD). This is followed by the (−3.35+1.0 mm) particle size with 5.55% ash content and the (−6.7+3.35 mm) size fraction with an ash content of 5.89%. At an RD of 1.5, coal A has a specific ash content of 16.65%, and coal B has an ash content of 13.56% for the (−6.7+3.35 mm) fraction. Upon separating with the wind sifter, the clean coal products from coal A have a higher ash content compared to those from coal B. Running the separator without the bins, clean coal products with cumulative ash content ranging from 22.42% to 19.44% for the (−6.7+3.35 mm), 24.61% to 21.43% for the (–3.35+1.0 mm) and 27.54% to 22.51% for the (–1.0+0.2 mm) fractions were obtained. For the particle size of (−6.7+3.3 mm) and with the bins closed, a clean coal product of 20.21% was obtained from coal A (feed coal with 37.38% ash content). A coal product with 19.55% ash content was obtained from coal B (from feed coal of 26.65% ash).

A second-stage test conducted on a first-stage coal product of 23.48% ash content yielded a coal product of 21.79% ash and 80% yield for coal A at (6.7+3.35 mm). This trend was also observed for other first-stage products at the three particle sizes used in this study. The E_p values obtained from this separator ranged between 0.035 and 0.16, with the E_p values increasing as the airstream velocity was reduced. For the (6.7+3.35 mm) fraction, Ep values (Probable Error of Separation) of 0.035, 0.095, and 0.16 were obtained at 6.0, 5.0, and 4.0 m/sec air velocities, respectively. Overall, the cleanest coal product with 16.73% ash and 26.70 MJ/kg was obtained in this study from coal A at bin 2. According to the study’s results, the separator was highly adaptable. The separator could also be used for upgrading and pre-concentrating other minerals in the mineral processing industry.

ACKNOWLEDGEMENTS

To God be the eternal gratitude!

My sincerest gratitude goes to my supervisor, Prof. Samson Bada, for his arduous guidance and dogged support to ensure the completion of this research. If not for my supervisor, I doubt my research would have been a success. I would also like to thank the team at Trade All Africa, as well as the laboratory technicians at Mechanical and Aeronautical Engineering, Wits-University, for helping me fabricate the separator assembly and cradles, respectively.

I am eternally grateful to the Coaltech Research Association, and the DSI/NRF South Africa's SARChI Clean Coal Technology grant (Grant Number: 86421), for their financial support. I also want to acknowledge the Clean Coal Technology Research Group of the University of the Witwatersrand and the School of Chemical and Metallurgical Engineering for access to research facilities.

My sincerest gratitude goes to my darling wife, Mary, eldest brother Mr. Israel Olorunfemi Alade, relatives and other siblings for their prayers and motivation, friends for their steadfast encouragement, and my parents for blessed memories for their tenets.

I also wish to particularly appreciate Mr. Andrew Morgan for his assistance, dedication, and selflessness, Mr. Hopewell Gumede for his illustrious help, and Mr. Msizi Mkhize, who was always available to help me. I would also want to acknowledge Dr. Gentil Kahilu for his selfless help, Dr. Orevaoghene Eterigho-Ikelegbe for his help and encouragement, as well as Mr. Sifiso Ncgobo, Mr. Vatsha Mhlawakhe and Mr. John Nkuna; I truly appreciate you all.

PRESENTATIONS AND PUBLICATION

The following presentations on this research were made:

I. Presentations to the Coaltech Research Association in April, July and November 2022 and April, July and November 2023.

II. Alade, J.J., and Bada, S.O., 2023. Wind-Sifting Separation: A Review. *ACS omega*, http://pubs.acs.org/doi/abs/10.1021/acsomega.3c01087

III. Jimmy Alade, Samson Bada. DRY COAL BENEFICIATION USING WIND-SIFTER SEPARATOR. Oral (In-person). Southern African Coal Processing Society Technical Presentations: 30^{th} November, 2023.

LIST OF ACRONYMS

ADMFB	Air-Dense Medium Fluidised Bed
CAGR	Compound Annual Growth Rate
DMVFB	Dense-Medium Vibrated Fluidised Bed
E_p	Probable Error of Separation
FGX	Fuhe Ganfa Xuanmei
MSFB	Magnetically Stabilised Fluidised Bed
RD	Relative Density
ROM	Run-of-Mine
SMART	Spatial Monitoring and Reporting Tool
VFB	Vibrated Fluidised Bed

TABLE OF CONTENT

LIST OF TABLES

LIST OF FIGURES

CHAPTER 1: INTRODUCTION

1.1. BACKGROUND AND MOTIVATION

Energy resources are needed globally for social, economic and industrial development as coal plays an integral role, particularly for nations endowed with this resource, notably for power generation, as well as for metallurgical applications (Dwari and Rao, 2007; Yu et al., 2016; Mutezo and Mulopo, 2021). Coal is the largest source of electricity generation and provides about a third of the world's electricity generation (Future Coal, 2023) According to the Future Coal (2023), coal contributes 36% of the global electricity supply and is predicted to be the single largest source of electricity in 2040 (Department of Mineral Resources and Energy, 2023; Future Coal, 2023; IEA Coal Market Update, 2023). Coal continues to play a crucial role in the energy supply of over 80 countries, not only in terms of electricity but also heat production. It provides process energy fuel and accounts for 70% of the global steel manufacturing, 90% of cement production and 61% of energy to make aluminium (Future Coal, 2023). Coal is a very valuable source not only for thermal energy but also for value-added carbon products such as carbon fibers, carbon-carbon, and carbon-metal composites, and specialty carbon products (EnergyGov, 2023).

Coal is the world's most abundant energy source owing to its abundance and relatively low cost; however, owing to the scarcity of high-grade coal, the use of low-grade coal for fulfilling the energy demands of modern civilisation becomes inevitably necessary (Behera et al., 2018). Coal serves as the main energy source in the Southern African region and is pivotal to the region's economic advancement. Being a significant mainstay of the South African economy, coal supplies nearly all the nation's electricity generation demands, accounting for 77% of the primary energy supply (Department of Mineral Resources and Energy, 2023) and presently meets 70% of installed power generation capacity (IEA, 2023).

According to Mantashe (2022), the coal sector produced around 248 million tons of saleable coal in 2020, the highest revenue earner and contributed about 21.4% of the total mining revenue of R608.99 billion. The coal sector generated about 53.42% of the total local sales revenue of R159.16 billion and around 10.13% of total foreign exchange earnings of R449.83 billion. In that same year, the sector was the third largest employer in the mining industry, employing 20.48% of the total mining industry employment of 437 288 people. These employees received around R31 billion in wages and salaries, around 20.27% of the mining industry's total wage income of R151.53 billion (Mantashe, 2022).

In terms of sustainability, coal is abundant in South Africa, with the estimated remaining reserves to last more than a century, assuming the current rates of usage and production remain the same (Prevost, 2004; Minerals Council South Africa, 2023). Many alternative energy sources, such as nuclear and solar energy, are projected to be progressively added to the total energy mix on the local and global stages. Nuclear energy, which is touted as the silver bullet to replace fossil fuel, is projected to play a significant role in this development. Despite this, coal is projected to remain the key energy source in the future owing to its relative abundance and minimal cost (Jeffrey, 2005; Future Coal, 2023; International Atomic Energy Agency, 2023). Based on the facts, coal is an invaluable resource not only to South Africabut globally.

For the continuous use of coal in the abovementioned sectors, it must have a quality suitable for these applications. The decline in coal quality in South Africa requires research on more effective beneficiation techniques to produce clean coal that meets different customer specifications (Taole, 2015; Mills, 2016; Reid, 2017). According to Jeffrey et al. (2014), high-grade coal products with an ash content lower than 15% are mostly exported, with the low grade used locally. These coal grades are achieved through a wet or dry coal beneficiation process, which separates the coal's inorganic minerals from its organic components. The wet beneficiation processes are well received within the mineral processing industry since they accomplish a higher quality product with high recovery. Some of these processes include dense-medium cyclone (Honaker et al., 2000; Zhang et al., 2014a, 2014b), spirals (Honaker et al., 2007), froth flotation (Lynch et al., 1981; Han, 1983; Shi et al., 2019; Cheng et al., 2020), wet jig (Rao and Vidyadhar, 2006; Tripathy et al., 2016; Kumar and Venugopal, 2017), etc.

There are, however, concerning challenges facing the wet beneficiation techniques ranging from water scarcity, effluent management and intensive capital requirements, amongst others. Dry beneficiation is, therefore, becoming the process of choice, and further studies are being carried out to increase its efficiency, particularly when upgrading smaller coal particles (Wang et al., 2018). In addition, energy is not utilised in drying the coal, ensuring the thermal value does not change (Dwari and Rao, 2007; Chagwedera et al., 2018; Alade et al., 2021). Dry coal beneficiation techniques depend on the coal's physical properties, as well as its associated mineral matter. Numerous studies have been conducted on dry coal beneficiation based on coal's physical properties, such as shape, size, density, electrical conductivity and magnetism (Bada et al., 2010b; Bada et al., 2012; Riazi and Gupta, 2016; He et al., 2017; Chagwedera et al., 2018; Alade et al., 2021). In fact, new dry beneficiation techniques are being developed, one of which is the wind-sifter technique, which Alade (2021)adapted for the beneficiation of dry South African coal for the first time.

The wind-sifter separation principle has been successfully implemented in other fields and industries, including the separation of municipal solid waste, opal sandstone, mica, food and other organic materials (Redemann et al., 2008; Krüger et al., 2014; Pettinari and Simone, 2015; Ragaert et al., 2017; De la Fuente et al., 2018). From the initial investigation conducted using the novel wind-sifter separator designed Alade (2021), a clean coal with an ash content of 16.75% and a calorific value of 27 MJ/kg was achieved. However, a few drawbacks were experienced by this separator, including particle misplacements and massive sample loss, particularly of the very fine coal size fraction. In addition, collection of coal products, and cleaning of the separator were cumbersome tasks for the old separator design. These drawbacks prompted the current study to optimise the already designed and fabricated separator to improve its separation performance for effective partitioning of the feed coal.

1.2. PROBLEM STATEMENT

In recent times, the quality of Run-of-Mine (ROM) coal found in South Africa has been declining, and this resource cannot be used for certain applications without beneficiating it (Bunt et al., 2015). Coal with more than 40% ash is being mined in situ in South Africa (Isaac and Bada, 2020), and to meet different applications or customers' specifications, the quality of the ROM coal must be improved. The wet beneficiation process has been the main technique utilised for many decades, producing clean coal with lower ash content and higher yield than dry processes. There is, however, an increase in the demand for dry beneficiation owing to the scarcity of water, large amounts of reagents and high operational cost associated with wet beneficiation processes like dewatering and wastewater treatment (Zhao et al., 2014; Shanmugam et al. 2022). Particle separation under dry beneficiation is based on the ore's properties, including the shape, size, density, electrical conductivity/resistivity, frictional coefficient and magnetic nature. The heterogeneous and near-density natures of South African coal are responsible for the difficulty faced in separating this coal efficiently, along with the mineral matter finely entrained within the coal (Falcon 1986; Bada, 2010a).

A prototype version of the wind-sifter separator for dry coal beneficiation was designed and fabricated in a previous study to upgrade South African coal (Alade, 2021). In the prototype version, the separator assembly has two chambers; chamber 1 is designed to collect the coal particles rich in mineral matter, while chamber 2 is designed to collect the coal particles rich in organic matter. Chamber 2 is integrated with a filter connected in tandem with it to filter the coal dust particles along with the air exiting the separator. One of the drawbacks of this prototype is that coal of finer particle size fraction (−1.0+0.2 mm) stick to the walls of the separator. Also, some clean coal particles (coal with less mineral matter) travel further into the filter section, ultimately resulting in the loss of valuable clean coal products.

The influence of factors such as particle shape, particle size and density were investigated in the optimised separator. The wider the particle size distribution, the more likely the particles will be exerted with more drag force, leading to different particle velocities in the airflow. In addition, factors such as the flow rate, velocity of the air, and drag-force in relation to particle size distribution, shape and density were observed critically using a computational fluid dynamic. As the coal will be fed into a flowing airstream in the separator and under gravity, the influence of gravity was monitored. It is expected that the inorganic and organic content of coal will follow different parabolic movements due to the differences in their densities, leading to different particle trajectories. This, in turn, will impact the separation of the particles in the first separation chamber's airstream. The particle density will also influence separation efficiency; coal dominated with higher-density particles (lower-grade coal) will travel a shorter distance in an airstream than lower-density particles (higher-grade coal).

The impact of settling velocity in association with the particle density was thoroughly investigated, with more emphasis on its influence on the separation of particles in the second chamber. The current study focused on redesigning the prototype separator and fabricating a new separator for beneficiating coal using wind-sifter technology. The effects of operational factors such as feed rate, air velocity, flow rate, the air-jet angle in the chamber, and static and dynamic pressure were investigated.

1.3.RESEARCH QUESTIONS

The primary research question was: Will the separation efficiency of this optimised version of the wind-sifter separator for dry coal beneficiation be viable enough to be applied for coal beneficiation; to match other dry beneficiation techniques and replace the wet beneficiation technique? This led to four sub-questions:

- At what particle size range will the highest efficiency be attained in this new design, and to what extent will the coal particle size influence the separation of the organic matter from the high ash mineral-rich particles?

- What influence will factors such as drag force, gravitational force, and particle shape have on the separation of particles in an airstream?
- How will the separation process of this optimised wind-sifter affect properties such as the ash content, volatile matter, carbon content, etc. of the coal feed?
- How would the performance of the new design of the wind-sifter separator when compared to that of the sink and float analysis?

1.4.RESEARCH AIM AND OBJECTIVES

This research aimed to design and fabricate an optimised wind-sifter separator and apply the separator for dry beneficiation of South African coal. The research objectives were:

- To design and simulate a new and optimised wind-sifter separator for dry coal beneficiation using the software tools Autodesk Inventor and Star CCM+, respectively.
- To fabricate the optimised wind-sifter separator design.
- To experimentally validate the simulated data results by performing sample runs on the fabricated unit and compare the obtained outcomes with the simulation results.
- To determine the impact of different particle size fractions ranging from (−6.7 mm+3.35 mm), (−3.35 mm+1.0 mm) and (−1.0 mm+0.2 mm) on the separator's yield and efficiency by analysing the influence of shape, size, density feed rate, air flow rate, etc. and comparing those results to that from the sink and float tests.
- To address the problems of sample loss observed, particularly for the (−1.0 mm+0.2 mm) size fraction.
- To determine an appropriate cut size for the separator.

1.5. HYPOTHESIS

It was observed from the prototype that the wind-sifting principle was effective in beneficiating the ROM coal. However, a few drawbacks, including highergrade coal particles travelling further than the collecting bins in chamber 2 of the prototype assembly and minimal separation effectiveness of the (−1 mm) size fraction, were observed. Optimisation of the current prototype separator was needed to address these drawbacks, and it is expected that the new design will significantly separate the inorganic mineral matter from the organic matter. The wind-shifting dry beneficiation principle is based on factors such as drag force, airflow velocity, pipe length and diameter in association with the coal's aerodynamic properties, such as shape, size and density. The extent of separation will depend on these variables and the airstream response.

1.6. LAYOUT OF THE THESIS

There are five chapters in this thesis, and they comprise of the following:

I. Chapter One introduces this research with its background and motivation. The study's aim and objectives are also presented.

II. Chapter Two details the available literature associated with the wet and dry techniques of coal beneficiation, and also on the wind-sifter technique.

III. Chapter Three gives a detailed research methodology. This chaptermeticulously looks at the simulation and experimental studies, including the sink and float tests, as well as the dry beneficiation process executed. It also includes the standards that were followed in this research.

IV. Chapter Four presents the results of the research and discussesthese results to illustrate the importance of the research. These results comprise the results of the simulation and experimental studies.

V. Chapter Five presents the conclusions drawn from the study, as well as the recommendations required to optimise the dry recovery process used in this study.

CHAPTER 2: LITERATURE REVIEW

2.1. INTRODUCTION

Coal mined from the ground, also known as ROM, is made up of different sizes ranging from small particles to large chunks. In most cases, ROM coal needs some degree of preparation and beneficiation to meet certain market requirements such as size, ash content, sulphur, and moisture content, as well as heating values (Charan et al., 2016). The quality of the mined coal varies greatly because of its heterogeneous nature and the unavoidable incorporation of non-coal bands and possibly a certain amount of out-of-coal seam rock material (Falcon, 1986; Bada et al., 2010a, 2010b; Charan et al., 2015; Wagner et al., 2018). This underscores the need for coal beneficiation which cannot be overemphasised as it encompasses a series of processes to meet specific end-user needs (gasifier fuel, steam boiler, etc.).

The separation efficiency of coal cleaning separators is usually assessed by the Probable Error in Separation (E_p) and Organic Efficiency (E_{org}). The E_p which will be the main index used in this study is a widely recognized measure is used to assess the separation efficiency of coal separators. It is determined from a Partition or Tromp curve based on precise cut point density of separation and implies that for ideal separation the error is zero. Figure 2.1 shows a display of a general partition curve.

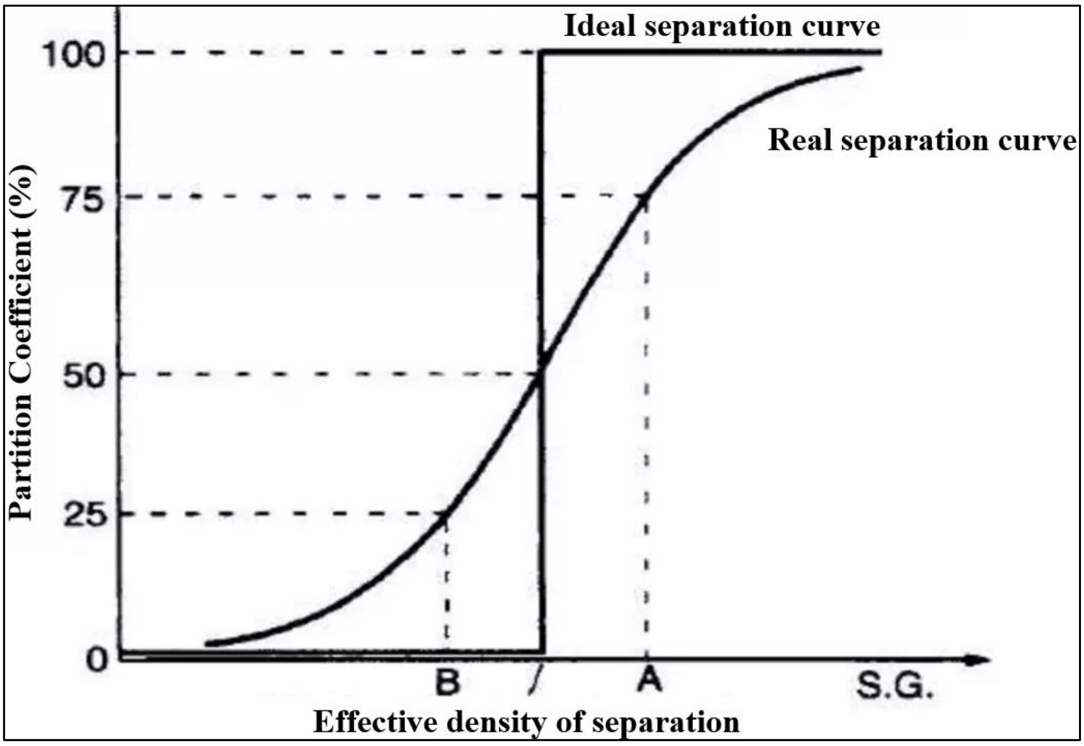

Figure 2.1: General design of a partition curve. Image adapted from Hussain, (2013)

Processes with the best separation efficiency are grouped under wet beneficiation, but in recent years, there has been renewed interest in dry coal beneficiation techniques. A few reasons for this include:

I. Eliminating the need for a large amount of water used in the wet beneficiation process, which leads to significantly large amounts of effluents (wastewater). These effluents seep into the water table and cause environmental degradation for man, animals and plants.
II. Mitigating challenges related to tailings disposal and water pollution through wet beneficiation processes.
III. Eliminating the high cost of drying coal prior to use to ensure the retention of the coal's thermal value.
IV. The capital and operating expenditures for the dry beneficiation plants are significantly less than the wet beneficiation plants. According to De Korte (2014), the operating expenditure of dry processing plants can be as low as half of that of wet beneficiation plants, while the capital expenditure can be as low as one-third.

This section provides an overview of the origin and extent of coal. The impact of beneficiation techniques (both wet and dry) on coal quality, with emphasis on dry coal beneficiation along with the fundamental principles driving these techniques, is discussed. Lastly, information on the global and local coal market is briefly discussed to further underline the importance of coal to the world economy.

2.2. OVERVIEW OF COAL (ORIGIN AND FORMATION)

Coal is a solid stratified, complex organic 'rock' and a natural fossil fuel, formed many millions of years ago from the remains of decaying trees and vegetation and occurs in layers in the earth's crust (Orem and Finkelman, 2003). The various conditions prevailing during the period of the flora accumulation and transformation of the vegetation, along with the extent of coalification resulted in coal with different grades, types and ranks. These properties impact the various fields of application or use (England et al., 2002; Orem and Finkelman, 2003). Thus, the prevailing conditions imply that coal is formed from the biological and geological processes that have acted on plant remains for an extended period. The complex (organic and inorganic matters) and heterogeneous nature of coal, along with the condition of its formation, are responsible for the difficulty faced in beneficiating coal.

Major coal deposits were formed over 400 million years ago, and the coal seams currently mined in South Africa were formed roughly between 285 and 200 million years ago (Minerals Council South Africa 2023). Formation of coal commenced during the first coal age (Carboniferous Period) at around 360 million to 290 million years ago, with the coal seams forming from the death and putrefaction of vegetable matter from densely populated tropical forests (Wills and Napier-Munn, 2006; Wagner et al., 2018). The dead plant materials are bio-chemically transformed into peat, and under appropriate conditions (swampy conditions), the formation of thick layers of peats occurs (England et al., 2002). A typical example showing peat occurrence in South Africa can be found in St. Lucia in KwaZulu-Natal (Scholtz et al., 2015).

The continuous accumulation and burial of these flora entities beneath the earth's crust over these periods caused the vegetation to be subjected to elevated pressures and temperatures, and the flora materials went through a metamorphosis, transforming into coal. ROM coal requires the separation of its ash-forming minerals from its organic matter to produce a clean coal product of higher quality for specific applications. In South Africa, clean coal products (washed coal products) with an ash content of less than 15% are mostly exported, while those with higher ash content, the low grades, are utilised locally by Eskom (Jeffrey et al., 2014).

2.3. COAL BENEFICIATION

In the area of coal utilisation, especially combustion, high-efficiency, low-emission technologies increase coal combustion efficiency while reducing the emission of pollutants. With this in mind and the high-cost implication of these technologies,coal processing industries globally must take on the challenge imposed by the decline in coal quality or coal grade (Reid, 2017). With the immense contribution of coal, locally and globally, as a source of energy, its inorganic mineral content, which results in gaseous emissions and other pollution, must be removed or reduced before use. According to Mills (2016), the quality of coal mined in South Africa and globally has reduced over time. The author pointed out that the average gross calorific value of coal supplied by India and the United States during the last half of the century decreased from 24.7 MJ/kg to 14.7 MJ/kg and from 28 MJ/kg to 20 MJ/kg, respectively. Given that most coal applications require high-quality coal, it is of the utmost importance to produce coal of acceptable quality to achieve the expected process efficiency; this can only be achieved through beneficiation.

The techniques employed in coal beneficiation to remove these ash-bearing minerals in coal are based on the differences in the physicochemical characteristics (specific gravity, surface and electrical properties, particle size and grindability/friability) between the organic and inorganic components of the coal. Despite research in beneficiating coal over many decades, there are still challenges impacting the recovery and the quality of the products produced. Some of these challenges are due to the inadequate liberation of the coal minerals from its organic matrix, as well as the coal origin. The following sections describe the two main techniques for beneficiating coal wet beneficiation and dry beneficiation – as well as a mini-review of a few wind-sifting techniques.

2.3.1. WET BENEFICIATION

The wet process uses water or other liquid medium in beneficiating ROM coal into a clean coal product and gangue material by using their inherent densities. In comparison to the water-only plant, the dense/heavy medium processing of coal over the years has proven to deliver more precise and accurate separation efficient and effective automatic control (England et al., 2002; Suresh et al., 2010). Owing to its adaptability in handling diverse coal qualities and particle fractions in the feed, it is a far more recommended technique than the water-only plant (Wills and Naper-Munn, 2006; Langner, 2016). The wet beneficiation techniques in this literature review include the float and sink technique, the dense-medium cyclones, the reflux classifiers, and wet jigs, as well as flotation (Langner, 2016).

2.3.1.1. Sink and float

The sink-float technique for coal beneficiation is a technique used to partition raw coal into two or more relative densities by means of different relative density (RD) solution(s) and can be used to determine coal properties (England et al., 2002; Meyer and Craig, 2014). In this technique, the principle of gravity separation is the principal factor that facilitates the partitioning of the coal feed. The coal feed is poured into a stationary liquid of known RD, and, by Archimedes' principle, particles that are less dense than the density of the liquid float. England et al. (2002) pointed out that there is a relationship between the ash content of a piece of coal and the specific gravity, implying that the ash content can be controlled by washing the coal at a specific RD. They also stated that the shape and size of the particle play almost no part in the stationary medium when the medium-to-ore ratio is adhered to, thus making it a very effective means for separating particles. Meyer and Craig (2014) illustrates this technique in Figure 2.2.

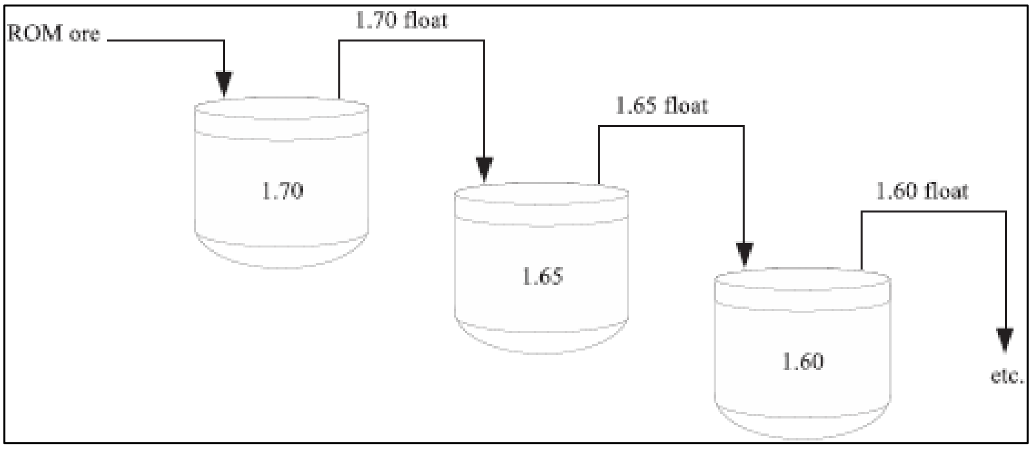

Figure 2.2: Principle of float-sink separation. Image adapted from Meyer and Craig (2014)

The efficiency of a centrifugal float-sink technique for upgrading different coal fractions (−217+83 µm), (−83+48 µm), (−48+14 µm) and (−14 µm) was determined by Killmeyer et al. (1992). The results of the study showed a higher mass yield of floats as the particle size fraction decreased. Aktaş et al. (1998) also conducted a coal beneficiation study using centrifugal float-sink equipment to upgrade lignite coal samples from Tunçbilek and Soma–Merkez collieries. According to the authors, as the RD of the media was increased from 1.30 to 1.50, the ash content of the lignite coal from Soma–Merkez and Tunçbilek collieries increased from 1.31% to 5.38% and 2.20% to 9.58%, respectively. The mass yield for the same coals increased from 4.5% to 96% and 4.40% to 94%, respectively. They concluded that the difference in the grade achieved between the two coal samples was due to the liberation difference between the two coal samples. Another study was conducted by Çetinkaya and Bayat (2020) on low-quality lignite coal from the Çanakkale lignite coalfield in Turkey at (−10+0.5 mm) particle size fraction using the float and sink technique. The ash content of the feed coal was reduced from 39.69% to 16.46% at an RD of 1.6. Coal's responsiveness can be predetermined, as well as its amenability to gravity separation, with the float-sink technique.

2.3.1.2. Dense-medium cyclone

The dense-medium cyclone separation process is well-known for processing coal. This approach is known to be one of the most efficient processes for removing inorganic minerals from ROM coal. The principle of dense media separation (Figure 2.3) is a technique based on density differences to separate mineral matter from raw coal (Honaker et al., 2000; England et al., 2002).

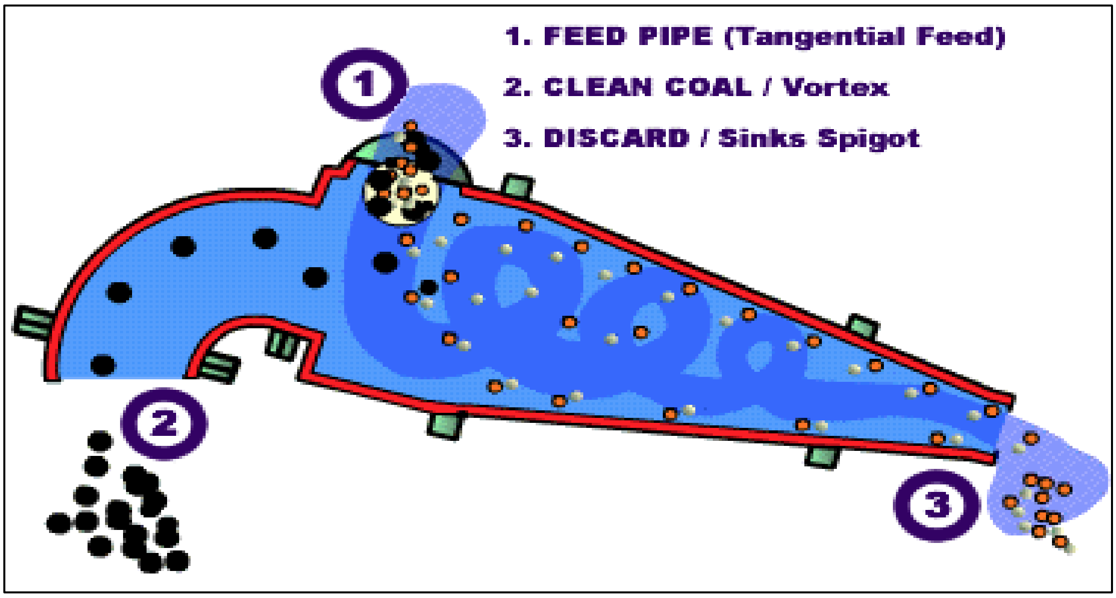

Figure 2.3: Basic working principle of the dense-medium cyclones. Image adapted from Millops Cyclones (2023)

Honaker et al. (2000) reported that fine coal (−1.0 mm) can be separated efficiently by increasing the centrifugal force in the cyclone. This is done by applying feed at high pressure into the dense-medium cyclone. This phenomenon was also supported by Suresh et al. (2010) and Napier-Munn (2018);the efficiency of a dense-medium cyclone for beneficiating fine coal (−1.0 mm) depends on the high-pressure feed injection, which provides significantly high centrifugal force in the unit. A pilot-scale medium cyclone separator to upgrade coal of (−6+2.0 mm) was used by Suresh et al. (2010) under different operating parameters, such as the coal feed inlet flowrate, pressure and RD. The study shows that at an RD of 1.6, a clean coal product of 12.5% ash and a yield of 52% is achievable from a feed coal of 32% ash. According to Suresh et al. (2010), a further 5% increase in yield is attainable when the air core in the unit is suppressed compared to the air core unsuppressed.

Zhang et al. (2014b) integrated a pump storage system into a dense-medium cyclone coal preparation plant to improve the energy efficiency of the plant while continuing to maintain the required supply of the medium. It was observed that the circulation loop of the medium reduced the associated energy consumption and, ultimately, the cost of separating coal using this unit. A life cycle cost analysis was conducted to ascertain the effectiveness of the pump storage system approach using the operation status quo of the dense medium cyclone plant, and the result showed that with a 160 m^3storage tank, a +50% energy cost reduction is achievable. Another scenario showed that a 38% overall cost reduction with a 2.7-year payback period was attainable.

Using dense-medium cyclones and spirals is well-known for upgrading coal, and a combination of the two techniques was used by Ma et al. (2018) in a study to upgrade coal (−1+0.125 mm). According to the authors, the presence of near-gravity materials in the coal feed was found to be minimal. A clean coal yield of 37.39%, organic recovery of 47.76% and ash content of 8.31% with a Probable Error of Separation value (E_p) of 0.150 was achieved from the spiral. Whereas a better result was achieved using a medium cyclone with a clean coal yield of 62.98%, ash content of 8.31%, organic recovery of 80.84% and an E_p of 0.118.

A novel dense-medium separation investigation was conducted by Williams et al. (2022) using calcium nitrate (from common fertiliser) rather than conventional calcium chloride solution to upgrade low-grade, high-ash Colombian coals. For this investigation, three low-grade coal samples from Valle, Cundinamarca and Antioquia, which are commonly used in Colombian stoker furnaces for sugar milling, were tested. The report shows that the calcium nitrate reduced the ash content to less than 7% for all the coals tested. This was particularly notable for Valle, whose ash content dramatically reduced across all size fractions from 29% to below 7%, which is an acceptable level for coking coals (less than 10% ash). The authors recommended further investigation to analyse the potential for the washed Valle coal to be used as metallurgical coal.

2.3.1.3. Reflux Classifier™

The Reflux Classifier is an advanced type of gravity separator used in the mineral and coal processing industries. The separator is efficient in upgrading coal of (−8.0 mm) and can go as low as 250 µm (Galvin et al., 2010; Kopparthi et al., 2019; Galvin et al., 2020). The Reflux Classifier as seen in Figure 2.4, separates fine particles based on the difference in their density or particle size. In addition, it combines a conventional fluidised bed separator with a set of parallel inclined plates that form lamella channels. A coal beneficiation study using the reflux classifier technique to upgrade coal was carried out by Galvin et al. (2010). In this study, the effectiveness of upgrading coal at (−8.0 mm) was critically investigated, and it was observed that the process effectively produces a clean coal product with significantly low ash content. Four runs of the process were carried out, and the separation result (run 1) shows a product mass yield of 80.3% and an ash content of 8.5% from a feed coal of 18.0%. For run 2 and run 3, a yield of 73.7% with an ash content of 16.1% and a yield of 87.9% with 18.0% ash content was obtained, respectively. From the fourth run, a product yield of 90.4% and 10.2% ash was obtained.

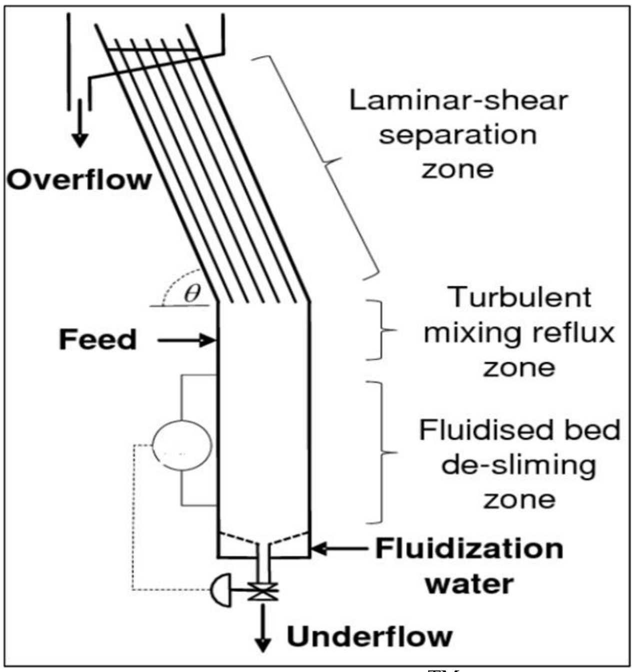

Figure 2.4: Working principle of the Reflux Classifier™. Image adapted from Galvin et al. (2020)

Another study conducted using the Reflux Classifier™ was reported by Campbell et al. (2015) on fine coal samples (−1400+150 µm) from Waterberg Coalfield, Limpopo. A laboratory scale Reflux Classifier™ (105 × 105 mm), with 23 steel plates arranged at a 70° inclination angle and 3.5 mm apart, was designed and built for this study. The test was carried out on different coal fractions (−1180+850 µm), (−850+600 µm), (−600+355 µm) and (−355+150 µm) under different water flowrates 25 to 80 L/min. At 35 L/min, a cut-point of RD 1.45 was attained for the (−1180+850 µm) size fraction, while a cut-point of RD 1.55 was obtained for the remaining size fraction. The ash content achieved in the clean coal product was less than 25% using the separator.

Kopparthi et al. (2019) also beneficiated high-ash coking coal fines of (−2+0.25 mm) particle size fraction using the same approach. The influence of parameters, such as the set point of the bed, the fluidisation velocity of water in the Reflux Classifier™ and the feed rate of the feed coal, were investigated. The results obtained under varying operational parameters show that the feed coal was de-ashed from 28% to an ash content range between 7.9 and 20%. The mass yield of the clean coal product ranged between 31 and 64% with an $E_P$value ranging from 0.07 to 0.1 as separation densities varied between 1.34 and 1.7 RD.

Iveson et al. (2019) also upgraded a (−6.0 mm) coal using a reflux classifier and comparedthe dense-medium cyclone, which processed (−6.0+4.0 mm), and the Reflux Classifier™ at

(−4+0.5 mm). Sixteen runs were carried out with the volumetric flowrate of the feed ranging from 210 to 368 m^3/h and pulp density ranging from 16 to 37 wt%. The results of the study show that at an RD ranging from 1.2 to 1.575, the mass yield of the products ranged from 35.7 to 93.9%. Ash content in the feeds ranging from 55.6% to 11.5% was reduced to 11.5% to 4.3% in the products, and a maximum E_p value of 0.1 was obtained. Rautenbach et al. (2019) also beneficiated 100 kg of coal at (−75+1.7 mm) using the same approach. The result from this study shows that the three coal samples, A, B and C, have an ash content of 35.9%, 32.9% and 25%, respectively. The ash was subsequently reduced to 7.8% for coal A, 12.4% for coal B and 10.5% for coal C.

2.3.1.4. Wet jig

Jigging is a long-lived and effective gravity separation method to upgrade large arrays of unwrought minerals such as gold, raw coal, etc., having approximately 20% near-gravity matter (Ambrós, 2020). As pointed out by England et al. (2002), wet jigging works on the same principle as the fluidised bed. In this separation technique, raw coal is fed on the washing deck of the jig and particles of various relative densities are partitioned based on the vertical water pulsation, viscosity and particle size (England et al., 2002; Terblanche, 2013; Woollacott and Silwamba, 2016; Woollacott, 2018). Langner (2016) pointed out that remixing can occur as pulsation strength increases in a wet jig. Figure 2.5 provides a representations of the jigging process, adapted from AllMineral (2018).

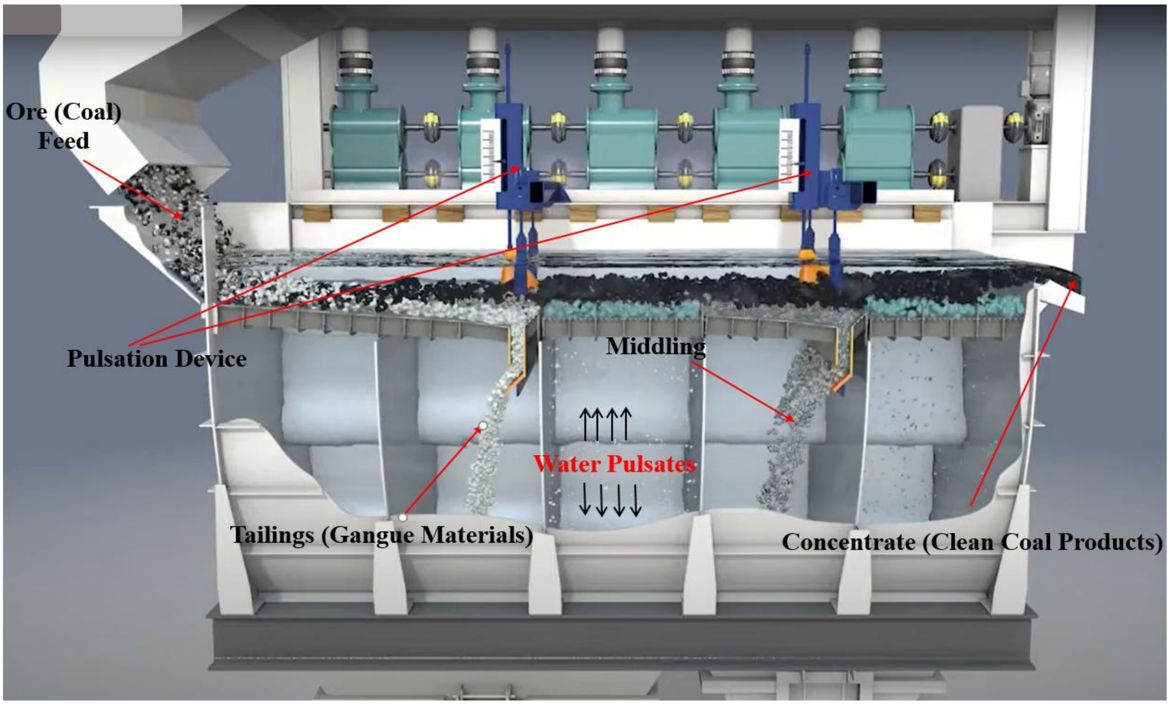

Figure 2.5: Working principle of the wet jig. Image adapted from AllMineralJig (2018)

The wet jig technique was used by Rao and Vidyadhar (2006) to upgrade (−10+6. mm), (−6.3+4.0 mm), (−4.0+1.0 mm) and (−1.0 mm) coking coal samples from Assam. A clean coal product of 2.67% ash and 70.7% mass yield was obtained from the (−10+6.3 mm) size fraction. The (−6.3+4.0 mm) size fraction had the lowest ash content of 1.89% with the highest yield of 73.7%, while the (−4.0+1.0 mm) fraction had an ash content and yield of 3.29% and 64.9%, respectively. Tripathy et al. (2016) upgraded non-coking coal of (−3+2.0 mm) and (−2+1.0 mm) using the laboratory scale Denver mineral wet jig by varying operating parameters such as the feed rate, water flowrate and feed particle size. Statistical analysis was carried out to ascertain the jig performance (combustible recovery and ash content of the clean coal product), and from this analysis, the Nelder-Mead multidimensional pattern was used for an optimisation investigation of the process. A clean coal of 64.15% combustible recovery and an ash content of 22.6% was obtained under optimised conditions.

Another study was carried out by Kumar and Venugopal (2017) using the wet jig on a coal sample with a (−10 mm) size fraction. The coal was screened into different particle sizes of (−10+6.73 mm), (−6.73+4.73 mm), (−4.73+3.0 mm), (−3+0.5 mm) and (−0.5 mm). Operating parameters such as jigging time, bed height and water flowrate were varied, and the Box-Behnken experimental design, a test programme that uses a completely randomised three-level factorial design, was used to optimise the operating parameter and to improve the separator's performance. The results obtained show that the height of the bed was the major factor influencing the ash content and yield of the clean coal product. It was observed that at a jigging time of 10 minutes and 2.0 L/min water flowrate, the ash content of 24.32% in the feed can be reduced up to 16.55% in the clean coal product.

2.3.1.5. Froth flotation

The froth flotation process is based on the contrast in surface properties of the materials in the raw coal (Han, 1983), and this process is a surface chemistry-based unit operation usually for fine solid-particle separation from an aqueous suspension (Jafarinejad, 2016). Several parameters (air bubbles, particle sizes and oil droplets) involved in this technique concurrently interface with each other and other species, like the molecules that boost reagents and ions that dissolve in water (Polat et al., 2003). A frothing agent is usually added to help stabilise the froth, which is skimmed off and becomes the clean coal product. A flotation aid, such as fuel oil, may also be used to increase the hydrophobicity of the coal and to help collect the particles. The bubbles introduced into the system lift the hydrophobic material to the top of the water suspension in which they are collected by skimming while the gangue is left behind in the water suspension (Lynch et al., 1981; Han, 1983). Figure 2.6 portrays a basic working principle of froth flotation.

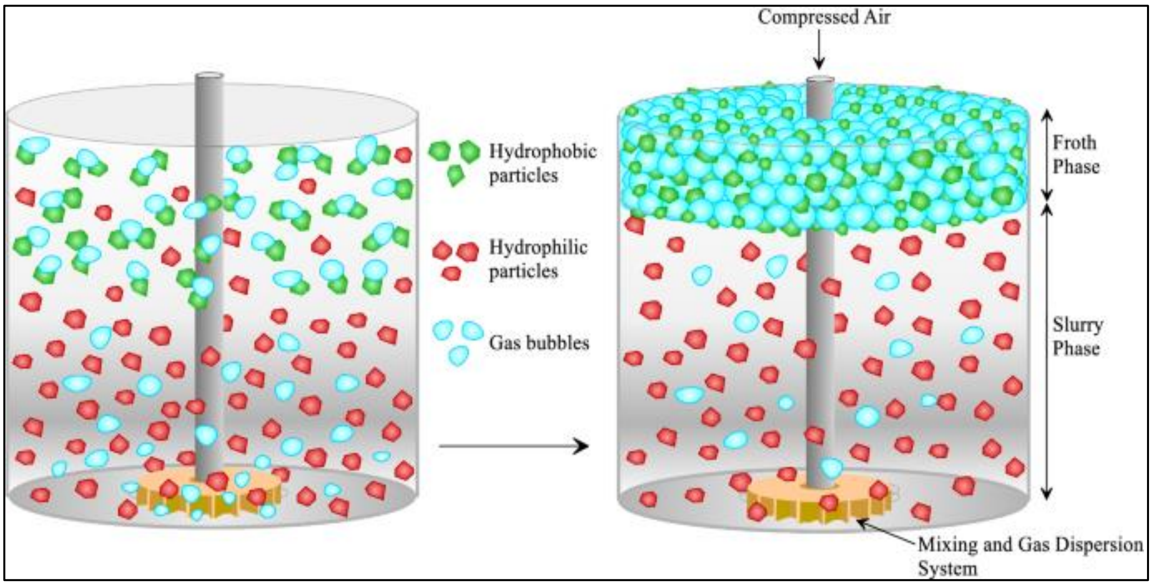

Figure 2.6: Working principle of the froth flotation process. Image adapted from Pawlik (2022)

Ozmak and Aktas (2006) carried out an investigation on the effects of reagent adsorption on the froth structure. This investigation determined the relationship between the reagents adsorbed on the solid particles, froth structure and froth flotation performance. A (−53 μm) bituminous coal was used to perform this experiment, and the results showed that the adsorption of a high amount of reagent on the coal particles decreased the system's separation efficiency. A recent study to beneficiate flotation tailings was carried out by Shi et al. (2019) using a flotation cell. In this study, a comparison was made of the performance of four different collectors. The depressant used was hexa-metaphosphate, and parameters, such as collector dosage, pulp inflation rate, stirring or revolving speed, frother dosage and the depressant mechanism, were investigated. The optimal flotation condition was achieved at 300 g/t collector dosage, pulp inflation rate of 0.25 $m^3/(m^2.mins)$, 4000 g/t of depressant, 500 g/t frother dosage, revolving speed of 2200 rpm and a pulp concentration of 100 g/L. At these parameters, the ash content of 62.01% in the feed coal was reduced to 10.64%, and a 71.88% mass yield was achieved.

Cheng et al. (2020) recently upgraded a coking coal of (−500 μm) size fraction using the froth flotation technique. The coal sample for this study was collected from the Linhuan coal preparation plant in the province of Anhui, China. The coal samples were screened into (−500+250 μm), (−250+75 μm), (−75+45 μm) and (−45 μm), and the influence of three flotation systems was investigated: the jet, counter-current and cyclone systems. The separation result shows that the counter-current system was very effective for the (−500+250 µm) size fraction and the cyclone for the (−250+45 µm) size fraction, while the jet system was effective for the (−45 µm) fraction. The authors reported that factors such as the flow field and the degree of turbulence (the turbulent kinetic energy and turbulent dissipation rate) were responsible for this observation. The turbulent kinetic energy and the different turbulence intensities resulted in different bubble sizes, as well as the collision, detachment and attachment of the different bubble and particle sizes. The counter-current system showed the least turbulent kinetic energy and dissipation rate, while the jet flow system displayed the maximum of the three systems. The clean coal product for the (−500+250 µm) size fraction showed that ash content lower than 10%, and combustible recovery in the range of 62.34 to 66.16% was obtained, while for the (−250+75 µm), combustible matter in the range of 49.19 to 84.09% with an ash content lower than 11% was obtained. An ash content lower than 12.5% and recovery in the range of 32.62 –to 73.03% was obtained for the (–75+45 µm), while combustible recovery in the range of 30 to 64.54% and ash content lower than 14.5% was achieved for the (−45 µm) size fraction.

2.3.2. DRY BENEFICIATION

Dry beneficiation techniques explore the differences in the coal's physical properties and its inherent mineral matter, which include the shape, density, size, magnetic susceptibility tendencies, lustrous nature and electrical conductivity for coal separation (Dwari and Rao, 2007; Bada et al., 2010a; Charan et al., 2016; Chagwedera, 2017). Numerous techniques have been used for the dry beneficiation of coal, such as the air table, air-dense medium fluidised bed (ADMFB), electrostatic separators, air jigging and a few innovative approaches (Chen and Wei, 2003; Bada et al., 2010a; Bada et al., 2010b; Bada et al., 2012; Scholtz et al., 2015; Chagwedera et al., 2018). In the sections that follow, three different types of dry fluidised bed techniques are discussed (ADMFB, dense-medium vibrated fluidised bed (DMVFB) and magnetically stabilised fluidised bed (MSFB)), followed by other dry processes.

2.3.2.1. Air-dense-medium fluidised bed (ADMFB)

The ADMFB is a major technique used in the beneficiation of dry coal and is deemed to be one of the most efficient methods for dry coal beneficiation (Fu et al., 2019). It makes use of a fluid-like mixture of the blend of a dense medium (magnetite powder) and fine coal powder as the separating medium, and the separation of the coal is attained through vertical stratification (Chagwedera, 2017). Skimmers are attached to the separator to remove middling and clean coal fractions along the table length (Kretzschmar, 2010). The pressure drop across a fixed bed height containing a single size of isotropic solids is determined using a model called Ergun's equation (Makokha et al., 2012). This phenomenon is similar to the sink-float process that depends on Archimedes' principle (Sahu et al., 2009; Zhao et al., 2014; Meshram et al., 2015; Zhao et al., 2015).

An investigation was carried out by Choung et al. (2006) using the ADMFB to upgrade subbituminous coal samples from Genesee, (Alberta, Canada). The effects of parameters, such as bed height, coal particle size and magnetite (medium), were investigated and their influence on separation efficiency. Coal samples of (−6+5.66 mm), (−5.66+3.35 mm), (−3.35+1.0 mm), (−1.0+0.42 mm), (−0.42+0.25 mm), (−0.25+0.04 mm) and (−0.04 mm) size fractions and magnetite (−300+150 µm), (−106+45 µm), (−75+45 µm), (−53+45 µm) and (−45 µm) size fractions with the bed density of 1.6 g/cm^3 were tested. Separation results show that for (−5.66+3.35 mm) coal size, clean coal with an ash content of 14% was achieved for magnetite of (−300+150 µm) size fraction at an air velocity of 23.5 m/sec. However, the ash content was further reduced to 6% with a mass yield at 90% when the particle size of magnetite was reduced to (−106+45 µm) at a velocity of 4.0 m/sec, with little to no significant improvement in the separation performance when using magnetite of (−75+45 µm) at a velocity of 2.9 m/sec. For the (−3.35+1.0 mm) coal and magnetite of (−106+75 µm), a clean coal with an ash content of 7% and yield of 70% was achieved as the bed density was reduced from 1.6 g/cm^3 to 1.4 g/cm^3. While the separation performance for the (−1+0.42 mm) coal size fraction was very small.

In a study carried out by Luo et al. (2007) using a (−50+6.0 mm) coal particle size, the effect of a low-density cut-point was studied using magnetic pearls as the solid medium. The formation of microbubbles was investigated, and the fluidisation characteristics of the pearls were established for a precise particle size fraction. The process produced a clean coal product of 90.80% mass yield with an ash content of 13.95%, while the ash content in the tailings was 56.82%. Prashant et al. (2010) investigated the influence of operating parameters, such as fluidising velocity, separating time and media type, on the separation performance in both continuous and batch ADMFB separators. ROM coal of (−6+2.0 mm) particle size range and 25% ash content were beneficiated, and a clean coal of 10% ash and 80% yield was achieved. A continuous ADMFB was used by Dave (2012) to beneficiate a (−22 mm) coal fraction from Genesee Mine, Alberta, Canada. A yield of 80% with an ash content of 10% from a feed coal of 26% ash content was obtained. Sahu et al. (2009, 2011, 2013) carried out an investigation to upgrade high-ash Indian coal using the ADMFD separator at (−25+6.0 mm) particle size fraction. A 600 kg/h capacity continuous ADMFD separator with nano-bubbling condition was fabricated by observing the fluidisation stability, and this characteristic was an important factor in the separation process. From these investigations, clean coal products of 60 to 72% yield and an ash content range between 32 and 35.5% were achieved with an E_p of 0.12.

Another study was conducted by He et al. (2013) on South African coal using the dense gas-solid fluidised bed technique utilising a (−50+6.0 mm) size fraction with 78.20% of the cumulative mass distribution being 1.6 g/cm^3. Simulation and experimental results of the hydro-mechanical and density distribution stability indicated that under stable operating conditions, the dense gas-solid fluidised bed gives steady separation with steady fluctuations in density. The feed coal sample was separated into three product streams: clean coal product with 73.25% mass yield and ash content of 9.59%, the middling with an ash content of 11.31% and the gangue material with 15.44% ash content. In another investigation by Azimi et al. (2013) on Canadian low-rank coal, the influence of bed height, residence time and superficial air velocity on the separation performance of the ADMFD was conducted. A clean coal product of 10.60% ash and 95.63% yield at optimal operating conditions of 150 mm bed height, a superficial air velocity of 0.15 m/sec and a residence time of 90 seconds was produced. The authors observed that with an increased feed rate, a lower ash clean coal product at a higher yield can be achieved.

Integrating a pulsating system with an ADMFB was utilised by Duan et al. (2015) to beneficiate a (−6.0+1.0 mm) coal particle size fraction. A feed coal of 56.15% was de-ashed to 33.69% with an E_p of 0.085 at a pulsation frequency of 1.82 Hz. Another novel ADMFB was designed by Zhao et al. (2017) from the University of Mining and Technology in China, using a binary mixture of magnetite of (−0.3+0.06 mm) and fine coal (−1.0 mm) as the heavy medium to upgrade coal feed of (−100+6.0 mm). The approach's industrial application became the world's first ADMFB modularised dry separator, achieving clean coal with an organic efficiency of 95%, ash content of 3.46% and 67.88% yield with an E_p 0.05. Although 0.42 kg loss per ton of the heavy medium occurred, less than two dollars was spent for the separation of a ton of coal feed. Chagwedera *et al*. (2018) also carried out an investigation to find an alternative dense media to magnetite with potential for use on (−13+6.0 mm) South African coal using ADMFB. In this study, silica sand, pyrrhotite, magnetite, coal discards and granulated blast furnace slag were investigated. Magnetite and pyrrhotite gave the most uniform and stable bed density, with a variation in the bed density under 0.7% and standard deviation under 0.0025 $\mathrm{kg/m^3}$. At 100% magnetite bed, a clean coal product of 25.24 MJ/kg and 20.30% ash content from a feed coal of 39.27% ash was achieved. From a bed of 40% pyrrhotite and 60% magnetite blend, a coal product with an ash content of 14.5% and a higher calorific value of 27.3 MJ/kg was also obtained. The total sulphur content of the product was also reduced from 2.49% in the feed to approximately 0.41% in the cleaner coal, and an E_p value of 0.083 was achieved.

Further investigation into the blending of different mediums to form a singular binary medium was investigated by He et al. (2018) in upgrading (−13+6.0 mm) coal. The two mediums of (−0.20+0.15 mm) of magnetite powder and quartz sand of (−0.35+0.25 mm) were investigated. Optimal separation results were achieved when the quartz sand was between 10 and 20% of the binary media. A high-grade coal product of 10.12% ash content and 68.29% yield was achieved. The combustible recovery of 92.09% and E_p of 0.085 was also achieved, indicating that this process has high separation efficiency.

2.3.2.2. Dense-medium vibrated fluidised bed(DMVFB) or vibrated fluidised bed(VFB)

Over time, the ADMFB has been relatively efficient in upgrading coal of (+ 6.0 mm) particle size; however, it has been relatively inefficient for (− 6.0 mm) (Luo et al., 2008). The DMVFB separator is a fluidised bed that utilises an external vibrating force to upgrade coal of (−6.0 mm) (Luo et al., 2008). Several investigations have been carried out on this technique, including understanding the energy transfer mechanism and the agitation effect on the bed characteristics (Luo et al., 2008; Yang et al., 2013a, 2013b; Wang et al., 2016). The investigations carried out by Luo et al. (2008) portrayed the following imperfections of the technique:

I. Increase back mixing when the vibration intensity increases, leading to a downside in forming a stable bed.
II. Occurrence of unevenly transmitted vibrational forces owing to significant adhesive frictional force that resides between the particles and walls of the bed.

Luo et al. (2008) carried out a study deploying the DMVFB to beneficiate the (−6.0 mm) particle size. The bubble-breaking mechanism was exhaustively studied, and the results showed that at optimal conditions, the coal of (−6 mm) with a lower limit of 0.05 mm was effectively beneficiated with an E_p of 0.07, and the mechanism proved to be more effective than the wet jig, which gave an E_p of 0.11. An experimental study was carried out by Yang et al. (2013a, 2013b) deploying the vibrated fluidised bed (VFB) to upgrade coal of (−6.0 mm) particle size. The results show E_p values of 0.190 to 0.225 and 0.175 to 0.195 for the particle size fractions of (−6.0+3.0 mm) and (−3.0+1.0 mm), respectively. In another study, a VFB was also used by Yang et al. (2015) to beneficiate fine coal of (−3.0+1.0 mm), and an E_p of 0.23 was achieved. The interaction between vibration and the gas phase in the VFB and its impact on density distribution and stable state of fluidisation was carried out by He et al. (2015). A lignite coal of (−6.0+1.0 mm) was tested and further split into (−6.0+3.0 mm) and (−3.0+1.0 mm). The respective samples attained a significant yield with cut-points of 1.68 and 1.75 RD and E_p values of 0.065 and 0.055. For the (−6.0+3.0 mm) sample, a mass yield of 84.46% and ash content of 10.40% was achieved from a feed coal of 23.52%, while the (−3.0+1.0 mm) size fraction produced a product of 11.43%.

Fu et al. (2017) likewise used the VFB technique to upgrade lignite coal of (−6.0 mm) particle size distribution. The particles were partitioned into different sizes (−6.0+4.0 mm), (−4.0+2.0 mm), (−2.0+0.5 mm) and (−0.5 mm) before beneficiating in the separator. The optimal separation for the (−6.0+0.5 mm) was obtained at operational parameters of 0.646 m/s air velocity, a fluidisation time of 360 seconds and a static bed height of 129.3 mm. The authors observed that the separator was not effective in upgrading coal of (−0.5 mm) size fraction.

2.3.2.4. Magnetically stabilised fluidised bed(MSFB)

The MSFB uses both air and a magnetic field for the beneficiation of fine coal. The generated magnetic field suppresses the formation of bubbles with the increase in gas velocity while suppressing back mixing of the solid or gas (Fan et al., 2001; Fan et al., 2002). Figure 2.7 is a generic schematic diagram of the working principle of the MSFB.

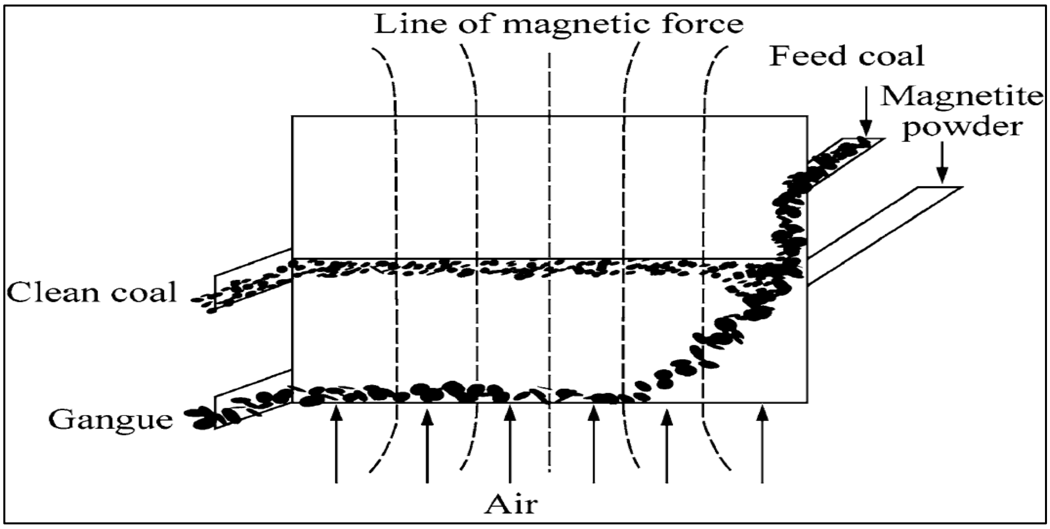

Figure 2.7: Schematic diagram of the crossflow magnetically stabilised air-dense medium fluidised bed. Image adapted from Song et al. (2012b)

An experimental investigation was conducted by Fan et al. (2001) using this approach to upgrade coal of (−6.0+1.0 mm) size fraction and magnetic pearls of 98 µm. The separation result shows that the process can effectively cut coal at an RD of 1.5 with an E_p value of approximately 0.07. Another coal beneficiation study was performed by Fan et al. (2006) to upgrade ROM coal at a top size of (−50 mm). The coal particles were split into three size fractions (−50+6.0 mm), (−6.0+0.5 mm) and (−0.5 mm) and subjected to three different beneficiation techniques: ADMFB, MSFB and electrostatic separation. ADMFB was very effective in upgrading the (−50+6.0 mm) coal; however, there was excessive back mixing and bubbling for the (−6.0+0.5 mm coal); therefore, MSFB was used for this fraction. Three magnetic beads, the Fushun, Shiliquan and Zouxian beads, were used independently in this study. This was to observe the bead with the highest magnetic stability in the fluidised bed, free of bubbles or pulsation. The Zouxian bead was chosen as it was the most suited for the stated requirements for this MSFB when the magnetic field was applied. An optimal separation efficiency was achieved with an air velocity of 12.3 m/s and 30 oersted magnetic field intensity. A clean coal product of 14.6% ash and an E_p value of 0.066 was achieved at a separation density of 1.52 g/cm^3.

In another study, Luo et al. (2002) conducted a study using the MSFB to upgrade Chinese coal of (−6.0+0.05 mm) size fraction of low ash coal. The optimal operating parameters used in this study were 55.0 m/sec gas velocity, 30 Tesla magnetic field intensity and bulk density of 1.5 g/cm^3. The results obtained show that after 25 seconds of the coal being introduced into the separator, a clean coal product of 12.62% ash content and yield of 61.30% was achieved, with an E_p value of 0.065. Song et al. (2012a, 2012b) also utilised a crossflow MSFB separator to beneficiate coal of (−6.0+0.5 mm) size fraction, using magnetite of (−0.074+0.045 mm) size fraction. A significant separation efficiency was achieved, with an E_p of around 0.068 to 0.095. The authors also stated that the separation efficiency decreases continuously as the particle size of the coal decreases below 0.5 mm.

2.3.2.5. Air/pneumatic table

The stratification of particles based on the difference in their density and terminal velocity is used in air table separation technology. The air table has a flat deck with uniformly distributed apertures and riffles. The filtered air enters the deck to fluidise the coal and stratifies the coal particles according to the terminal velocities of the particles. A particulate layer is formed as the lighter particles move to the top and then travel down the slope towards the discharge opening, while the heavier particles travel to the bottom in the direction of the deck’s vibration along the riffles (Zhao et al., 2014). Material in the air table moves in different directions, and separation is achieved through vertical stratification of the coal particles. Skimmers are used to remove fractions of clean coal and middling along the table's length (Kretzschmar, 2010). Figure 2.8 shows the basic working principle of the air/pneumatic table.

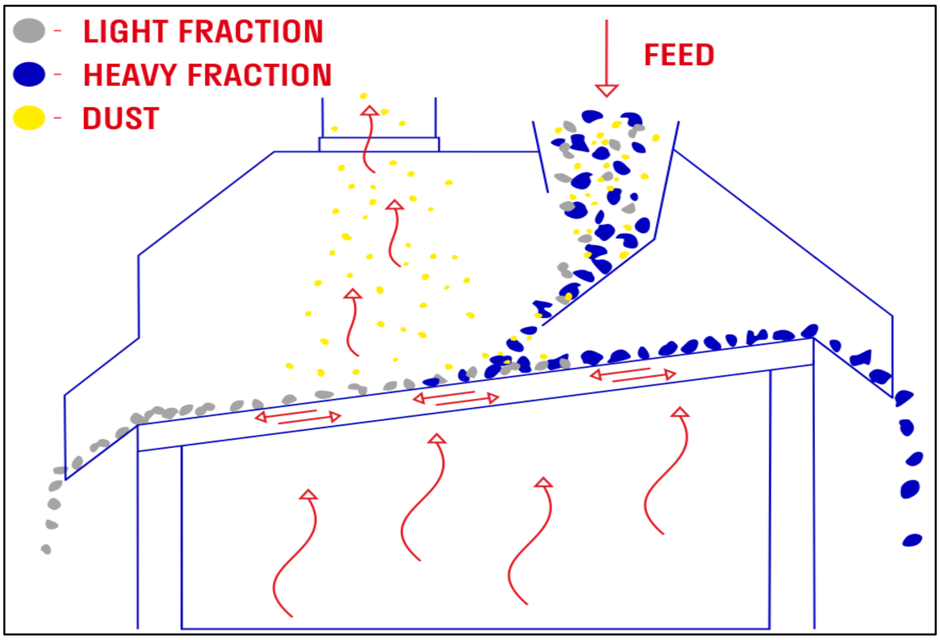

Figure 2.8: Basic air/pneumatic table. Image adapted from Rusmagnet (2022)

The technical and economic feasibility study of the air table was carried out by Çicek (2008). Two coal feed samples (A and B) of three different particle size ranges (−8.0+5.0 mm), (−5.0+3.0 mm) and (−3.0+1.0 mm) were upgraded and the results showed that the coal feed of (−3.0+1.0 mm) size fraction portrayed the best results, as the ash content of the coal feeds (A and B) were reduced from 42.36% and 29.72% to 21.82% and 17.94 %, respectively, with an E_P of 0.09 and 0.20, respectively.

A study to ascertain the effects of operating parameters, i.e., frequency of the table and the transverse and longitudinal angles, on the yields of clean coal products using statistical design experiments was carried out by Patil and Parekh (2011). Results from this investigation show that the mass yield of the clean coal was around 75% to 80%, while the ash content was reduced from 27% to 12%. According to the authors, the clean coal yield decreases as the table frequency increases; however, this increases as the transverse inclination increases.

Chalavadi and Das (2015) used an air table separator to beneficiate fine coal at (−1.0 mm) size fraction. Feed coal of 43% ash content was upgraded using the air table. Based on the separation results, it was established that a 10% (absolute) reduction in ash with a significantly high quantity of clean coal was achieved. Using the force balance approach, a set of mathematical equations was used to describe the separation of the fine coal in the air table, and it was discovered that the two key factors responsible for the separation are horizontal segregation and vertical layering. The trajectories of the particles with various particle sizes and densities on the surface of the deck were identified using simulation, which then led to the product's mass yield and ash content being computed. The authors discovered that the data computed and the observations from the experiment concurred with minimal discrepancies.

A modified air table, known as the Southern Illinois University air table, was utilised by Akbari et al. (2017) to upgrade coal of (−6.35+1.0 mm) size fraction. The separator was integrated with a novel deck and air distribution channel for fluidising fine coal particles. In this study, the efficiency of the Southern Illinois University air table for coal beneficiation was optimised, and the performance of an integrated Liwell flip-flow screen to the separator was also evaluated for 1.0 mm and 2.0 mm coal fractions. The two coal samples were from seam 6 in Illinois, and the separation results showed that coal A and B had cut-points of 1.70 and 1.89 and E_p values of 0.36 and 0.65, respectively. The product ash content of samples A and B was 13.8% and 14.5%, respectively, while the tailing ash contents were 59.7% and 52.9%, respectively. The efficiency of screening for 1.0 mm and 2.0 mm were 88.7% and 85.1%, respectively.

2.3.2.6. Air jig

The dry jig is a deep bed separator, unlike the air table; however, it works on the same principle of separating gangue from clean coal. The separator applies the difference in the particles' densities and settling velocities, which is practically equivalent to the wet jig (Zhao et al., 2014; Charan et al., 2016; Chagwedera, 2017). Although, during the beneficiation process, the clean coal and the gangue material move in the same direction, separation is achieved using a splitter (Charan et al., 2016; Chagwedera, 2017). The air supply into the jig can be achieved through two structures: a consistent air stream and a superimposed pulsated air stream that gives the driving force for stratification (Zhao et al., 2014). Stratification is achieved by first delivering constant airflow, which helps to unbind or loosen the bed, and then superimposed pulsating air is supplied to boost the stratification sufficiently (Zhao et al., 2014; Charan et al., 2016). Combining vibration with air supply boosts stratification and transportation of materials across the jigging bed (Honaker, 2007). Sampaio et al. (2008) utilised an air jig separator to beneficiate a high ash Brazilian coal from Candiota. This low-rank coal with 1.8% sulphur content and 51% ash content was upgraded using this approach. The sulphur and the raw ash content were reduced to 0.7% and 47%, respectively, with a mass yield of approximately 71%.

An air jig, which was fabricated by Allmineral with a 50 t/h capacity, was used by Charan et al. (2011) to beneficiate an Indian high-ash non-coking coal. With this separator, a clean coal product of 33% ash was produced from a feed coal of 40% ash at a particle size of (−40+5.0 mm). In another study, an Allair stratification jig was also used by Boylu et al. (2015) to upgrade a feed coal of (−13+4.0 mm) particle size fraction and 43% ash content. A clean coal of 17.4% ash and 48.8% mass yield was achieved. Another study was conducted on the Barro Branco seam in Brazil using a dry batch jig by Feil et al. (2012). The results demonstrated that effective separation was accomplished when the coal was jigged at a frequency of 88/min, with the uppermost layer having an ash level of 39.1% and the lowest layer 74.93%, contrasted with a feed coal of 54.89% ash content.

A recent study was carried out by Kumar and Venugopal (2020) using a laboratory model of the Denver air jig to upgrade coking coal of (−10+3.0 mm) size fraction. In this study, the coal particle size was split into three size fractions of (−10+6.73 mm), (−6.73+4.73 mm) and (−4.73+3.0 mm). The influence of parameters such as the size of the coal particles, the jigging time and the height of the bed were studied to understand their effects on the separator's efficiency. The separation results showed that a clean coal product of less than 17% ash content was achieved, which was the targeted ash content for coal particle size of (−5 mm) and 40 mm bed height. Figures 2.9 and 2.10 illustrate details of the working principle of the air/dry jig.

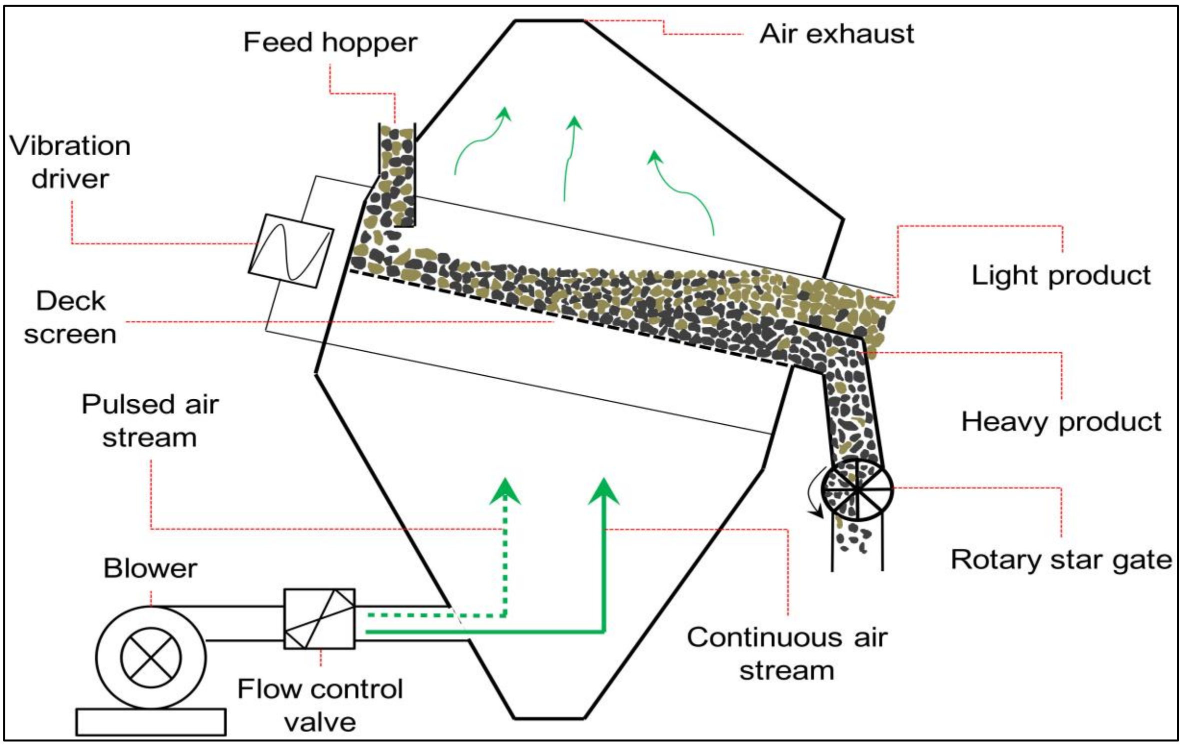

Figure 2.9: The basic working principle of an Air/dry jig. Image adapted from Ambrós (2020)

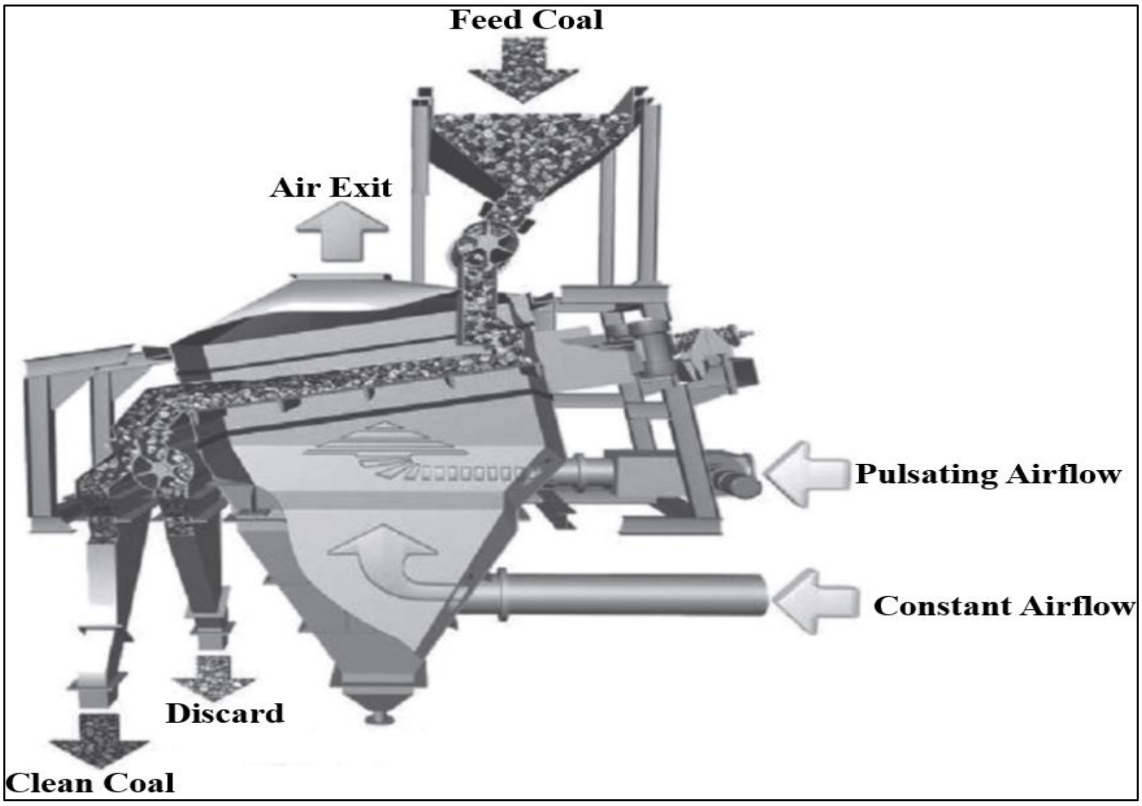

Figure 2.10: The working principle of an air jig. Image adapted from , Charan et al. (2011)

2.3.2.7. Dry magnetic separation

Dry magnetic separation is effective in beneficiating coal fines based on how responsive the coal organic (clean coal product) and its inherent minerals (mineral/gangue material) are to magnetisation. As pointed out by Zhao et al. (2014), dry magnetic separation, like the tribo-electrostatic separation technique, requires a high degree of the liberation of the feed coal to promote clean coal and mineral matter separation. Separation under a high magnetic field occurs owing to the paramagnetic and ferromagnetic properties of mineral matter and the clean coal product that is diamagnetic in nature (Zhao et al., 2014; Meshram et al., 2015). Zhou et al. (1996) carried out an investigation using the gravity-enhanced magnetic separator to separate mineral matter within the feed coal. In this study, a four Tesla (T) superconducting solenoid magnet to induce the magnetic field was needed for the separation process. From the optimal separation of the process, ash content and pyritic sulphur were reduced by 44% and 72%, respectively, while achieving a combustible recovery yield of 95%.

An exhaustive study to de-ash fine coal using the dry magnetic separator was carried out by Jiao et al. (2009). A key aim of the study was to ascertain the degree of the magnetic susceptibility and the density of the magnetic field, as well as the field's intensity of the coal organic and its mineral content. It was observed that a linear correlation exists between the magnetic field density and magnetic susceptibility. Magnetic susceptibility is the measure of the degree to which a material becomes magnetised in response to an external magnetic field. In addition, an opposite polarity in the magnetism of the low- and high-density coal was observed. The results from the separation performance of the tested coal show that the fine coal was de-ashed and de-sulphurised by 64.41% and 55.52%, respectively. Zhang et al. (2020) conducted a study on the de-sulphurisation of (−0.5 mm) coal using a high gradient magnetic separator. The feed coal was screened into three different particle sizes (−0.5+0.3 mm), (−0.3+0.15 mm) and (−0.15+0.074 mm), and the effects of the background field intensity, specific susceptibility and microwave pretreatment time were investigated for the coal-feeds. The experimental results show that 31% sulphur rejection was achieved for the (−0.15+0.074 mm) at a microwave pretreatment time of 240 seconds and a background field of 2750 tesla (T). In addition, a maximum sulphur rejection of 52% was achieved for (−0.074 mm) coal size fraction at 240 seconds microwave pretreatment time with a background field strength of 5000 tesla (T).

2.3.2.8. Fuhe Ganfa Xuanmei dry separator

The Fuhe Ganfa Xuanmei (FGX) dry separator is one of the few dry coal separators that has been utilised commercially for the beneficiation of South African coal (De Korte, 2015). The separator was initially designed by a Chinese dry coal specialist, with a few hundred separators designed and sold worldwide (Zhao et al., 2014). It utilises the separation standards of an autogenous medium and a table concentrator (Charan et al., 2016). The deck vibration frequency, feeder frequency, height of the baffle plate, longitudinal deck angle, vibration and the air stream all considerably influence the separator's efficiency (Zhao et al., 2014). The FGX separator gives a moderately effective separation at high values of separation densities between 1.8 RD to 2.2 RD. The typical E_p is about 0.25 (Charan et al., 2016). Riazi and Gupta, 2015 illustrate the principle of operation of the FGX dry separator in Figure 2.11.

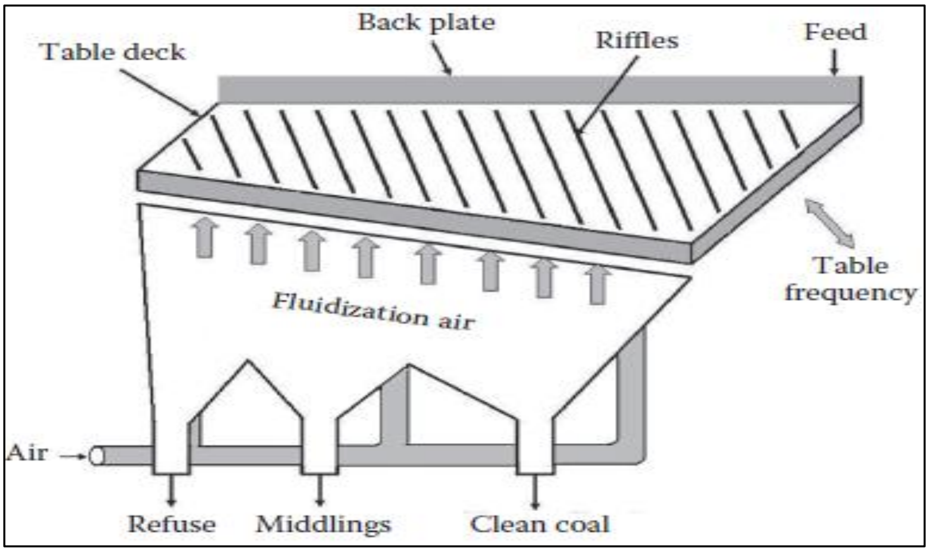

Figure 2.11: Schematic diagram of the Fuhe Ganfa Xuanmei dry separator and its processing system. Image adapted from FGX Sep. Tech, LLC, USA (Riazi and Gupta, 2015)

A 5 t/h pilot-scale FGX dry separator was utilised by Honaker et al. (2008) to produce clean coal with characteristics that meet contract requirements and improve the measure of rejecting rocks of high density before transportation and processing the coal. The results from the separation evidently demonstrate that the FGX can reject more than 70% of rocks of high density from ROM coal at high separation density estimations of around 1.8 to 2.2 g/cm^3, with an E_P value of about 0.25. Boylu et al. (2015) used an Allair stratification jig to beneficiate a feed coal of 43% ash content and (−13+4.0 mm) particle size fraction. The separation results show a clean coal with a yield of 48.8% and 17.4% ash content. The FGX dry separator was also used by Ling et al. (2018) to upgrade ROM coal from the Dafeng mine in China. In this study, the FGX-3 dry separator was used to upgrade coal of 80 mm top size. The study's results show an ash content of 48.7% in the feed reduced to 31.28% in the clean coal, with a yield of 65.12%. The authors observed that the yield for a cleaner product increased as the size distribution of coal decreased from (−80+50 mm) to (−6.0+3.0 mm). In addition, the FGX could beneficiate the (−3.0 mm) fraction effectively.

Hacifazlioglu (2018) used the FGX dry separator to carry out a beneficiation study on low-rank lignite Turkish coal. In this study, the FGX dry separator integrated with infra-red increased the net calorific value of the coal to 10.46 MJ/kg from 6.90 MJ/kg, reaching the minimum energy requirement of lignite coal for the Turkish coal market. The FGX dry separator's optimal result was achieved at operational parameters of 15 mm baffle height, 50% air rate, a longitudinal angle of (−1º) and a (5º) latitudinal angle, and 48Hz motor frequency. A clean coal product of 70.30% yield with an ash content of 35.20%, combustible recovery of

82.57% and 84.70% organic efficiency was achieved from this process. The net calorific value of the coal product from the FGX dry separator was 9.37 MJ/kg. The humidity decreased with the infra-red drying process, leading to an increased net calorific value of 10.46 MJ/kg.

2.3.2.9. Tribo-electrostatic separator

The tribo-electrostatic beneficiation process is an advanced coal cleaning process that can upgrade (−300 µm) particle size fraction feed coal (Dwari and Rao, 2009; Xin-xi et al., 2009; Zhao et al., 2014). Meshram et al. (2015) also stated that this technique can effectively beneficiate fine coal (−74 µm) size fractions. This technique utilises contrasts in the electrical conductivity characteristic of the clean coal and mineral matter in the coal feed (Bada et al., 2010a, 2010b). Three key mechanisms involved in the electrostatic separation process, as stated by Dwari and Rao (2007), are conductive induction, tribo-electrification and corona bombardment. Coal feed particles in this technique are charged as they pass through the tribo-electrostatic charger, where they become either positively or negatively charged, and the charged particles undergo a free fall as they pass through an electrostatic field in the separation chamber, attracting the mineral matter and the clean coal to opposite plates thus producing clean coal and gangue stream (Chagwedera, 2017; Zhao et al., 2014).

It is important to note that this process requires a certain amount of particle liberation in the feed material. This implies that each particle must be independent of each other to allow for separation when passing through the electrostatic field (Zhao et al., 2014). The yield of this technique is known to be low on average, but high-grade clean coal products with significantly low ash content are achievable (Soong et al., 2001; Xin-xi et al., 2009; Zhao et al., 2014). Xin-xi et al. (2009) showed the principle of this process in Figure 2.12.

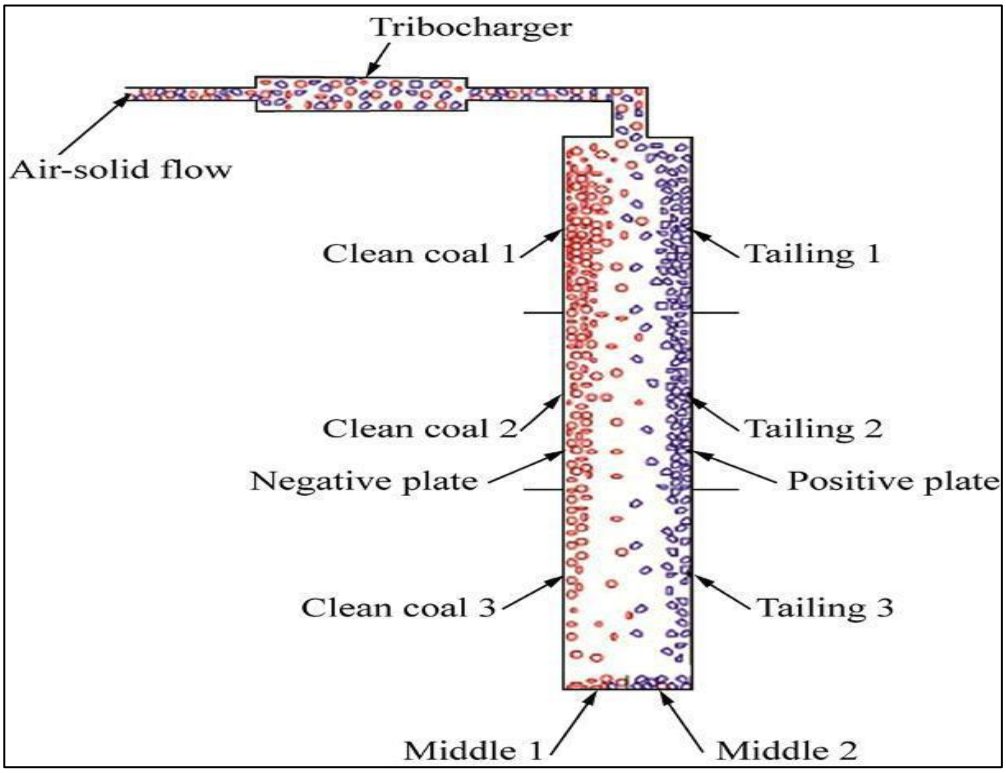

Figure 2.12: Principle tribo-electrostatic separator and sampling rule (Xin-xi et al., 2009)

In a study carried out by Soong et al. (2001) utilising the triboelectric separation technique to upgrade three coal samples from Cigel, Handlová and Nováky in Slovakia, the feed coals were screened to a particle size of (−15 µm) for the Cigel coal, (−20 µm) for the Handlová coal, and (−12 µm) for the Nováky coalThe separation process was modest, with ash contents of 51.58% in the Handlová coal feed reduced to 39% and a combustible recovery of 78%. This was further reduced to 31% ash with a corresponding 38% combustible recovery. The Cigel coal feed had 48.74% ash content reduced to 40% in the product with a 58% combustible recovery, and the ash content was reduced further to 33%, but the combustible recovery dropped to 28%. The Nováky coal feed with 28.24% ash content was reduced to 22% in the product, with a combustible recovery of 22%. Dwari and Rao (2009) also utilised a tribo-electrostatic separator to upgrade Indian thermal non-coking coal at (−300 µm). A clean coal product of 18% ash from 43% feed coal and a yield of 30% was achieved.

Xin-xi et al. (2009) conducted coal beneficiation using a tribo-electrostatic separator on a (−75 µm) particle size fraction. Results from this test show that 69.31% to 71.27% of quartz, 75.66% to 81.93% of kaolin and 86.74% to 90.52 % of pyrite in coal can be removed. Bada et al. (2010a) utilised a rotary tribo-electrostatic separator for the separation of South African coal at (−177 µm). The investigation was carried out under various process parameters, such as air injection velocity, feed rate, applied charging and separating voltage, and splitter position. The results showed that Majuba raw coal with 30% ash content was de-ashed to 14.30% and 10.82% after two stages of separation and at different separating voltages. A coal beneficiation study was conducted by Dwari et al. (2015) to upgrade high-ash Indian coking coal. In this study, the electrical and chemical properties of the carbon, kaolinite and quartz constituents of the coal sample were investigated. The tribo-charging medium used was copper, and the separator's design parameters, such as the plate angle and gap, were studied to determine the separator's optimal performance. It was observed that the carbon, kaolinite and quartz acquired different amounts of absolute charge, and as the tribo-charging time increased, the magnitude of charge also increased. Separation results from this research show that at an angle of 5º plane inclination, the feed coal of 53% ash content was upgraded to 33% ash, with a feasibility of attaining 10% ash content with a yield of 61%. Table 2.1 compares the EPM/E_p values of a few wet and dry coal beneficiation techniques.

Table 2.1: Comparison between fine coal (−6.0 mm) beneficiation techniques for wet and dry processing

Separation Technique	**Ecart Probable Moyen/Probable Error of Seperation**
Dense-Medium Cyclones (Wet Beneficiation)	~0.08 – 0.150 (Ma et al., 2018)
Wet Jigging (Wet Beneficiation)	~0.04 – 0.18 (Paul and Bhattacharya, 2018)
Reflux Classifier (Wet Beneficiation)	~ 0.07 – 0.10 (Iveson et al., 2019; Kopparthi et al., 2019)
Froth Flotation (Wet Beneficiation)	~ 0.125 (Horsfall et al., 1986)
Air-Dense Medium Fluidised Bed (Dry Beneficiation)	~ 0.05 – 0.12 (Zhenfu and Qingru, 2001; Sahu et al., 2009)
Air Jig (Dry Beneficiation)	~ 0.16 – 0.27 (Boylu et al., 2015)
Fuhe Ganfa Xuanmei (Dry beneficiation)	~ 0.25 (Charan et al., 2016)
Air Table (Dry Beneficiation)	~ 0.18 – 0.65 (Akbari et al., 2017)

2.4. INNOVATIVE BENEFICIATION CONCEPTS

This section discusses some of the unorthodox (innovative) techniques for dry coal beneficiation, and one such technique is the planar air jet used by Yang et al. (2018) to upgrade coal of (−6.0+2.0 mm) size fraction. This separation technique uses the difference in the densities of the coal particles when travelling through the planar air jet flow field in a horizontal direction to separate coal particles. The result obtained shows a clean coal yield of 56.75% with an ash content of 16.61% from feed coal of 26.92%. Figure 2.13 illustrates an overview of the planar air jet principle.

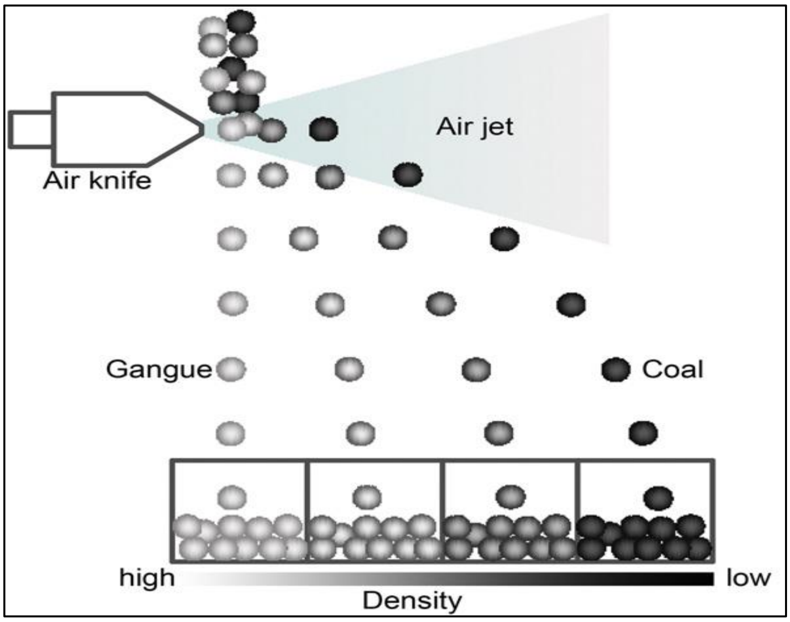

Figure 2.13: The planar air jet’s working principle (Yang et al., 2018)

Another novel technique was also applied by Dong et al. (2019) on coal of two particle size fractions (−100+50 mm) and (−50 mm). The innovative approach for this study entailed a combination of two separators: an ADMFB and an FGX dry separator connected in series. The fluidisation characteristics were studied for the AMDFB and FGX dry separators, and the process of coal transportation and the extent of de-ashing under different vibration parameters (i.e., the vibration amplitude and vibration frequency) were investigated. The result from the study showed that optimum separation efficiency for the ADMFB was attained at an air velocity of 0.11 m/sec, yielding a 90.96% clean coal product with a 7.86% ash content. The separation efficiency for the FGX was optimal at a vibration frequency and amplitude of 18 Hz and 2.2 mm, respectively, with a yield of 90.30% and a 13.28% ash content.

In a recent study by Dong et al. (2022), a novel dry coal beneficiation approach combining the ADMFB and the FGX to upgrade Chinese coal was investigated. In this study, an ADMFB in tandem with an FGX separator were arranged in series to upgrade low ash coal of (−100 mm) particle size fraction with 14.86% ash content. The raw coal was sized into two size fractions of (−100+50 mm) and (−50 mm); the former size fraction was upgraded using the ADMFB, while the latter was beneficiated with the FGX separator. For the ADMFB, fluidisation characteristics were investigated, and results showed that at a gas velocity of 0.11 m/sec, a clean coal product of 90.96% and ash content of 7.86% was achieved. For the FGX, results show that a clean coal product of 90.30% cumulative yield and 13.28% ash content was achieved at operating parameters of 18 Hz frequency and a vibration amplitude of 2.2 mm.

2.5. THE SOUTH AFRICAN COAL MARKET

As of 2021, South Africa produces an average of 224 million tons of coal annually (ESKOM, 2021), meeting around 70% of the installed power generation capacity (IEA South-Africa, 2023). The largest coal deposits in South Africa are found in the Ecca deposits, which are part of the Karoo supergroup and cover around two-thirds of the country. These deposits contain more than a third of the coal reserves in the entire Gondwanan region (Cairncross, 2001; Mining Africa, 2022). Present coal reserves are deemed to sustain the nation's coal consumption for over a century, assuming production rates remain the same (Minerals Council South Africa, 2023).

The interest in coal mining began to shift many years ago to the Waterberg and other coal fields in the Limpopo province, owing to the collieries in Emalahleni coalfields gradually approaching their useful life (Minerals Council South Africa, 2023). The Grootegeluk Coal Mine in the Limpopo province is presently the country's largest colliery, producing an estimated 32.46 million tons of coal in the year 2022 (Mining Technology, 2023a). Figure 2.14 from Hancox and Götz (2014) shows nineteen generally accepted coalfields in the nation.

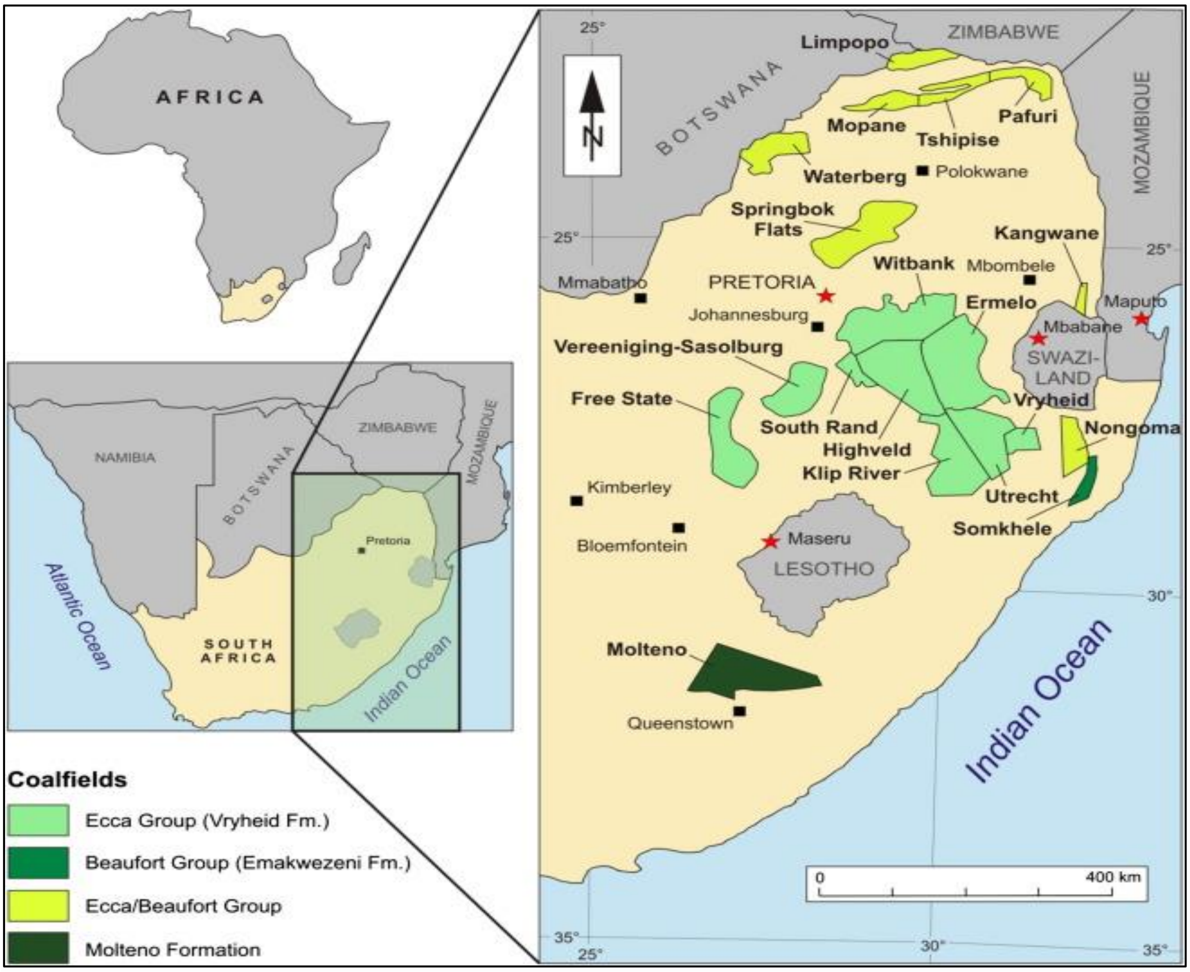

Figure 2.14: South African coalfields (Hancox and Götz, 2014)

In the year 2022, coal remained the dominant fuel for power generation, with a stable share of around 35.4%, marginally down from 35.8% in the previous year (BP, 2022). From 1990 to 2017 in South Africa, energy production increased by 37.39% from 115 to 158 million tons of oil equivalent (IEA, 2023). The total primary energy supply increased by 46.67% from 90 million tons of oil equivalent, and electrical final consumption increased by 45.51% from 156 TWh to 227 TWh, which caused a 72.95% increase in carbon dioxide emissions from 244 to 422 million tons (IEA, 2023). As the Minerals Council South Africa (2023) points out:

I. The coal industry employed 92 230 individuals in 2019, making 19% of the total employment in the mining industry. Likewise, in 2018, it employed 86 647 people and 82 248 in 2017. In 2022, the coal industry employed nearly 91 000 people (90 977), who together earned R31.7 billion.

II. About 231.2 million tons of coal was produced in 2022, and total sales for that year were R252.3 billion. For the year 2019, 258.9 million tons of coal were produced with a total sale of R139.3 billion; in 2018, 253 million tons were produced with a total sale of R146 billion.

III. About 70% of coal produced is consumed locally, with more than 70% meeting the electricity demand.

In 2022, South Africa was the seventh-largest coal producer globally, with a 12% output increase compared to 2021. Five years prior to 2021, production from South Africa reduced by a compound annual growth rate (CAGR) of 3.05% and is expected to rise by a CAGR of 0.74% between 2022 and 2026. South Africa accounts for 3.0% of global coal production, with the largest producers being China, India, Indonesia and Australia. Exports of coal from South Africa increased by 11% in 2022 compared to the previous year, with the highest share being exported to India. South Africa's coal exports are expected to grow at a CAGR of 0.67% between 2022 and 2026 (Mining Technology, 2023b). South Africa currently ranks 7th largest coal producer (Global Fire Power, 2023a) and 6th largest consumer globally (Global Fire Power, 2023b).

2.6. WIND-SIFTER

The concept of particle sorting is essentially a method of separating mineral particle mixtures into two or more particles based on the continuous decline in the velocity with which the travelling particles fall through a fluid medium (Wills and Napier-Munn, 2006). This concept is well-used in several industries, including agriculture, food processing and, particularly, mineral processing. Particle classification is made possible by the particles' physical properties, such as their shape, size and density. Solid particles falling freely in a vacuum are subject to constant acceleration as their velocity increases indefinitely, regardless of size and density. However, in air or water, there is resistance to this movement because of viscosity. Resistance increases with velocity, and when equilibrium is attained between the gravitational and fluid resistance forces, the particles come to rest as they attain what is known as terminal or settling velocity (Wills and Napier-Munn, 2006; Alade et al., 2021). Particle separation is possible when these solid particles reach their respective settling velocities due to different sizes and densities.

There are two types of particle classification based on the fluid used: the wet classification and the dry classification. The wet classification entails using hydraulic fluid (liquids) like water for particle separation. While this classification provides excellent separation efficiency, some drawbacks, including negative environmental impacts and high operational capital costs, have made dry classification a viable alternative (Chagwedera, 2017; Alade et al., 2021; Kaas et al., 2022). The primary purpose of classification is to separate coarse particles from fine particles in a particle mix. With dry classification, the processing of particles in various sizes ranging from fine powder to pellets, flakes and even two-dimensional materials such as paper and aluminium foil are achievable (Shapiro and Galperin, 2005; Kuyumcu and Rosenkranz, 2009). The separation of particles without using water as a sorting medium has been implemented for decades, with many new inventions and techniques now in the literature. Some of these techniques involve ballistic air separators, winnowing separators and wind-sifting separators, among others (Bao et al., 2009; Jang et al., 2014; Luijsterburg and Goosens, 2014; Mielke, 2018;; Roloff et al., 2019; Cappelli et al., 2020; Netsch et al., 2022).

In the case of wind-sifting, this technique sometimes involves using sieves for the classification of particles and without sieves, as seen with the Zigzag wind-sifter, which uses air primarily for particle sorting (Stebbins, 1932). The wind-sifting separation techniques have been used in various applications and in the diverse recycling of materials, like electronic waste (e-Wastes), municipal solid wastes, food, furniture, pharmaceuticals, minerals, chemicals and metallurgical, and, recently, in the field of coal processing (Goran, 1951; Heinrich 1962; Rumpf and Leschonski, 1979; Ericsson, 1991; Nishinari et al., 1992;Gornet et al., 2002; Krauß et al., 2002; Kimmeyer and Schnartz, 2003; Eichert et al., 2008; Redemann et al., 2008; Pehlken and Müller, 2009; Giani et al., 2014; Krüger et al., 2014; Pettinari and Simone, 2015; Adamčík et al., 2017; De la Fuente et al., 2018; Evangelopous et al., 2018; Roloff et al., 2019; Alade et al., 2021). In a study conducted by Redemann et al. (2008), the technology was used in managing ash production in the circulating fluidised bed combustors during the co-firing of refuse-derived fuel and coal. In addition, it was employed in monitoring the transportation of a mixture of fuel and limestone from a hammer mill into the combustion chamber. The same technique was also used by Krüger et al. (2014) to separate toxic substances from the waste stream to obtain a higher quality refuse-derived fuel.

A study on Material Advanced Recovery Sustainable Systems conducted by Giani et al. (2014) and funded by the European Union, referred to as the Life Plus Program, also employed the wind-sifter in the sorting of waste streams. The research included a combination of mechanical and biological treatments of municipal solid waste to generate biomass fuel to feed the biomass plant. The municipal solid waste was subjected to a thorough waste characterisation programme. The wind-sifter was utilised to partition the heavy inert portion from the lighter desired fuel to obtain the required particle size distribution. The results showed that the biodegradable portions were in the fraction (−40 mm) particle size, whereas the fraction (−10 mm) had about 45% of the stream's energy content (calorific value). The study recommended that screening municipal solid wastes to (−11.5+4.0 mm) size fraction will boost the heating value of the stream to 13.3 MJ/kg. Hagemeier et al. (2014) used computational fluid dynamic simulations and discrete particle modelling in a coupled manner to numerically investigate the separation efficiency of a pilot-scale zigzag wind-sifter separator. The influence of process parameters such as air flow velocity and particle size was investigated under various turbulence models. The results showed that process performance varied with changes in process parameters. The authors also observed that the residence time for finer particles was much longer than for coarser particles because finer particles are more easily influenced by the slight change in air velocity than the coarser particles, making them easily affected by the vortices, thus increasing their residence time.

In a study conducted by Lotfi et al. (2015), the author applied a combination of SMART demolition technologies coupled with innovative techniques to produce high-grade recycled aggregates with very low pollutants. The sifting technology combined with near-infrared was used by the author to sort plastic and wood fragments, with the (−16+4.0 mm) particle size fraction achieved within the stipulated European Union standard. Overall, the study shows that the combination of wind-sifter and near-infrared sorting proved very valuable when compared with using the near-infrared sensor sorting system alone. Mann et al. (2017) conducted a study using the zigzag wind-sifter to investigate the processing of agricultural raw materials, minerals and their products using gravel and sand as models for the feed of non-homogenous sized particles. The influence of airflow velocity and feed rate on particle properties such as size, shape and density was investigated. A SMART (Spatial Monitoring and Reporting Tool) analysis was conducted to identify optimal process parameters, like the appropriate feed rate and airflow velocity, as well as cut size. A study by Adamčík et al. (2017) utilised the wind-sifter in a rotor air classifier for the classification of particulate material into fine and coarse particles. Operating parameters such as the inlet air velocity, feed rate of the particulate material, the speed of the rotor and their influence on turbulent flow field patterns within the air classifier were investigated. The wind-sifter unit was installed together with a centrifugal fan (for air recirculation) and was used for the separation and transportation of particles.

The recovery of useful metals from the automotive shredder residue was carried out by Evangelopoulos et al. (2018) using the wind-sifter technique. The automobile shredder residue is the remaining fraction, which are the lighter particles of municipal metallic vehicle waste. In another investigation carried out by Roloff et al. (2019), a multi-camera shadow imaging system was installed in a wind-sifter separator to capture the dynamics of the particles in the separator. The fabricated wind-sifter separator was used to separate glass beads of 1.0 mm to 4.0 mm at different particle loads (mass flowrates) and air velocities. The results revealed that the particle air velocity has more influence on the separation efficiency of the separator than the particle loading for the classification of the particles. Reddy et al. (2021) used the zigzag wind-sifter separator to separate food particles such as milk, spices, starch, sugar, salt, flour and grain. The wind-sifting principle was used to circumvent the challenges, as well as high capital and operational expenditures, that would have been encountered with the conventional approach of using sieves for separation. Reddy et al. (2021) also noted that it was easier to maintain the zigzag separator due to its wear-resistance and not sensitive to changes in the composition of the feed material.

The most recent wind-sifter separator was fabricated by Alade et al. (2021). The separator was used by the author to upgrade ROM coal from the Witbank coalfield, South Africa. The separator was effective in upgrading a feed coal of 30.28% ash content and 21 MJ/kg calorific value to a clean coal of 18.94% ash content with a calorific value of 26.8 MJ/kg. This was the first time that this technology was applied in the field of dry coal beneficiation and served as a prototype with an optimised version in view.

Although various configurations of wind-sifter separators exist, the three major types of wind-sifters are zigzag sifters, rotary/drum/centrifugal sifters and air-wheel sifters. This section reviews these types of wind-sifter separators, including their design features, modes of operation, their respective components, and the feasibility of the technique in the mineral processing field of various minerals other than coal. This section also looks at some recent innovative approaches to using the wind-sifting principle for particle separation.

2.6.1. THE ZIGZAG WIND-SIFTER

2.6.1.1. General design features and mode of operation

The zigzag wind-sifter consists of cascading connected vertical channels. The channels alternatively slant left and right and facilitate the separation of a solid dispersed particle phase into its light-fine and heavy-coarse fractions (Roloff et al., 2019). The zigzag sifter is the most common type of sifting separation technique used for various applications, such as waste processing and recycling, agriculture, furniture, mineral processing, etc. The main component of this kind of wind-sifter is its zigzag section, from which its name is derived. Figure 2.15 provides a general representation of the segmented section in question.

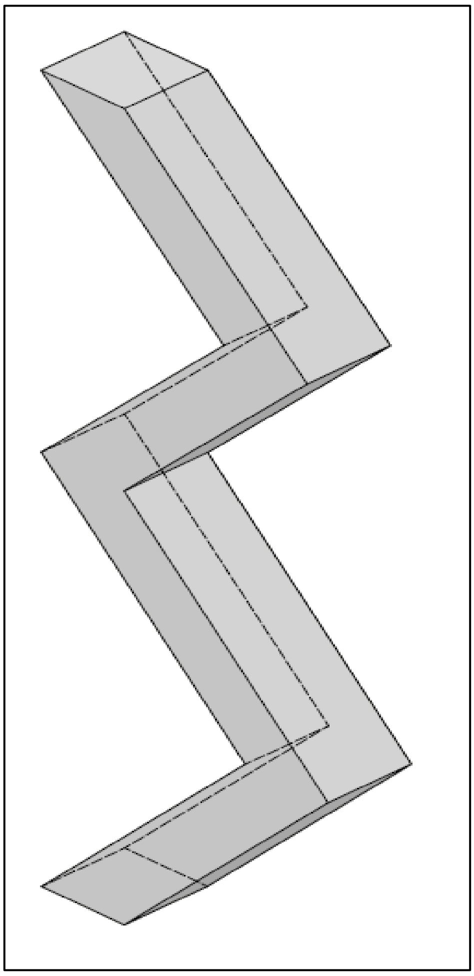

Figure 2.15: General design of the zigzag section (Alade and Bada, 2023).

Kaas et al. (2022) provided an elucidating review of the zigzag wind-sifter, outlining the design parameters of the zigzag section, some of which include stages and step angles. Each stage is the amount of the segmented zigzag cross-sections, while the step angle of the section in each stage is shown in Figure 2.16. The separator design can vary based on manufacturer's design, like Impact Air Systems, etc., for their respective applications. In the Kaas et al. (2022) design, the step angle for each stage was 120 degrees to ensure an adequate amount of kinetic energy in the sifting and transportation of the lighter particles.

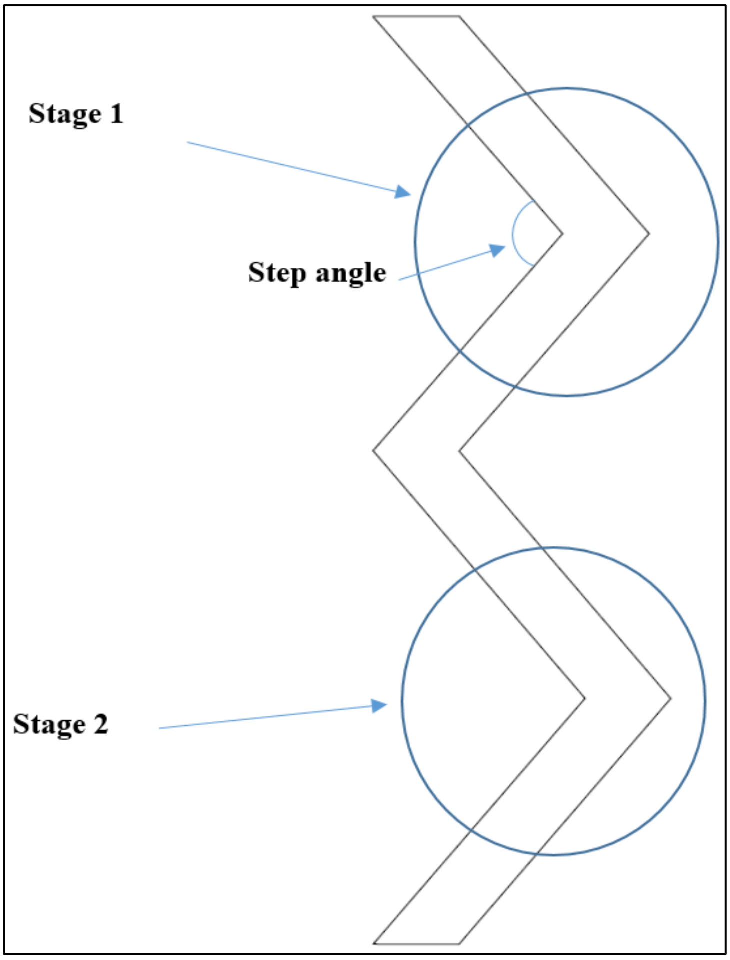

Figure 2.16: Side view of the zigzag wind-sifter. Image adapted from Kaas et al. (2022).

2.6.1.2. Operational principle

Figure 2.17 shows the basic function of a zigzag wind-sifter separator. Air is supplied by a mechanical draft (forced draft), usually with the aid of a blower from the bottom of the zigzag section of the separator. The feed material to be separated is fed directly from the top of the zigzag separator, usually with the aid of a rotary valve, as indicated in Figure 2.18. This is then distributed over the complete sifter channel's cross-section. In the zigzag section, the feed materials bounce through this section as they cascade down the stage(s), with the heavier particles bouncing more than the lighter particles. This is due to the incoming air supply sifts, leading to the lighter particles being transported further while the heavier particles fall into their designated collection zone.

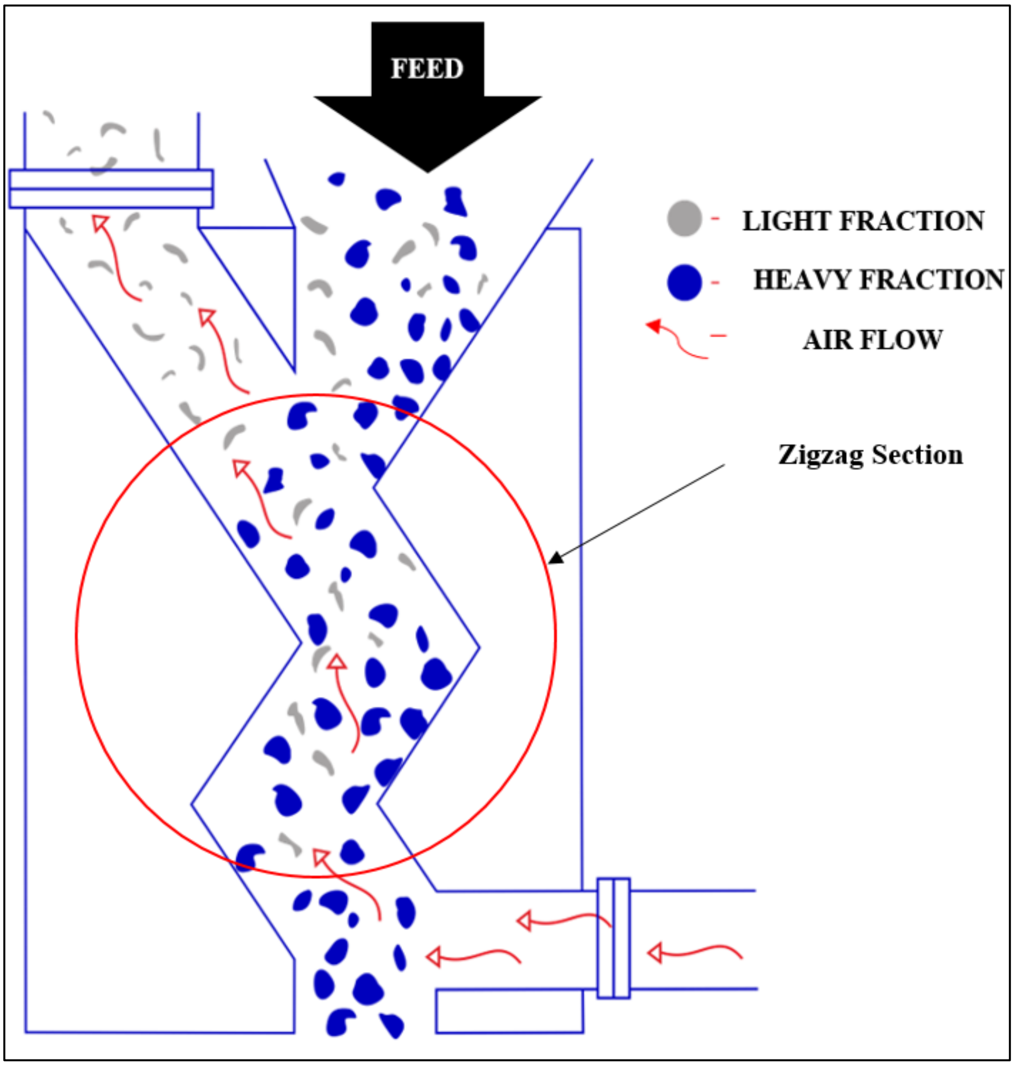

Figure 2.17: Working principle of the zigzag separator. Image adapted from ERGA Global zigzag separator (2022)

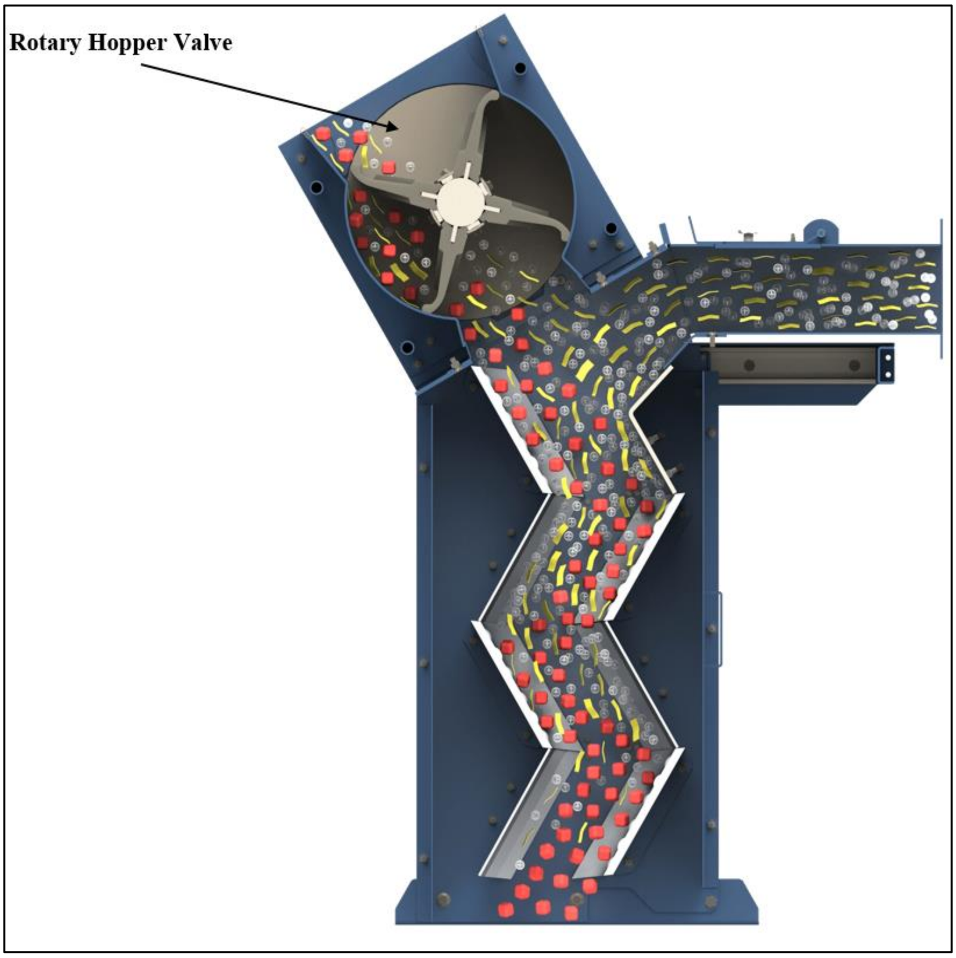

Figure 2.18: Image showing the rotary hopper valve. Image adapted from Impact Air Systems (2021)

Generally, the zigzag sifter separator is used alongside other equipment rather than as a standalone unit. Although the separator classifies lighter particles from heavier ones, it does not ensure the lighter particles attain their settling velocities. This type of wind-sifter engages both the counter-current and co-current modes of particle separation. The counter-current separation occurs when the incoming air meets with the incoming feed, while for the co-current separation, the lighter particles are transported to their settling zones. Major companies like Trennso Technik and Impact Air Systems, etc., usually combine their zigzag separators with a gas cyclone equipment to ensure adequate classification. Some researchers have combined the zigzag separator with other separators, like the ballistic air separator, depending on the nature of the application, like municipal solid wastes and e-waste treatment (Trennso Technik, 2018; Impact Air Systems, 2021). Figure 2.19 shows a typical zigzag sifter and gas cyclone assembly.

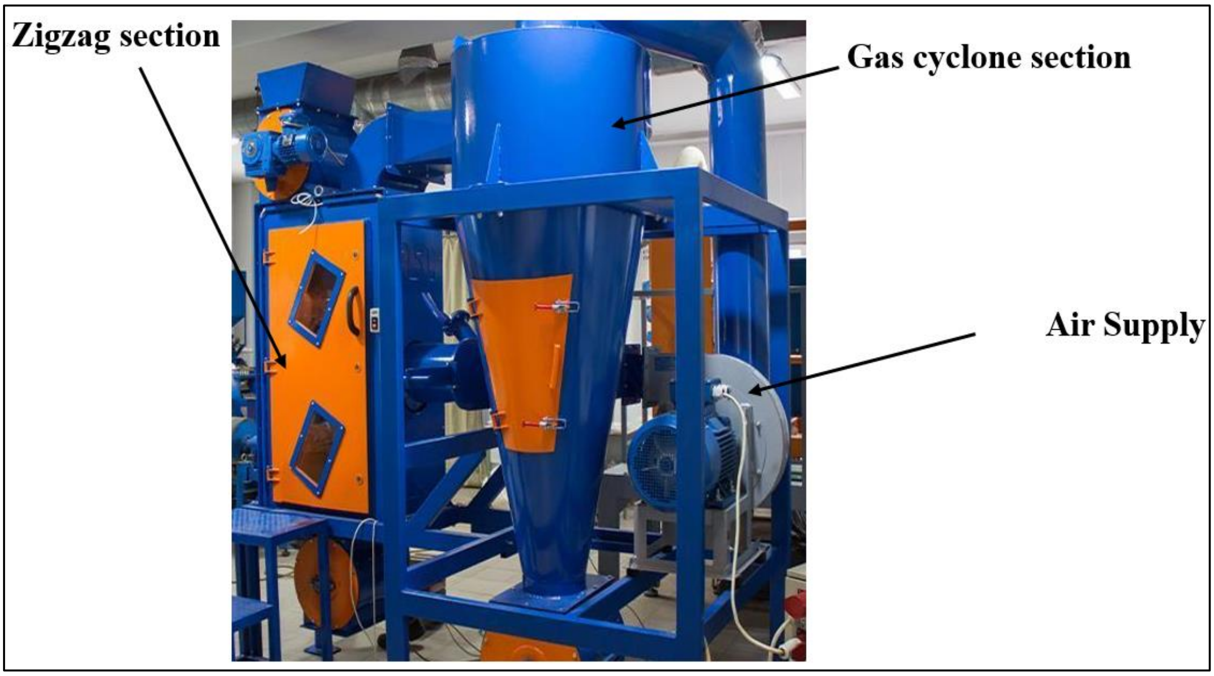

Figure 2.19: A zigzag separator with a gas cyclone. Image from ERGA Global Zigzag Separators (2022)

The research conducted by Alade (2021) for dry coal beneficiation entailed using the zigzag separator in tandem with a diffuser separation chamber. The diffuser chamber ensures clean coal products are separated based on their relative densities (the cleaner the coal, the further the particles travel to their settling points). The labelled schematic of the separator designed by Alade (2021) is provided in Figure 2.20, demonstrating that the zigzag separator is very flexible. The particles are separated based on their sizes and densities by varying process parameters, such as particle loading (feed rate), size disbributions of the particles fed, and air flowrate into the separator (Blanke 2015; Walton et al., 2015; Alade, 2021; Alade et al., 2021; Kaas et al., 2022).

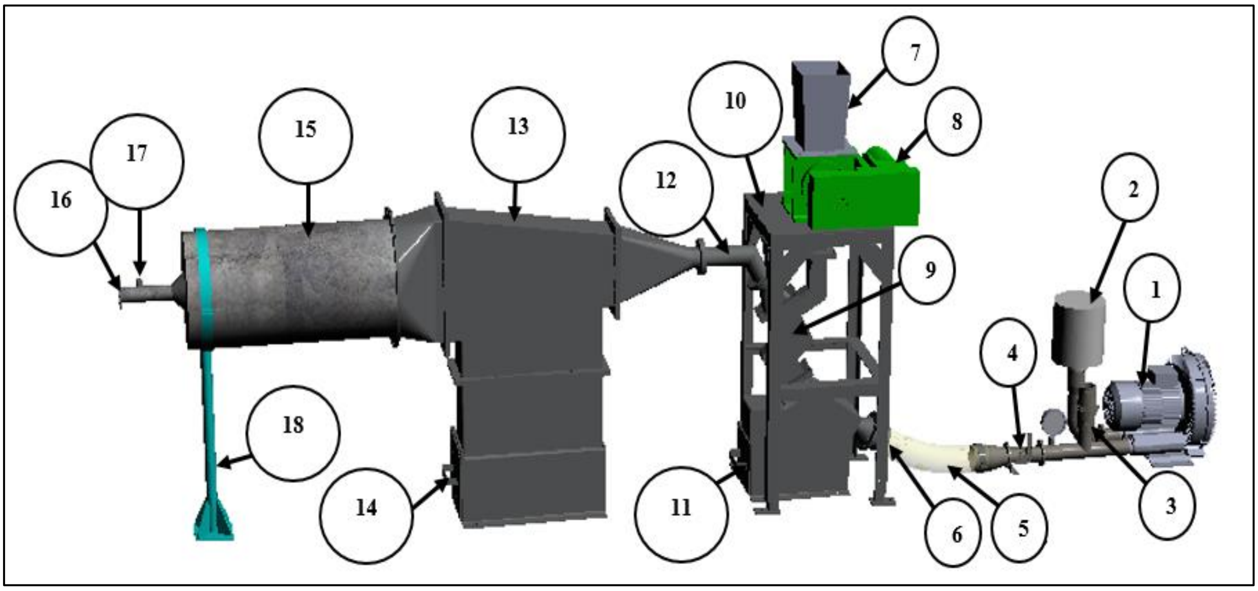

Figure 2.20: Designed zigzag separator for dry coal beneficiation by Alade et al. (2021)

1- Air blower

2- Air filter

3- Safety relief valve

4- Throttle damper

5- 100 mm diameter flex

6- Air-inlet into the first chamber

7- Rotary airlock valve for the coal feed

8- The variable frequency drive motor drive for the rotary hopper valve

9- The first chamber (the wind-sifter) with the zigzag section

10- Support frame for the wind-sifter

11- Coal bin for the first chamber

12- Exit of the clean coal from the first chamber into the second chamber

13- Second chamber (diffuser chamber) to collect the clean coal

14- Coal bin for the second chamber

15- Filter section (with filter cartridge) to prevent coal dust from escaping to the environment

16- Air exit from the separator

17- Velocity measuring port

18- Support stand for the filter compartment

2.6.2. THE ROTARY/DRUM/CENTRIFUGAL WIND-SIFTERS

2.6.2.1. General design features and mode of operation

The rotary centrifugal sifter, which is not as common as the zigzag sifter, works primarily on the principle of applying centrifugal force to the feed particles. Major components of this sifter (Figure 2.21) include a feed inlet, a cylindrical mesh or screen, rotating paddles, a cantilever shaft driven by an electric motor and a screw conveyor, which is a screw wound around the shaft in a helix form, also called an auger.

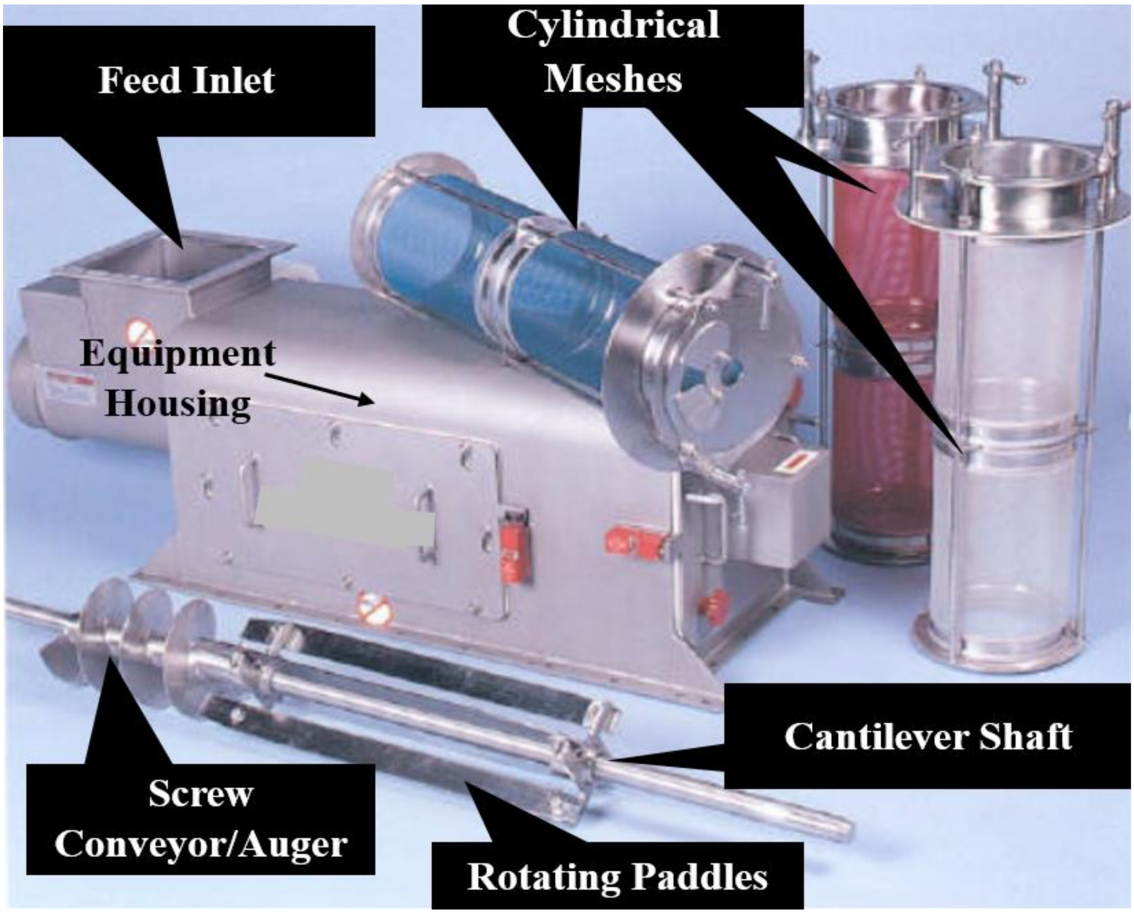

Figure 2.21: Major components of a centrifugal sifter. Image courtesy of Gericke (2022)

2.6.2.2. Operational principle

In operation, the feed material to be separated is fed through the feed inlet, which is at the upper section of the housing and the rotating paddles (also known as rotating scrapers). The paddles transport the feed material into the mesh section of the centrifugal sifter through centrifugal force and cyclone propelling action (Walton et al., 2015). Figure 2.22 illustrates the flow path of the feed material through the separator.

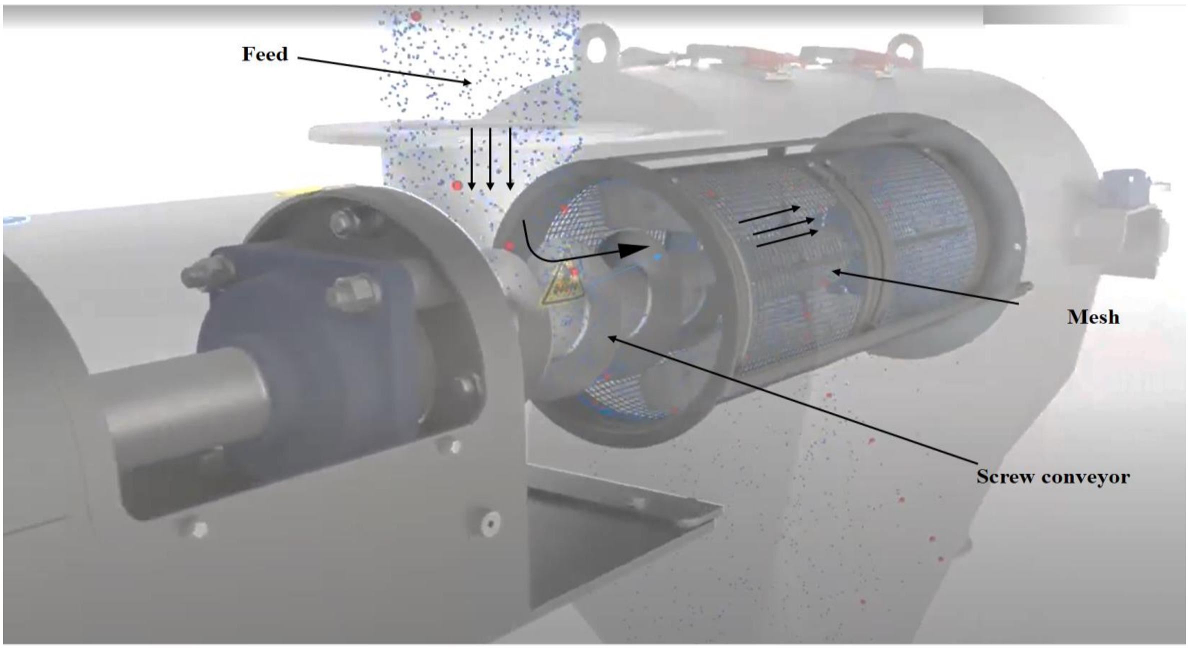

Figure 2.22: Side view of a centrifugal sifter. Image adapted from Kemutec (2022)

The finer particles pass through the cylindrical mesh while the coarser particles, which cannot pass through the mesh, continue moving forward as they are transported by the rotating paddles. Figure 2.23 displays the respective outlets for the fine and coarse particles in a typical centrifugal sifter, while Figure 2.24 shows the centrifugal sifter when closed. It is important to note that the air in this wind-sifter is generated by the rotating action of the paddles that are coupled to the cantilever shaft and not an external air supply. This contrasts with the zigzag wind-sifter, which mainly uses a co-current airflow. Also, this sifting classifies particles mainly on size as opposed to the zigzag sifter, which classifies on size, shape and density.

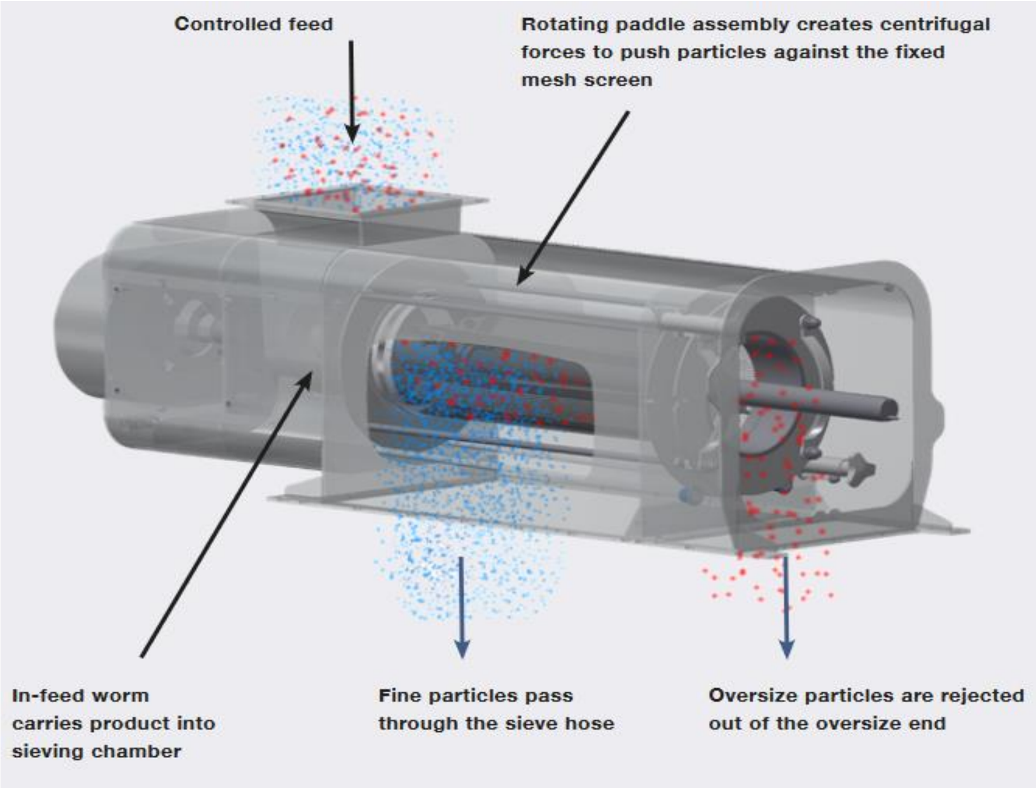

Figure 2.23: Side view of a centrifugal sifter. Image adapted from Gericke (2022)

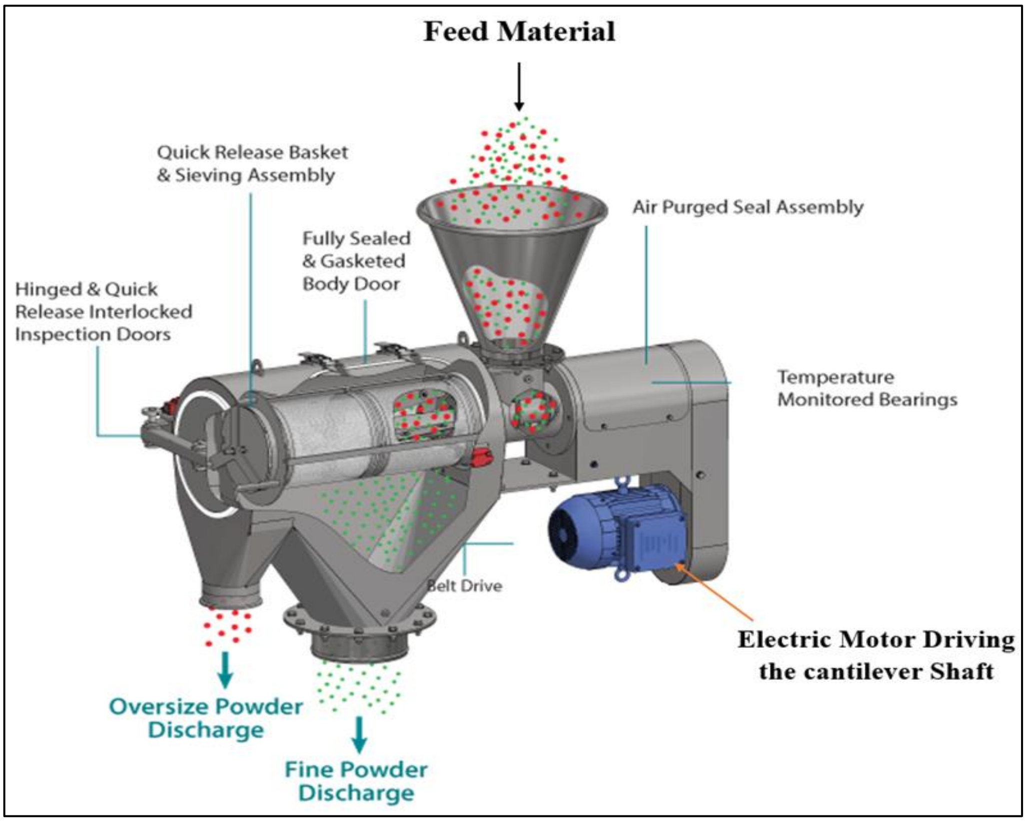

Figure 2.24: Closed centrifugal sifter. Image adapted from Kemutec (2022)

The flexibility of this sifting process depends on the ability to change the cylindrical mesh to different aperture sizes to obtain a product of different qualities. Figure 2.25 shows different cylindrical meshes of various aperture sizes.

Figure 2.25: Mesh of different apertures. Image adapted from Gericke (2022)

2.6.3. THE 3-FRACTION WIND-SIFTER

The 3-fraction wind-sifter is compared to the zigzag wind-sifter, a recent technique of wind-sifting. In this technique, an air-wheel is used to partition the air, which is transporting the particles to heavy, medium and light fractions at the operator’s discretion.

2.6.3.1. General design features and mode of operation

The 3-fraction wind-sifter is a relatively new approach wind-sifter, which works primarily on the principle of applying centrifugal force to the feed particles. Major components of this sifter include the air-inlet section separation chamber doors and hand rails (Figure 2.26), and the feeder for the raw materials, as well as an air-wheel (Figure 2.27).

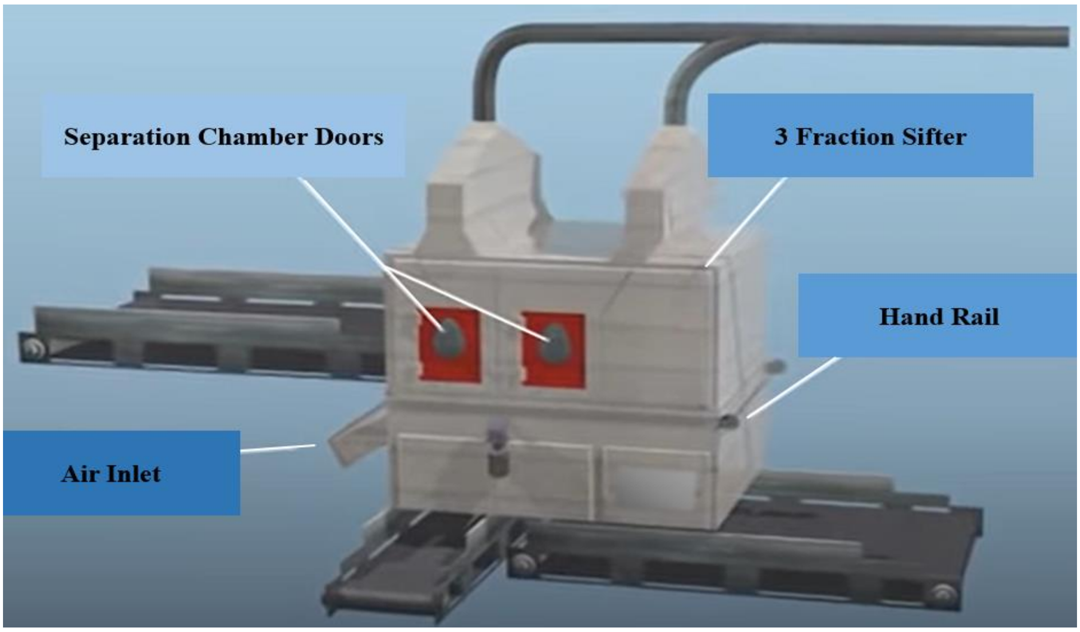

Figure 2.26: The 3-fraction sifter. Image adapted from Schulz & Berger (2014a)

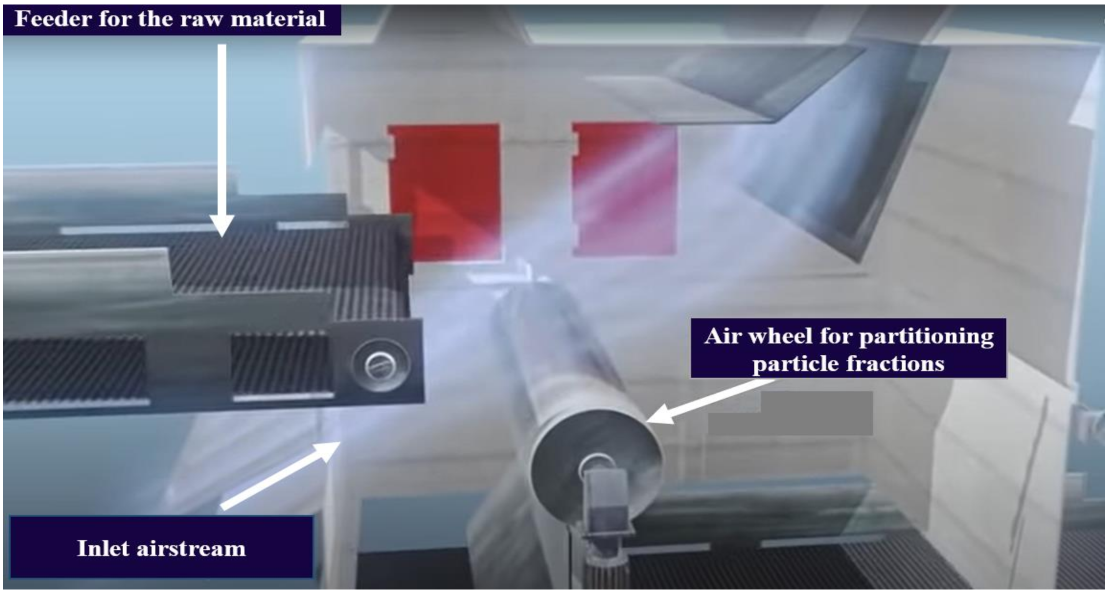

Figure 2.27: Image showing inlet air and air-wheel. Image adapted from Schulz & Berger (2014a)

2.6.3.2. Operational principle

In operation, the raw material undergoing the separation process is fed by means of a feeder, usually a conveyor belt with an adjustable feed rate, into the already flowing airstream, as shown in Figure 2.28. The heavy fractions fall into their designated discharge tray or belt, the middle fraction flows into its designated discharge, while the light particles are sucked upwards out of the separation chamber into their designated collection point (Figure 2.29).

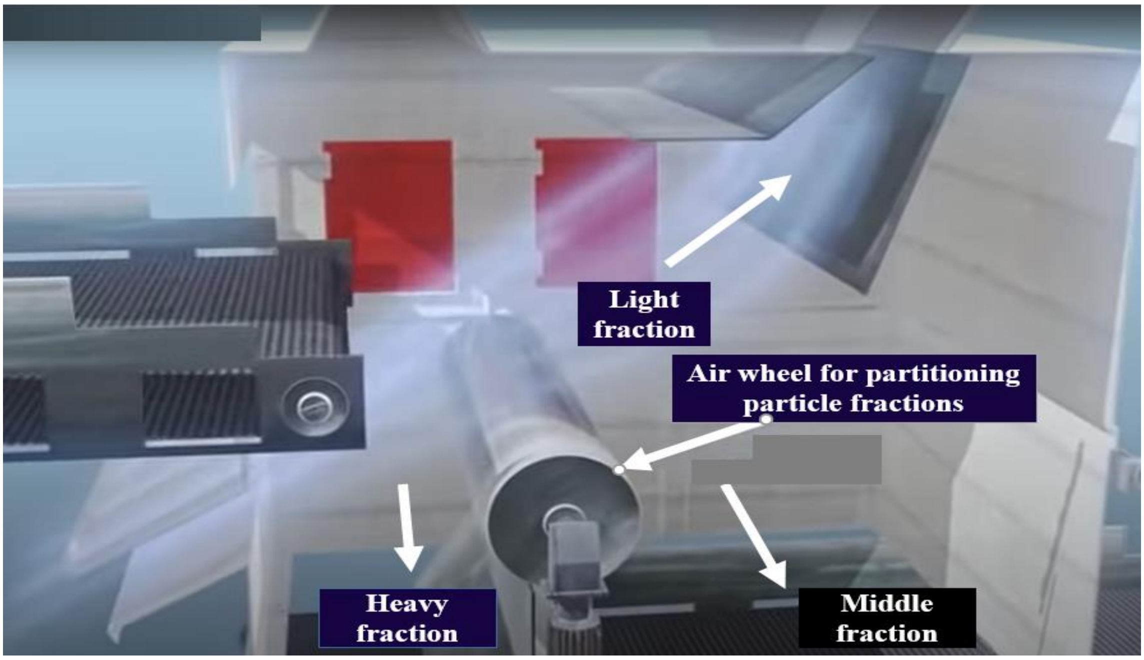

Figure 2.28: Image showing fractions locations after classification. Image adapted from Schulz & Berger (2014a)

The major function of the air-wheel is to partition the airstream carrying the particles into their respective sections. The air-wheel is driven by the airstream, reducing the airstream's kinetic energy so that the particles being transported attain their terminal velocities. The three fractions from the separation process are portrayed in Figure 2.29.

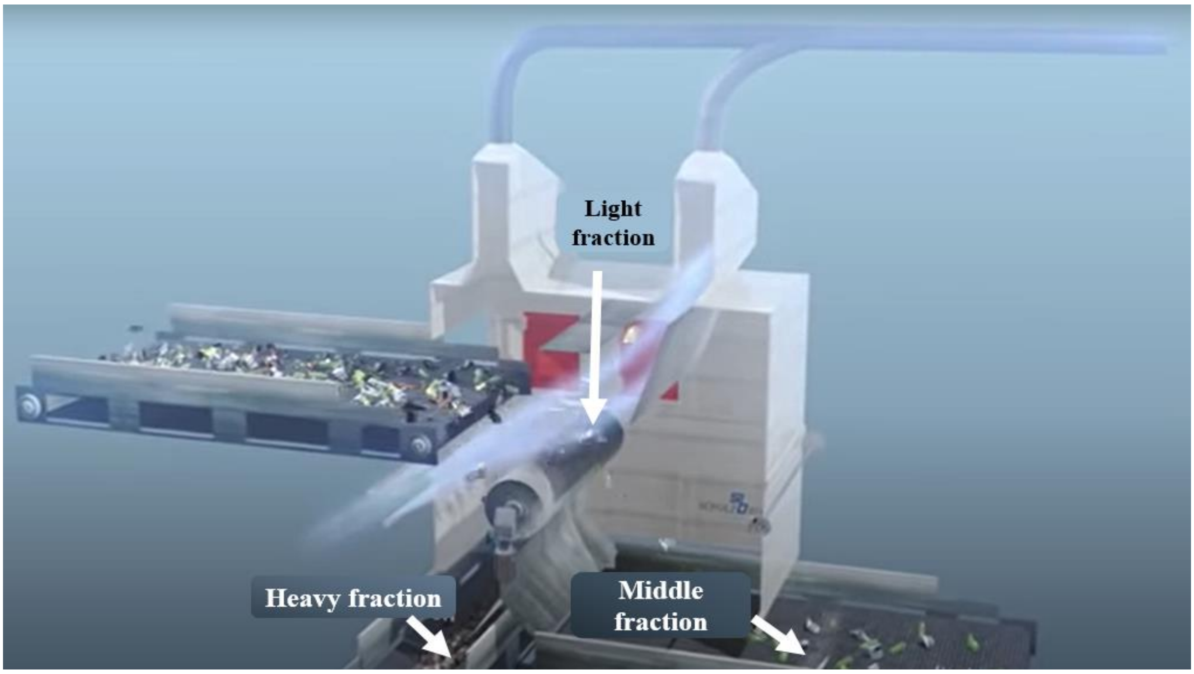

Figure 2.29: Image showing fractions after classification. Image adapted from Schulz & Berger (2014a)

This type of wind-sifting separator, like the other two, can be a standalone unit or can be used in tandem with a dust extraction chamber or with a cyclone, as seen in Figures 2.30 and 2.31. These enable the separator unit to deal effectively with the lighter fractions of the separated particles, and the separation operation is usually a closed circuit, as seen in both figures. Figure 2.30 shows the 3-fraction wind-sifter separator connected in tandem to a light-fraction separator and then to a filter chamber dust container. The light-fraction separator separates the light fractions into fine and super-fine particles, which may be entrained in the airstream, while Figure 2.31 shows the 3-fraction separator connected to a gas cyclone for processing.

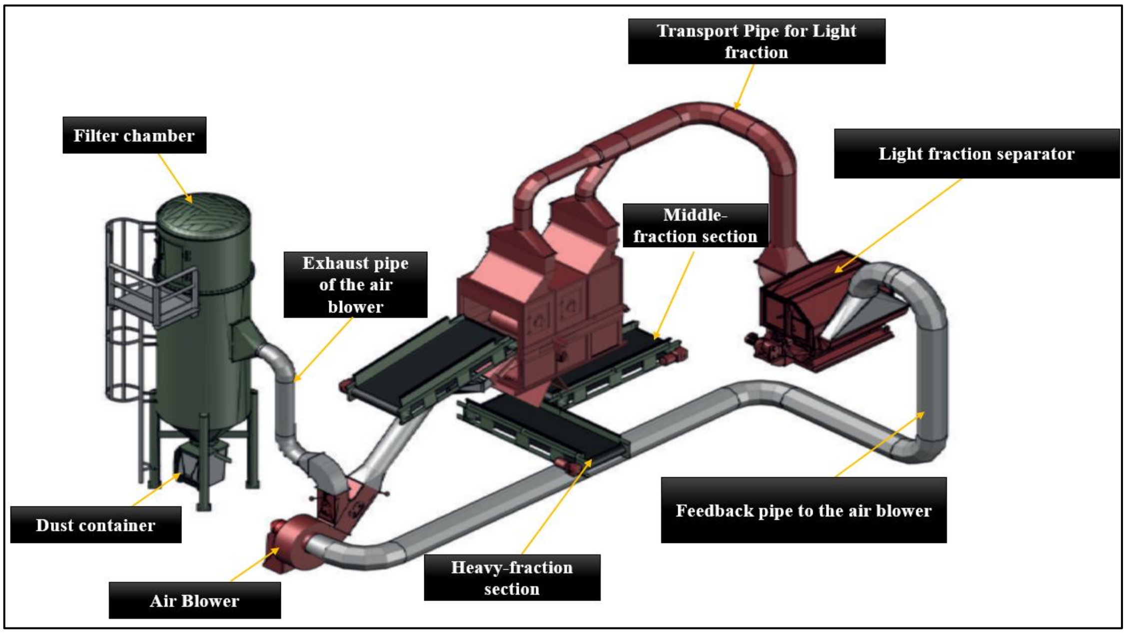

Figure 2.30: Image showing the 3-fraction connection to a light fraction separator and filter chamber. Image adapted from Schulz & Berger (2014b)

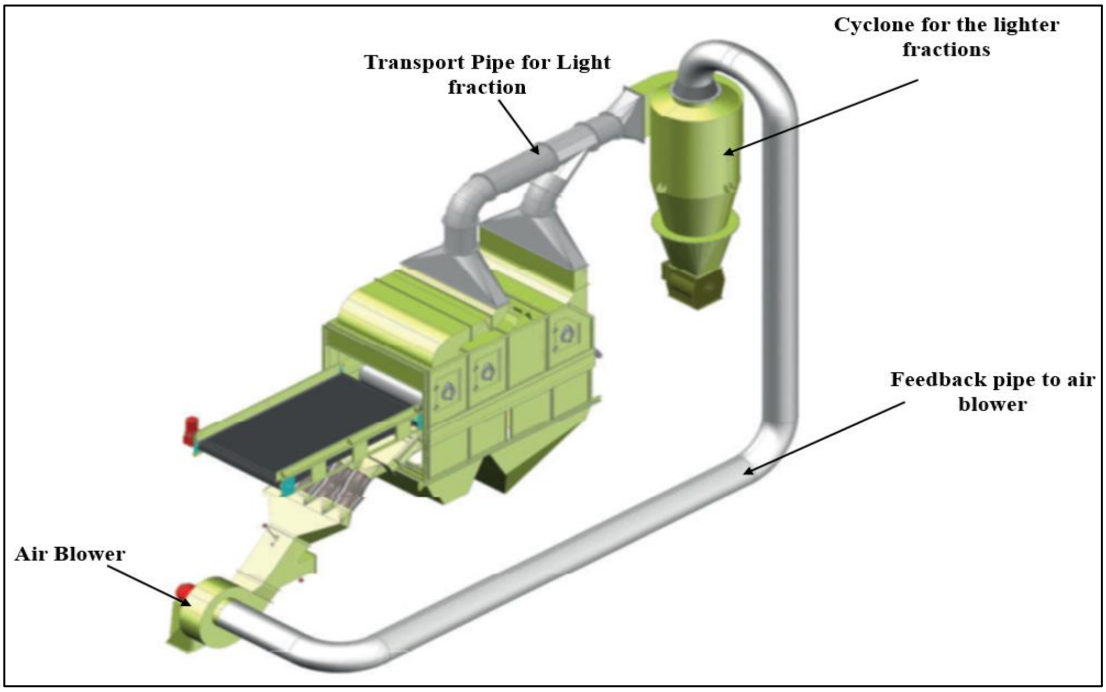

Figure 2.31: Image showing the 3-fraction connection to a gas cyclone. Image adapted from Schulz & Berger (2014b)

2.7. SECURITY CONCERNS: HEALTH, SAFETY AND ELECTRIFICATION OF POWDERS DURING PROCESSING

In the pneumatic processing of fine particles, particularly powdery materials, some concerns must be outlined. One of these issues is the safety of processing and managing fine/powdery materials. Powdery materials could generate a dust atmosphere containing inhalable particles during management or processing, ultimately posing a health hazard to individuals within their proximity. Some of these health issues range from mild irritation to auto-immune diseases and cancerous growth (Benson, 2012; Steiling et al., 2018). Another safety concern is the issue of the combustible powder posing an explosion hazard. The issue of explosion of powders can either be because the powders are highly reactive in the presence of an ample amount of the particle dust cloud (Benson, 2012) or because of electrostatic discharges or mechanically generated sparks (Hoppe et al., 2000; Jaeger, 2001). To prevent this from happening, in most cases, the machines are designed for ATEX (explosive atmosphere) classification that mitigates the creation of a spark (Kemutec, 2022; HSA, 2023). In the pharmaceutical industry, Hoppe et al. (2000) suggested that an inert environment, e.g., a nitrogen atmosphere, be maintained as this inhibits the availability of oxygen for combustion during the pneumatic transportation of these inflammable powdery materials.

A second concern with the pneumatic processing of powdery (fine) particles that must be outlined is the issue of powder electrification. When powdery materials are being pneumatically transported, the particles tend to collide with each other and with the walls of the transport chamber, leading to the accumulation of electrostatic charges. This phenomenon is known as triboelectric charging and may result in hazardous spark discharges (Nifuku and Katoh, 2003; Ceresiat et al., 2019). To avert this phenomenon, Nifuku and Katoh (2003) suggest earthing the granular/powdery materials' pneumatic transport vessels to discharge any charge build-up, as well as increasing the air velocity to facilitate a dilute phase as this greatly minimises inter-particle collisions.

2.8. SUMMARY

The wind-sifter has been used in numerous studies for diverse applications; however, there is not much literature on this technology in the field of dry beneficiation of coal. The ability of this technique to separate lighter particles from heavier ones is an integral feature, as was observed from the previous version designed by Alade (2021) in Figure 2.20. This feature makes the wind-sifting technology a good and viable addition of techniques in the field of dry coal beneficiation. The potential to optimise the wind-sifting separator for dry coal beneficiation will be meticulously investigated in this study. This will add more to the available literature in the public domain on dry coal beneficiation techniques and provide insight into the performance of the separator designed, with the possibility of improving the design and its operating parameters. Alade and Bada (2023) comprehensively review wind-sifting separation, adding to Sections **2.6** and **2.7** of this literature review.

CHAPTER 3: RESEARCH METHODOLOGY

3.1. INTRODUCTION

In this chapter, the procedures and characterisation techniques used to analyse the coal samples utilised in this study, along with the simulation and experimental investigation conducted, are outlined. The computer design and simulation softwares, the equipment and materials utilised, as well as information on the experimental standards utilised, are provided.

3.2. EXPERIMENTAL PROCEDURE

The procedures followed in this study is depicted in Figure 3.1, with designing the optimised separator being the first of the task conducted. Thereafter, the fabricated separator was used in the beneficiation of two sets of coal samples (coal A and coal B) from Witbank Coalfield at different particle size fractions of (−6.7+3.35 mm), (−3.35+1.0 mm) and (−1.0+0.2mm). Float and sink analysis, as well as the dry beneficiation separation process, were conducted for coal A and coal B, and the clean coal products obtained from each of the two coal, under different conditions, were analysed for their calorific value, ash content, carbon content, etc.

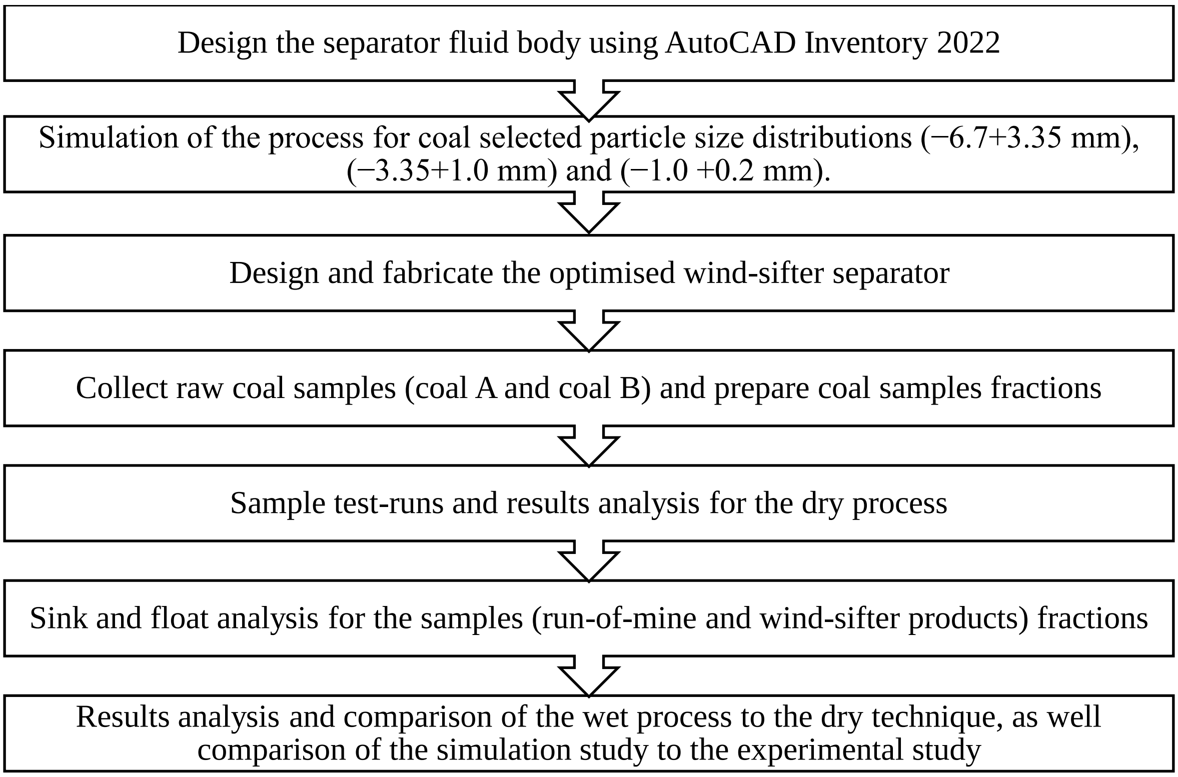

Figure 3.1: Summary of experimental methodology

3.3. DESIGN AND SIMULATION OF THE SEPARATOR

3.3.1. GEOMETRY DESIGN OF THE SEPARATOR

The wind-sifter separator was first generated using Autodesk Inventory 2022 and then exported into Star-CCM+ for simulation. Important factors, like the velocity of the airstream, air-jet angle, size and density of the particle, drag force, buoyant force, the force of gravity and friction on the separator's wall, were considered major parameters during the design of the separator. The inter-particle interactions are negligible owing to the minimal mass flowrate, which ensure that a dilute phase of the particles in the airstream is established. The gas phase (airstream) was treated as a continuous phase, with Equations 3.1 to 3.3 providing the guiding model used in describing the forces experienced by the particles at any location in the separator. The basic equation used arises from the Euler equation.

$$\begin{cases} \left(\dfrac{d\rho}{dt} = -\rho\nabla.u\right) & \text{(Equation 3.1)} \\ \left(\dfrac{du}{dt} = -\nabla\left(\dfrac{P}{\rho}\right) + \mu\nabla^2 u + g\right) & \text{(Equation 3.2)} \\ \left(\dfrac{de}{dt} = -\left(\dfrac{P}{\rho}\right)\nabla.u\right) & \text{(Equation 3.3)} \end{cases}$$

When written in their derived material form, Equations 3.1, 3.2 and 3.3 show the conservation of mass, impulse and energy, respectively. The flow is assumed to be a steady state. Hence, the velocity is constant, and $\nabla \mathrm{u} = 0$. This implies that the terms $\frac{\mathrm{d\rho}}{\mathrm{dt}}$ and $\frac{\mathrm{de}}{\mathrm{dt}}$ equals zero. The air temperature is assumed to be 20^0C. This implies that the dynamic viscosity (µ) of air with a value of 1.6×10^{-5} Pa. s is infinitesimal and considered negligible (tends to zero). Hence, Equations 3.1, 3.2 and 3. 3 can be rewritten as:

$$\begin{cases} \left(\dfrac{dp}{dt} = -\rho\nabla.u = 0\right) \\ \left(\dfrac{du}{dt} = -\nabla\left(\dfrac{P}{\rho}\right) + g\right) \\ \left(\dfrac{de}{dt} = -\dfrac{P}{\rho}\nabla u = 0\right) \end{cases}$$

Therefore, the above equation becomes:

$$\left(\rho\frac{du}{dt} = -\nabla P + \rho g\right) \qquad \text{(Equation 3.4)}$$

When explicated, the equation becomes:

$$\left(\frac{\partial(\rho\, u)}{dt}\right) + \nabla(\rho\, u\, u) = -\nabla P + \rho g - F_{ap} \qquad \text{(Equation 3.5)}$$

Where ρ is the fluid density, u is the fluid velocity, e is the specific energy of the fluid, P is the air pressure, t is time, g is the acceleration due to gravity and F_{ap} is the total force of the interaction between the fluid and the particles per unit volume of fluid (air). The expression of F_{ap} is given in Equation 3.6:

$$F_{a\,p} = \sum_{j=1}^{n} \frac{f_{a\,p,j}}{V} \qquad \text{(Equation 3.6)}$$

Where a represents the fluid (air), p, j represents the particle 'j', n represents the number of particles considered, V represents the volume of particle 'j' and $f_{a\,p,j}$ is the force of interaction for individual particles, which is shown in Equation 3.7.

$$f_{a\,p,j} = F_B - F_w - F_D \qquad \text{(Equation 3.7)}$$

According to Equations 3.8 and 3.9, F_B is represented as the buoyant force, ρ is the density of the fluid (air), V is the displaced body volume of the fluid (this is also the volume of the particle since it is fully immersed in air), and g is the acceleration due to gravity.

$$F_B \geq F_W + F_D \qquad \text{(Equation 3.8)}$$

$$F_B = \rho\, V\, g \qquad \text{(Equation 3.9)}$$

$$F_W = m \times g \qquad \text{(Equation 3.10)}$$

In Equation 3.10, F_W represents the weight of the particle, m is the mass of the particle, and g is the acceleration due to gravity.

$$F_D = \left(\frac{C_D \times A \times \rho \times u^2}{2}\right) \qquad \text{(Equation 3.11)}$$

In Equation 3.11, F_D is the drag force on the particle, C_D denotes the drag coefficient of the particle, A is the cross-sectional area, ρ is the density of the fluid (air), and u is the flow velocity relative to the air.

When $F_B > F_W + F_D$, the particles are being transported in the airstream, and when $F_B = F_W + F_D$, which implies that $f_{a\,p,j}$ is zero, the particle velocity in the airstream terminates, and the particles fall at constant velocity. An important factor that must be stated when dealing with dry particle separation, particularly using air as the separating medium, is the particle settling ratio. The settling ratio is equal to the limiting ratio of diameters of particles that may be separated by free settling, given by Equation 3.12.

$$Settling\ ratio = \frac{d_L}{d_H} = \frac{\rho_h - \rho_m}{\rho_l - \rho_m} \quad \text{(Equation 3.12)}$$

Where,

$d_L = diamter\ of\ the\ lighter\ particles$

$d_H = diamter\ of\ the\ heavier\ particles$

$\rho_L = density\ of\ the\ lighter\ particles$

$\rho_H = density\ of\ the\ heavier\ particles$

$\rho_m = density\ of\ the\ separating\ medium\ (air)$

To also factor in the influence of shape, the following model (Equation 3.13) for the coefficient of drag was developed as this is the same coefficient of drag used by the simulation software.

$$\varphi = \frac{Surface\ area\ of\ volume\ equivalent\ sphere\ of\ the\ particle}{Surface\ area\ of\ the\ particles} = \frac{\pi \times d_v^2}{\pi \times d_s^2} = \frac{d_v^2}{d_s^2} \quad \text{Equation 3.13}$$

Where,

φ is the Sphericity factor of the particle

d_v and $d_s$are the diameters of the volume equivalent sphere of the particle(s) and the diameter of the particle(s), respectively.

$$\varphi = \frac{\pi \times d_v^2}{\alpha_{sv} \times d_v^2} = \varphi = \frac{\pi}{\alpha_{sv}} \quad \text{(Equation 3.14)}$$

Where, α_{sv} is the shape factor and is expressed as:

$$\alpha_{sv} = S_w \times \rho \times \frac{\pi}{6} \times \frac{\sum n_i \times d_{vj}^3}{\sum n_i \times d_{vj}^2} \quad \text{(Equation 3.15)}$$

Adapted from Barreiros et al. (1996)

Where,

S_w (m^2/g) is the powder-specific surface area determined using gas adsorption,

ρ is the density of the particle of the number of equivalent volume diameter in sample j,

d_{vj} is the equivalent volume diameter of particles in sample j,

n is the number of particles,

i is the size class (particle size distribution).

The expression for the coefficient of drag C_D accounting for shape, which will then be put into Equation 3.11 is then given by Equation 3.16.

$$C_D = \frac{8}{Re} + \frac{1}{\sqrt{\varphi}} + \frac{16}{Re \times \sqrt{\varphi}} + \frac{4 \times \varphi}{\sqrt{Re}} + 0.4210^{0.4(-log\varphi)^{\frac{0.2}{\varphi}}} \qquad \text{(Equation 3.16)}$$

Adapted from Hölzer and Sommerfeld (2008).

Following the guiding mathematical model derived above, the optimal separator design from the simulation was attained following these steps:

I. The first chamber of the separator assembly was designed using the Autodesk Inventor software and was then imported into the simulation software.
II. A Simulation test was then carried out using the assumptions listed in section **3.3.2.**, whilst varying operational parameters like the airstream velocity and the feed rate of the particles.
III. The particle tracks for each RD were observed, and the operational parameters were changed to observe the separation effectiveness of that design at the cut-point of 1.6 RD like the prototype.
IV. Continuous augmentations were made based on the flow tracks observed from each design until an optimal separation was attained in the first chamber.
V. A second chamber was designed, and the same steps listed above (for the first chamber) were carried out based on the optimal results achieved through the particle tracks, leading to the design of the optimised separator assembly.

Figures 3.2 and 3.3 depict the individual chambers and their respective flow boundaries, with ***A*** (Figure 3.2) representing the air supply inlet into the separation chamber, while ***B*** denotes the particle inlet into the separation chamber, and ***C*** is the outlet of the clean coal particles elutriated by the airstream from the first chamber. **B8**, **B9** and **B10** represent the coal bins 8, 9 and 10 for the collection of gangue material's particles, respectively.

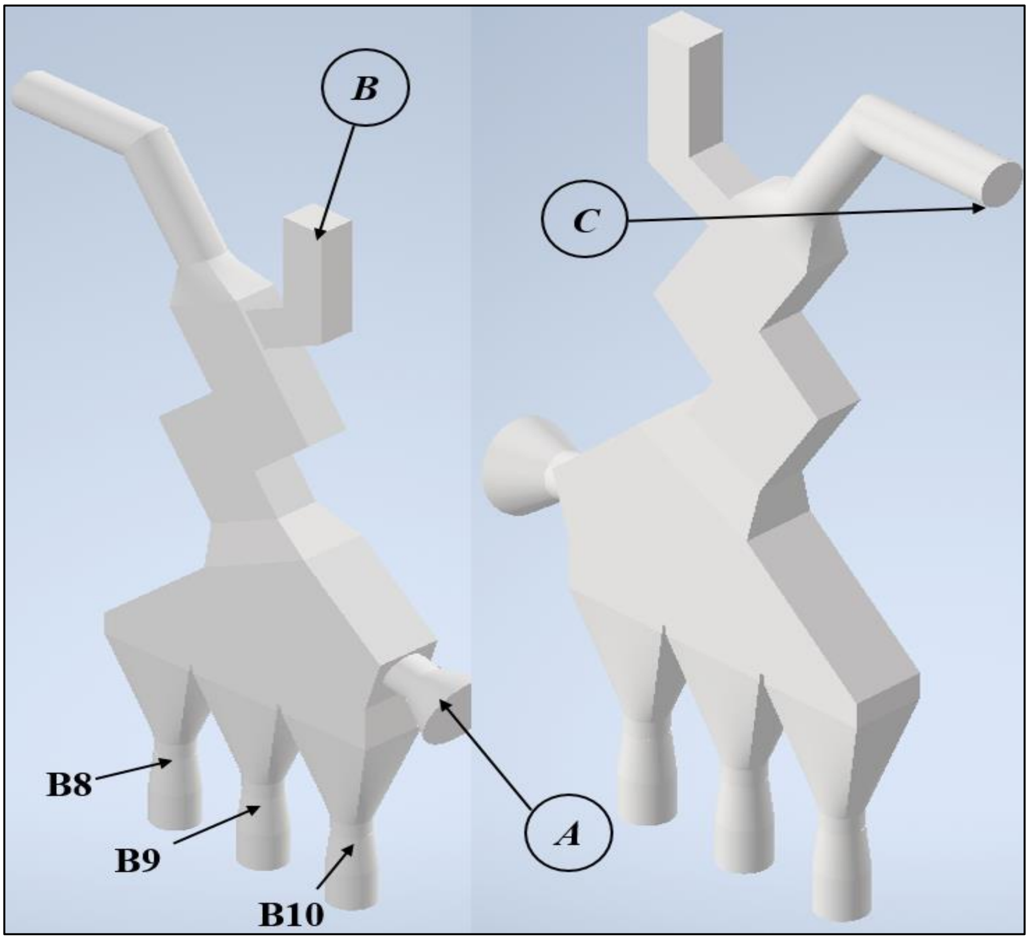

Figure 3.2: Flow boundaries of the first chamber (chamber 1) with its collection bins

In Figure 3.3, ***D*** represents the inlet of the partitioned particles, i.e., through which the lighter particles are transported into the second chamber, while ***E*** is the air outlet from the separator. **B1**, **B2**, **B3**, **B4**, **B5**, **B6** and **B7** represent the particle collection bins 1, 2, 3, 4, 5, 6 and 7, respectively, while **B0** represents the collection point for particles that go past **B1**. The design of the separator was carried out in such a way that coal samples fed into the system are maximally recovered, either as a product or discard. This helps to prevent the samples from being retained in the separator, which was observed in the previous design, as seen in Figure 2.20. Figure 3.4 shows the full assembly of the separator with bins, and Figure 3.5 shows the assembly without bins.

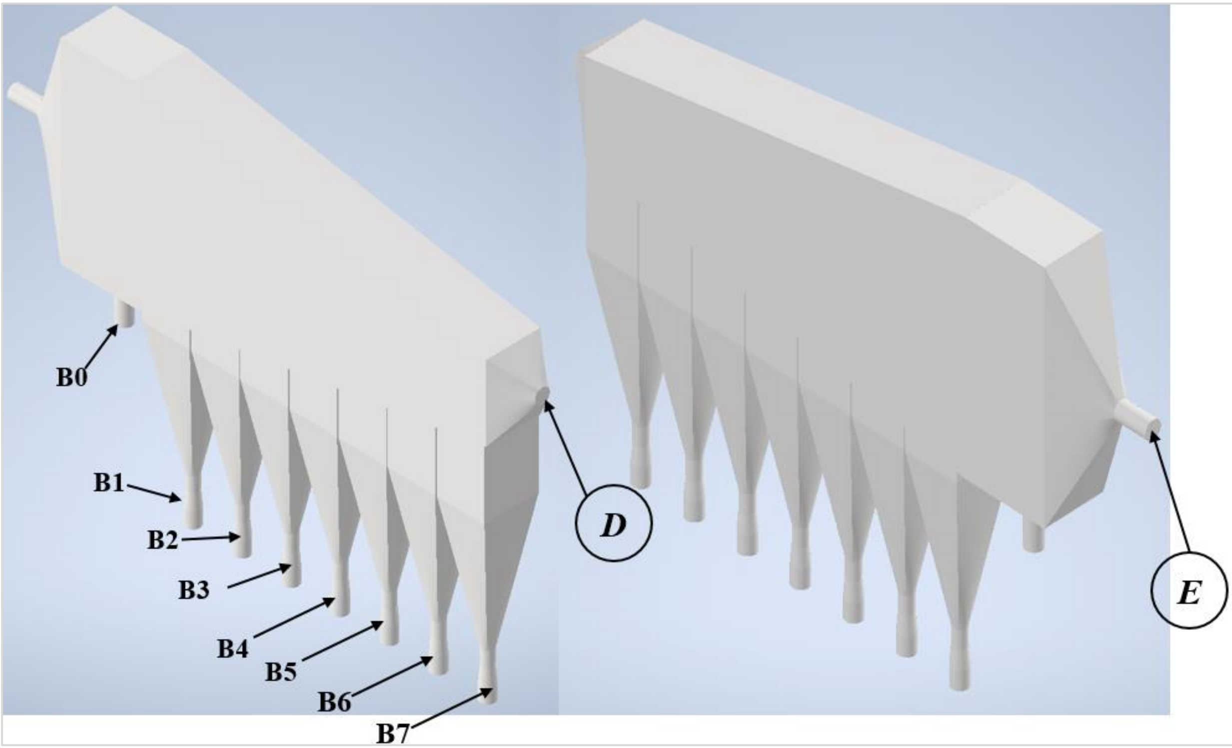

Figure 3.3: Flow boundaries of the second chamber (chamber 2) with its collection bins

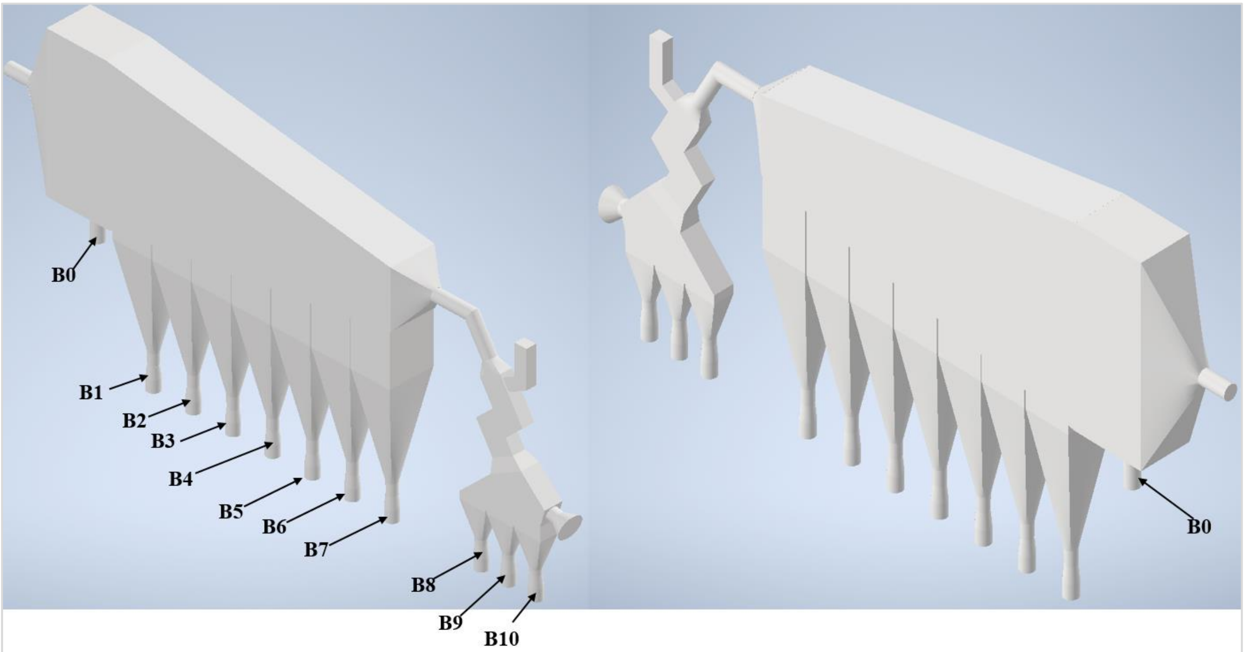

Figure 3.4: The optimised separator assembly with bins

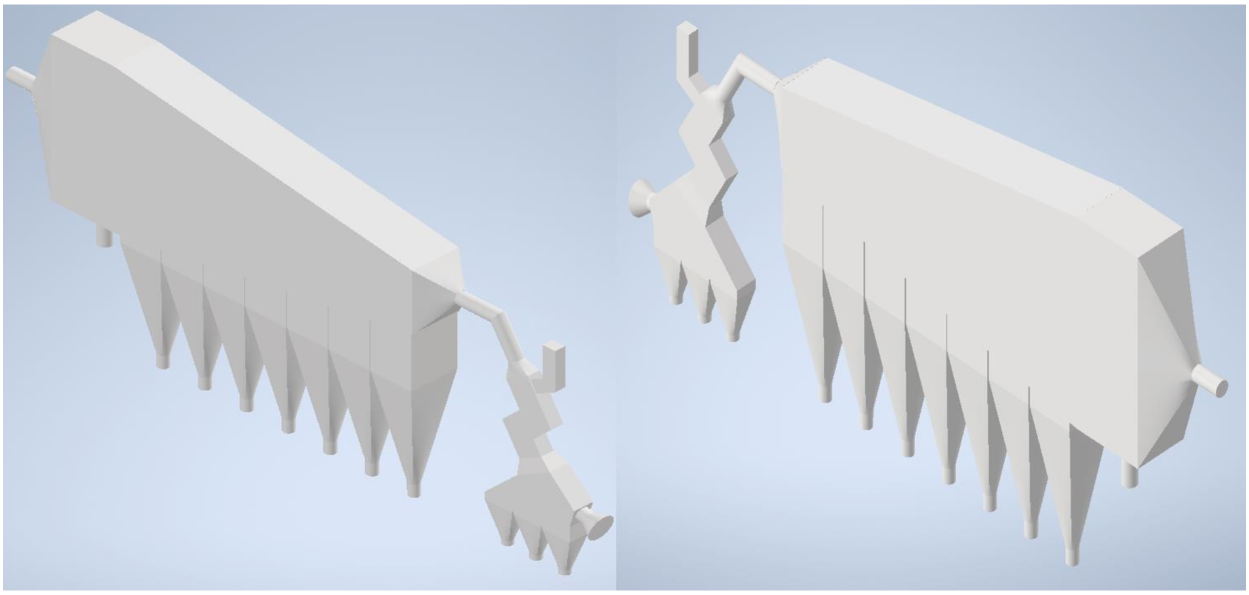

Figure 3.5: The full separator assembly without bins.

As can be seen from Figure 3.6, the upper part of chamber 1 was designed and then merged with the chute that transfers the particles into collecting bins 8, 9 and 10. The same approach was also applied to the second chamber design. The merging was done to form a contact region/surface between the two connecting faces when imported into the simulation software. This design approach enabled the determination of the amount of the particle recovered in each bin. Each of the two chambers was designed as an assembly, as shown in Figures 3.6 to 3.8.

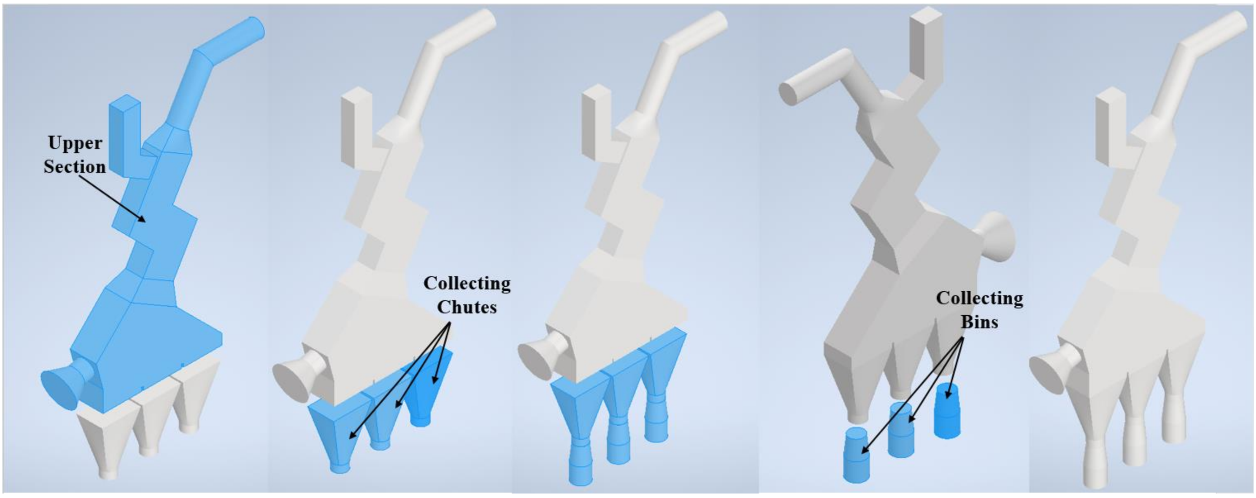

Figure 3.6: The designed assembly of chamber 1 to depict contact regions

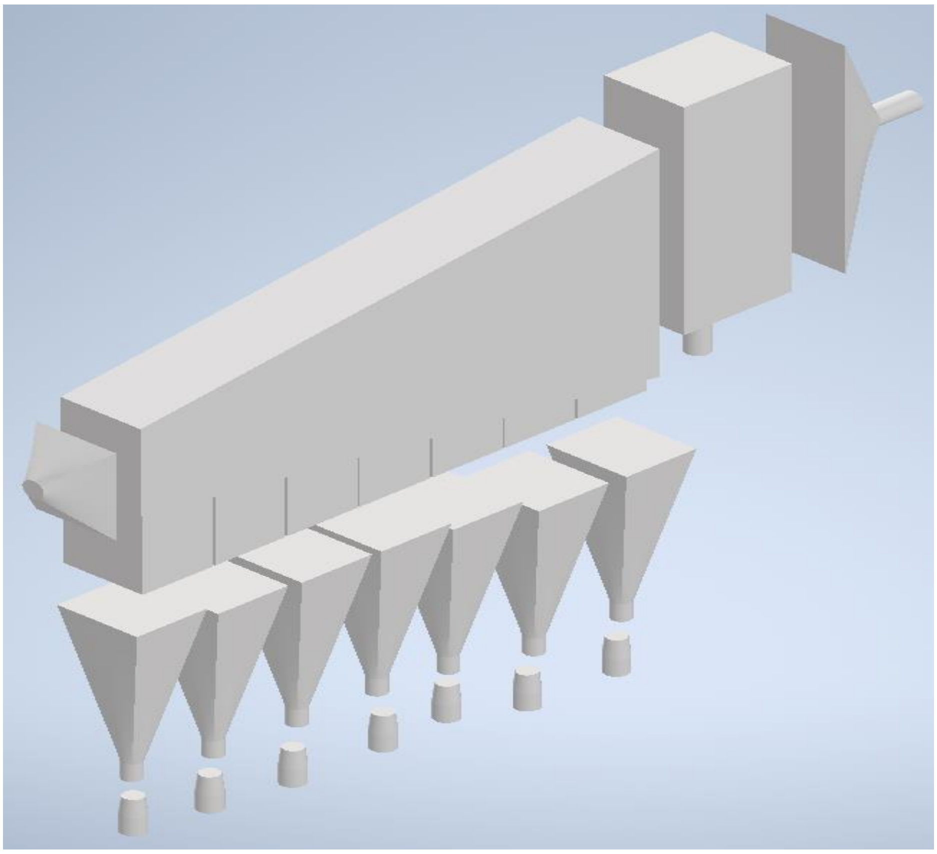

Figure 3.7: Designing chamber 2

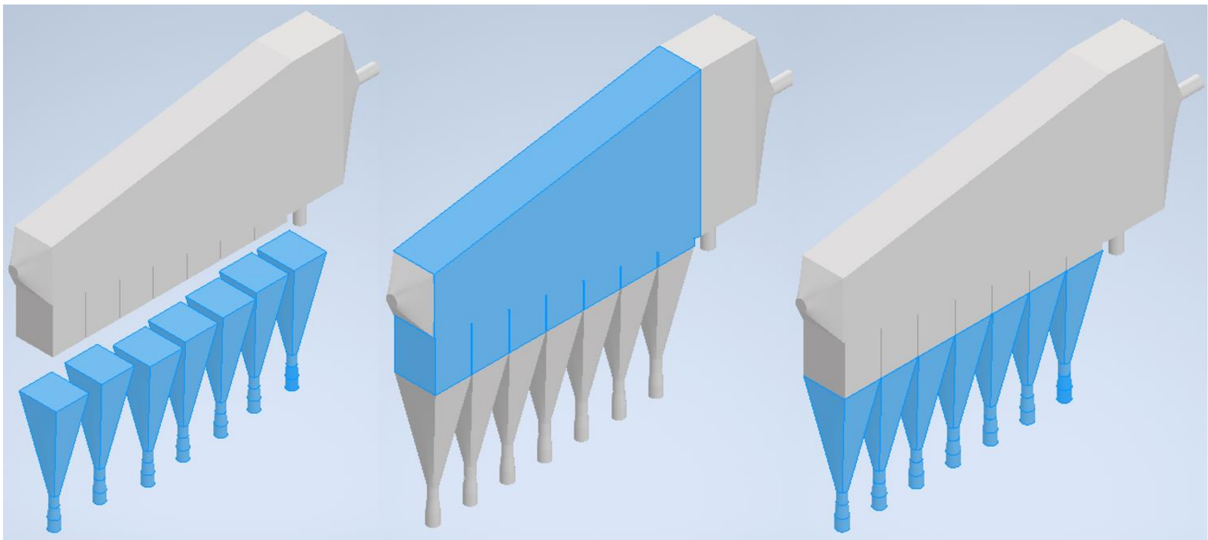

Figure 3.8: The designed assembly of chamber 2 to depict contact regions

3.3.2. THE SIMULATION PROCESS

The mesh is an integral component of this design and was generated for both chambers (1 and 2) to optimise these geometries and obtain a highly accurate measurement. The meshing models used were the *surface remesher*, the *polyhedral mesher* and the *prism layer mesher*. The surface remesher meshing model is used to improve the overall quality of an existing surface and to optimise it for the volume mesh model, which is the polyhedral mesher, as used in this study. The polyhedral mesher is a volume core mesh model that provides a balanced solution for complex mesh generation as it uses arbitrary polyhedral cell shapes to build the core mesh. The polyhedral mesher was utilised in this design because it is straightforward and requires no further surface preparation, unlike the tetrahedral mesher model. It is very effective in the analysis of the simulation and contains approximately five fewer cells than the tetrahedral mesher model. Figures 3.9 and 3.10 show the mesh generated for both chambers with the bins and without the bins, respectively.

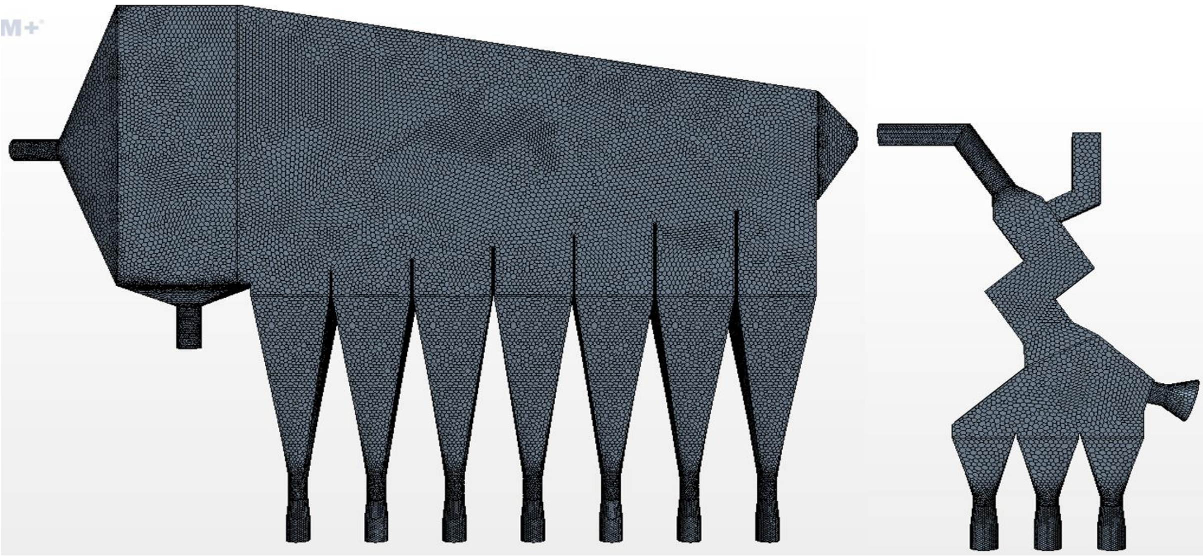

Figure 3.9: Mesh generated for chambers 1 and 2 with bins

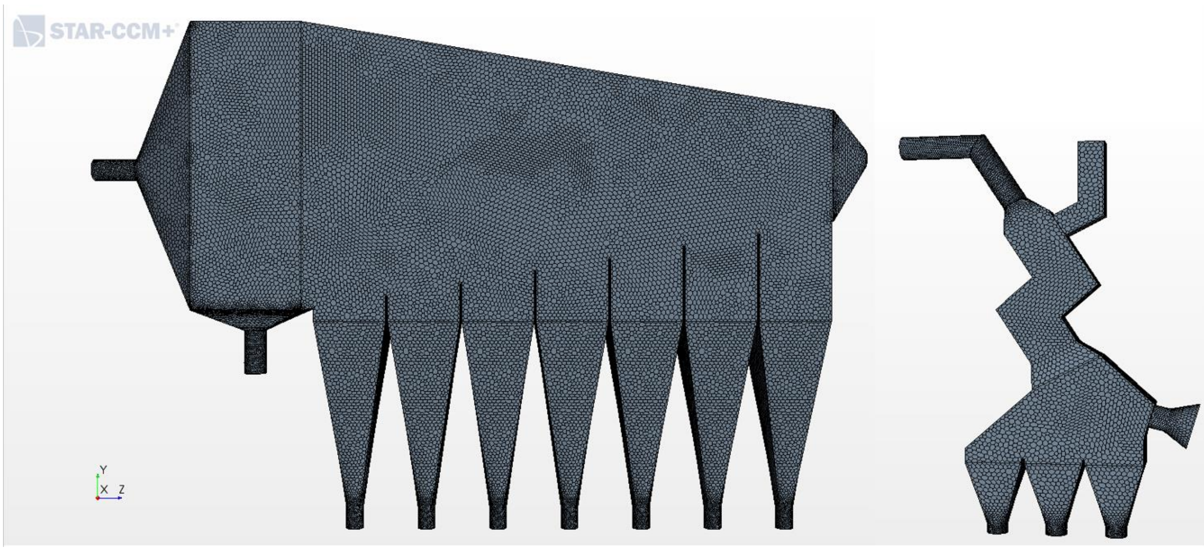

Figure 3.10: Mesh generated for chambers 1 and 2 without bins

The prism-layer mesher model was also applied with the core-volume mesher (polyhedral mesher). The prism-layer model was used to generate orthogonal prismatic cells next to the walls (surfaces) of the separator and to give accurate results in the simulation test runs even with just a few prism layers. Figures 3.11 and 3.12 show the prism layers of the generated meshes for chambers 1 and 2, respectively.

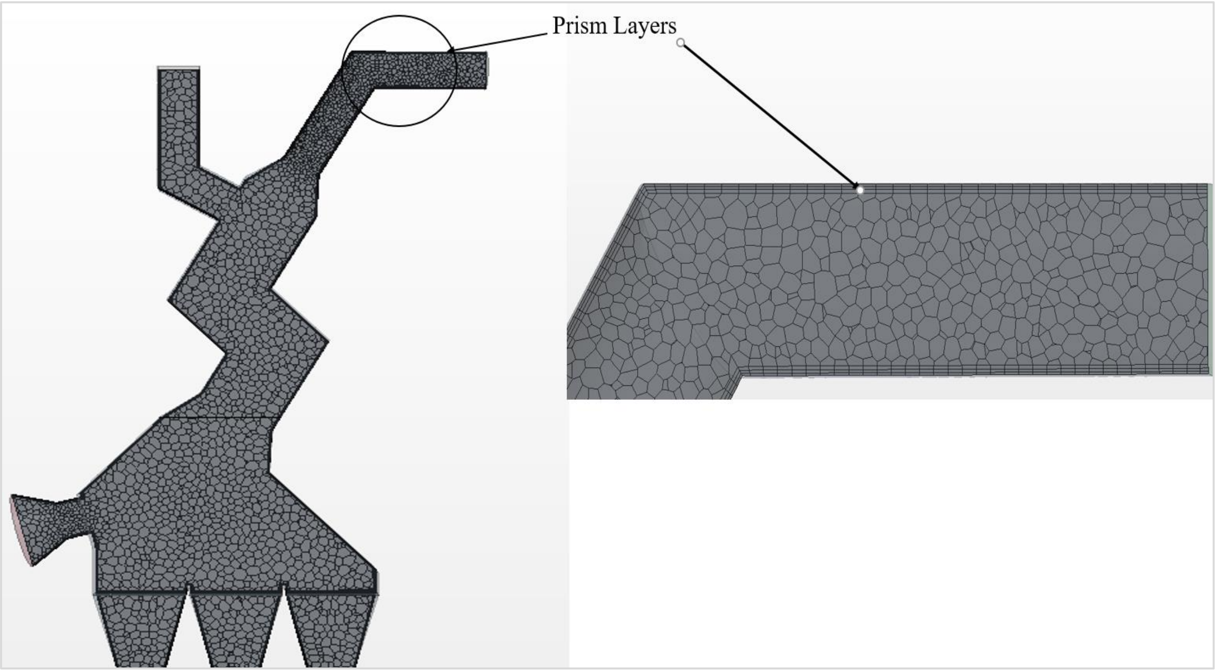

Figure 3.11: Prism layer in chamber 1

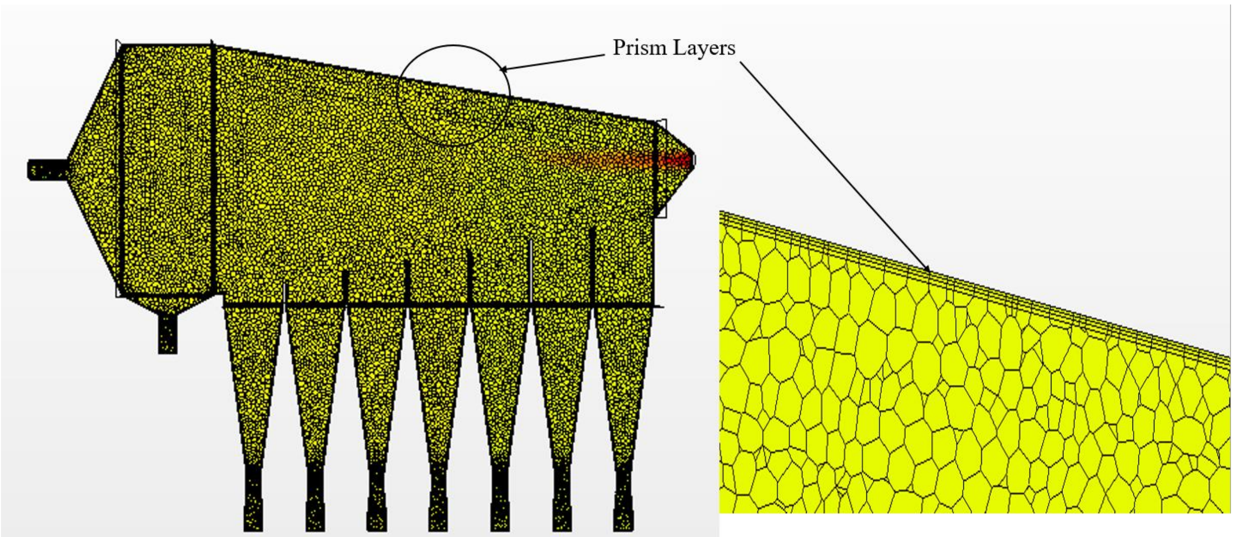

Figure 3.12: Prism layers in chamber 2

As earlier stated, the contact regions generated were used to determine the number of particles, as well as the RDs of the particles entering the individual collecting bins. Figures 3.13 and 3.14 show the yellow patches, which are the contact regions in the first and second chambers, respectively, and help to ascertain the number of particles entering each bin, as well as the number of misplacements in both chambers of the separator assembly.

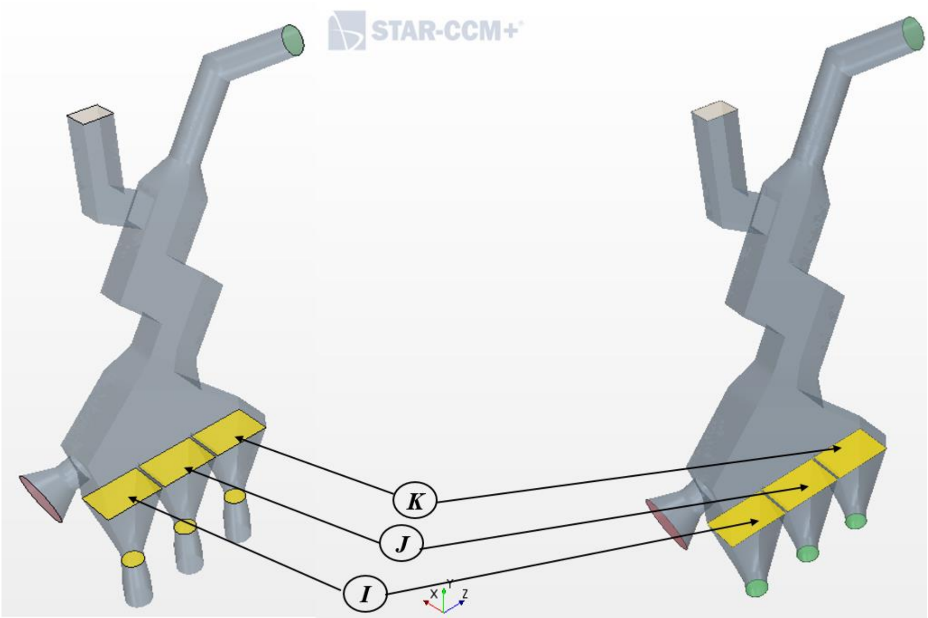

Figure 3.13: Contact regions in the first chamber with and without the bins

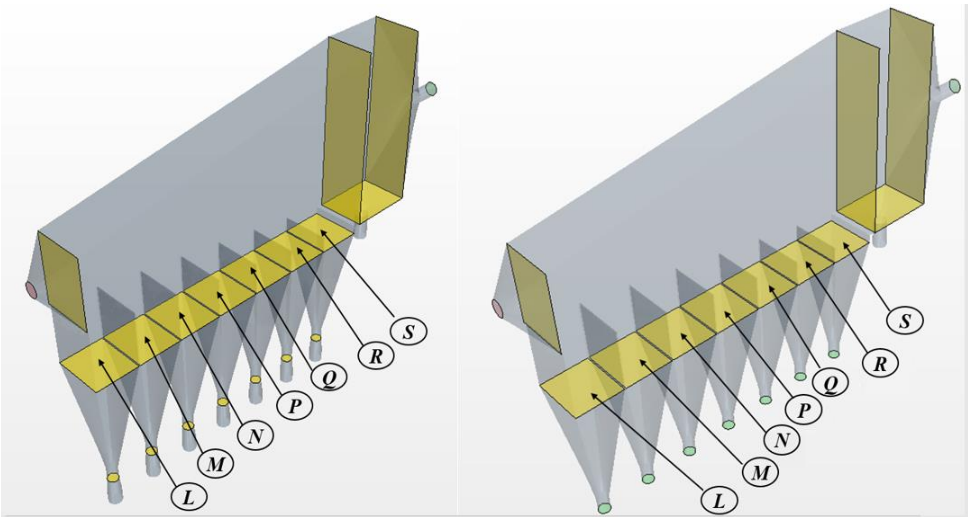

Figure 3.14: Contact regions in the second chamber with and without the bins

Physics models are very important in determining the primary variables of the process being simulated, for example, velocity, temperature, pressure, etc (Maharaj, 2014; Alade et al., 2021). The *physics* models to be used in any simulation are dependent on factors such as if the flow is three-dimensional, and is steady, unsteady, transient or stationary. In this study, parameters such as flow velocity and mass flowrate were also considered, and the *physics* models chosen were the *three-dimensional* and *time* models, and the flow was *steady state*. It is important to point out that steady state flow indicates that properties at every point in the separator remain constant; although the flow properties may change at different points, the overall properties in the separator do not change. Equation 3.17 is the general equation that defines steady flow with respect to density (ρ) and velocity (u):

$$\frac{\partial \rho}{\partial t} = 0, \frac{\partial u}{\partial t} = 0 \qquad \text{(Equation 3.17)}$$

The *Gravity* and *Lagrangian* models were used in the simulation investigation of this dry beneficiation process, while air was used as the *Material* (continuum) for this simulation study. For the *Gravity* model, values of (0, −9.81 m/s, 0) were used in the (x, y, z) dimension to ensure proper action of gravity of the 'negative' y-direction in the separator and, seven *phases*, the same as Alade (2021) (densities of 1.3 g/cm^3 to 1.9 g/cm^3) for the *Lagrangian* model as particles fed into the computational geometry (separator) via the coal inlet boundary of the first chamber. The following assumptions were made regarding the simulation test runs:

I. The shape factors of the particles are between 32.5 and 0.03. This was done to create a spectrum of particles between the low and high drag coefficients of the particles.
II. The particle RDs are equally represented in terms of mass.
III. Each RD within the coal was represented in the simulator and assigned a size (mm) to simplify the simulation, which can be seen in Table 3-1.
IV. Normal and tangential restitution coefficients of the boundary for the wind-sifter separator were assumed to be 0.7. This was to account for the inner section of the separator, which was lined with linatex rubber HD 60 (heavy duty) to help cushion the travelling coal particles as they are transported in the airstream.

Table 3.1: The assigned particle diameters for each particle size fractions per density fraction

Relative Density	**(−6.7+3.35 mm)**	**(−3.35+1.0 mm)**	**(−1.0 +0.2 mm)**
1.3	3.35	1.00	0.20
1.4	3.80	1.40	0.35
1.5	4.60	1.80	0.40
1.6	5.40	2.30	0.55
1.7	6.10	2.70	0.70
1.8	6.35	2.90	0.85
1.9	6.70	3.35	1.00

From Table 3.1, the cut-size appropriate for the finest size fraction in the separation process was determined using the velocity indicated for this size fraction and then observing the flow tracks of the particles. The size that had a smoothened flow track (0.2 mm) was then used as the cut-size, as portrayed in Figures 4.24 to 4.26 in Section **4.3**.

3.4. WIND-SIFTER SEPARATOR

The optimised wind-sifter, with its bins and without auxiliaries, has a footprint of 2.46 meters in length, 1.30 meters in height and 0.2 meters in width. With its auxiliaries, the footprint is 4.0 meters in length, 2.5 meters in height and 0.9 meters in width. The separator assembly was designed to sit on a cradle that suspends it from the ground so that it can operate with and without its bins at the operators' discretion. Like the previous version, the first chamber has two inlets and an outlet; the top inlet serves as an inlet for the coal, and the other inlet is for the airstream. The second chamber only has one inlet to feed the clean coal and an outlet for the air to exit the separator. Figures 3.16 and 3.17 show the designed chambers 1 and 2, alongside their respective angle irons, to help them sit on their respective cradles. The design of the fluid bodies of both separator assembly chambers can be seen in APPENDIX **A.** and the design of the separator, as well as fabricated parts of the separator chambers, are not shown in this thesis. This is because documentations still need to be filed to protect the design for intellectual property.

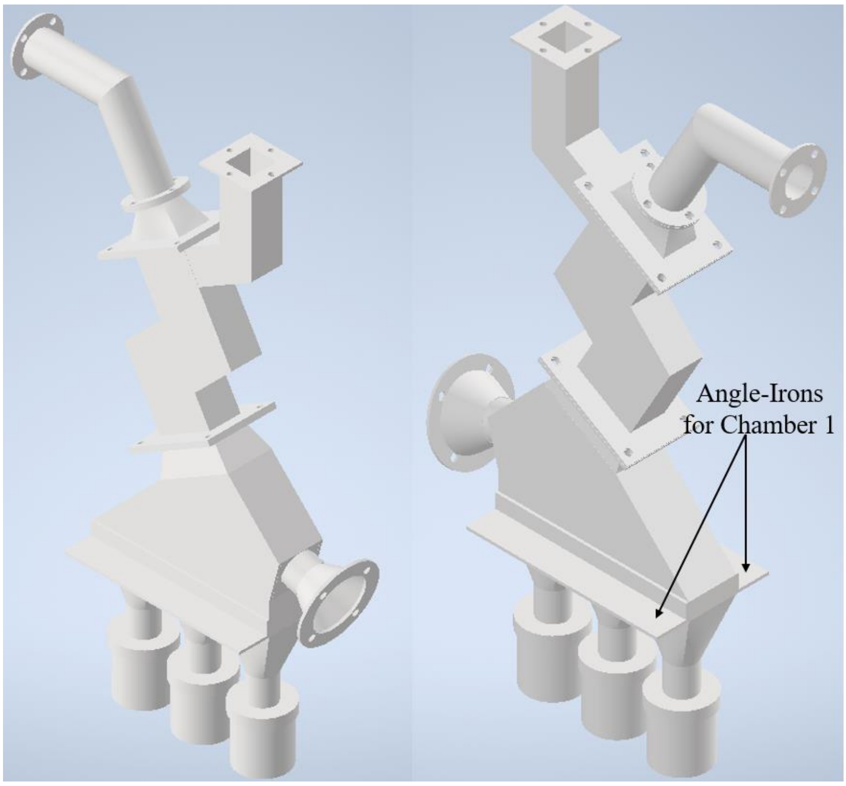

Figure 3.15: The designed chamber 1 with its angle irons

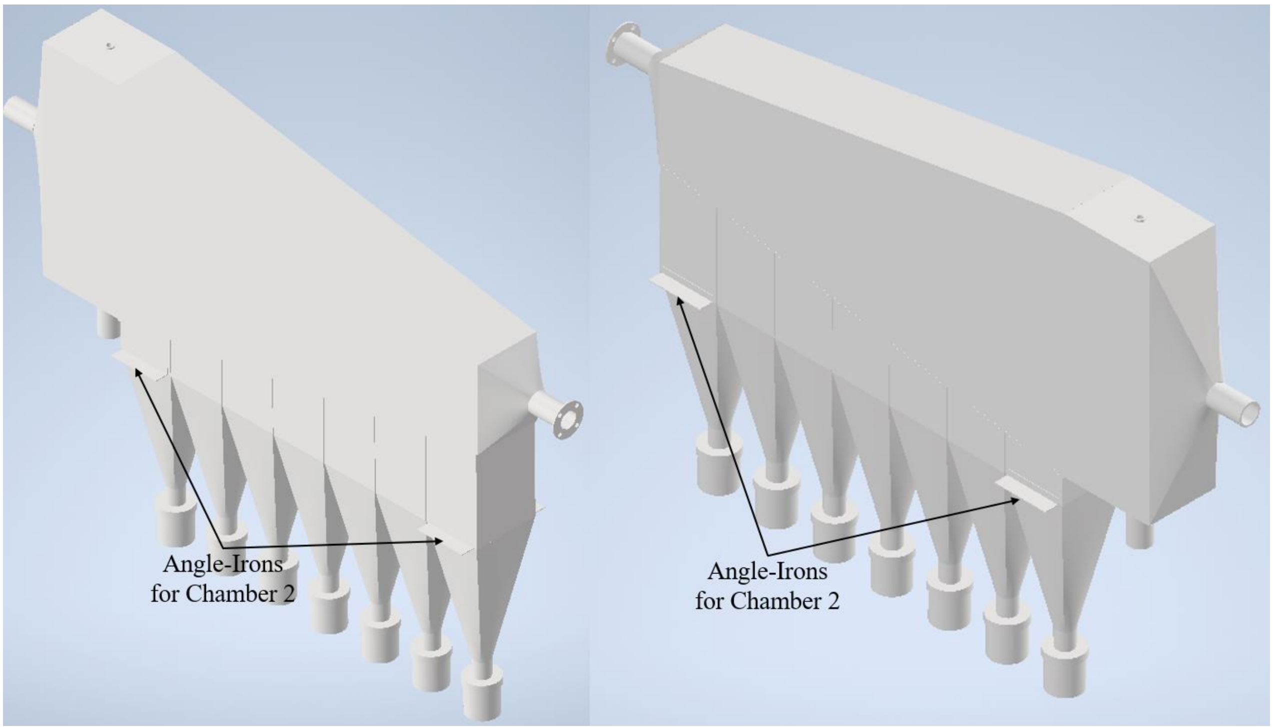

Figure 3.16: The designed chamber 2 with its angle irons

The designed cradles for chambers 1 and 2 are displayed in Figures 3.17 and 3.18; each figure depicts each cradle without and with its respective chamber. Figure 3.19 shows the designed full assembly on cradles without auxiliaries.

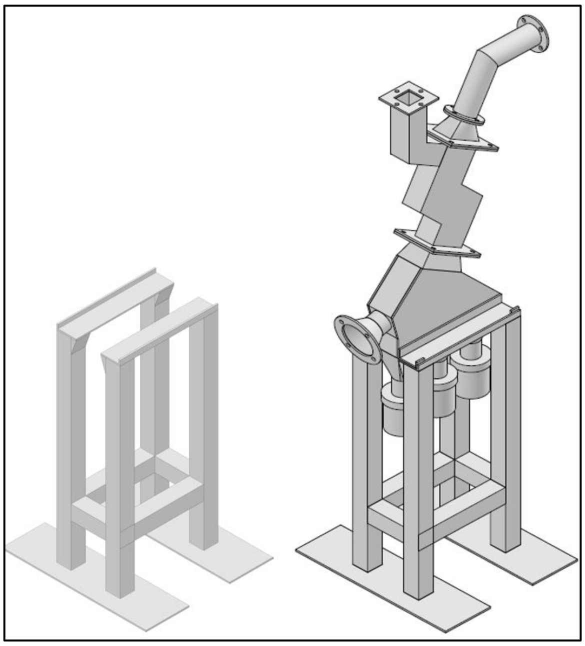
Figure 3.17: Chamber1 on cradle 1

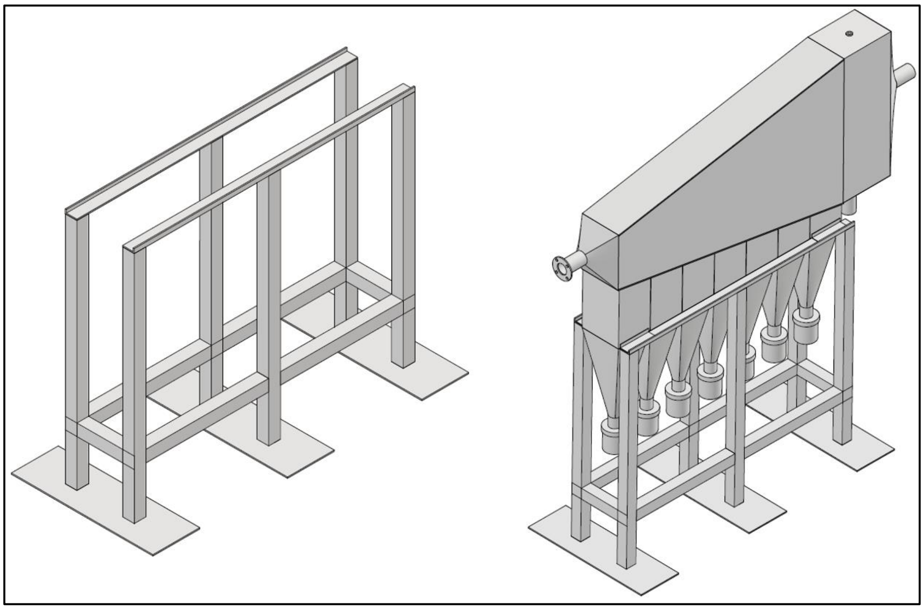

Figure 3.18: Chamber 2 on cradle 2

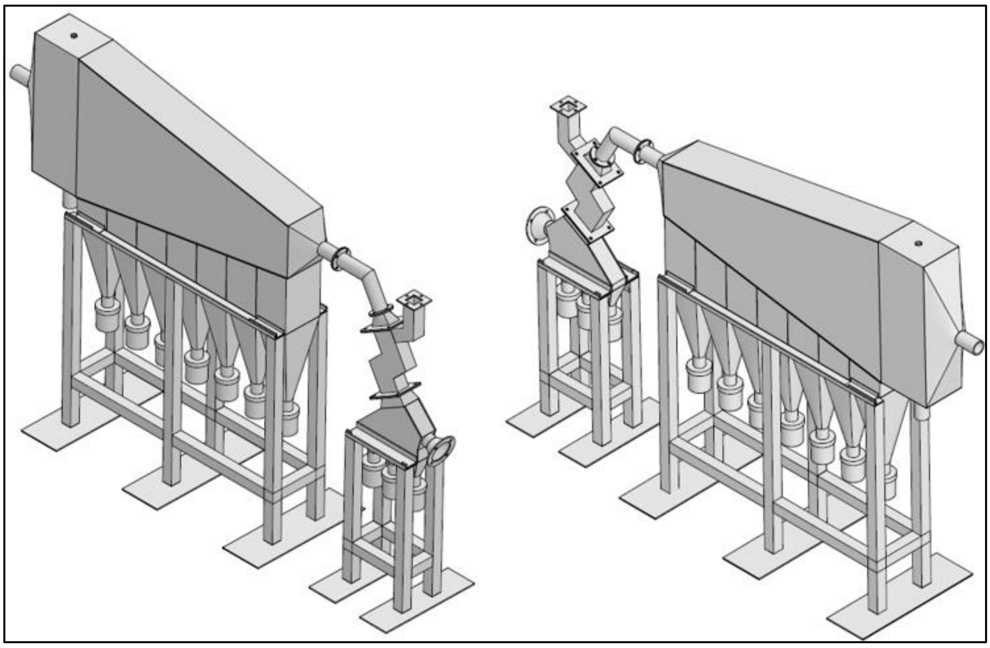

Figure 3.19: The optimised wind-sifter separator assembly design

3.4.1. OPERATING PRINCIPLE

As in its preceding design, the optimised wind-sifter separator separates lighter particles from heavier ones. As can be seen from Figure 3.20, the air blower supplies the air into the separator, which is drawn into the system through the inlet filter. The air then flows through a control valve (ball valve) for regulation and the regulated air flows into the separator through the flex. The gauge displayed in this figure is used to know if the filter is clogged: the higher the pressure reading the more the filter is clogged.

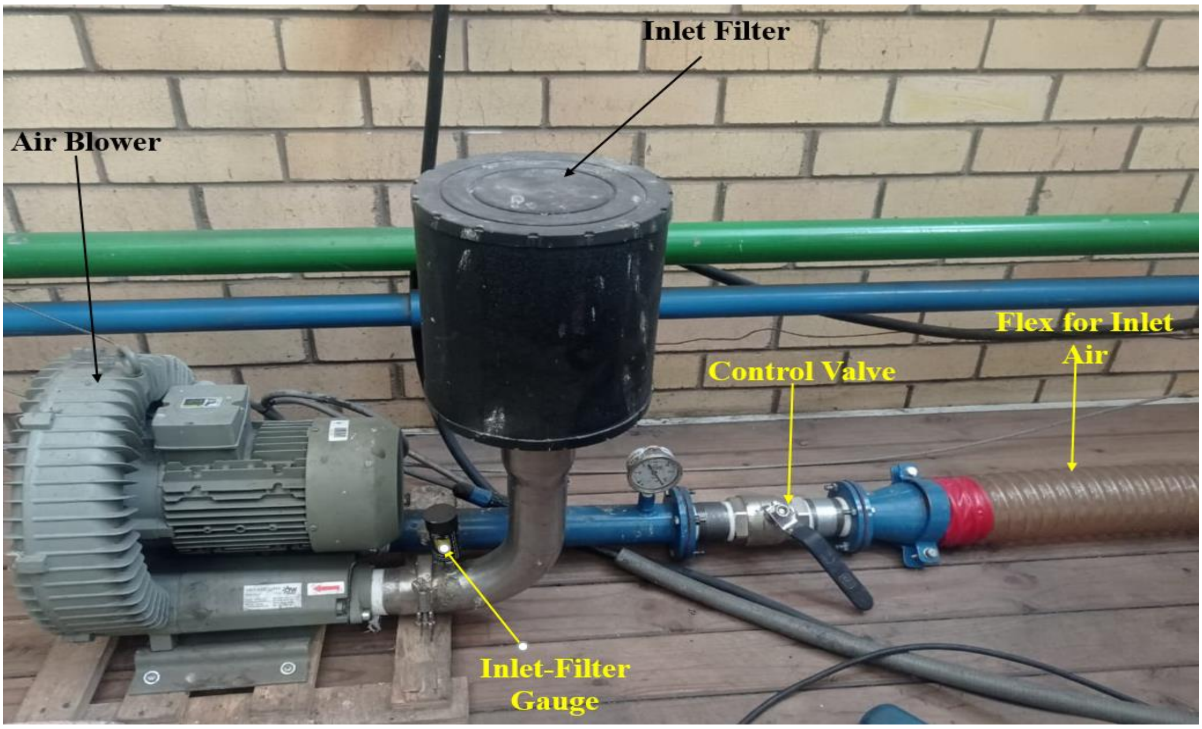

Figure 3.20: The separator's auxiliaries (a)

The safety/relief valve shown in Figure 3.21 below serves as a measure to depressurise the separator assembly from excessive pressure build-up and is also used together with the control valve when the percentage opening of the control valve is reduced for velocity control. The air that flows in through the flex enters chamber 1 of the separator assembly, and its velocity is measured. The value of the velocity is measured using a velocity probe/sensor (Figure 3.21).

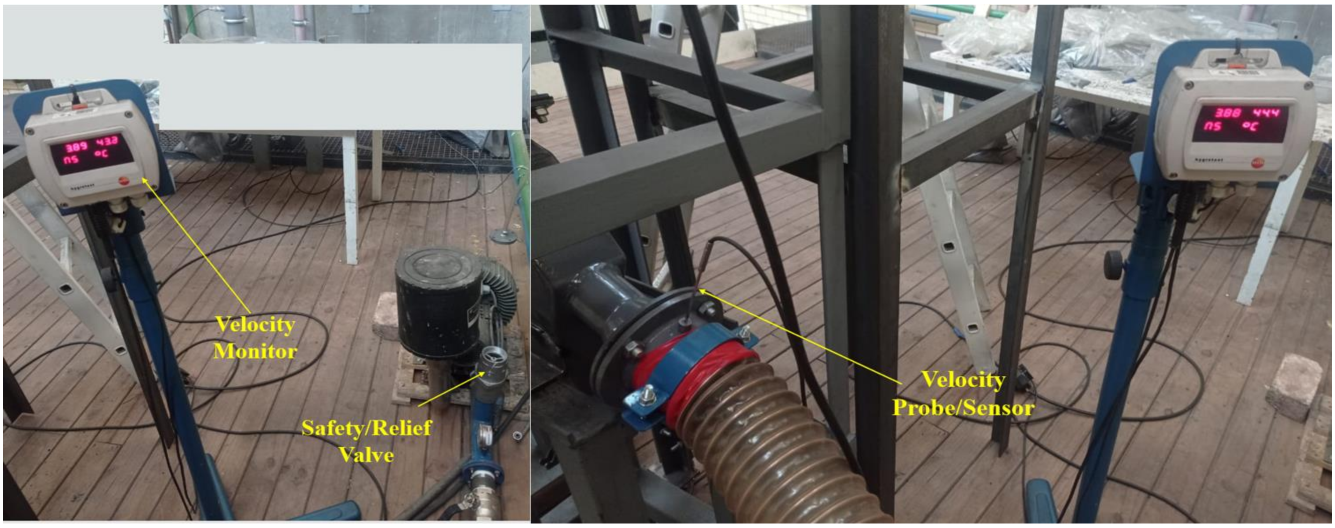

Figure 3.21: The separator's auxiliaries (b)

The airstream then travels through the air-inlet, the zigzag section and into the diffuser section, and then exits the separator assembly via its air outlet. Coal is fed into the separator through the coal-feed inlet, the particles then fall into the zigzag section, and as they bounce in this section, some separation occurs because of their varying weights. The continuously flowing incoming air then separates the lighter particles from the heavier ones in a counter-current manner and then transports them into the second chamber, where they are collected. As the clean coal product enters the second chamber, under the differential drag acting on particles in an airstream, the particles are further separated into different bins based on their densities. This chamber was designed under a different principle from that of the first chamber. The coal is fed with the aid of a vibratory feeder and a rotary hopper valve. The rotary hopper valve helps to feed the coal particles directly into the system and to seal the coal-feed inlet section so it does not serve as an outlet for the flowing airstream. Figure 3.22 shows the fabricated separator with the mentioned sections labelled, while Figure 3.23 shows the vibratory feeder, the rotary hopper valve and the control panel upon installation. The control panel powers both the electric motor-driven rotary hopper valve, as well as the air blower.

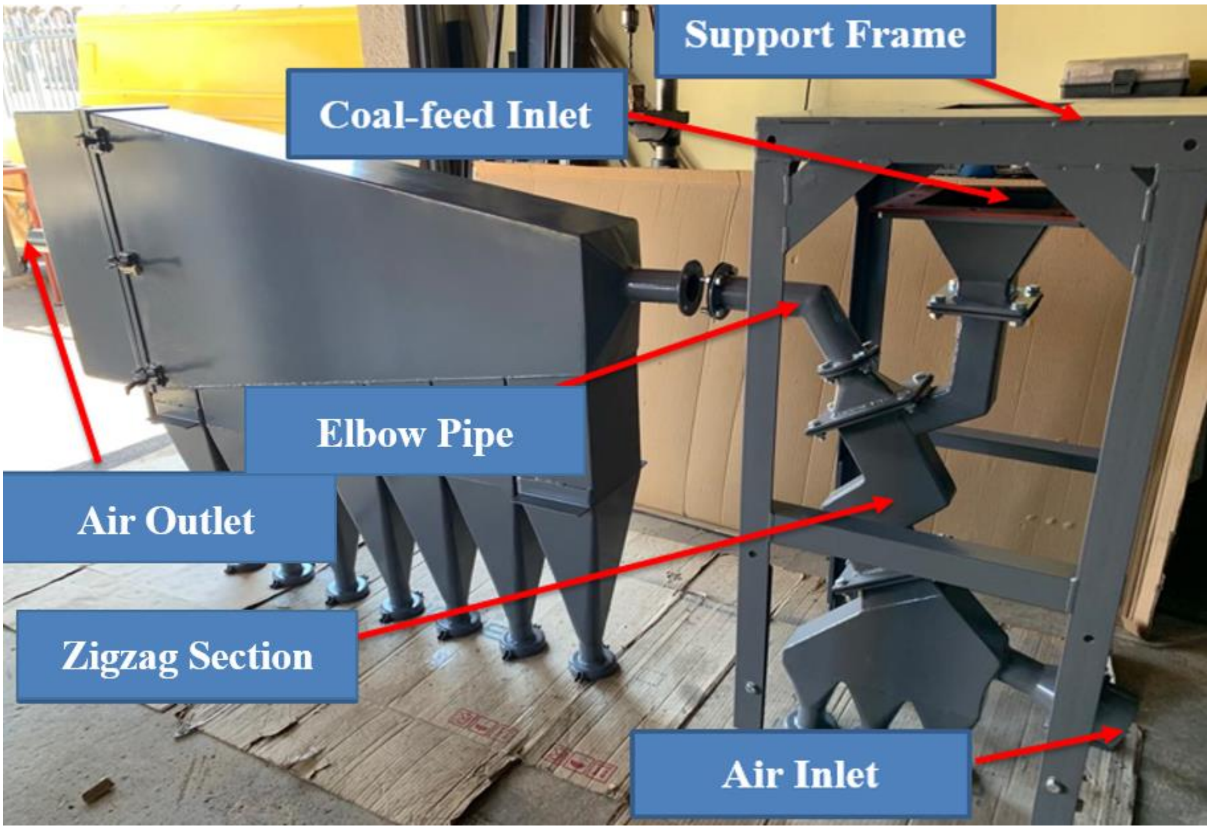

Figure 3.22: The Fabricated Optimized Wind Sifter Separator

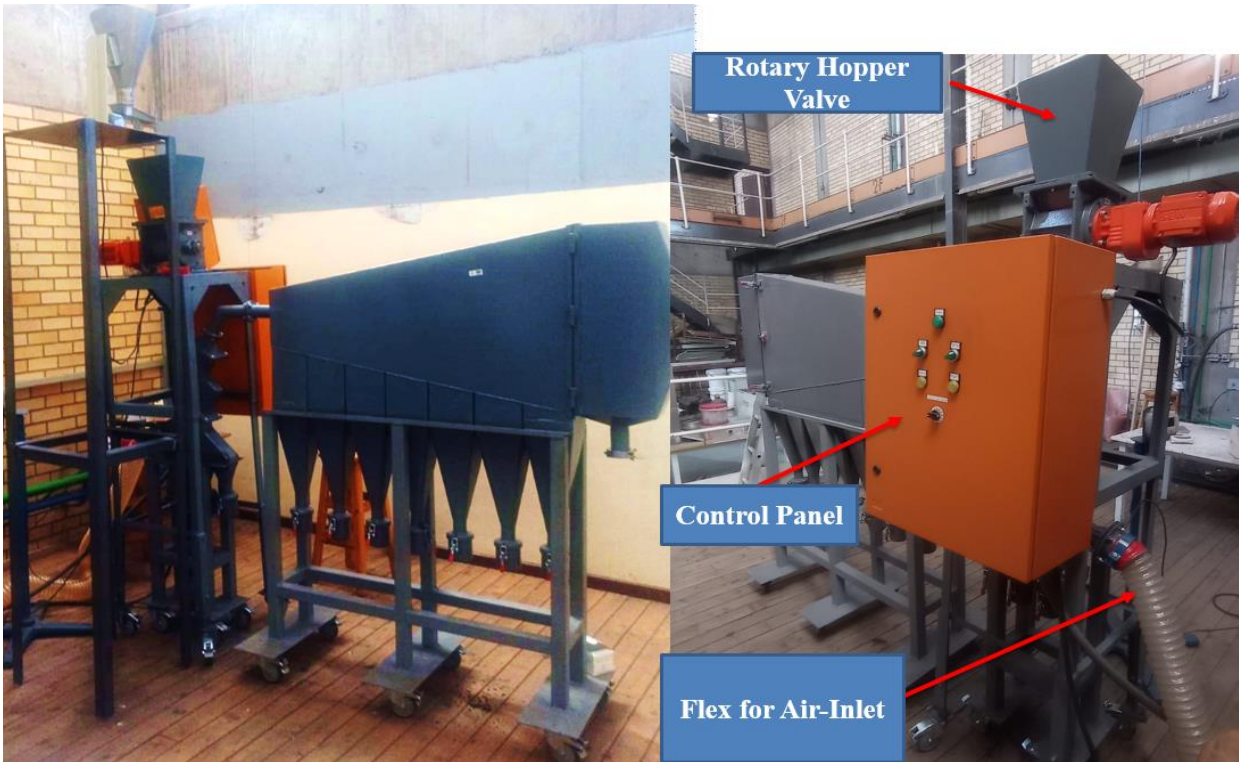

Figure 3.23: The installed separator assembly setup with its auxiliaries and cradles.

Equation 3.18 was used to calculate the wind-sifter separator's efficiency:

$$\%\text{Yield} = \left(\frac{Total\ mass\ of\ coal\ collected\ in\ the\ coal\ bins\ of\ the\ second\ chamber}{Total\ Mass\ of\ Coal\ feed}\right) \times 100$$

(Equation 3-18)

Comparisons were made between the simulation test results, the fabricated laboratory scale separator and that obtained from the float-sink tests (for coal A). The evaluations were then made in terms of their respective mass yield and separation efficiency and the extent to which the separator can beneficiate (ash content).

3.4.2. CALIBRATION OF THE COAL FEEDER

A vibratory feeder was used to feed the coal into the separator. It is important to note that the vibratory feeder was calibrated by increasing its 'carrier frequency', while 200 g of representative feed coal was fed into the chute of the vibratory feeder assembly, as shown in Figure 3.24.

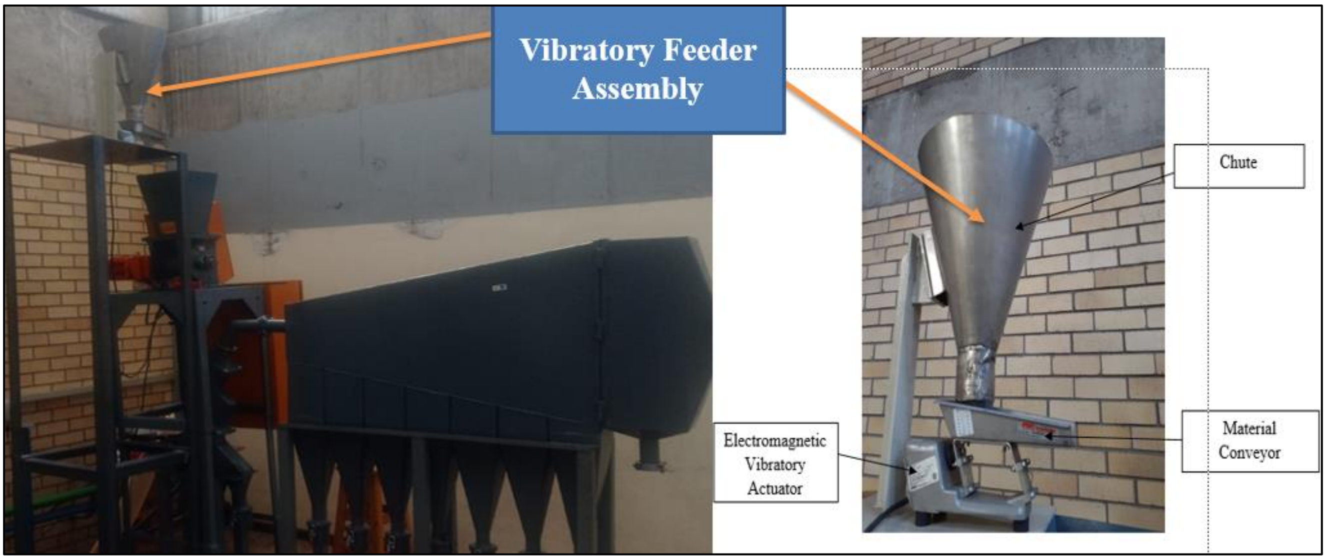

Figure 3.24: The vibratory feeder assembly

The time that it takes for the coal to be completely fed into the system is recorded, and mass flowrate is derived by dividing the mass of the feed by the time it takes for the feed to be completely fed into the separator. The feed rate of the system can be varied with changes to the vibration intensity and carrier frequency from the electromagnetic actuator of the feeder.

3.5. SINK AND FLOAT ANALYSIS

The sink and float laboratory scale test, deployed in accordance with the ASTM-D4371 and ISO 7936:1992 standards, was used to beneficiate samples from coal A and coal B at (−6.7+3.35 mm), (−3.35+1.0 mm) and (−1.0+0.2 mm) at different RDs. The float and sink analysis entails the use of a heavy medium solution to partition particles based on the solution's RD. Zinc chloride was used as a medium of separation, and the washability data obtained was used as a benchmark to compare against the designed separator to ascertain its separation efficiency. The test was conducted at six RDs ranging from 1.8 to 1.3 (in 0.1 decrements), with the sinks in the 1.8 RD solution considered as the sink of the test.

Already prepared zinc chloride solutions in six 5 L beakers ranging from 1.8 to 1.3 g/cm^3 at 0.1 intervals were used as the heavy medium for 500 g ROM coal samples for all the test work. The density of the solution was determined using a digital density metre with a buffer solution of high concentration, also prepared to account for any decreasing RD in any of the solutions. The 500 g ROM coal sample was added stage-wise into the first solution of 1.8 RD, and 3:1 (medium: ore) was maintained, agitated for a few minutes, and allowed to stand for separation to take place. As the separation was achieved, the light-density particles floating on the medium's surface were collected using a sieve, drained to remove the excess zinc chloride, and then poured into the beaker of 1.7 RD. The same process is repeated for each solution with the floats collected and poured into the next until the floats of the 1.3 RD solution are obtained.

The results attained were used to construct a washability profile, which is a plot of RDs against the cumulative mass for the individual fractions. Equations 3.19 to 3.29 were used to find the percentage yield of the clean coal products for the three size fractions.

% Float recovery = $\left(\frac{Mass\ of\ recovered\ at\ specific\ relative\ density}{Total\ Mass\ of\ Coal\ feed\ (500\ g)}\right) \times 100$ (Equation 3.19)

Float analysis (wt. %) = $\left(\frac{Mass\ of\ product\ recovered\ at\ specific\ density\ fraction}{Total\ Mass\ of\ the\ Coal\ product}\right) \times 100$

(Equation 3.20)

Sink analysis (wt. %) = $\left(\frac{Mass\ of\ coal\ discard\ at\ specific\ density\ fraction}{Total\ Mass\ of\ Coal\ reject}\right) \times 100$

(Equation 3.21)

% Float of the feed $\left(\frac{Mass\ of\ product\ recovered\ at\ specific\ density\ fraction}{Total\ mass\ of\ coal\ feed}\right) \times 100$

(Equation 3.22)

% Sink of the feed = $\left(\frac{Mass\ of\ coal\ discard\ recovered\ at\ specific\ density\ fraction}{Total\ mass\ of\ the\ coal\ feed}\right) \times 100$

(Equation 3.23)

% Yield = $\left(\frac{Total\ mass\ of\ the\ Coal\ product}{Total\ Mass\ of\ Coal\ feed}\right) \times 100$ (Equation 3.24)

Reconstituted feed = $Floats\ \%\ of\ feed + Sinks\ \%\ of\ feed$ (Equation 3.25)

Nominal Relative Density (RD) $= Average\ R.D.per\ density\ fraction$

(Equation 3.26)

Partition coefficient $= (Sinks\ \%\ of\ feedReconstituted\ feed) \times 100$

(Equation 3.27)

Organic efficiency (%)= $\left(\frac{Actual\ yield\ at\ specific\ ash\ content}{Theoretical\ yield\ at\ specific\ ash\ content}\right) \times 100$

(Equation 3.28)

The separation efficiency of the process was determined by calculating the mean probable error (E_p) using Equation 3.29.

$E_p = \frac{D_{75} - D_{25}}{2}$ (Equation 3.29)

Where D_{75} is the RD at which 75% of the particles report to the sinks, and D_{25} is the RD at which 25% of the particles report to the sinks.

3.6. ANALYTICAL TECHNIQUES

Coal analyses, such as proximate analysis, ultimate analysis and calorific value, were conducted to ascertain the physico-chemical properties of the ROM coals and the clean coal products from each bin and from the sink and float fractions.

3.6.1. PROXIMATE ANALYSIS

The inherent moisture, volatile matter, ash content and fixed carbon (calculated by the difference) are determined in accordance with ASTM D7582 – 15 standard, in which 1.0 g of representative sample was added stage-wise in each crucible in the TGA 701 Leco equipment. The proximate analysis entails the use of nitrogen in the first step, which is the drying step. The moisture content was determined by mass loss starting from room temperature (around 20ºC) to 107ºC, as the temperature ramps up at a heating rate of 8ºC/min.

The volatile matter was determined as the mass loss within a temperature range between 107ºC to 950ºC, whereas the combustion step that follows evaluates the mass loss under oxygen between the temperature range of 650ºC and 750ºC. The residual mass left after the analysis is then taken as the total ash content in the sample, while the fixed carbon is calculated as (100−(Moisture content + Volatile Matter + Ash Content)) %.

3.6.2. ULTIMATE AND TOTAL SULPHUR ANALYSIS

The ultimate (carbon, hydrogen, nitrogen, sulphur and oxygen (by difference)) and total sulphur analyses of all samples were performed according to ASTM D 5373-14:2015 and ASTM D 4239-14:2015 for carbon, hydrogen and nitrogen, and sulphur content, respectively, using LECO CHN 628 with add on 628 S module. Approximately 0.25 g of each sample was used for the analyses at a temperature up to 1 450 C with an analysing time between 60 to 300 seconds.

3.6.3. CALORIFIC VALUE DETERMINATION

The calorific value is the measure of the heat content in the coal and was determined in accordance with ASTM D5865-04. This analysis was carried out for some selected samples, particularly the coal samples from bin 1, using a Leco AC 500 bomb calorimeter. The bomb calorimeter calculates the total amount of heat released from the complete combustion of one-unit mass (1 g) of fuel under the oxygen atmosphere at a high pressure of about 3,000 kPa. The temperature was controlled at 25 degrees Celsius by recirculating cooling water in the equipment with the aid of a pump. The system uses an electronic thermometer with an accuracy of 0.0001 0C to measure the temperature every six seconds, with the results obtained within 4.5 to 7.5 minutes.

3.7. SUMMARY

The design of the separator and simulation were carried out to ascertain the dimensions of the separator, which then ultimately led to its fabrication. Coal samples used in this study were screened into three particle size fractions (-6.7+3.35 mm, -3.35+1 mm and -1+0.2 mm). The proposed experimental tests were carried out on the separator, and the results were compared with those from the simulation study. Sink and float tests were also carried out to serve as a basis of comparison for the physico-chemical properties of both the wet and dry beneficiation process. The next chapter (Chapter 4) will present the results and discussions of the simulation and experimental investigations that were carried out on the separator.

CHAPTER 4: RESULTS AND DISCUSSION

4.1. INTRODUCTION

In this chapter, the results of the simulation and experimental study are presented. The simulation results were used to design and fabricate the optimised wind-sifter separator, and the experimental results were obtained from the fabricated separator. Simulation tests for all the fractions were executed according to the assumptions outlined in Table 3.1 of Section 3.3.2 for both instances of the shape factors (32.5 and 0.03). The shape analysis was carried out for the three-size fractions when the separator's bins were closed (with the bins) and when it was open (without the bins). The values for the shape factor in this study were based on a study conducted by Barreiros et al. (1996), which ranged from 32.5 to 0.03. The upper limit (32.5) provides the least coefficient of drag, while 0.03 (lower limit) provides the greatest coefficient of drag. The effect of the airstream velocity on the three particle size fractions (−6.7+3.35 mm), (−3.35+1.0 mm) and (−1.0+0.2 mm) was also determined during the simulation test work.

Similar to the previous investigation conducted by Alade (2021), the experimental study on this separator was based on the results obtained from the simulation study. The impact of air velocity on the separation performance and ash contents of the products achieved was investigated through experimental studies. The vibratory feeder for the feed sample was calibrated, and the mass flowrates for the test runs were kept constant and low to maintain a dilute phase and minimise particle-to-particle interactions that can lead to fines electrification in the separator.

4.2. SIMULATION RESULTS

To ensure that the dilute phase was achieved, the simulation study was carried out according to the study by Santos et al. (2011), where a dilute phase of 6.0 g of particles to 11 g of air in the flowing airstream was used. The density of air used during the simulation process was 1.204 kg/m^3 (1.204×10^{-3} g/cm^3) as the air is assumed to be at room temperature (20^{o}C). The mass yield of the separator was determined according to Equation 4.1:

$$Mass\ Yield\ (\%) = \frac{100 \times \mathrm{M_O}}{\mathrm{M_I}} \qquad \text{(Equation 4.1)}$$

Where, $\mathrm{M_O}$ represents the mass of the lighter particles at a cut-point of 1.6 g/cm^3, which flows from the first chamber into the second chamber, and $\mathrm{M_I}$ is the total mass of the particles fed into the separator through the separator coal-feed inlet. Following the condition from the study conducted by Santos et al. (2011), the mass flowrate of the particles was determined using Equations 4.2 and 4.3.

$$Air\ mass\ flowrate = \rho_{air} \times u \times A \qquad \text{Equation 4.2}$$

Where, ρ_{air} is the density of air at 20 ^{0}C, u is the velocity of air entering the separator, and the diameter of the cross-sectional area of the air inlet channel was 100 mm.

$$Particle\ mass\ flowrate = Air\ mass\ flowrate \times \frac{6\ g\ of\ particles}{11\ g\ of\ air} \qquad \text{Equation 4.3}$$

4.2.1. Optimal velocity determination

The optimal airstream velocities for all particle size fractions when the bins were closed were obtained from Alade (2021). The reason for this was that the new separator design, chamber 1, was not too different from the previous design, with only some minor adjustments. Setting the cut-point of 1.6 RD, the airstream velocities were 6.0 m/sec for (−6.7+3.35 mm), 4.2 m/sec for (−3.35+1.0 mm) and 1.7 m/sec for (−1.0+0.2 mm) size fractions.

To determine the optimal velocity for the separation of each size fraction without the bins (open), different airstream velocities were simulated to observe the particles' separation behaviours. For the (−6.7+3.35 mm), airstream velocities from 6.0 m/sec to 12 m/sec were used. It was observed that at 6.0 and 7.0 m/sec, an insignificant yield was realised; however, as the airstream velocity increased, so did the yield. This is because an increase in the airstream velocity also leads to an increase in the buoyant force. To obtain an optimal mass yield for this size fraction (29.46 to 44.97%), the airstream velocity range was between 9.0 and 10.5 m/sec, as seen in Figure 4.1.

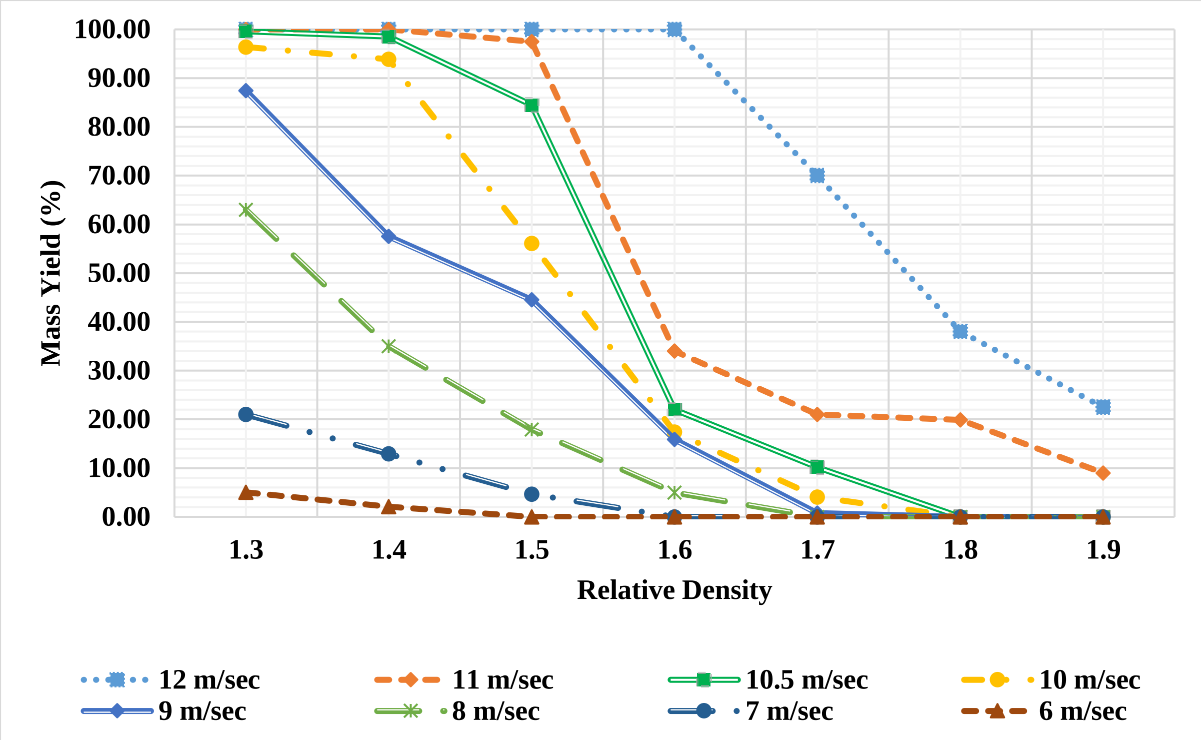

Figure 4.1: Optimal velocity determination for the (−6.7+3.35 mm) size fraction (***open bin***)

A similar investigation was also conducted for the (−3.35+1.0 mm) and (−1.0+0.2 mm) size fractions, the results of which are shown in Figures 4.2 and 4.3, respectively, until their optimal mass yields were attained. The optimal mass yield (30.47 to 44.65%) was obtained at velocities ranging between 5.0 and 7.0 m/sec and was attained for the (−3.35+1.0 mm) for a cut-point of 1.6 RD. The velocity range attained for the (−1.0+0.2 mm) size fraction was between 3.5 and 2.5 m/sec for the same cut-point, with the optimal mass yield of 21.00 to 38.65%.

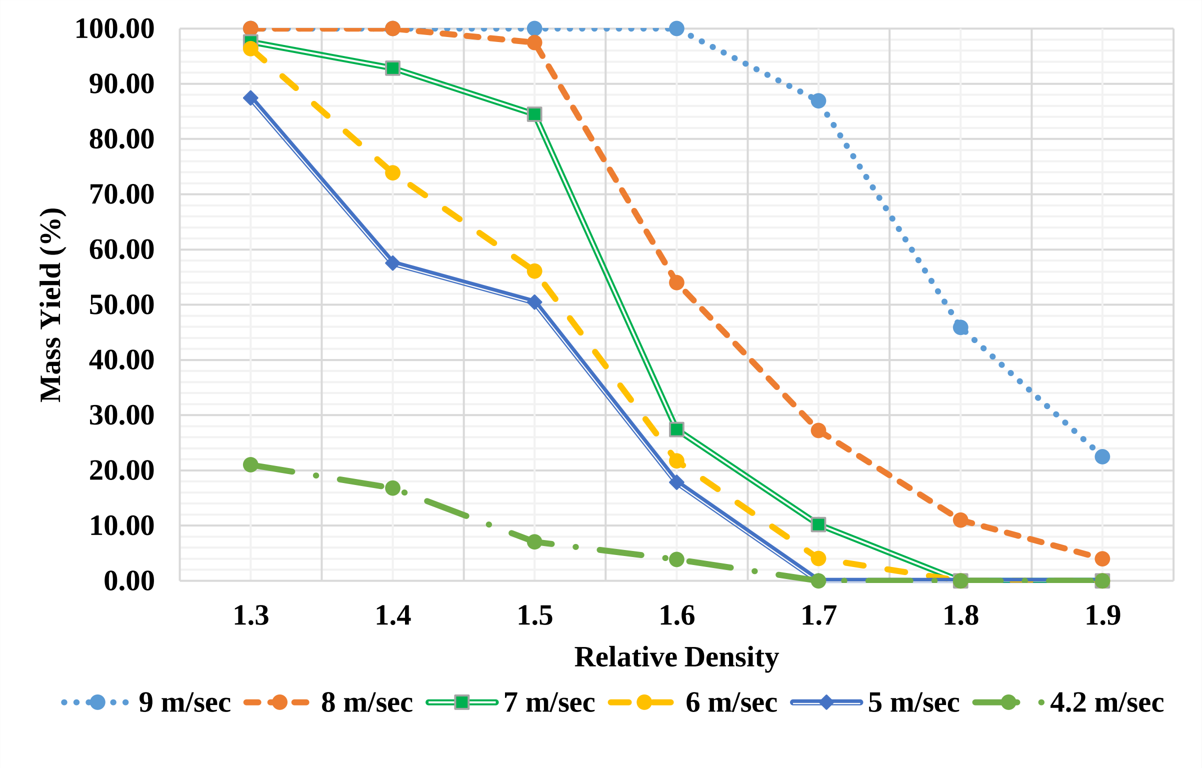

Figure 4.2: Optimal velocity determination for the (–3.35+1.0 mm) size fraction (***open bin***)

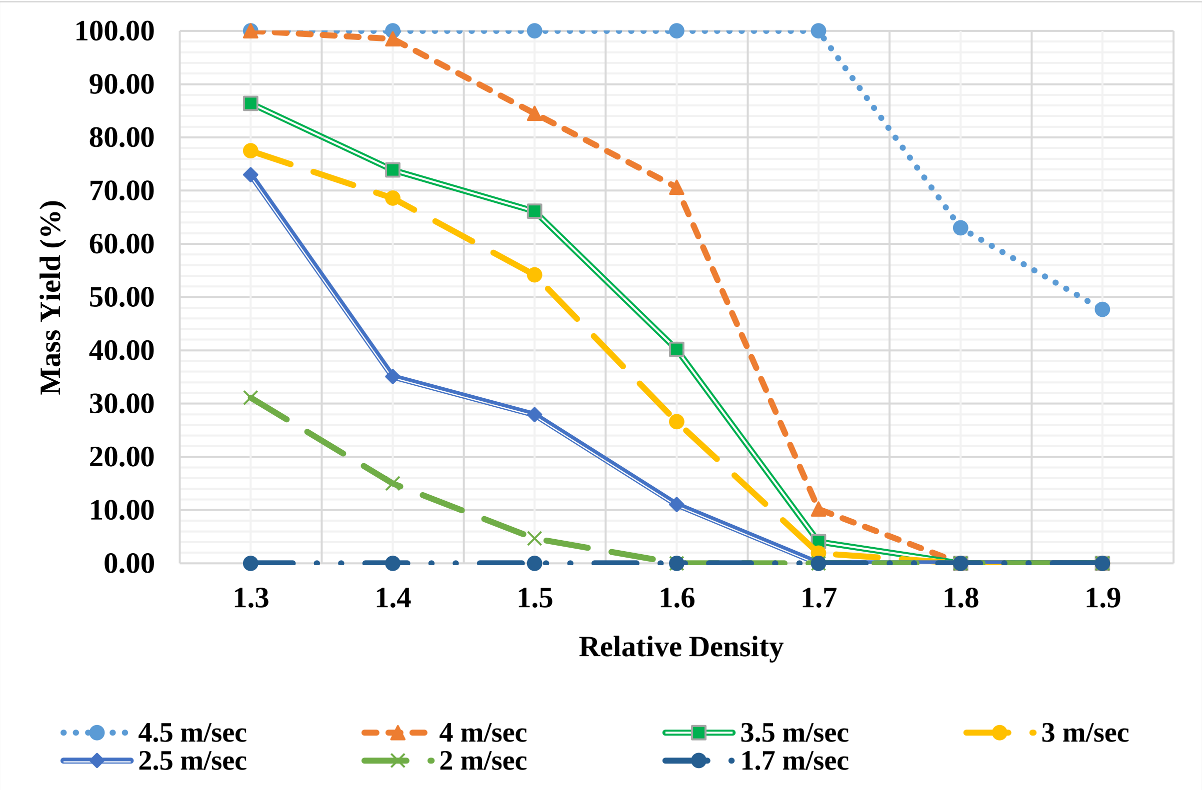

Figure 4.3: Optimal velocity determination for the (–1.0+0.2 mm) size fraction (***open bin***)

4.2.2. Shape analysis (effect of shape factor) based on assumptions

After determining the optimal velocities for all particle size fractions, simulation tests were carried out based on the assumptions earlier stated in section ***3.3.2***. The simulation test results at a shape factor of 32.5 and 0.03, representing the process separation efficiency, are presented in Figures 4.4, 4.5 and 4.6 for all fractions. The bold lines represent the percentage mass yield at a shape factor of 32.5, and the broken lines represent the mass yields at a shape factor of 0.03. Figures 4.4a, 4.5a and 4.6a show the washability or separation process with all the separator's outlet bins closed, while Figures 4.4b, 4.5b and 4.6b show the washability with open bins. Regardless of the shape factor, it was observed from Figure 4.4a that the yield for the (−6.7+3.35 mm) fraction for each RD was the same. When the bins were open, the yields recovered were noticeably different.

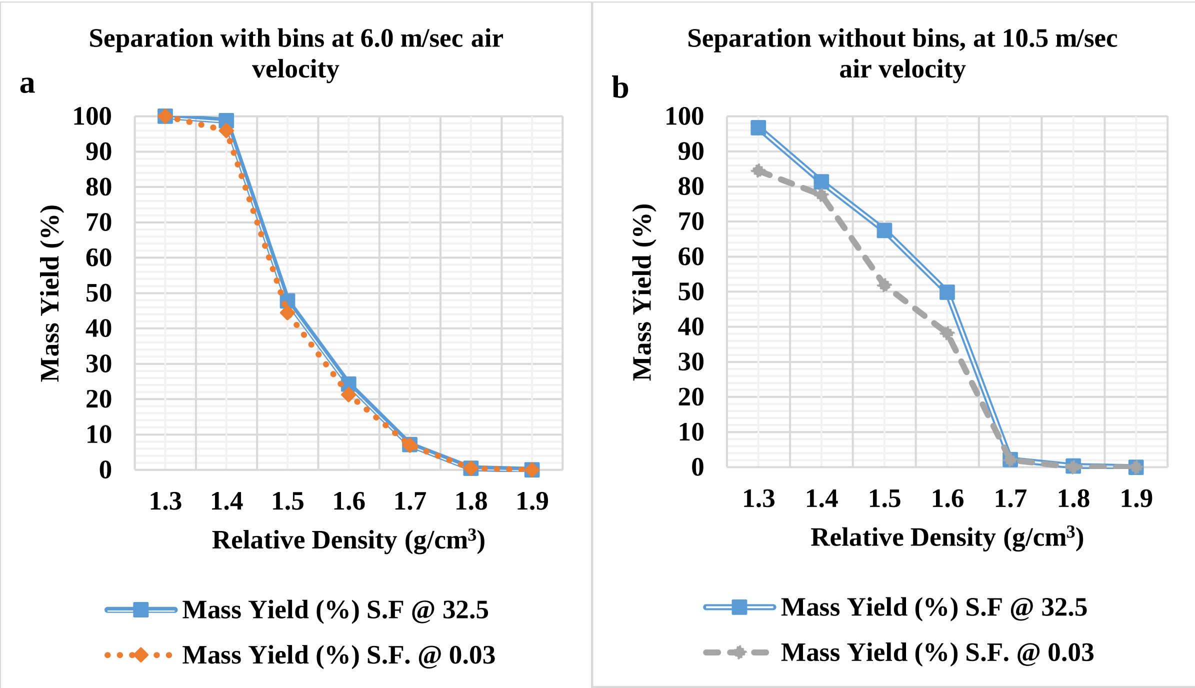

Figure 4.4a and b: Particle recoveries of the (−6.7+3.35 mm) size fraction for both particle shape factors (S.F)

In Figures 4.5a and 4.6a for the (−3.35+1.0 mm) and the (−1.0+0.2 mm) size fractions, respectively, it can be observed that the trend for both shape factors in terms of recoveries is similar for the closed bins. An overlap was observed for the (−3.35+1.0 mm) with an open bin (Figure 4.5b). This was more pronounced in the yields for both shape factors in the coarsest size fraction (−6.7+3.35 mm). It can be concluded that the influence of shape on the mass yield when the bins are closed is not as noticeable as when the separator is operating without the bins. It was observed that the finer the particle size fraction, the less influence the shape factor has on the particles and the mass yield.

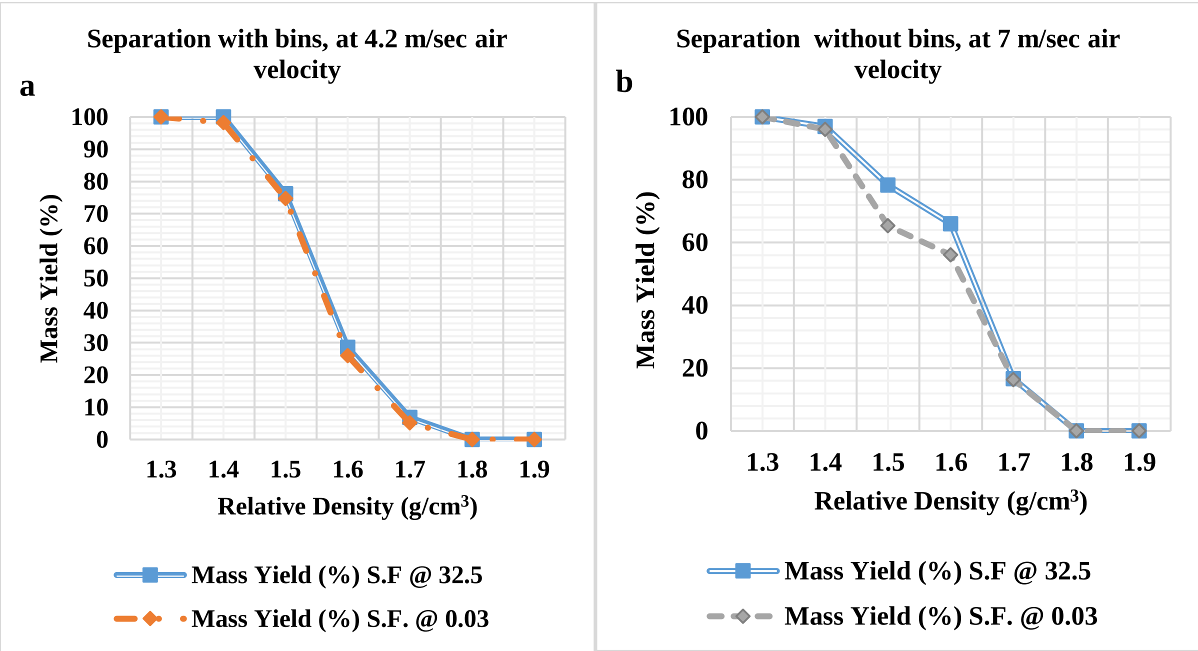

Figure 4.5 a and b: Particle recoveries of the (−3.35+1.0 mm) size fraction for both particle shape factors (S.F).

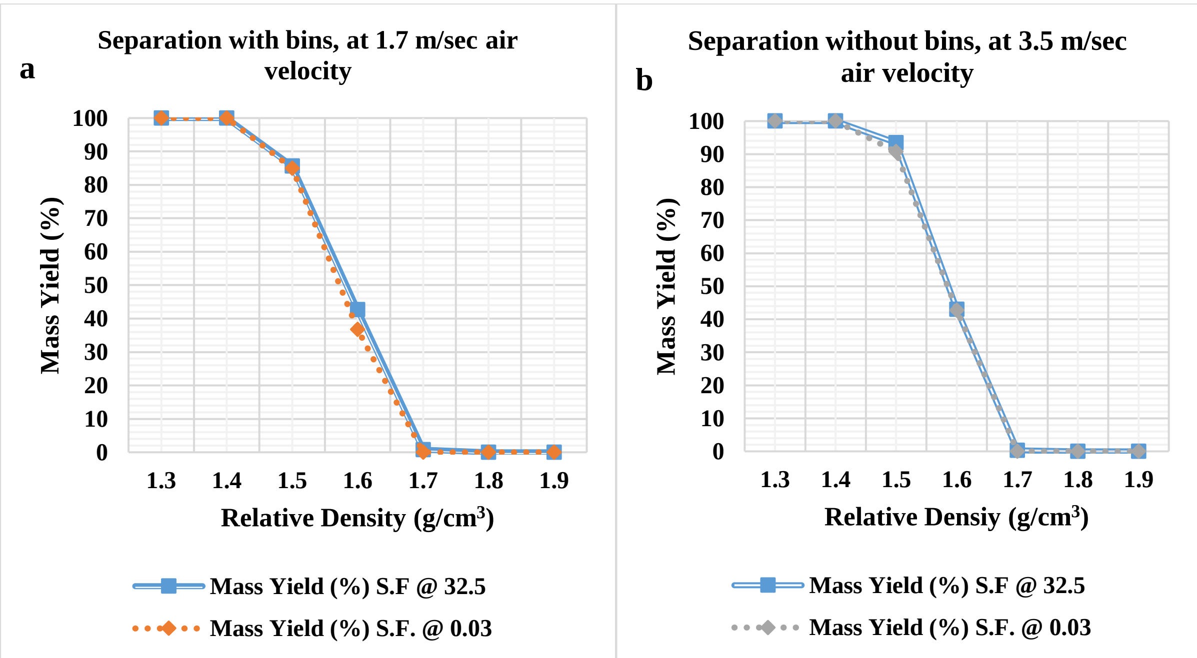

Figure 4.6 a and b: Particle recoveries of the (−1.0+0.2 mm) size fraction for both particle shape factors (S.F)

4.2.3. Particle tracks for the (−6.7+3.35 mm) size fraction at different relative densities and airstream velocities

The particle track presents the particle flow pattern during separation. Figures 4.7 to 4.14 show the particle separation (with and without the bins) for the (−6.7+3.35 mm) fraction. It can be observed that the lighter the particles, the more particles are recovered in chamber 2 (chamber with seven bins). The particle shape factor used to inspect the particle track flow had a shape factor of 32.5, as this will experience a lower drag force. This, in turn, ultimately travels further than those with the 0.03 shape factor. The flow patterns are also similar for the other two size fractions in APPENDIX B.

Figures 4.7 and 4.8 (with and without the bins, respectively) show that the particle flow tracks for the 1.3 RD particles travel the furthest in chamber 2. This is due to the delay in particles achieving their settling velocity as they enter the diffuser chamber. The kinetic energy of the airstream transporting the particles decreases as they enter the diffuser section of chamber 2 due to the expansion of the airstream channel. As the airstream expands, the trajectory of particle flow tends to follow the airflow trajectory as they attain their respective settling velocities. The particles travel further when they are lighter. This means that the 1.3 RD particles, which were the lightest for this study, were transported the furthest by the transporting airstream. Following the same phenomenon, the next step was identifying the 1.4 RD particles, as shown in Figures 4.9 and 4.10 (with and without bins, respectively).

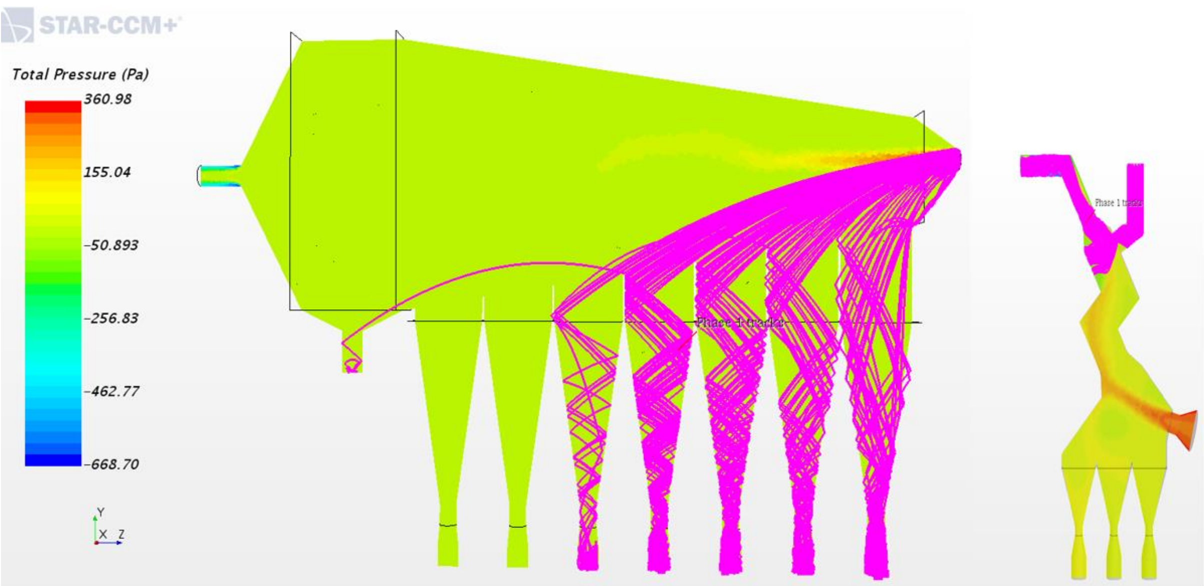

Figure 4.7: Particle tracks for the (−6.7+3.35 mm) size fraction at 1.3 relative density in both chambers at 6.0 m/sec (***closed bins***)

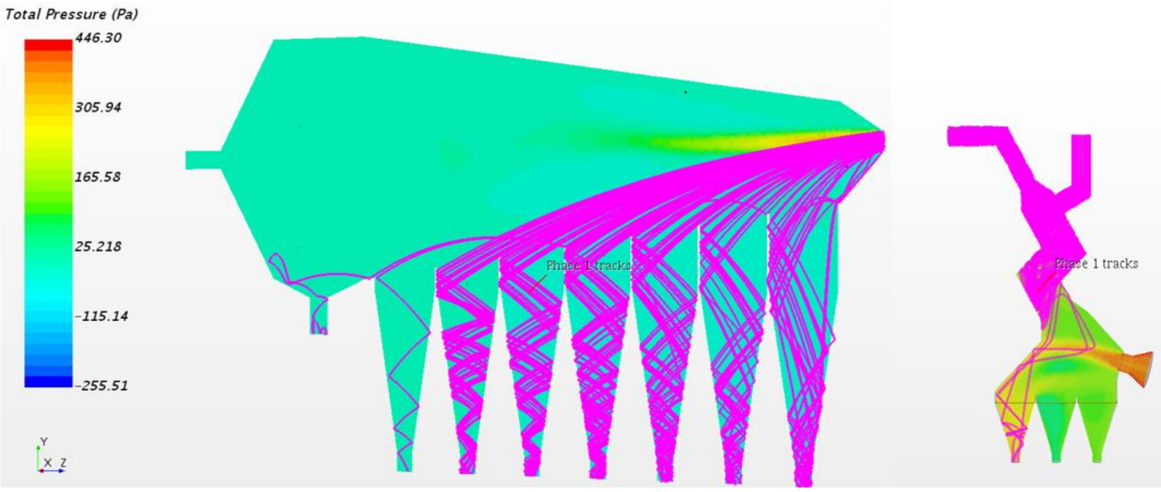

Figure 4.8: Particle tracks for the (−6.7 + 3.35 mm) size fraction at 1.3 relative density in both chambers at 10.5 m/sec (***open bins***)

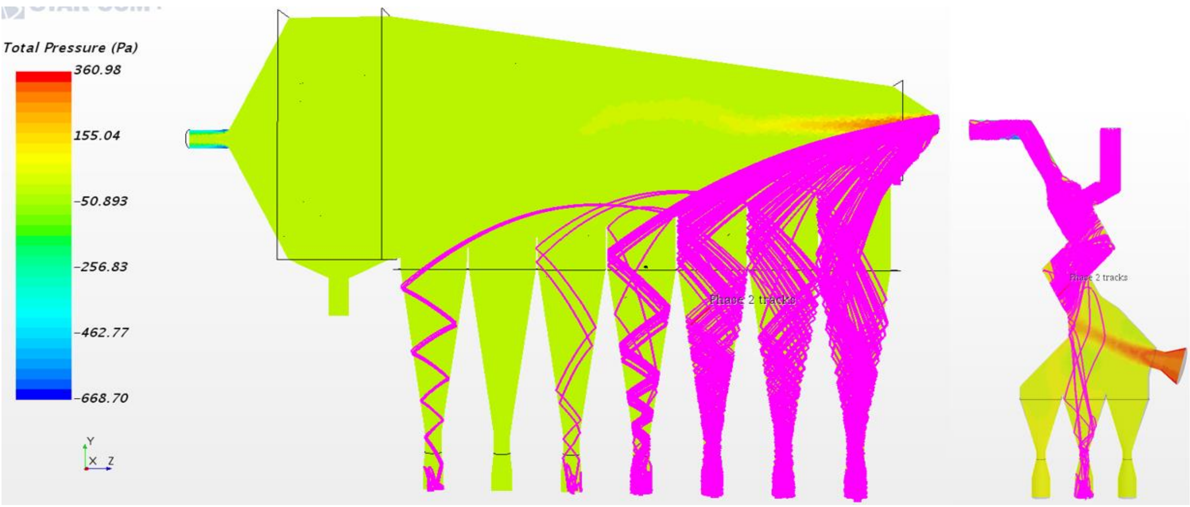

Figure 4.9: Particle tracks for the (−6.7+3.35 mm) size fraction at 1.4 relative density in both chambers at 6.0 m/sec (***closed bins***)

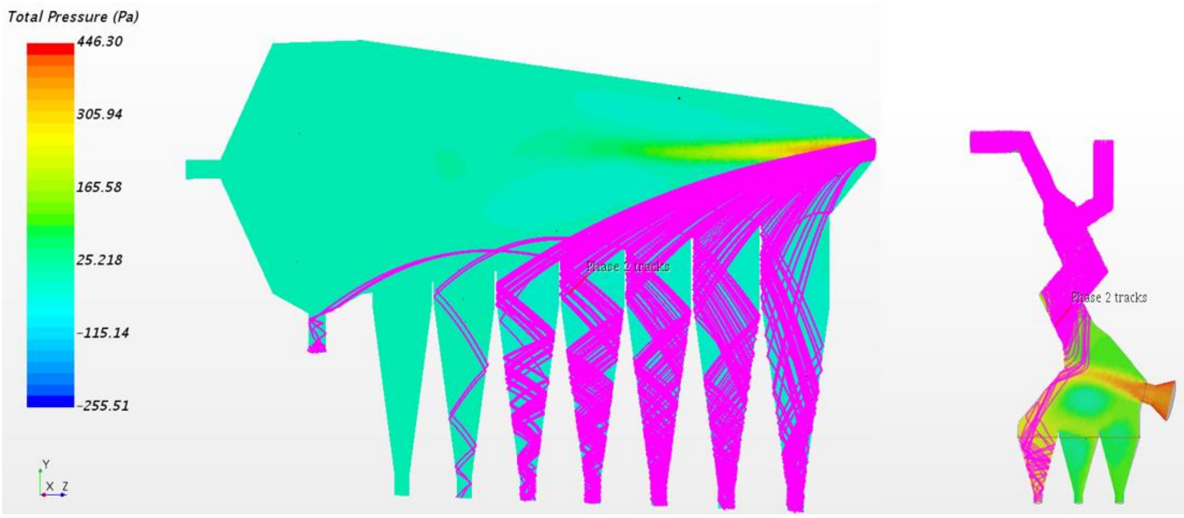

Figure 4.10: Particle tracks for the (−6.7 + 3.35 mm) size fraction at 1.4 relative density in both chambers at 10.5 m/sec (***open bins***)

The particle tracks for the 1.5 RD particles are shown in Figures 4.11 and 4.12 (with and without the bins, respectively), and the 1.6 RD particle tracks are shown in Figures 4.13 and 4.14 (with and without the bins, respectively). A decrease in the sample's yield or collected in the second chamber was observed as the density increased for both open (Figures 4.12 and 4.14) and closed bins (Figures 4.11 and 413). More samples are recovered when the separator is operated without the bins (***open***) than running the separatorwith the bins (***closed***). This result is expected, as an increase in airstream velocity results in an increase in buoyant force, leading to higher elutriation of particles into chamber 2 (from Equations 3 to 8).

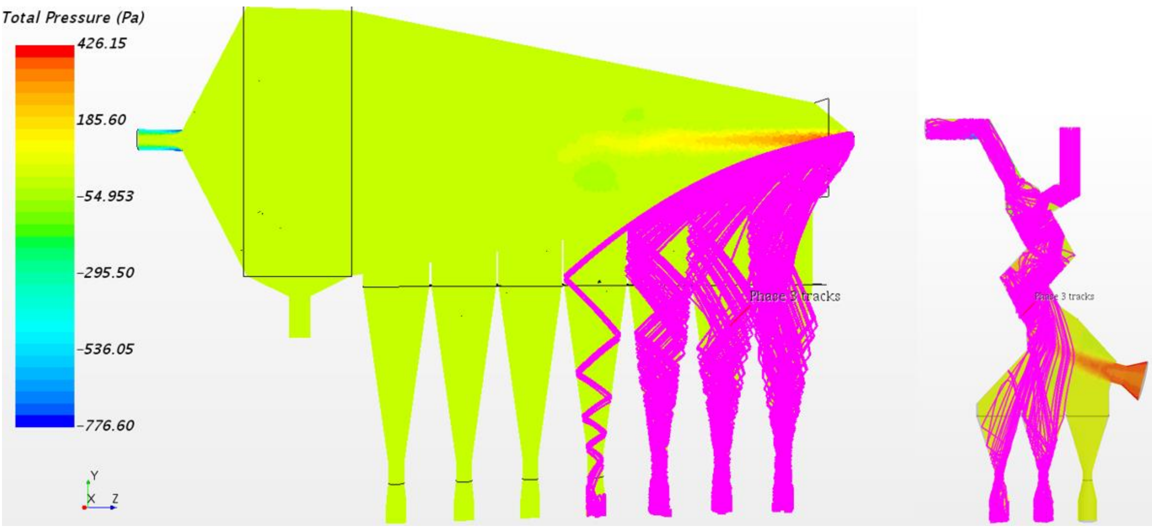

Figure 4.11: Particle tracks for the (−6.7+3.35 mm) size fraction at 1.5 relative density in both chambers at 6.0 m/sec (***closed bins***)

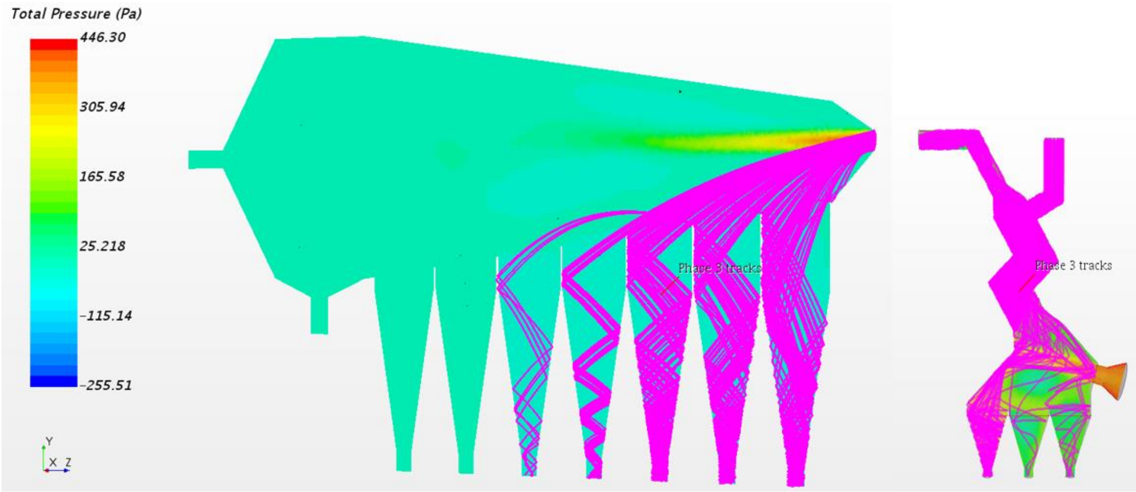

Figure 4.12: Particle tracks for the (−6.7+3.35 mm) size fraction at 1.5 relative density in both chambers at 10.5 m/sec (***open bins***)

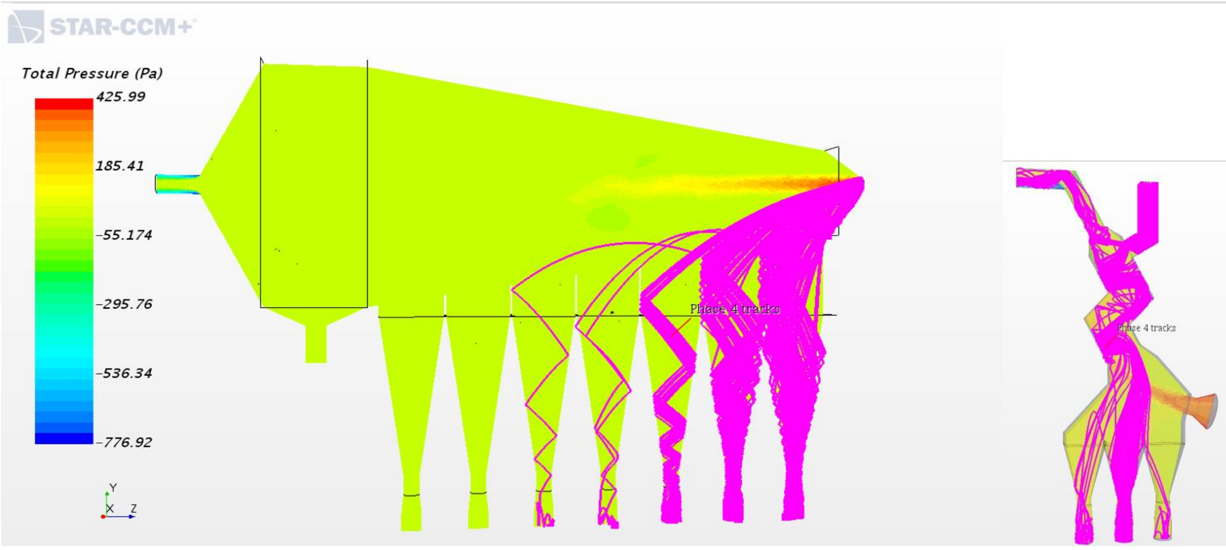

Figure 4.13: Particle tracks for the (−6.7+3.35 mm) size fraction at 1.6 relative density in both chambers at 6.0 m/sec (***closed bins***)

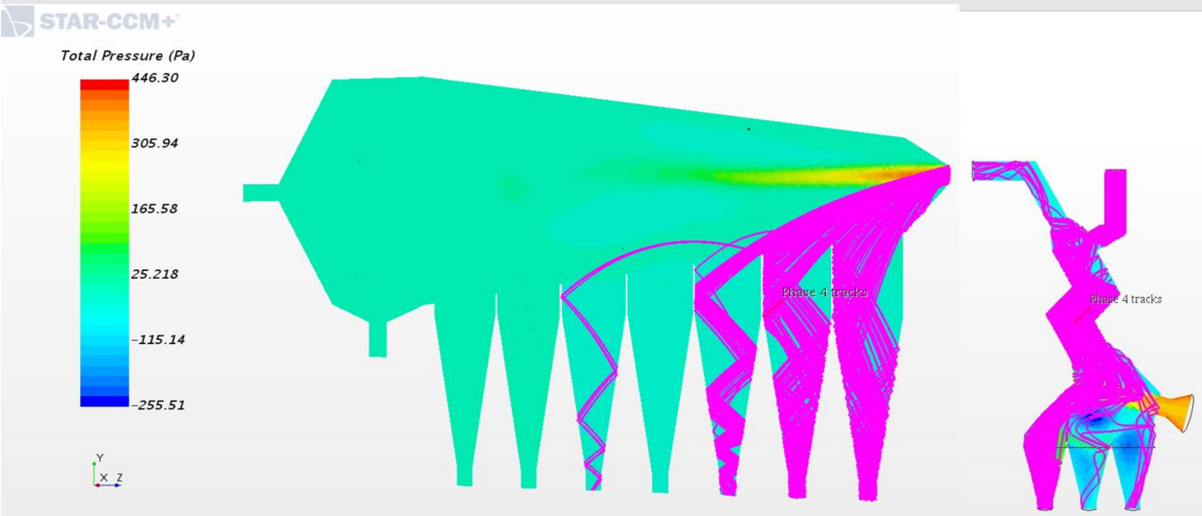

Figure 4.14: Particle tracks for the (−6.7+3.35 mm) size fraction at 1.6 relative density in both chambers at 10.5 m/sec (***open bins***)

4.2.4. Effect of shape factor on mass yield(s) of individual particles within (−6.7+3.35 mm)

From the computer simulator program, each RD within the coal was assigned a size (mm) to simplify the simulation, as seen in Table 3.1 (Chapter 3). This test was carried out to determine the effect of the shape factor at 32.5 and 0.03 on the mass yield(s) of the individual particles within the (−6.7+3.35 mm) size fraction at constant RD and velocity. The simulation results for the (−6.7+3.35 mm) size fraction for the 32.5 and 0.03 shape factor, respectively, for ***closed bins*** and at ***6.0 m/sec*** are shown in Figures 4.15 and 4.16. Figures 4.17 and 4.18 show the simulation results for the same size fraction with an ***open bin*** at ***10.5 m/sec***.

Figure 4.15 shows that particles with a size of 3.35 mm had a 100% mass yield for 1.3 to 1.6 RDs for a shape factor of 32.5. This was not the case for the same 3.35 mm particle size, as seen in Figure 4.16, for a shape factor of 0.03. Only the 1.3 RD particles had a 100% mass yield, while mass yields of 98.45%, 96.10% and 91.95% were achieved for the 1.4, 1.5 and 1.6 RD, respectively. As the individual sizes increase (Figures 4.15 and 4.16), the sample's mass yield for shape factor 32.5 (Figure 4.15) is higher than for shape factor 0.03 (Figure 4.16). For the same size fraction, the yield obtained at a 32.5 shape factor was much higher than the yield at a 0.03 shape factor. This is because the shape influence is more predominant in the coarsest size fraction. In addition, the yield from the 32.5 shape factor particles was much higher than the 0.03 shape factor due to a lower coefficient of drag in the former than the latter with a higher coefficient of drag.

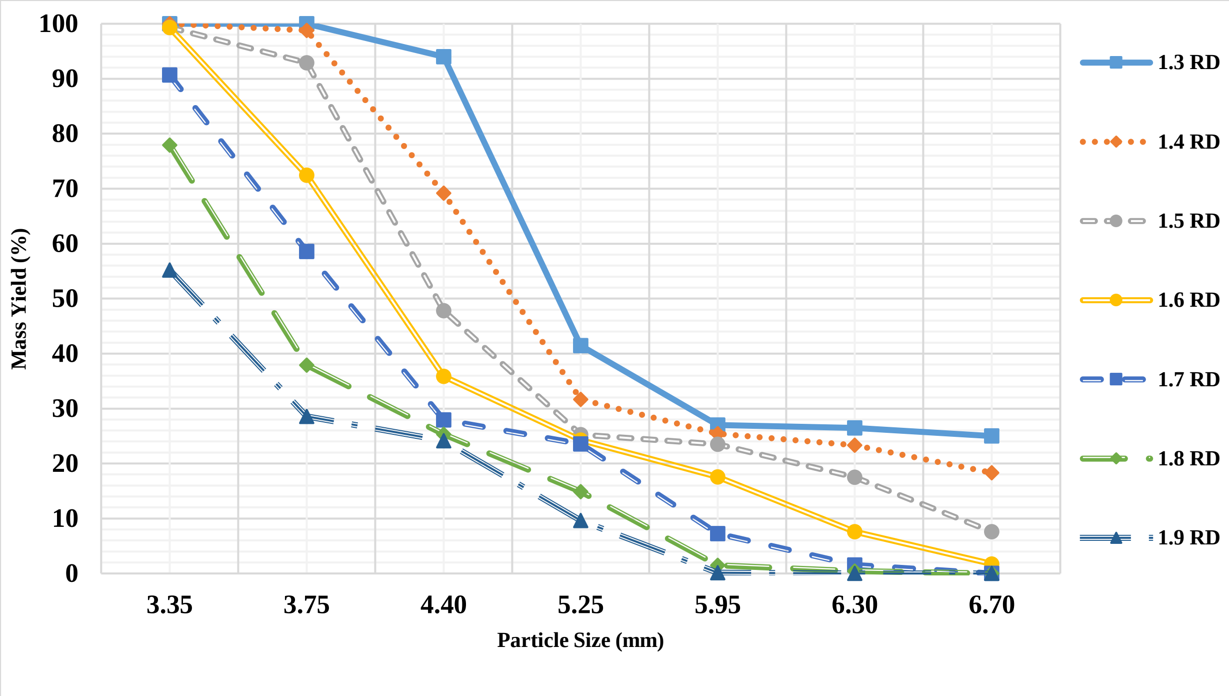

Figure 4.15: Mass yield(s) of individual particles in the particle size distribution of the (−6.7+3.35 mm) size fraction as a function of relative density (for a 32.5 shape factor with bins) at 6.0 m/sec

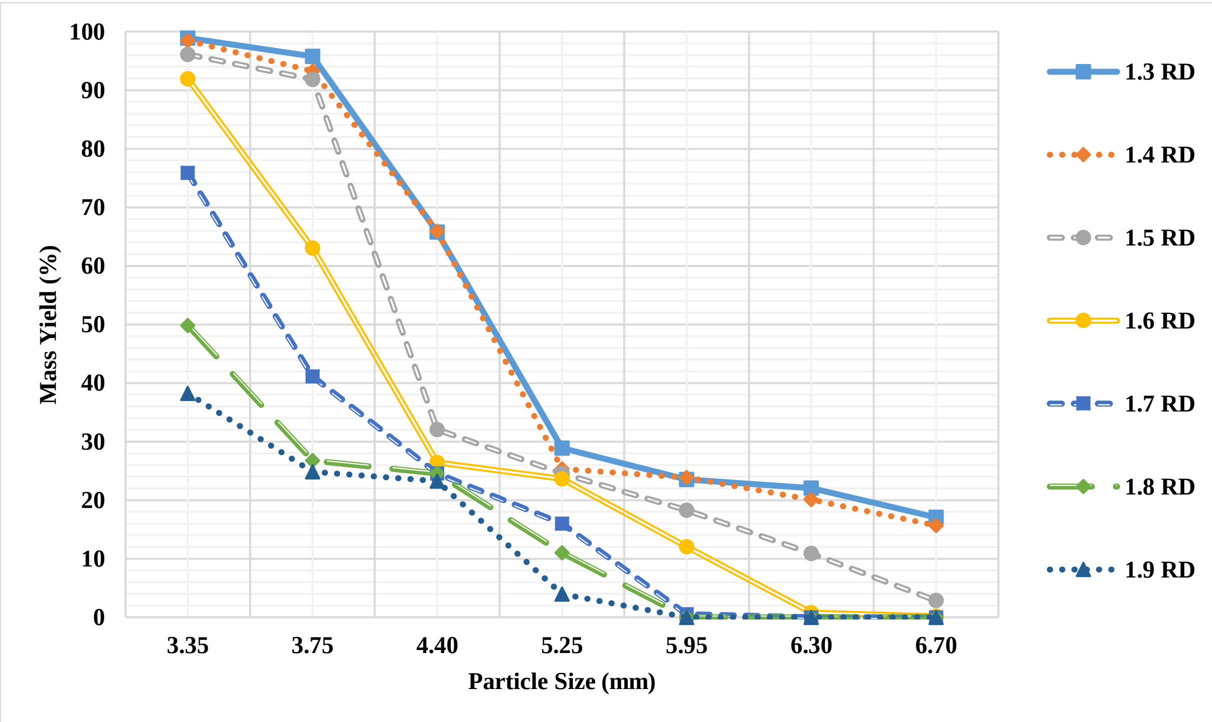

Figure 4.16: Mass yield(s) of individual particles in the particle size distribution of the (−6.7+3.35 mm) size fraction as a function of relative density (for a 0.03 shape factor with bins) at 6.0 m/sec

Figures 4.17 and 4.18 show the results from the simulation test conducted when the separator's outlets were open (without the bins). The separation was simulated at a higher velocity to accommodate for the observed pressure loss. Comparing Figures 4.17 and 4.18, it is apparent that the mass yields at 32.5 shape factor (Figure 4.17) were different from those at 0.03 shape factor (Figure 4.18). The mass yields of the 3.5 mm particle size for relative densities of 1.3 and 1.4 were 99.23% and 97.6%, respectively (Figure 4.17). For the same particle size, the mass yields were 97.29% and 90.12%, respectively (Figure 4.18). The trend was observed for other relative densities in this size fraction (3.5 mm). Considering the impact of the drag coefficient, the test conducted at a lower shape factor (0.03), i.e., higher drag coefficient, resulted in a lower yield (Figure 4.18) than at a higher shape factor (32.5) (Figure 4.17), for the same particle size. The lower mass yield obtained in the ***open bin*** circuit compared to the ***closed bin*** in this study is due to the higher pressure drop in the ***open bin*** circuit, resulting in a decreased buoyant force.

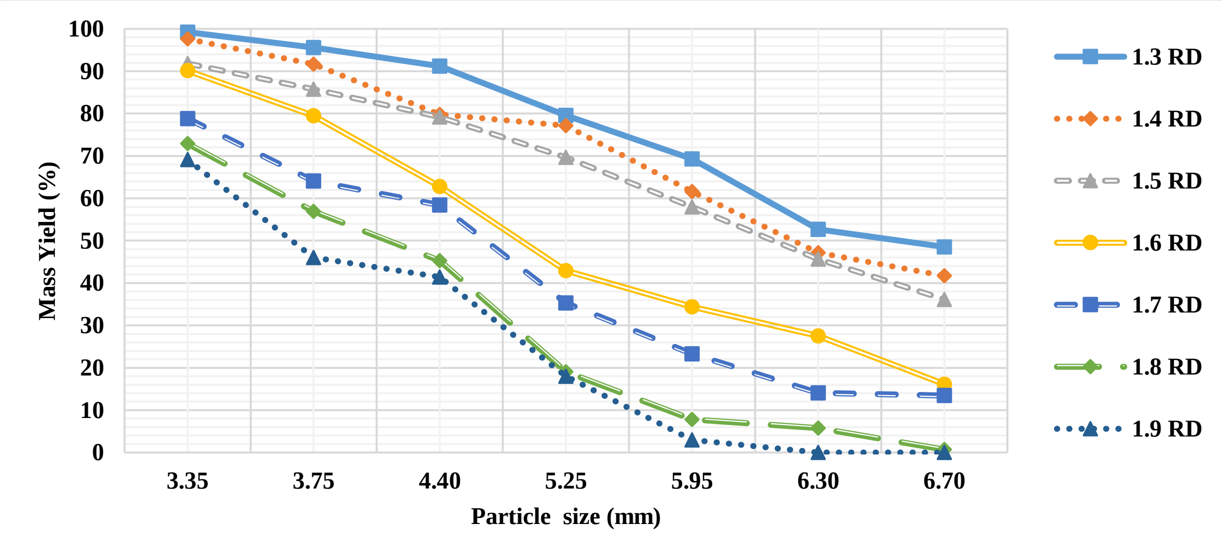

Figure 4.17: Mass yield(s) of individual particles in the particle size distribution of the (−6.7+3.35 mm) size fraction as a function of relative density (for 32.5 shape factor without bins) at 10.5 m/sec

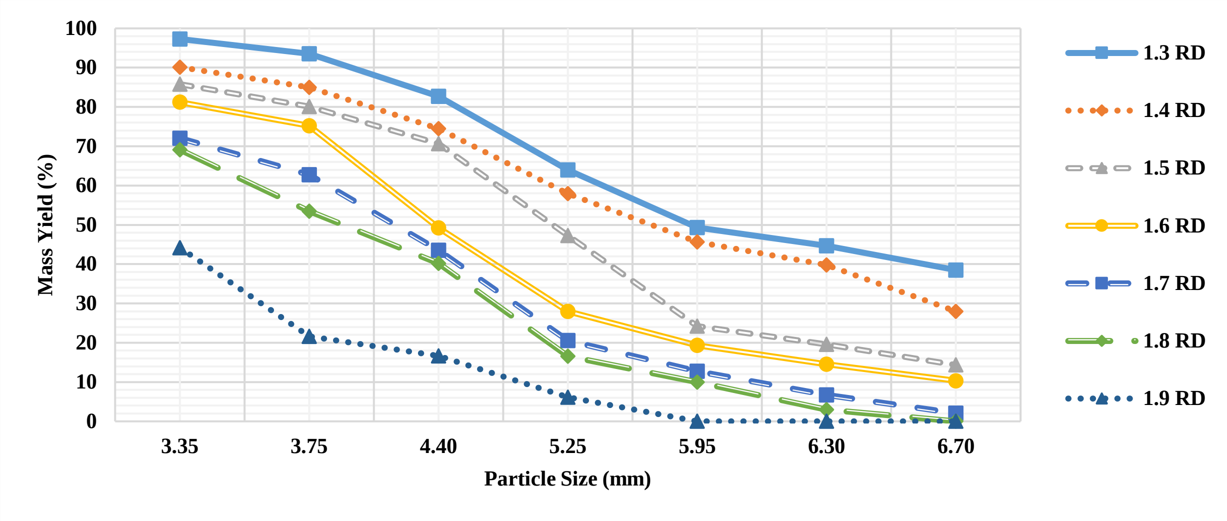

Figure 4.18: Mass yield(s) of individual particles in the particle size distribution of the (−6.7+3.35 mm) size fraction as a function of relative density (for 0.03 shape factor without bins) at 10.5 m/sec

4.2.5. Effect of shape factor on mass yield(s) of individual particles within (−3.35+1.0mm)

Figures 4.19, 4.20, 4.21 and 4.22 show the simulation results for the (−3.35+1.0 mm) size fraction. Figures 4.19 and 4.20 show the results for the 32.5 and 0.03 shape factors, respectively, with a constant air velocity of 4.2 m/sec and ***closed bins*** (with bins). For Figures 4.21 and 4.22 at a 32.5 and 0.03 shape factor, respectively, the test conditions were ***open bins*** (without bins) and 7.0 m/sec. The result obtained follows the same trend as in Figures 4.15 and 4.16. The recoveries of all the individual sizes in Figure 4.19 (the 32.5 shape factor) are much higher than the recoveries in Figure 4.20 (the 0.03 shape factor). In addition, the mass yields of the smallest particle in the particle size fraction (**1.0 mm particle**) in Figures 4.19 and 4.20 are much higher than the smallest particle in the (−6.7+3.35 mm) fraction (**3.35 mm particle**) with closed bins. This occurrence points to the difference in size; as the particle size reduces, so do the weight and drag force, making it much easier for the particles to be transported by the flowing airstream.

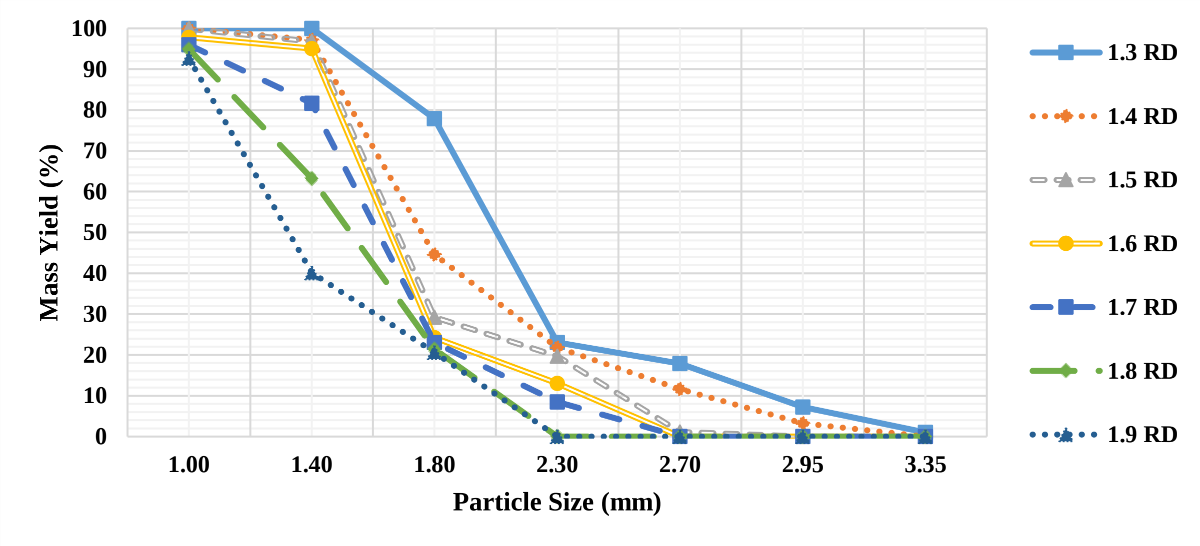

Figure 4.19: Mass yield(s) of individual particles in the particle size distribution of the (−3.35+1.0 mm) size fraction as a function of relative density (for 32.5 shape factor with bins) at 4.2 m/sec

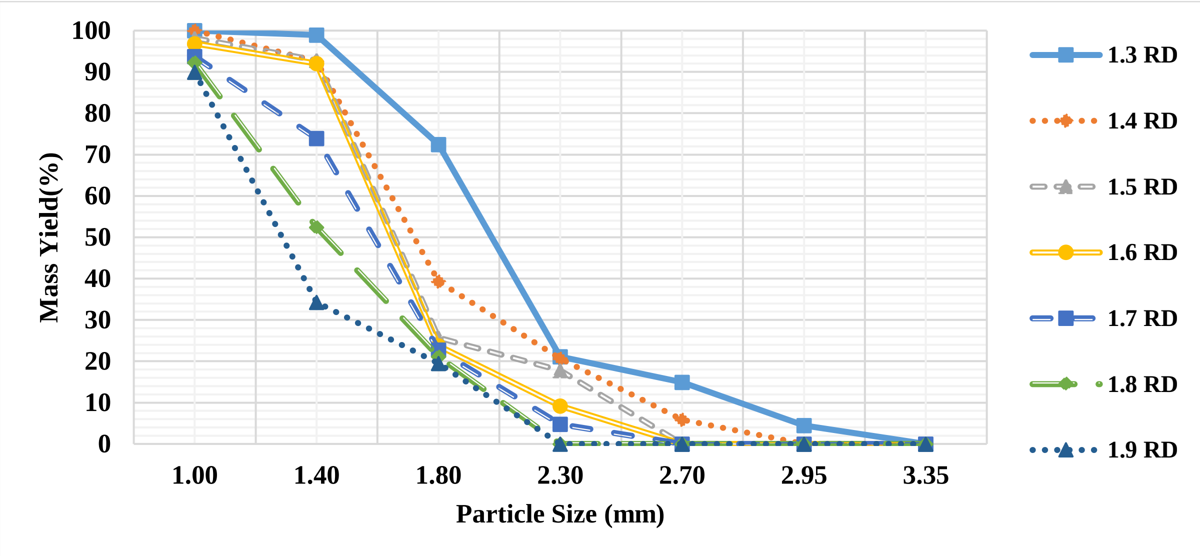

Figure 4.20: Mass yield(s) of individual particles in the particle size distribution of the (−3.35+1.0 mm) size fraction as a function of relative density (for 0.03 shape factor with bins) at 4.2 m/sec

Figures 4.21 (32.5 shape factor) and 4.22 (0.03 shape factor) show the simulated result for ***open bins*** (without bin) for the (−3.35+1.0 mm) size fraction. It was observed in Figure 4.21 a much higher mass yield was experienced compared to Figure 4.22. This follows the same trend as that of the (−6.7+3.35 mm) size fraction without bins (figures 4.17 and 4.18). The shape factor impacts the mass yield obtained for this fraction, but not to the same degree as when the (−6.7+3.3 mm) fraction is separated.

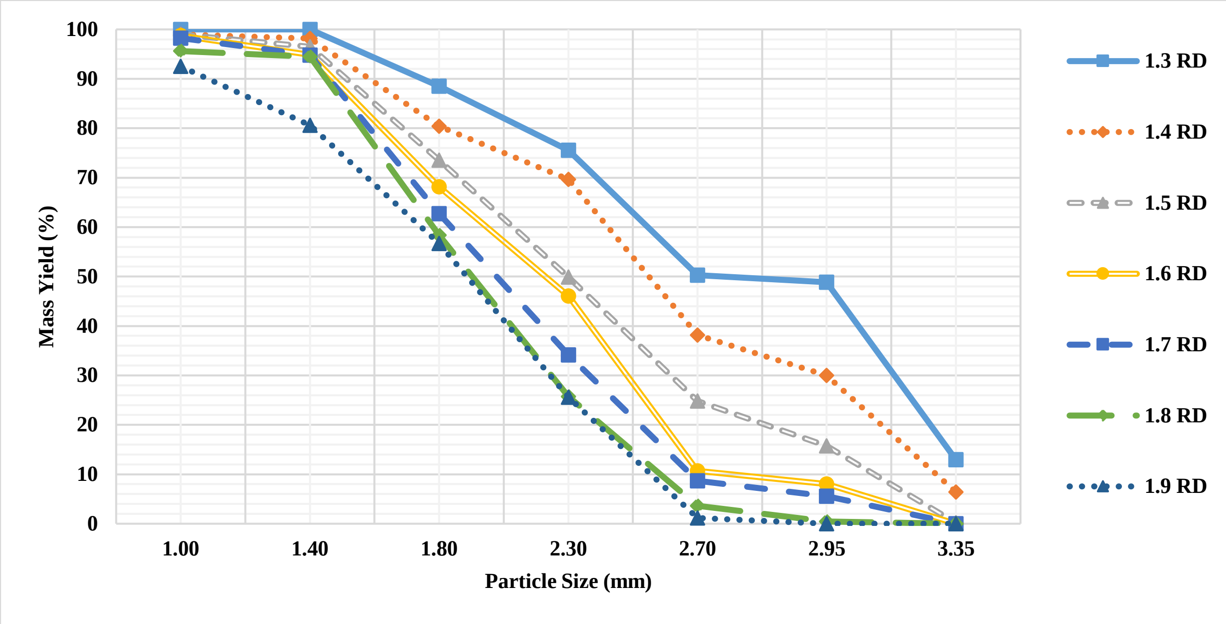

Figure 4.21: Mass yield(s) of individual particles in the particle size distribution of the (−3.35+1.0 mm) size fraction as a function of relative density (for 32.5 shape factor without bins) at 7.0 m/sec

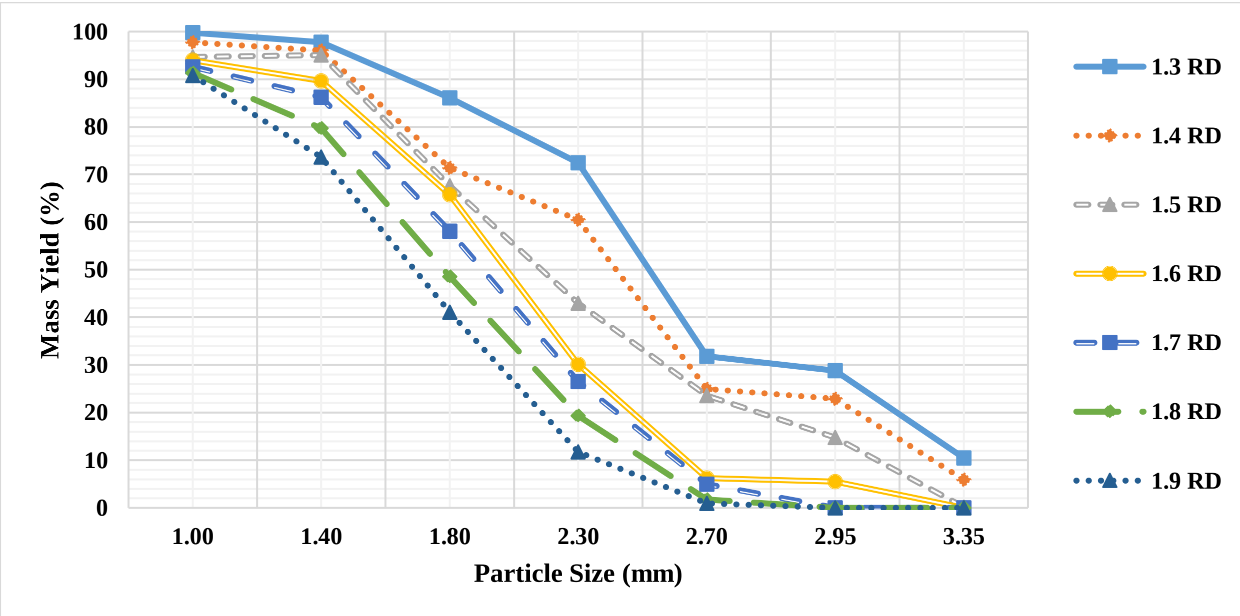

Figure 4.22: Mass yield(s) of individual particles in the particle size distribution of the (−3.35+1.0 mm) size fraction as a function of relative density (for 0.03 shape factor without bins) at 7.0 m/sec

4.2.5. Effect of shape factor on mass yield(s) of individual particles within (−1+0.2 mm)

Figures 4.23, 4.24, 4.25 and 4.26 show the simulation results for the finest particle size fraction (−1.0+0.2 mm). Figures 4.23 and 4.24 show the results for the 32.5 and 0.03 shape factor, respectively, for ***closed bins*** at an air velocity of 1.7 m/sec. The simulation results without the bins (***open bin***) at 3.5 m/sec for the 32.5 and 0.03 shape factors are presented in Figures 4.25 and 4.26, respectively. A 100% mass yield was obtained for particles with a size of 0.2 mm and 0.3 mm at 32.5 and 0.03 shape factors with closed bins (Figures 4.23 and 4.24).

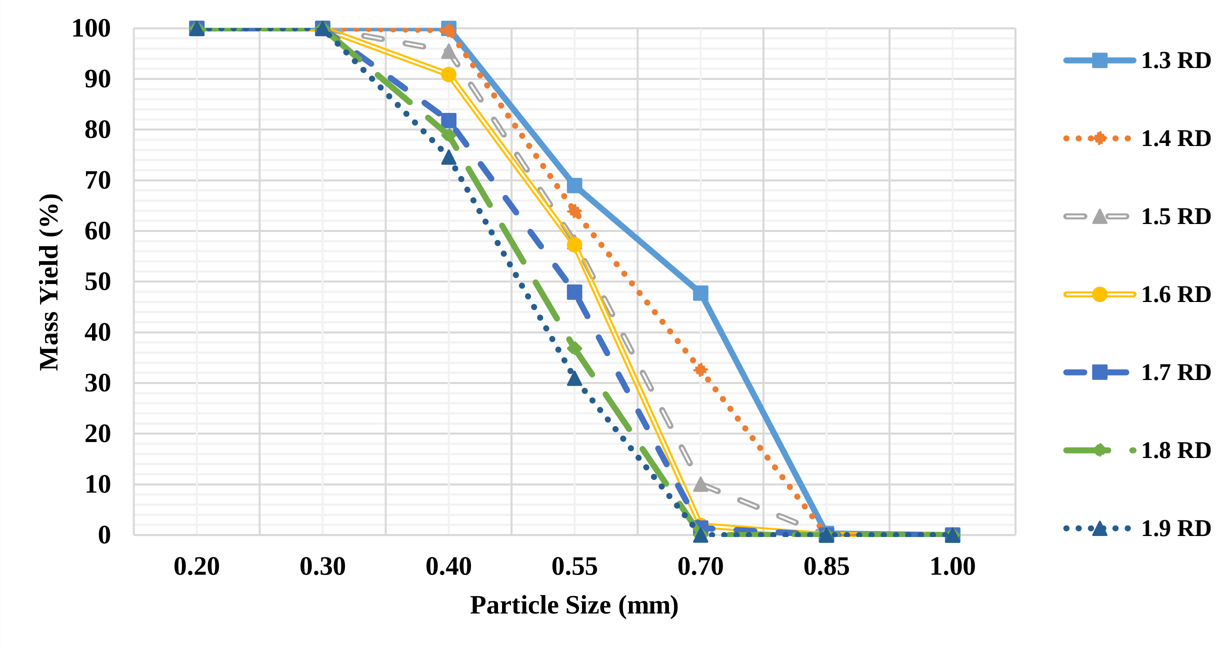

Figure 4.23: Mass yield(s) of individual particles in the particle size distribution of the (−1.0+0.2 mm) size fraction as a function of relative density (for 32.5 shape factor with bins) at 1.7 m/sec

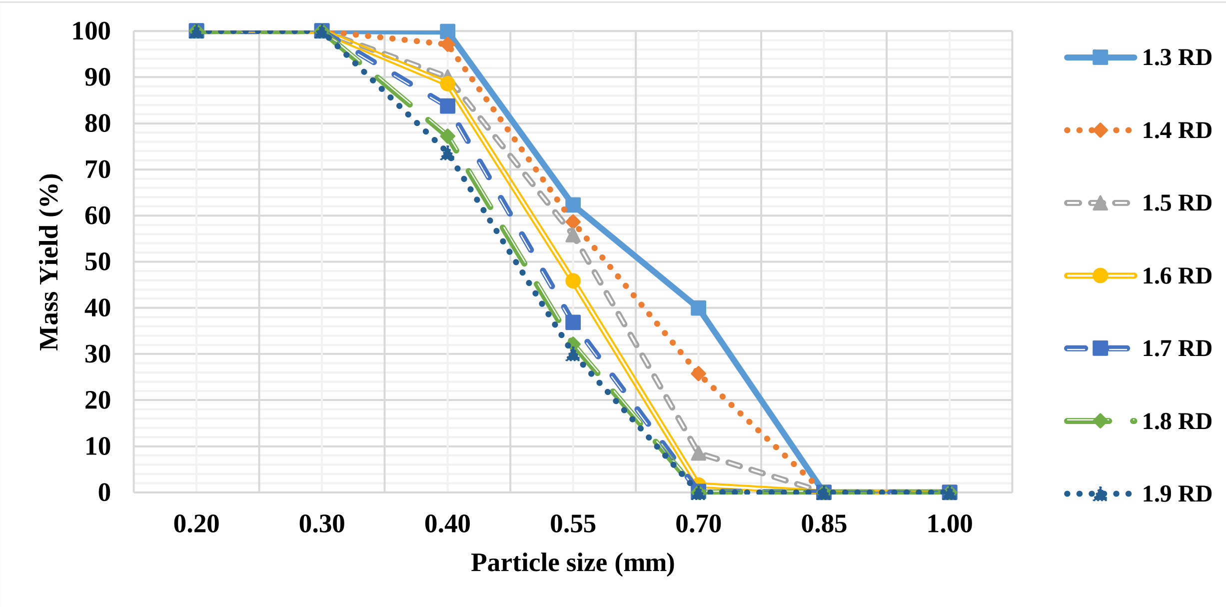

Figure 4.24: Mass yield(s) of individual particles in the particle size distribution of the (−1.0+0.2 mm) size fraction as a function of relative density (for 0.03 shape factor with bins) at 1.7 m/sec

The results from the simulation of the (−1.0+0.2 mm) size fraction without bins for the 32.5 shape factor are presented in Figure 4.25. The yield was higher than that obtained for the 0.03 shape factor (Figure 4.26). The difference in mass yield for the (−1.0+0.2 mm) size fraction (Figures 4.25 and 4.26) was smaller than that achieved for the (−3.35+1.0 mm) size fraction. This is because the influence of particle shape decreases as the particle size decreases. Also, a smaller particle size implies lesser weight and drag force and a higher likelihood of the particle being elutriated by the flowing airstream.

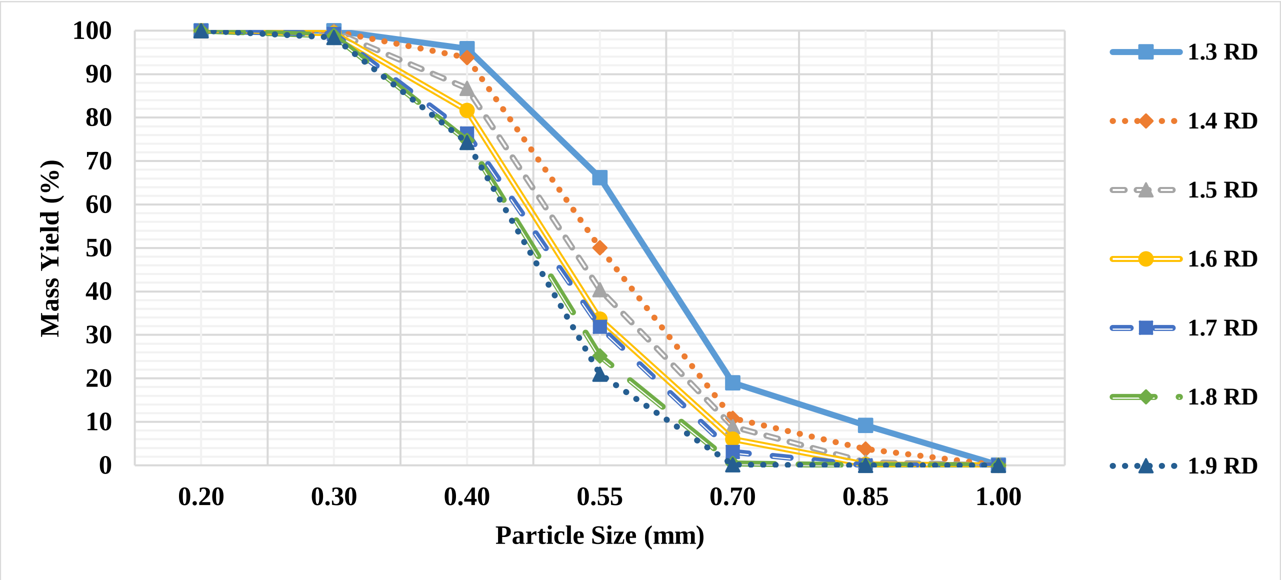

Figure 4.25: Mass yield(s) of individual particles in the particle size distribution of the (−1.0+0.2 mm) size fraction as a function of relative density (for 32.5 shape factor without bins) at 3.5 m/sec

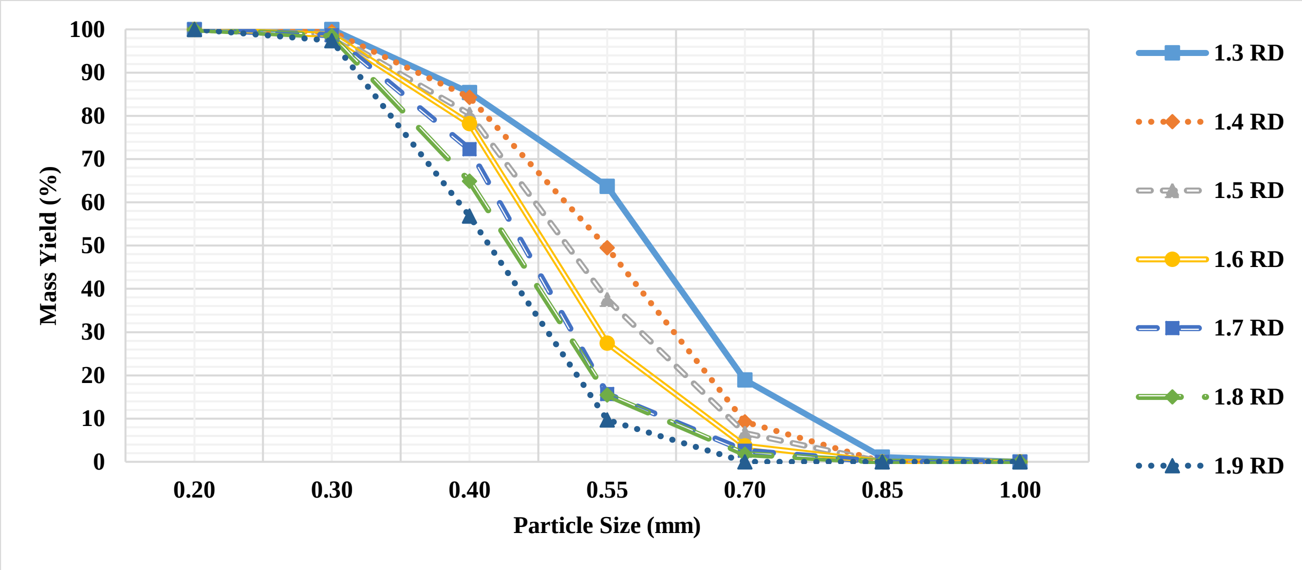

Figure 4.26: Mass yield(s) of individual particles in the particle size distribution of the (−1.0+0.2 mm) size fraction as a function of relative density (for 0.03 shape factor without bins) at 3.5 m/sec

These results show that a particle's density and size play a role in its transportation and separation in an airstream. In addition, it was observed that the shape factor of the particles is highly significant in the separation of coarse particle size fractions and vice versa when the particles are finer. As the particle sizes decrease, the influence of the particle shape on the separation of particles, as well as the mass yield, is less. This is not the case for the sink and float method, which partitions coal particles based on their RD with minimal influence on shape. Section 4.3 summarises why the (−1.0+0.2 mm) particle size was used in the simulation of the separator rather than the (−1.0 mm) size fraction.

4.3. DETERMINATION OF THE PARTICLE SIZE FRACTION (CUT-SIZE) FOR THE (−1 MM PARTICLE SIZE)

Using the previous separator designed and fabricated by Alade (2021), a massive sample loss was observed when beneficiating coal of a size of (−1.0 mm). The smaller particles in this size fraction tended to be constantly entrained in the airstream, and some of them stuck to the walls of the separator. To prevent the issues that were initially encountered in the previous design, it was essential to determine a suitable cut-size for this new design with minimal sample loss. Three particle size distributions (−1.0+0.1 mm), (−1.0+0.15 mm) and (−1.0+0.2 mm) were simulated at 1.7 m/sec air velocity for closed bins and 3.5 m/sec air velocity for open bins. The particle tracks for the cut-size determination are presented in Figure 4.26 (for 0.10 mm), Figure 4.28 (for 0.15 mm) and Figure 4.29 (for 0.20 mm). For all three figures (Figures 4.27 to 4.29),

A represents the particle flow tracks for ***closed bins*** (with bins), while **B** represents the tracks for ***open bins*** (without bins).

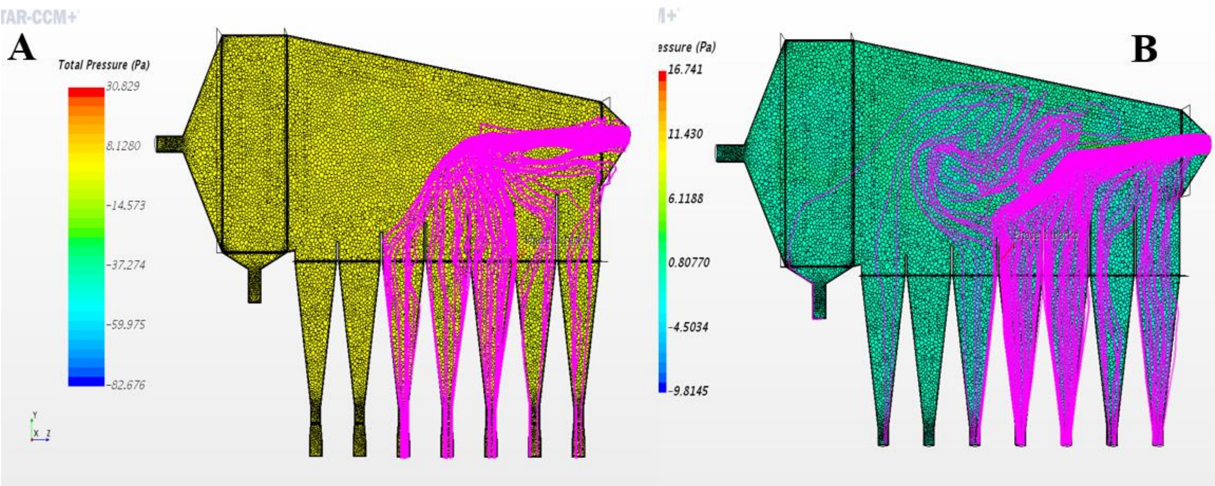

Figure 4.27: Test for 0.1 mm particle for closed (a) and open bins (b)

To determine the cut-size for the (−1.0 mm) size fraction, three different cut sizes, 0.10 mm, 0.15 mm and 0.2 mm [(−1.0+0.1 mm), (−1.0+0.15 mm) and (−1.0+0.2 mm), respectively], were simulated at 1.7 m/sec air velocity with bins and 3.5 m/sec air velocity without bins. The particle density at 1.3 RD was maintained during all experiments to observe the flow of the smallest and lightest particles in the airstream. The particle flow tracks for the cut-size determination are shown in Figure 4.24 (for 0.10 mm), Figure 4.28 (for 0.15 mm) and Figure 4.29 (for 0.20 mm). For all three figures (4.27 to 4.30), **A** represents the particle flow tracks for **closed bins** (with bins), while **B** represents the tracks for **open bins** (without bins). Figure 4.27b indicates that the particles recirculate with the airstream, particularly when the separator bins are open. Figure 4.28 demonstrates that the particles for the separation process were smoother with and without bins. Figure 4.29a displays the particles' flow tracks that settle appropriately, resulting in a cut-size for particle size fraction (−1.0+0.2 mm).

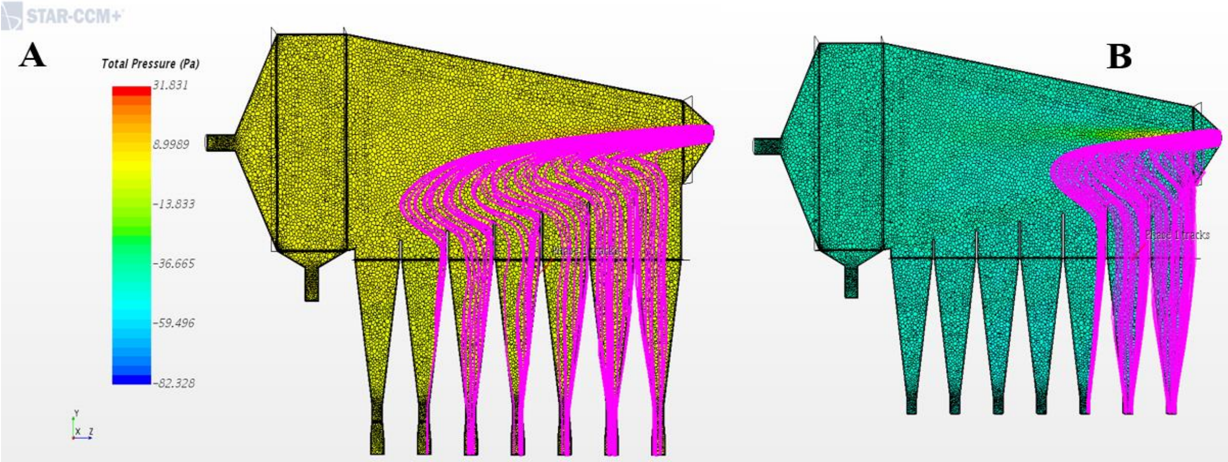

Figure 4.28a and b: Test for 0.150 mm (150 µm) particle for closed (a) and open bins (b)

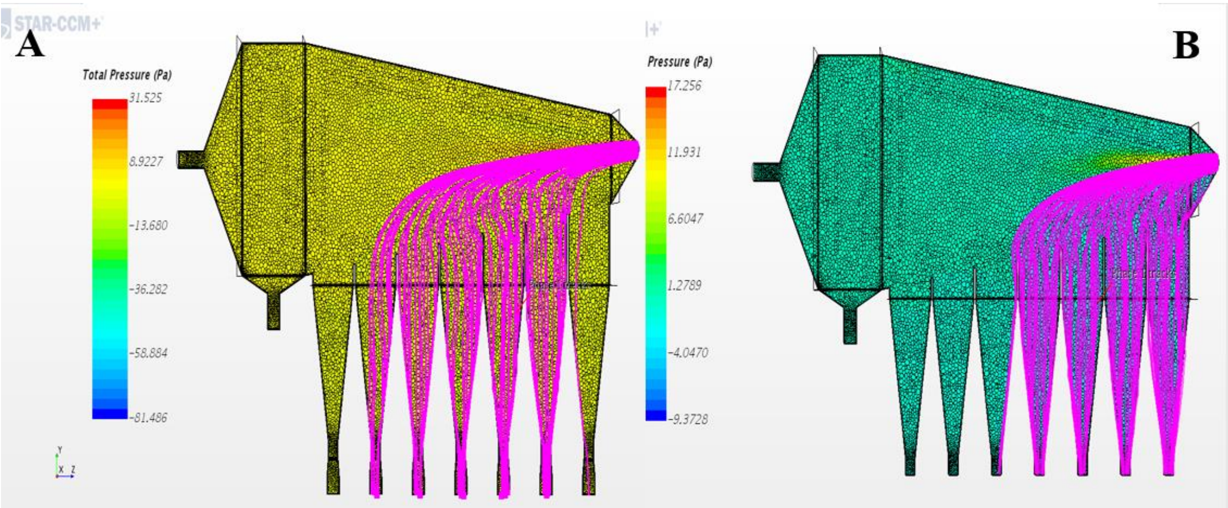

Figure 4.29: Test for 0.2 mm (200 µm) particle for closed (a) and open bins (b)

The results of the wet analysis test conducted to ascertain the degree of separation efficiency of the designed separator for beneficiating coal, as well as the results from the fabricated separator, are presented in section 4.4.

4.4. EXPERIMENTAL RESULTS

4.4.1. Sink and float results for coal A and coal B

The sink and float tests were carried out to beneficiate the as-received two feed coals and compared their results with those from the optimised wind-sifter separator. The washability plot from this test displays the cumulative yield at each RD with their corresponding cumulative ash contents (Figures 4.30 to 4.31). It can be observed in Figure 4.30 that for coal A, the (−1.0+0.2 mm) size fraction has the lowest ash content of 4.29% at 1.3 RD. This is followed by the (−3.35+1.0 mm) size fraction with 5.55% ash content and the (−6.7+3.35 mm) size fraction with ash content of 5.89%. A similar trend was observed for coal B (Figure 4.31);

at RD of 1.3, the lowest ash content was obtained from the (−1.0+0.2 mm) particle size fraction. The reason is that the lower the particle size fraction, the higher the tendency for particle liberation, i.e., the liberation of the inorganic minerals from the organic component of the coal.

It can also be observed from coal A (Figure 4.30) that the cumulative yield of 1.8 RD particles ranged from 59.90% to 73.33% from the coarsest to the finest, which means that the 1.8 RD sinks ranged from 40.10% to 26.67%. For coal B (Figure 4.31), the cumulative yield of 1.8 RD particles ranged from 81.42% to 84.36%, from the coarsest to the finest. This means that the 1.8 RD sinks ranged from 18.58% to 15.64%, from the coarsest to the finest size fraction. The phenomenon indicates coal A has more mineral-rich particles (particles with densities above 1.8 RD) than coal B.

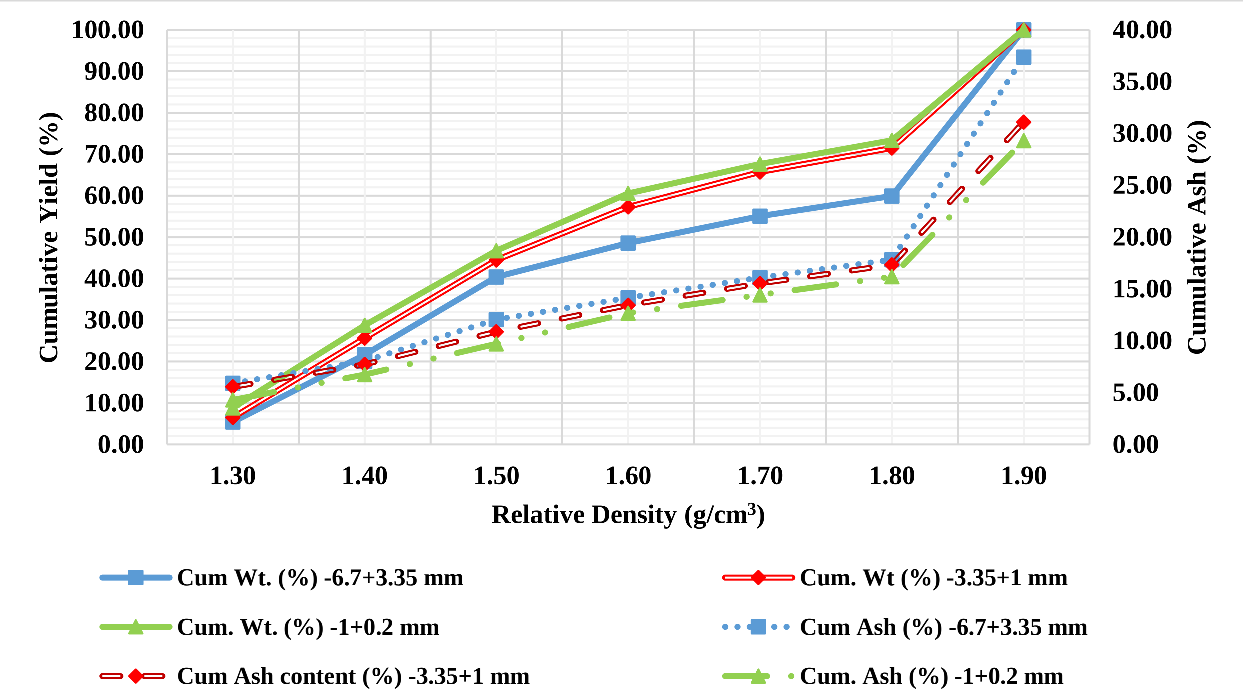

Figure 4.30: Relative density versus cumulative yield (%) and cumulative ash (%) of all three particle sizes (**coal A**)

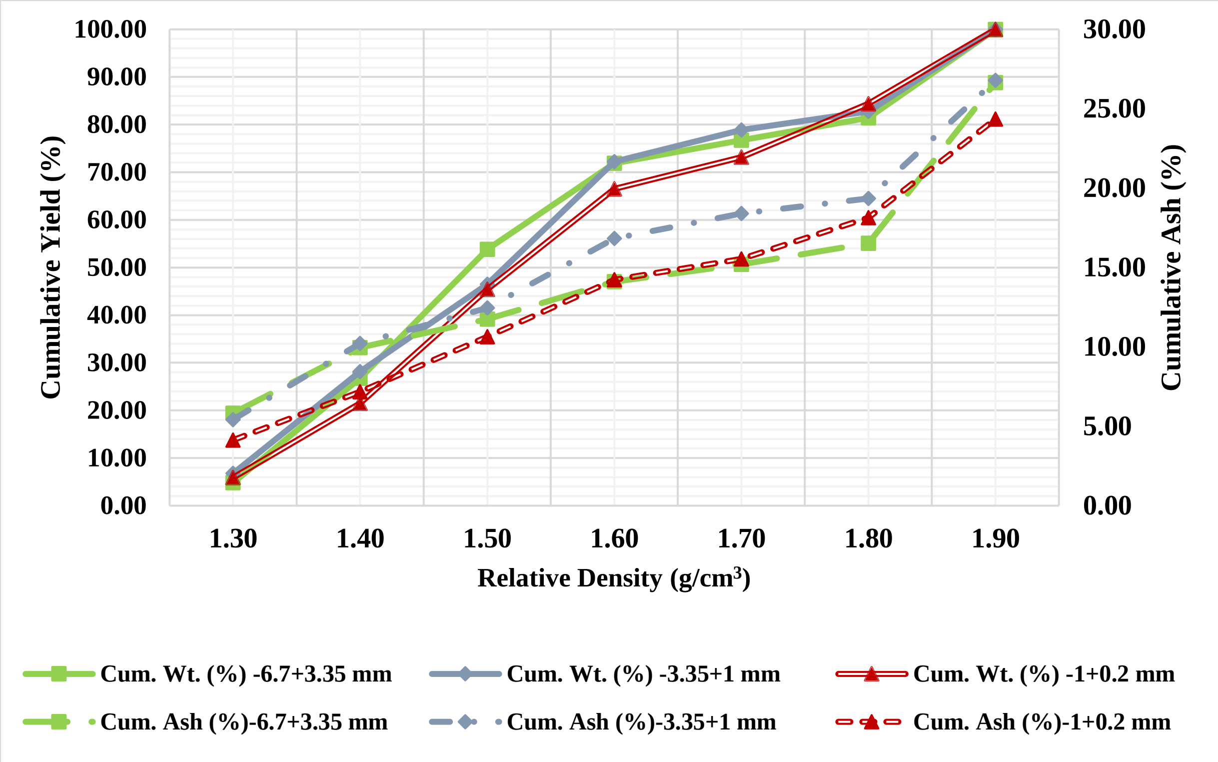

Figure 4.31: Relative density versus cumulative yield (%) and cumulative ash (%) of all three particle sizes (**coal B**)

Table 4.1 depicts the ash content of the raw feed coals for coal A and coal B for the three particle size fractions, and this shows that coal A is of lower grade than coal B. Tables 4.2 to 4.4 give the results of the inherent moisture and ash contents of the sink and float products for both coal samples.

Table 4.1: Ash content for the raw feed coal for coal A and coal B from the sink and float analysis

Particle Size Fraction (mm)	**Coal A**	**Coal B**
–6.7+3.35	37.38%	26.65%
–3.35+1	31.11%	26.78%
–1.0+0.2	29.3%	24.35%

Table 4.2: Results of proximate analysis (air dry basis) for the feed coal of the (−6.7+3.35 mm) particle size fraction

Relative Densities (g/cm^3)	Coal A Moisture Content (%)	Coal A Specific Ash Content (%)	Coal B Moisture Content (%)	Coal B Specific Ash Content (%)
1.3 floats	2.55	5.89	2.03	5.83
1.3 sinks	2.90	8.74	6.06	10.85
1.4 sinks	2.84	16.65	5.00	13.56
1.5 sinks	2.56	24.67	6.94	21.10
1.6 sinks	2.55	30.45	3.21	31.40
1.7 sinks	2.40	37.48	2.74	38.24
1.8 sinks	1.69	66.60	0.98	71.00

Table 4.3: Results of proximate analysis (air dry basis) for the feed coal of the (−3.35+1.0 mm) particle size fraction

Relative Densities (g/cm^3)	Coal A Moisture Content (%)	Coal A Specific Ash Content (%)	Coal B Moisture Content (%)	Coal B Specific Ash Content (%)
1.3 floats	2.91	5.55	3.17	5.43
1.3 sinks	2.90	8.47	4.84	11.74
1.4 sinks	3.22	15.11	5.02	15.89
1.5 sinks	3.02	22.40	6.06	24.76
1.6 sinks	2.55	29.40	2.31	35.27
1.7 sinks	2.40	37.70	1.47	38.50
1.8 sinks	1.69	65.68	1.45	62.52

Table 4.4: Results of proximate analysis (air dry basis) for the feed coal of the (−1.0+0.2 mm) particle size fraction

Relative Densities (g/cm^3)	Coal A Moisture Content (%)	Coal A Specific Ash Content (%)	Coal B Moisture Content (%)	Coal B Specific Ash Content (%)
1.3 floats	3.21	4.29	3.30	4.13
1.3 sinks	3.06	7.82	3.33	8.31
1.4 sinks	3.08	14.45	3.36	13.75
1.5 sinks	2.84	22.56	3.00	21.99
1.6 sinks	2.62	29.24	2.76	28.73
1.7 sinks	2.40	37.44	2.59	35.04
1.8 sinks	1.58	65.32	1.77	57.84

4.4.2. Calibration of the wind-sifter separator vibratory feeder

4.4.2.1. Coal feeder calibration

The vibratory feeder of the separator was calibrated before the coal samples were beneficiated, just like in the previous study conducted by Alade (2021). A detailed calibration test was carried out on the Coal A sample due to its ample amount compared to Coal B. The calibration was carried out to determine the mass flowrates at each carrier frequency of the vibratory feeder to ascertain the range of sample mass flowrate in which the dilute phase can be maintained in the separator. The results from the calibration operation from 6.0 kHz to 14.4 kHz are shown in Figures 4.32 to 4.34. The (−1.0+ 0.2 mm) size fraction (Figure 4.34) showed the slowest mass flow at a carrier frequency of 6.0 kHz, with a mass flowrate of 24.54 g/min. This is followed by the (−3.35+1.0 mm) size fraction with 32.43 g/min and the (−6.7+3.35 mm) size fraction with a mass flowrate of 33.90 g/min. This occurrence is likely because the smaller the size fraction, the higher the particles tend to spread more in the vibratory feeder conveyor. As a result, they would only proceed into the rotary hopper valve with an increased vibration frequency. Based on this, the carrier frequency for the smaller size fraction over the coarse fraction would have to be increased to feed particles with the same mass flow rate.

To maintain a dilute phase for this study, a carrier frequency between 6.0 and 8.0 kHz was used for the (−6.7+3.35 mm) size fraction with mass flowrate between 33.90 and 428.57 g/min. The carrier frequency for the (−3.35+1.0 mm) size fraction (Figure 4.33) is between 7.2 kHz and 8.0 kHz (mass flowrate ranging between 32.43 and 266.67 g/min). Lastly, a carrier frequency between 8.0 and 10 kHz was used for the (−1.0+0.2 mm) size fraction (mass flowrate ranging between 95.24 and 240 g/min).

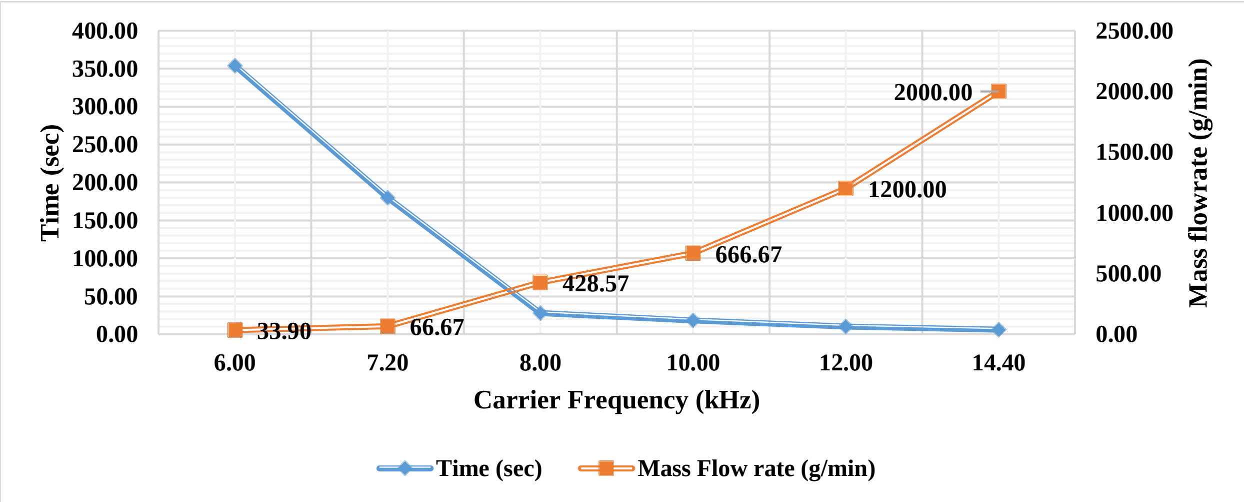

Figure 4.32: Calibration of the vibratory feeder for the separation of the (−6.7+3.35 mm) size fraction

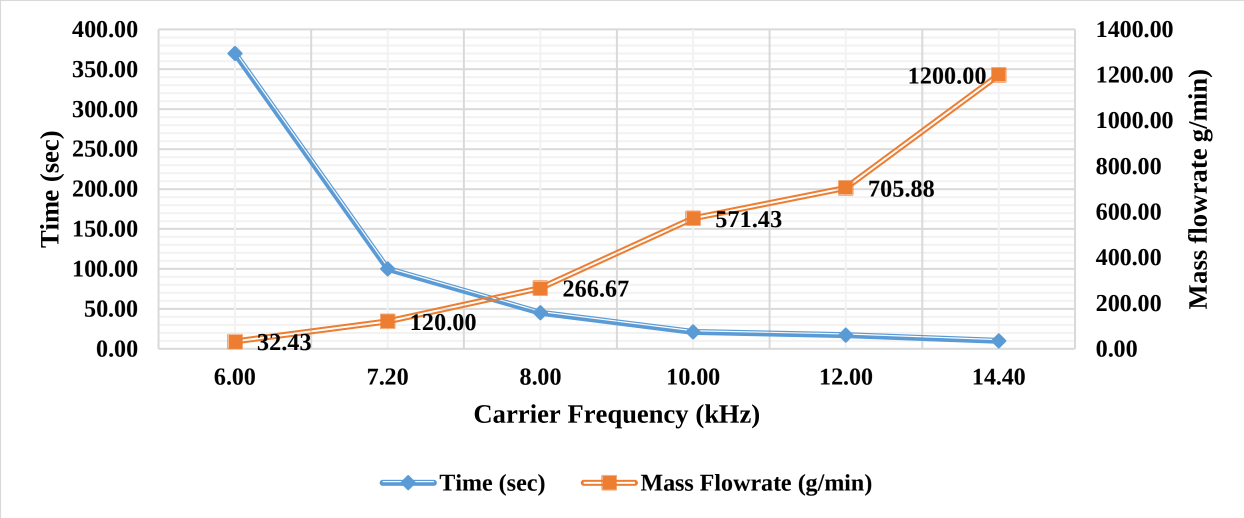

Figure 4.33: Calibration of the vibratory feeder for the separation of the (−3.35+1.0 mm) size fraction

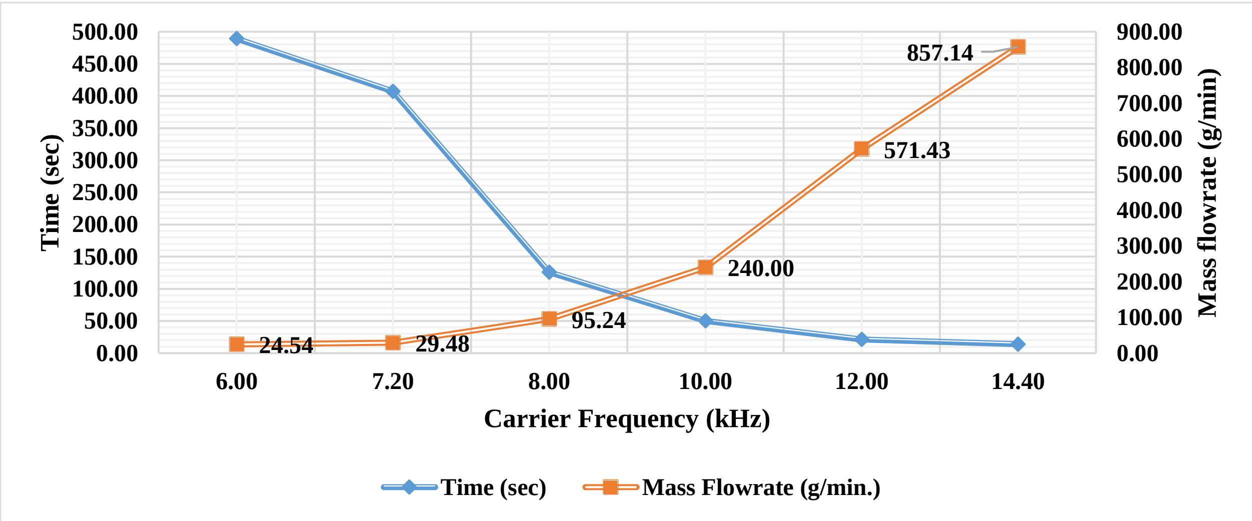

Figure 4.34: Calibration of the vibratory feeder for the separation of the (−1.0+0.2 mm) size fraction

4.4.2.2. Repeatability tests for sample mass recovery for each particle size fraction

All three particle size fractions were subjected to repeatability tests using all the airstream velocity values obtained from the simulation study. In addition, other airstream velocity values used in the experimental studies for all size fractions were also subjected to repeatability tests. This was done to verify the repeatability and consistency in the mass recovery of the separator. Results of the repeatability test are presented in Figures 4.35 to 4.37 for the (−6.7+3.35 mm) size fraction, Figures 4.38 to 4.40 for the (−3.35+1.0 mm) size fraction and Figures 4.41 to 4.43 for the (−1.0+0.2 mm) size fraction.

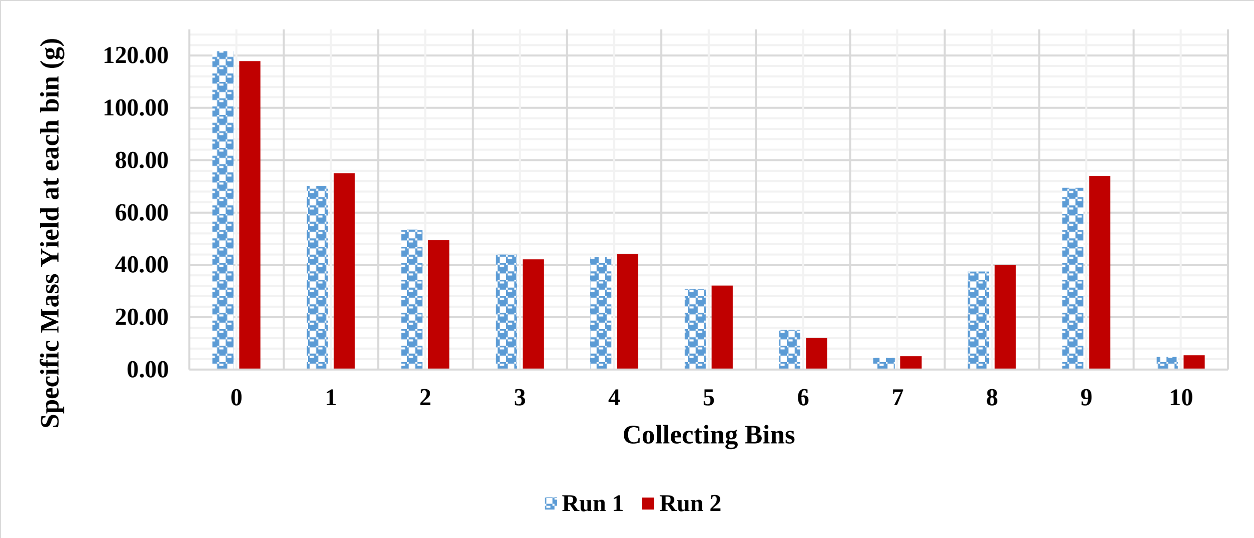

Figure 4.35: Repeatability test of the (−6.7+3.35 mm) particle size fraction at 6.0 m/sec

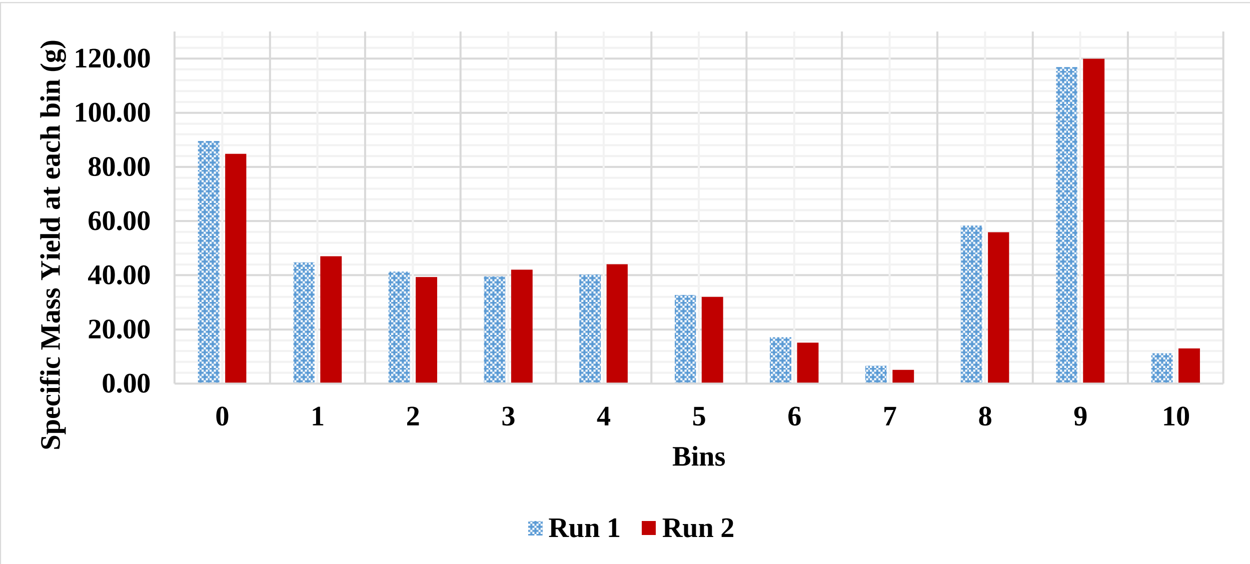

Figure 4.36: Repeatability test of the (−6.7+3.35 mm) particle size fraction at 5.0 m/sec

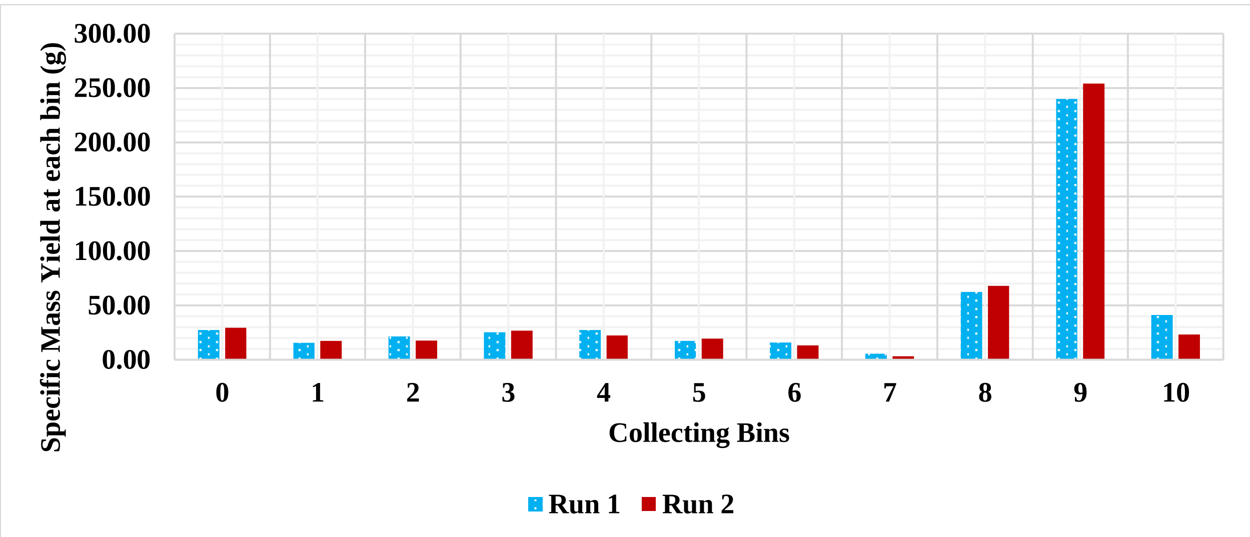

Figure 4.37: Repeatability test of the (−6.7+3.35 mm) particle size fraction at 4.0 m/sec

The mass recoveries of the (−6.7+3.35 mm) size fraction at different air velocities (Figures 4.35 to 4.37) were repeatable. The same trend can be seen for the (−3.35+1.0 mm) particle size fraction (Figures 4.38 to 4.40) with minimal losses. For the (−1.0 + 0.2 mm) size fraction, some sample loss was observed. The mass recoveries remained consistent and repeatable. The sample loss may be due to very fine particles (in the size range) being trapped on the linatex rubber used to line the separator wall. Another potential cause might be that the particles get crushed (make contact with the rotary feeder) into very fine sizes, which may cause them to recirculate with the airstream.

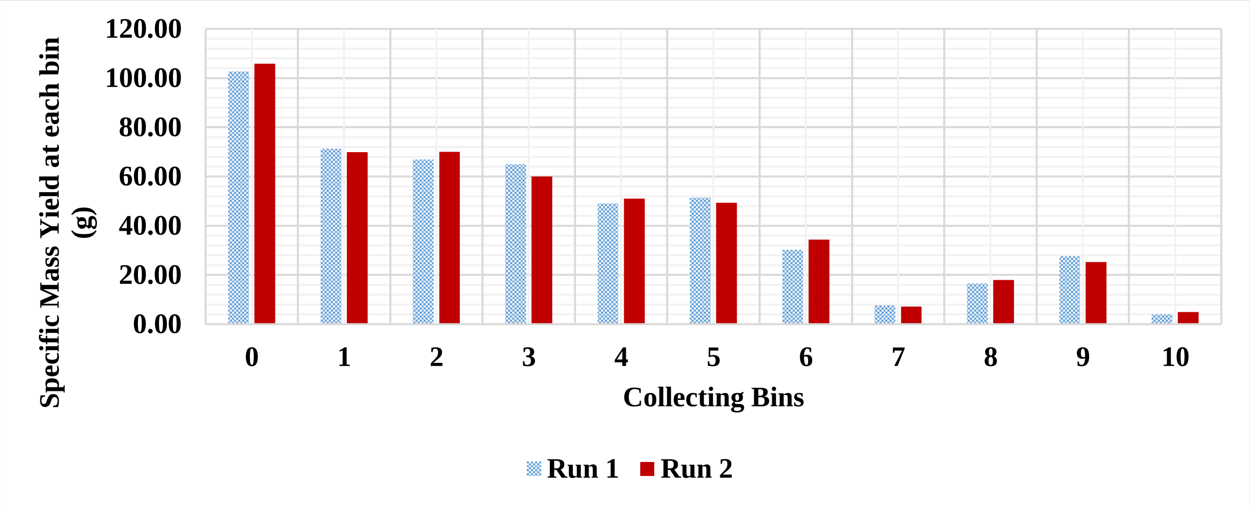

Figure 4.38: Repeatability test of the (−3.35+1.0 mm) particle size fraction at 4.2 m/sec

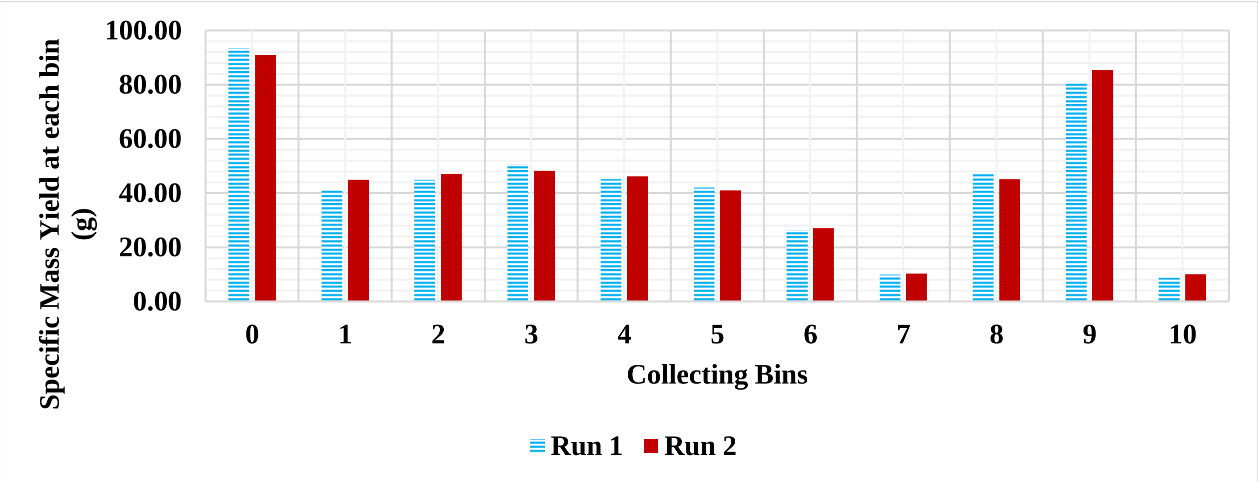

Figure 4.39: Repeatability test of the (−3.35+1.0 mm) particle size fraction at 3.0 m/sec

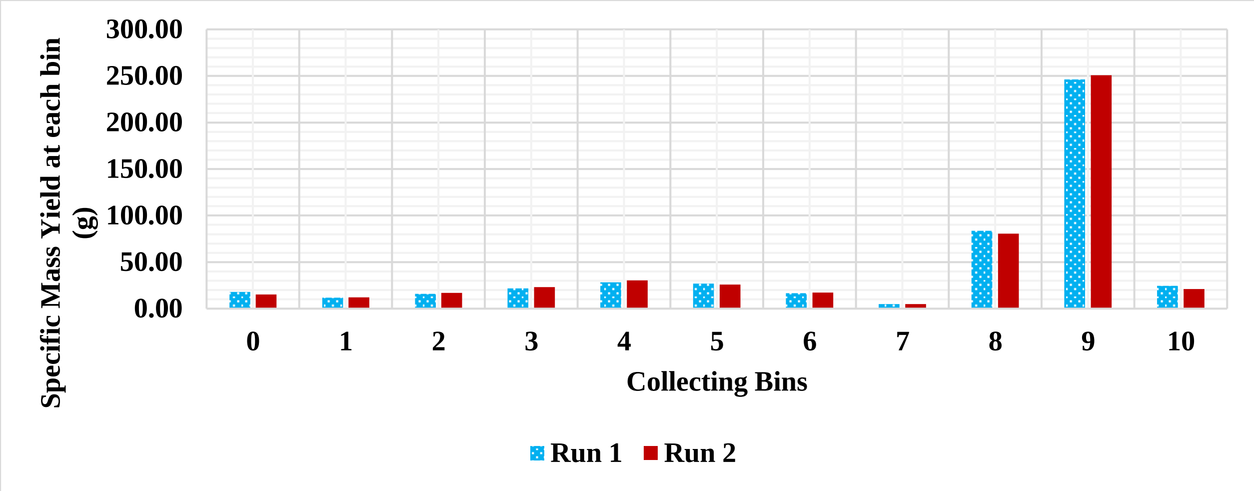

Figure 4.40: Repeatability test of the (−3.35+1.0 mm) particle size fraction at 2.0 m/sec

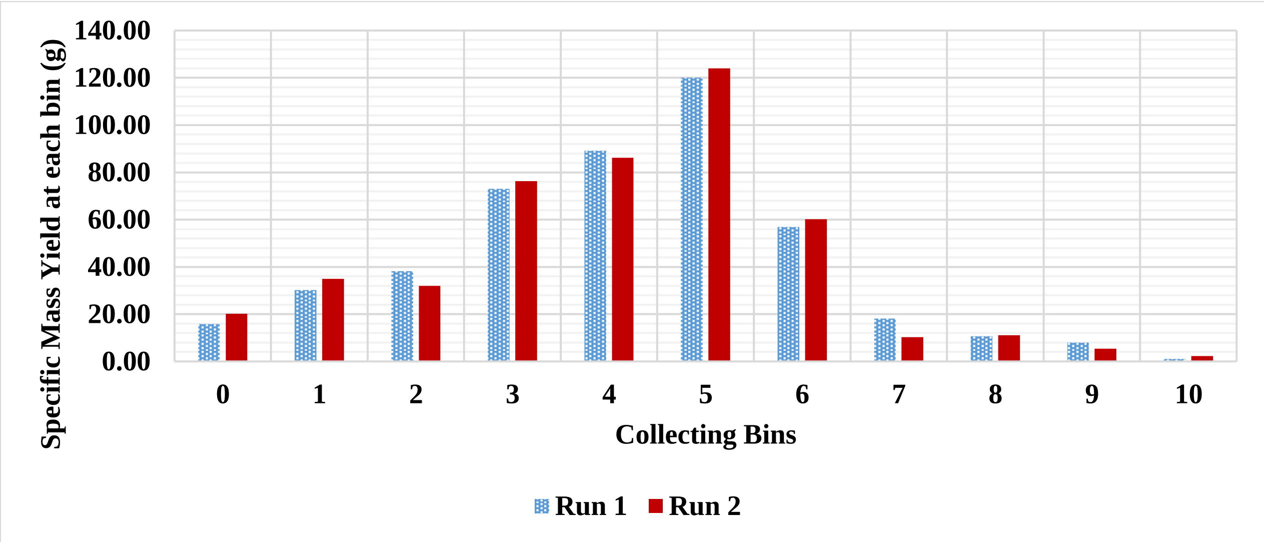

Figure 4.41: Repeatability test of the (−1.0+0.2 mm) particle size fraction at 1.7 m/sec

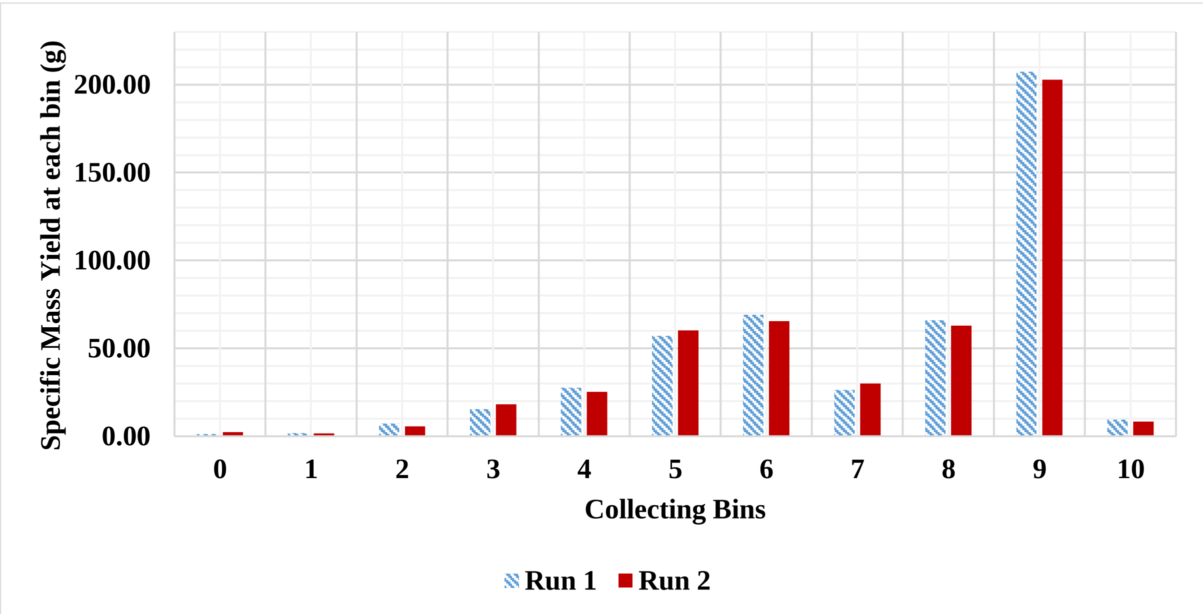

Figure 4.42: Repeatability test of the (−1.0+0.2 mm) particle size fraction at 1.0 m/sec

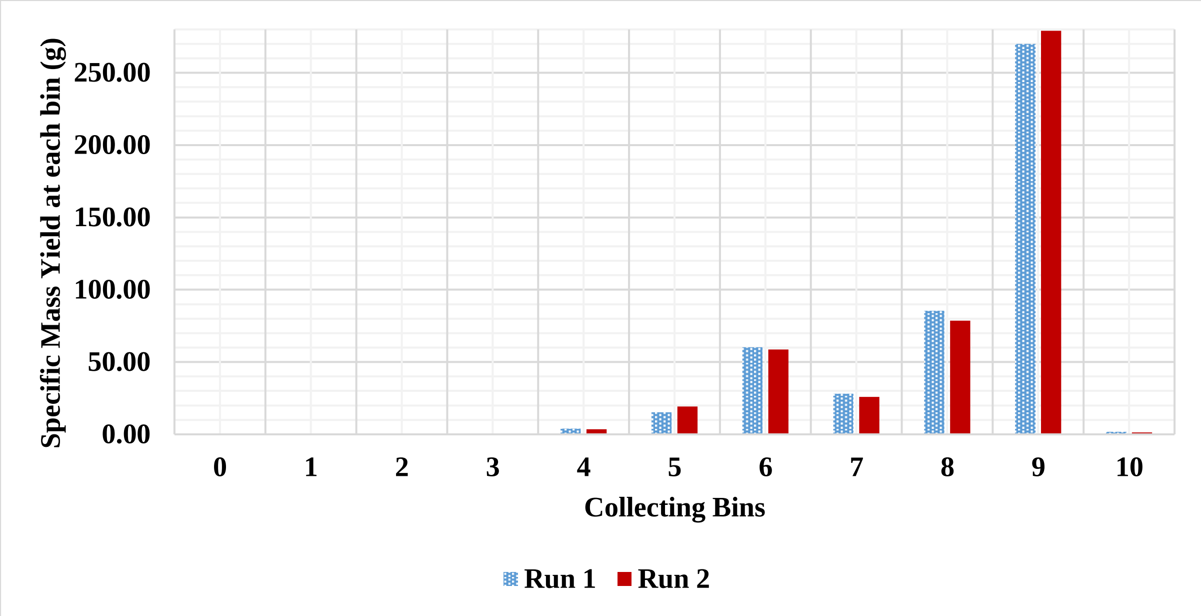

Figure 4.43: Repeatability test of the (−1.0+0.2 mm) particle size fraction at 0.75 m/sec

4.4.3. Wind-sifting beneficiation of coal A

4.4.3.1. Dry beneficiation results for coal A (with bins) for the (−6.7+3.35 mm) size fraction

A 500 g sample of coal A of (−6.7+3.35 mm) size fraction was fed into the separator for each test conducted. A constant mass flowrate of 66.67 g/min was used at different airstream velocities of 6.0 m/sec, 5.0 m/sec and 4.0 m/sec. From Figure 4.44, it can be observed that reducing the air velocity lowered the ash content, which correspondingly resulted in a drop in cumulative yield. At an airstream velocity of 6.0 m/sec, a clean coal product of 26.97% cumulative ash and 77.40% cumulative yield was achieved from the bins of **chamber 2** from a feed coal with an ash content of 37.38%. When the velocity was reduced to 5.0 m/sec, the bins of **chamber 2** yielded clean coal product with 24.84% cumulative ash and 62.59% cumulative yield. At an airstream velocity of 4.0m/sec, a further reduction in ash content was achieved with 20.21% cumulative ash and 31.17% cumulative yield in the same **chamber 2**. Under the same 4.0 m/sec airstream velocity, bin 8 (**chamber 1**) produced a clean coal product with a cumulative ash of 22.27% and a cumulative yield of 43.64%. The cleanest coal product obtained from this size fraction was 19.09% ash content under an airstream of 4.0 m/sec in bin 7. This is followed by the 19.79% ash content from the hatchet, which is denoted as bin 0 in Figure 4.44.

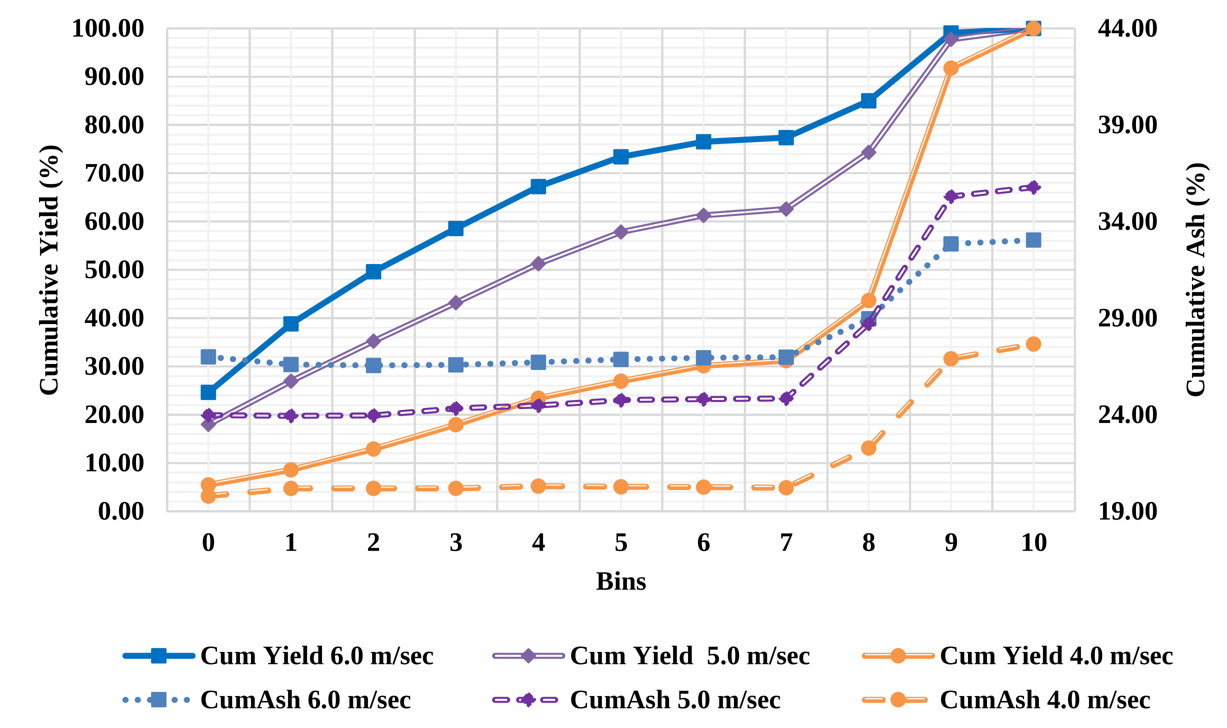

Figure 4.44: Cumulative yield and cumulative ash contents for the (−6.7+3.35 mm) size fraction at different airstream velocities (**coal A, with bins**)

The optimised separator used in this study was evaluated against the old prototype design by comparing the cumulative yields of both separator assemblies. At 6.0 m/sec, 58.38% cumulative yield was obtained in chamber 2 of the old design (Alade, 2021), while 77.40% was achieved in the optimised separator. Using a benchmark of 500 g sample feed, a sample loss of 37.15 g (7.43%) occurred in the old design. At 4.0 m/sec, a sample loss of 13.15 g (2.63%) and 5.02 g (1.0%) was obtained in chamber 2 of the old and optimised separator, respectively. The same was observed for the other size fractions, which is likely due to increased sifting effectiveness in the optimised separator. This addresses the issue of sample loss in the previous design.

4.4.3.2. Dry beneficiation results for coal A (with bins) for the (−3.35+1.0 mm) size fraction

The (−3.35+1.0 mm) size fraction was beneficiated at a constant mass flowrate of 120 g/min and under three different airstream velocities of 4.2 m/sec, 3.0 m/sec and 2.0m/sec. The separation of the coal’s organic from its inorganic components also follows a similar trend as that of the (−6.7+3.35 mm) size fraction. A clean coal product with cumulative ash of 27.29% and a cumulative yield of 83.39% was achieved from the bins in **chamber 2** at 4.2 m/sec airstream velocity (Figure 4.45). The cumulative ash decreased to 24.11% with a cumulative yield of 71.63% at a lower air velocity of 3.0 m/sec. At 2.0 m/sec airstream velocity, the clean coal product produced 20.48% cumulative ash and 28.89% cumulative yield. Adding recoveries from bin 8 (**chamber 1**) with the coal recovered from all the bins in **chamber 2** at 2.0 m/sec, a clean coal product of 22.68% cumulative ash and 45.66% cumulative yield was achieved. It can be observed from Figure 4.45 that the airstream velocity acts as the primary separation factor for this separator.

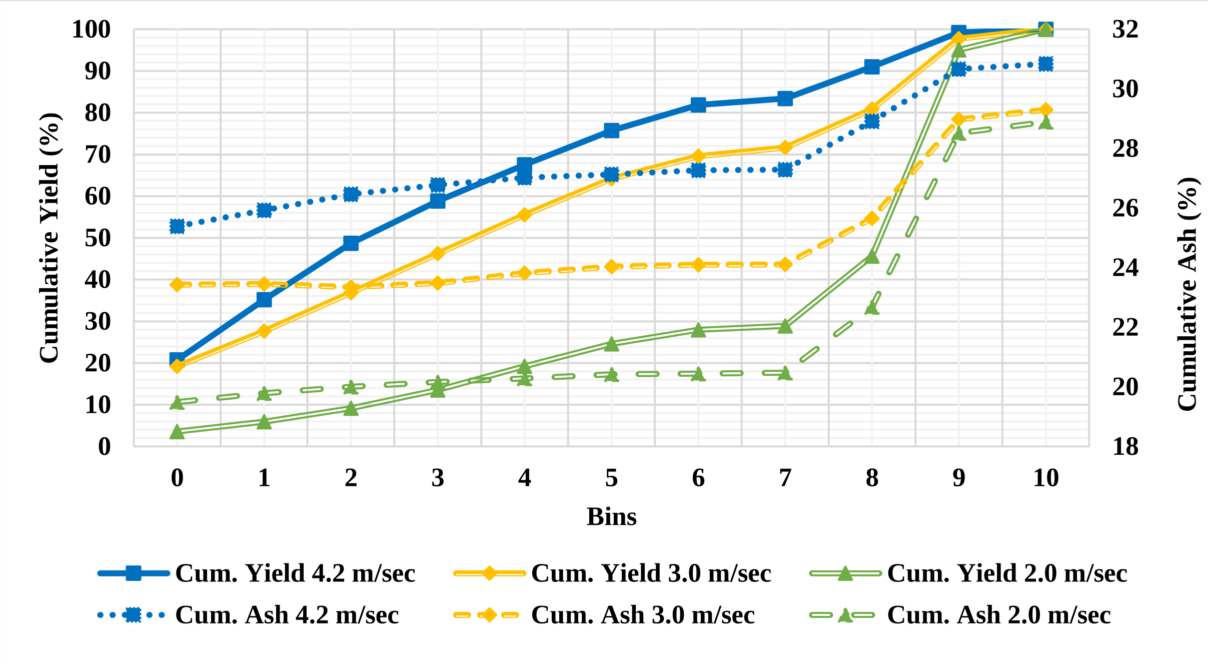

Figure 4.45: Cumulative yield and cumulative ash contents for the (−3.35+1.0 mm) size fraction at different airstream velocities (**coal A, with bins**)

4.4.3.3. Dry beneficiation results for coal A (with bins) for the (−1.0+0.2 mm) size fraction

Although the beneficiation of the smallest size fraction in this study resulted in some sample loss, upgrading it using this optimised separator was easier than using the previous one. A sample loss in the range of 11.23 to 35.31 g (2.25% to 7.06%) was experienced with the optimised design, whereas more than 50% of the sample was trapped within the old separator. The improper lining of the wall of the old separator might have been responsible. This test was conducted at airstream velocities of 1.7 m/sec, 1.0 m/sec, 0.75 m/sec and 0.5 m/sec. Like the two coarser size fractions, a decrease in airstream velocity reduced the cumulative ash contents and cumulative yields of the clean coal products.

The beneficiation results for the (−1.0+0.2 mm) size fraction at four different airstream velocities are shown in Figure 4.46. At 1.7 m/sec, a clean coal of 26.74% cumulative ash and 95.76% cumulative yield was obtained in chamber 2 of the separator from a feed coal of 29.30% ash content. With an airstream velocity of 1.7 m/sec, minimal separation was achieved, as the cumulative ash plot showed a flat line. When the airstream velocity was reduced to 1.0 m/sec, a clean coal product with a cumulative ash of 25.22% and a cumulative yield of 42.13% was achieved in chamber 2. As the air velocity was further reduced to 0.75 m/sec, the cumulative ash of the clean coal product in chamber 2 decreased to 20.14%, and a cumulative yield of 23.24% was achieved. At a minimum airstream velocity of 0.5 m/sec, a clean coal product with cumulative ash of 19.59% and cumulative yield of 14.29% was achieved.

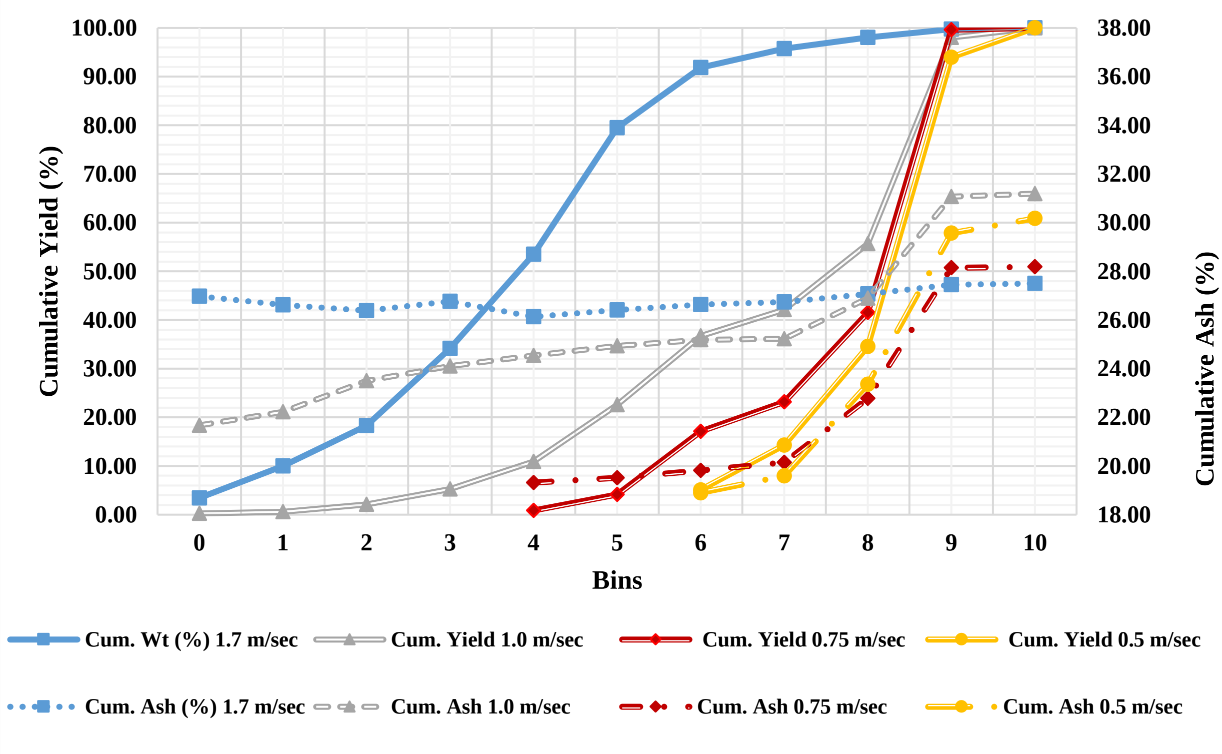

Figure 4.46: Cumulative yield and cumulative ash contents for the (−1.0+0.2 mm) size fraction at different airstream velocities (**coal A, with bins**)

4.4.4. Wind-sifting beneficiation of coal B

4.4.4.1. Dry beneficiation results for coal B for the (−6.7+3.35 mm) size fraction

Similar to coal A, 500 g of coal B feed was fed into the separator for each particle size fraction. The mass flowrate used was 66.67 g/min, the same as that for the (−6.7+3.35 mm) fraction for coal A. Unlike coal A, only two airstream velocities of 5.0 m/sec and 4.0 m/sec were used in beneficiating coal B. At 5.0 m/sec, ca lean coal product with cumulative ash of 21.42% was obtained in **chamber 2** bins with a cumulative yield of 43.70% from feed coal of 26.65% (Figure 4.47). When the velocity was reduced to 4.0 m/sec, a cumulative ash of 19.55% with 30.49% cumulative yield was attained in the bins of **chamber 2**. With the addition of coal product in bin 8, the cumulative ash content increased to 20.10%, with a cumulative yield of 42.93%. The cleanest coal product obtained from this size fraction was 17.38% ash content under an airstream of 4.0 m/sec in bin 2, and the next was 18.90% ash content in the hatchet (bin 0).

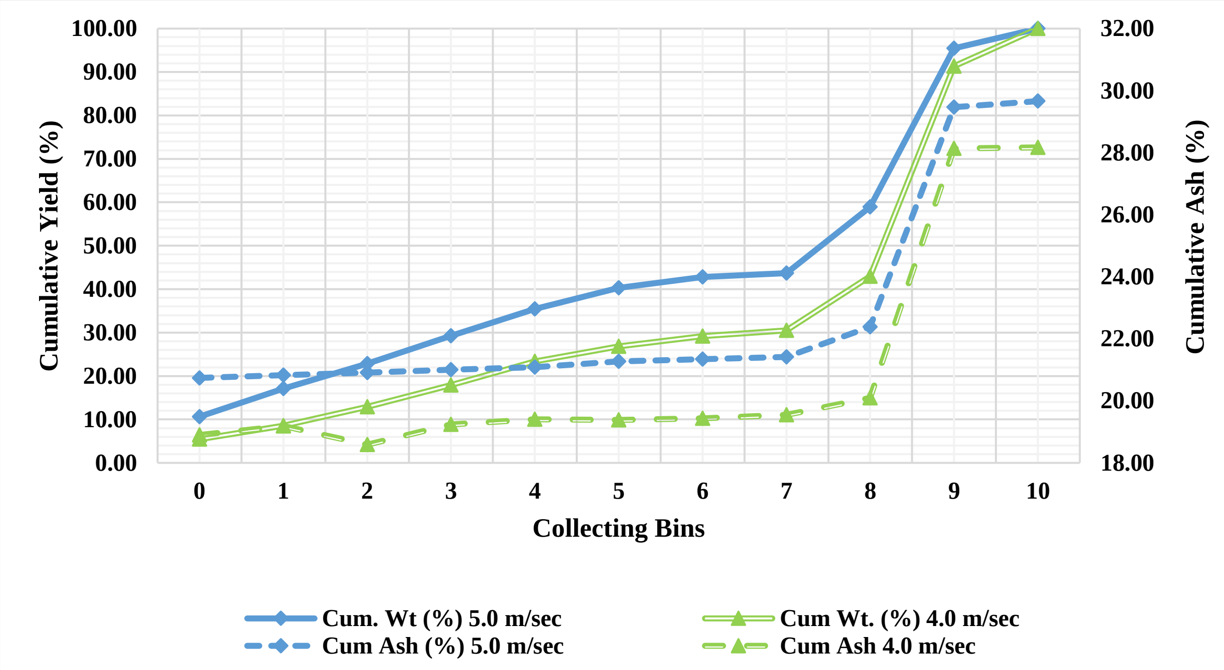

Figure 4.47: Cumulative yield and cumulative ash contents for the (−6.7+3.35 mm) size fraction at different airstream velocities (**coal B, with bins**)

4.4.4.2. Dry beneficiation results for coal B for the (−3.35+1.0 mm) size fraction

This test was conducted for the (−3.35+1.0 mm) size fraction at a mass flowrate of 120 g/min under two airstream velocities of 3.0 m/sec and 2.0 m/sec. The separation of the coal organic from its inorganic also follows a similar trend to that of coal A, as shown in Figure 4.44.

A clean coal product with cumulative ash of 21.87% and a cumulative yield of 60.22% was achieved in **chamber 2** at an airstream velocity of 3.0 m/sec (Figure 4.48). At 2.0 m/sec, a clean coal product of cumulative ash of 19.11% and 27.82% yield was achieved from a feed coal of 26.78% ash. The addition of coal product in bin 8 (**chamber 1**) to products from all the bins in **chamber 2** increased the cumulative ash of the products. This is expected as chamber 1 is more of a destoning chamber with a higher ash content coal.

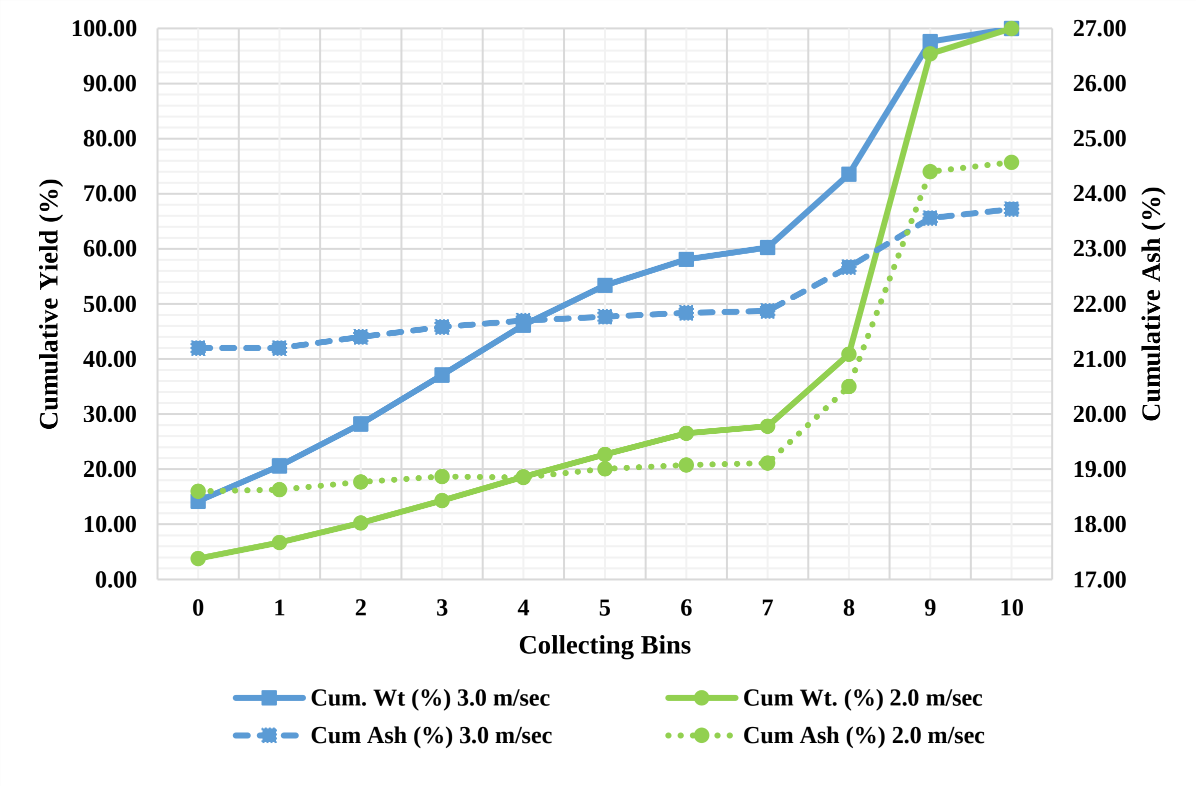

Figure 4.48: Cumulative yield and cumulative ash contents for the (−3.35+1.0 mm) size fraction at different airstream velocities (**coal B, with bins**)

4.4.4.3. Dry beneficiation results for coal B at the (−1.0+0.2 mm) size fraction

For the (−1.0+0.2 mm) size fraction of coal B, the beneficiation tests were conducted at airstream velocities of 1.0 m/sec and 0.75 m/sec. The two airstream velocities were applied for coal B because there was insignificant separation at 1.7 m/sec for coal A and insignificant yield (< 20%) at 0.5 m/sec. At an airstream velocity of 1.0 m/sec, a clean coal product of 23.55% cumulative ash and 32.74% cumulative yield was achieved from feed coal of 24.35% ash (Figure 4.49). The cleanest coal at this velocity was achieved in bin 1 with a specific ash content of 21.20%. As the air velocity was reduced to 0.75 m/sec, the grade of coal improved with a cumulative ash of 20.78% and 29.32% cumulative yield. For the 0.75 m/sec air velocity, when the recovery of bin 8 was added, cumulative ash of 22.03% and 42.07% cumulative yield was achieved.

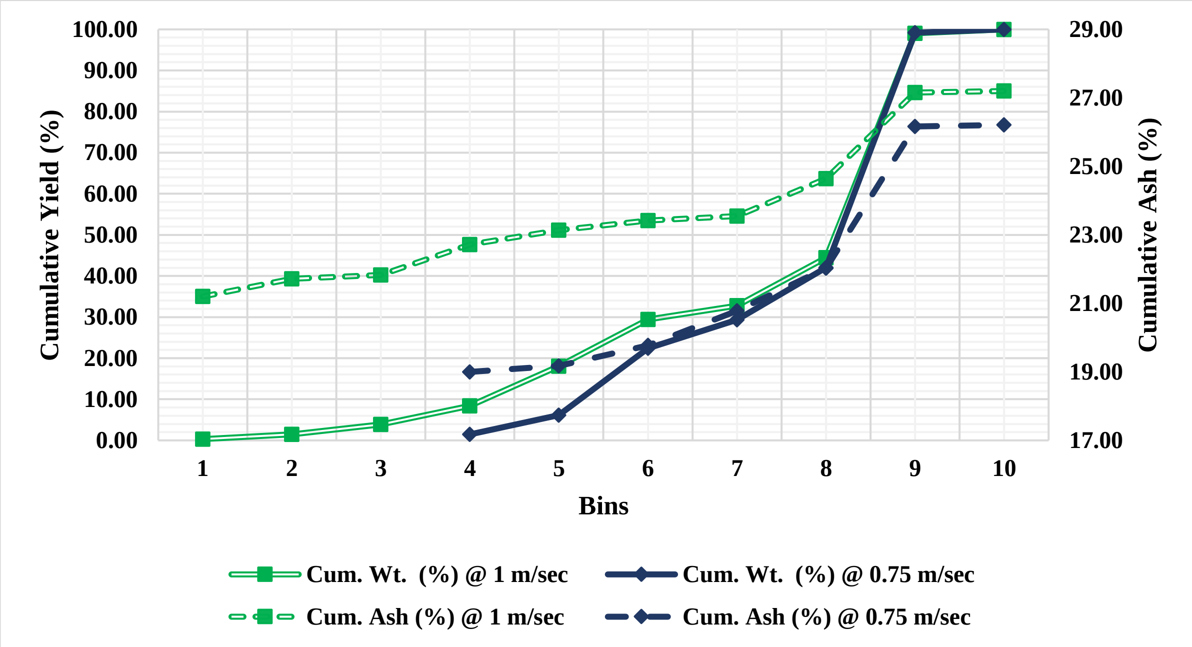

Figure 4.49: Cumulative yield and cumulative ash contents for the (−1.0+0.2 mm) size fraction at different airstream velocities (**coal B, with bins**)

4.4.5. Second-stage wind-sifting beneficiation of coal A

4.4.5.1. Dry beneficiation results for coal A (second-stage test)

A second-stage test was conducted to determine the lowest ash content the separator could achieve due to the high ash content in the coal products from each bin during the first-stage test. The test was conducted on the (−6.7+3.35 mm) and (−3.35+1.0 mm) size fractions, excluding the (−1.0+0.2 mm) size fraction because of the sample loss experienced from this fraction. For this test, the separator was first fed with 500 g of coal, then the combined products obtained from chamber 2 and the discard from chamber 1 were beneficiated again, separately. That is, the first-stage products from bins 0 to 7 were combined as a feed for the second-stage test, while products from bins 8 to 10 were combined as a feed for the second-stage test. The test was carried out at airstream velocities of 5.0 m/sec and 4.0 m/sec for the (−6.7+3.35 mm) fraction and at 3.0 m/sec and 2.0 m/sec for the (−3.35+1.0 mm) size fraction.

Figures 4.50 and 4.51 show the results for the second-stage test of the (−6.7+3.35 mm) size fraction at 5.0 m/sec and 4.0 m/sec, respectively. For the second-stage test, a clean coal product of 21.79% ash and 79.78% yield was obtained in chamber 2 from the product feed (Figure 4.50). The mass and ash content of the product feed (bins 0 to 7 from the first stage) were 278.01 g and 23.48%, respectively. For the combined discard feed of 212.70 g (bins 8 to 10 from the first stage), a cumulative ash of 28.14% and cumulative yield of 28.99% was achieved after the second-stage test from **chamber 2.** At an airstream velocity of 4.0 m/sec, a product yield and ash content of 170.50 g and 19.52%, respectively, were realised from the first stage (bins 0 to 7). A cumulative ash of 18.49% and a cumulative yield of 52.60% were achieved from the product feed (Figure 4.51). For the combined discard products (bins 8 to 10 from the first stage) used as second-stage feed, cumulative ash of 18.82% and cumulative yield of 2.23% were achieved in the bins of chamber 2. With the addition of coal in bin 8 after this second-stage test (from the discard feed), cumulative ash and yield of 23.45% and 14.32%, respectively, were achieved. It must be stated that the second-stage test gives the equipment operator more flexibility to obtain coal products of the desired grade from low-grade coal or any coal grade.

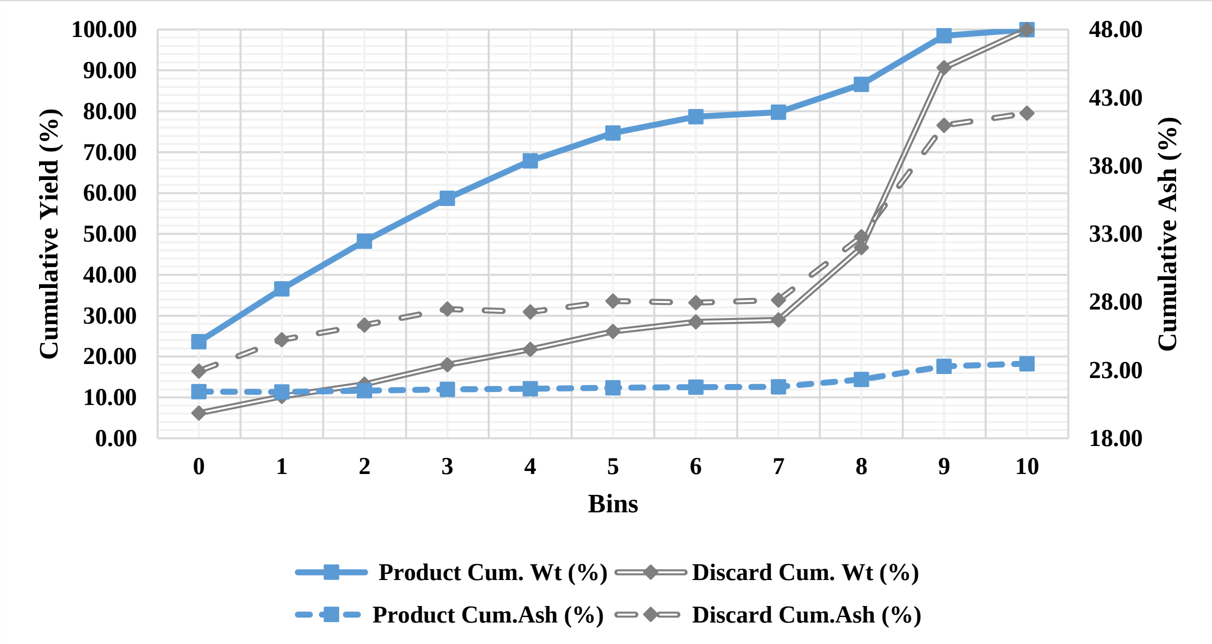

Figure 4.50: Second-stage test of the (−6.7+3.35 mm) size fraction at 5.0 m/sec airstream velocity (product mass of 278.01 g, discard mass of 212.70 g)

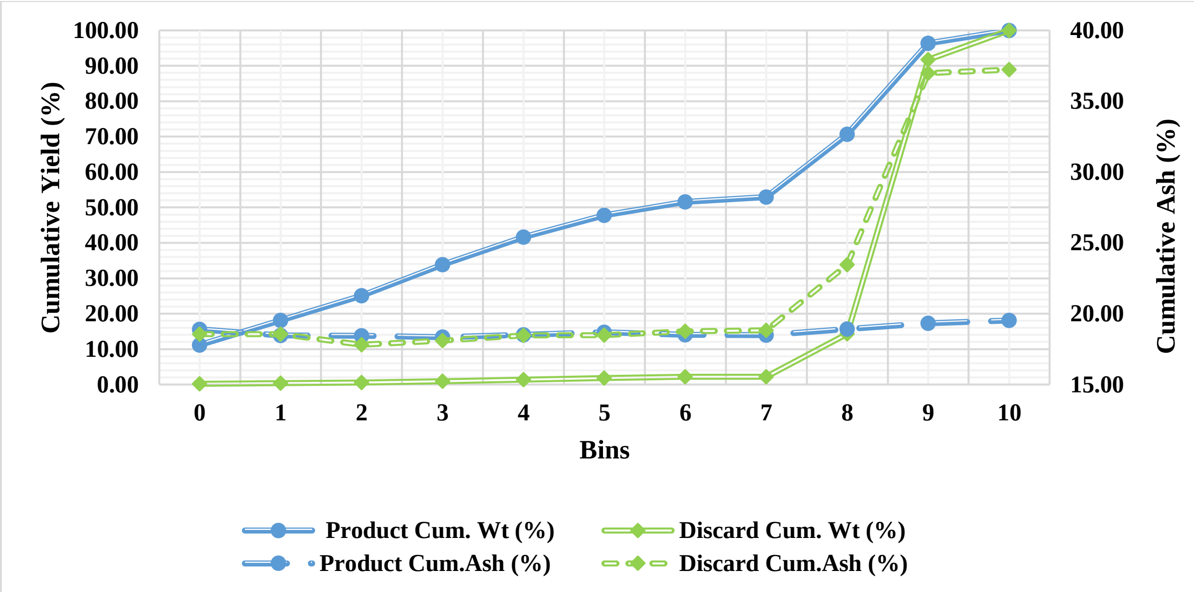

Figure 4.51: Second-stage test of the (−6.7+3.35 mm) size fraction at 4.0 m/sec airstream velocity (product mass of 170.50 g, discard mass of 328.76 g)

4.4.5.2. Dry beneficiation results for coal A (second-stage test) for the (−3.35+1.0 mm) size fraction

Figures 4.52 and 4.53 present the results for the second-stage test at 3.0 m/sec and 2.0 m/sec for the (−3.35+1.0 mm) size fraction. At 3.0 m/sec, a clean coal product (in chamber 2) of 20.88% ash content and 86.03% yield was attained from the product feed (bins 0 to 7 from the first stage). The mass and ash content of the product feed was 293.72 g and 22.41%, respectively. Adding the product from bin 8 after the second-stage test resulted in cumulative ash of 21.34% and a cumulative yield of 91.63% (Figure 4.52). For the combined discard products (bins 8 to 10 from the first-stage test), cumulative ash of 26.72% and a cumulative yield of 24.71% were achieved from chamber 2 after the second-stage test.

At an airstream velocity of 2.0 m/sec, cumulative ash of 19.77% and 82.64% cumulative yield were obtained from the product feed (bins 0 to 7) of 143.84 g and an ash content of 20.09% (Figure 4.53). From the combined discard products (bins 8 to 10) of 354.17 g and ash content of 28.30%, cumulative ash of 22.89% and a cumulative yield of 4.66% was achieved in chamber 2 after the second-stage test. When the product from bin 8 was added, cumulative ash and yield of 24.47% and 21.73%, respectively, were achieved. This means that for a coal sample of higher ash content, a second-stage test can be conducted to lower its ash content.

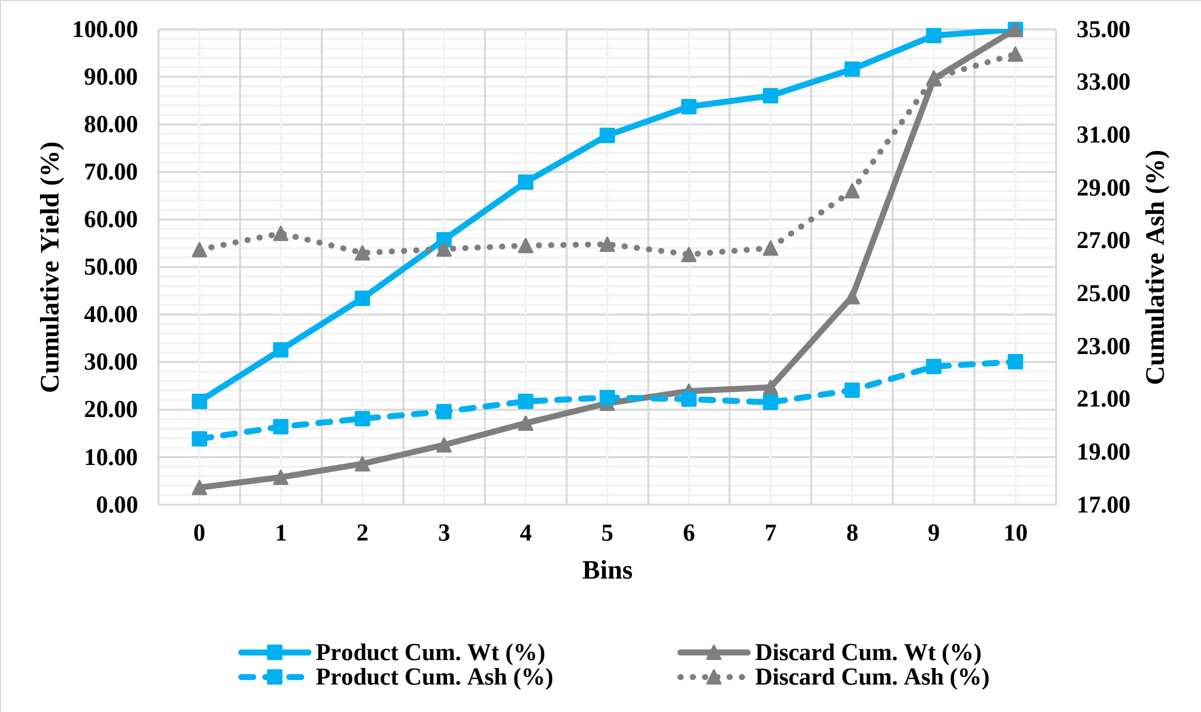

Figure 4.52: Second-stage test of the (–3.35+1.0 mm) size fraction at 3.0 m/sec airstream velocity (product mass of 293.72 g, discard mass of 198.69 g)

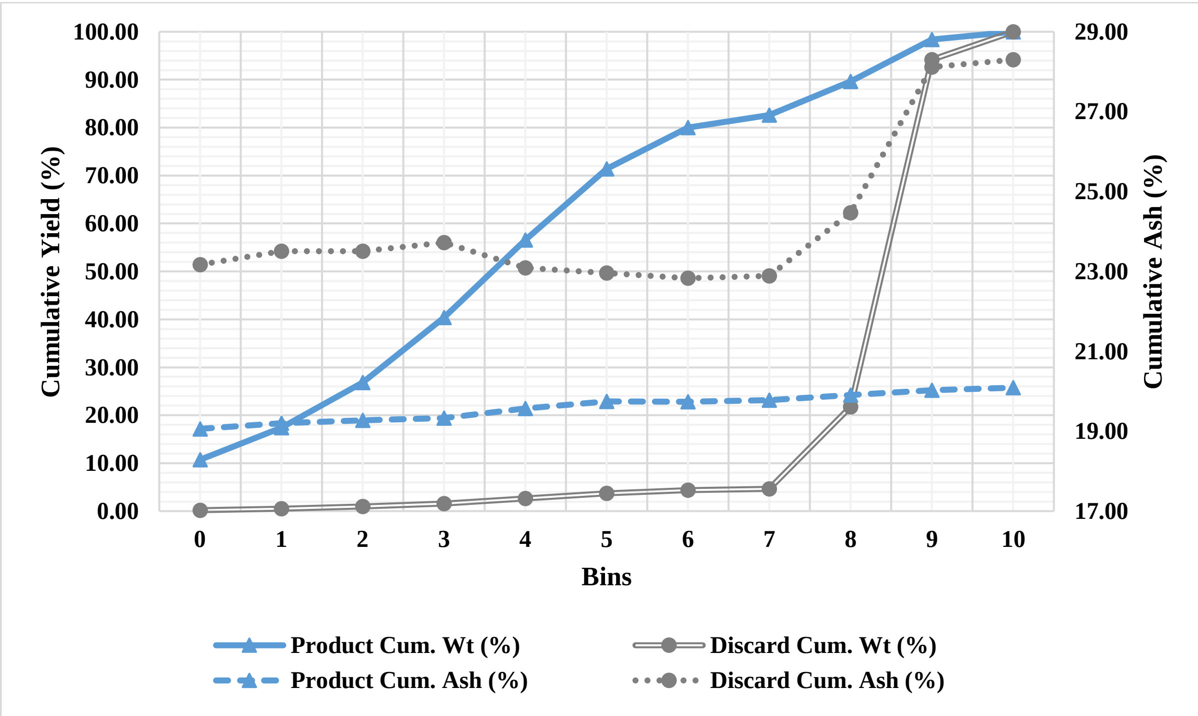

Figure 4.53: Second-stage test of the (−3.35+1.0 mm) size fraction at 2.0 m/sec airstream velocity (product mass of 143.84 g, discard mass of 354.17 g).

4.4.6. Dry beneficiation results for coal A (without bins)

The optimised separator's design was made flexible in its mode of operation, allowing it to run either with closed bins or without collecting bins (open). Thus, this investigation was carried out to examine the separation results when running the separator without collecting bins for all three particle size fractions. Figure 4.54 shows the results obtained for the (−6.7+3.35 mm) size fraction at 10.5 m/sec and 9 m/sec. Figure 4.55 depicts the results for the (−3.35+1.0 mm) size fraction at 7 m/sec and 5 m/sec. The results for the (−1.0+0.2 mm) size fraction at 3.5 m/sec and 2.5 m/sec are depicted in Figure 4.56. For all the tests conducted, 500 g of coal was used.

For the (−6.7+3.35 mm) size fraction (Figure 4.54) at 10.5 m/sec airstream velocity, a clean coal product with 22.49% cumulative ash was recovered with 58.43% yield (bins 0 to 7). The coal obtained was a better grade than the 26.97% cumulative ash achieved when the bin was closed (Figure 4.41) at a lower velocity of 6 m/sec. At 9 m/sec, a clean coal product with cumulative ash of 19.44% and 36.90% cumulative yield was achieved. By adding the coal products from bin 8 (**chamber 1)** to the products from **chamber 2**, a coal product with cumulative ash of 23.12% and a cumulative yield of 60.32% was achieved. The cleanest coal product from this study (16.73% ash content) was obtained from bin 2 at 9 m/sec for this size without the bins. Tables 4.5 and 4.6 show the physico-chemical properties of feed coal (−6.7+3.35 mm) size fraction.

The separator's operation without bins resulted in a higher yield and lower ash content products for the coarsest size. This is likely because as the air velocity increased from chamber 1, so did the buoyant force. However, as the particle travels in the separator assembly from chamber 1 to chamber 2, the buoyant force drops drastically due to the high pressure drop. The particles' settling velocities are faster due to the pressure drop caused by opening all the bins. This phenomenon occurred for the other two particle size fractions as well. The results for the (−6.7+3.35 mm) size fraction are shown in Figure 4.54.

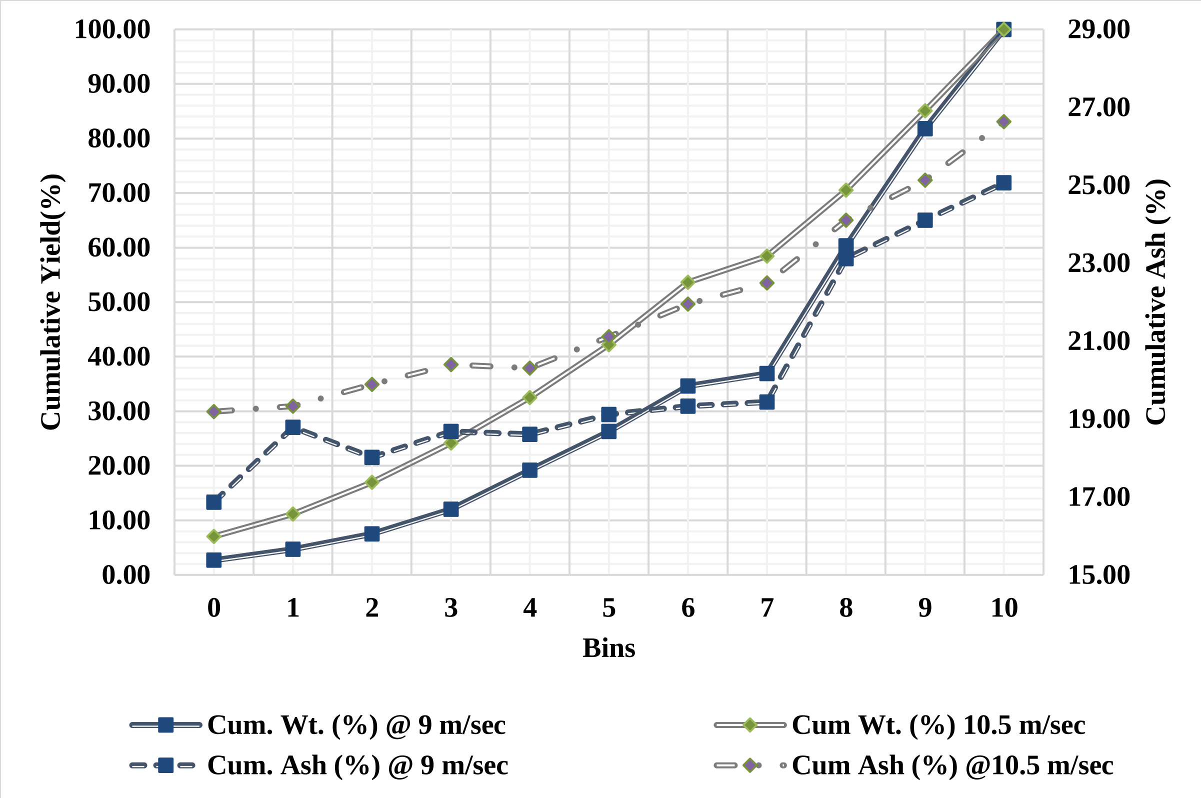

Figure 4.54: Cumulative yield and cumulative ash contents for the (−6.7+3.35 mm) size fraction at different airstream velocities (**coal A, without bins**).

Figure 4.55 presents the results from the (−3.35+1.0 mm) particle size fraction at an airstream velocity of 7 m/sec and without bins (***open bins***). A clean coal product of 23.75% cumulative ash and 62.67% cumulative yield was obtained from chamber 2. When the airstream velocity was 5 m/sec, a clean coal product with cumulative ash of 20.94% and 28.96% cumulative yield was achieved. The (−1.0+0.2 mm) size fraction resulted in a clean coal product with cumulative ash of 27.94% and a cumulative yield of 91.28% at 3.5 m/sec air velocity (Figure 4.53). A clean coal product of 22.69% cumulative ash and 68.16% cumulative yield was achieved at a lower air velocity of 2.5 m/sec.

The optimised wind-sifter separator can operate with and without bins, as demonstrated by the results of this test. The complete data of the washability studies for all the tests performed is provided in APPENDIX C.

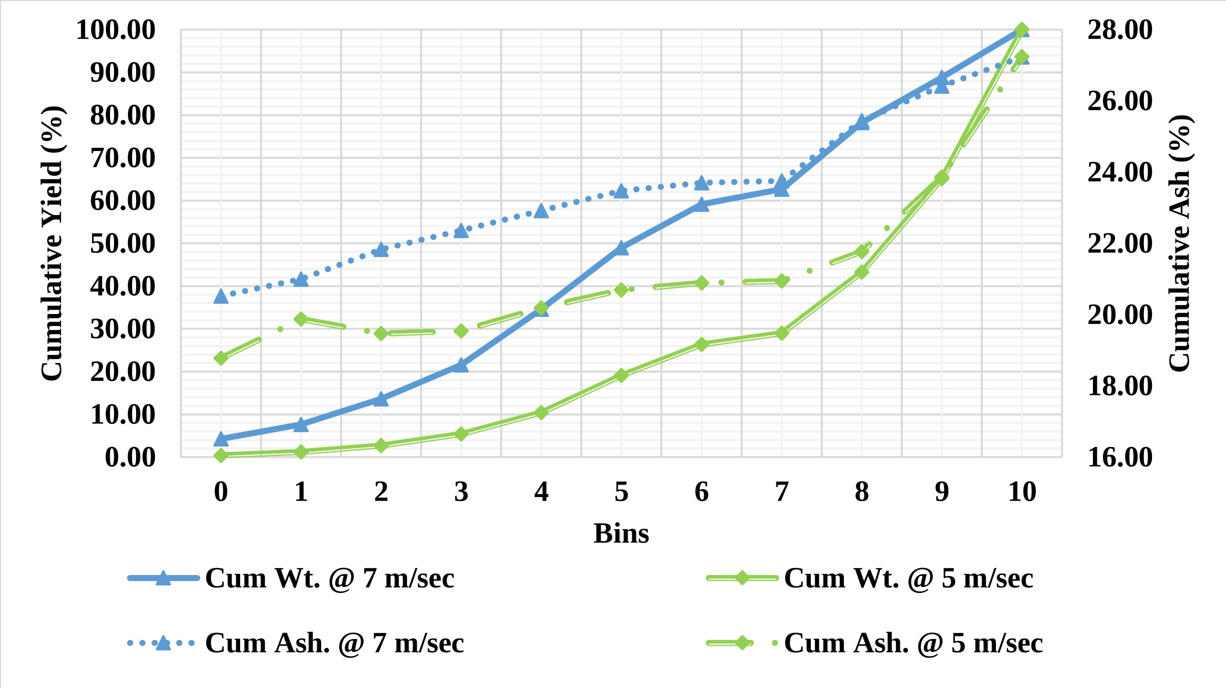

Figure 4.55: Cumulative yield and cumulative ash contents for the (−3.35+1.0 mm) size fraction at different airstream velocities (**coal A, without bins**)

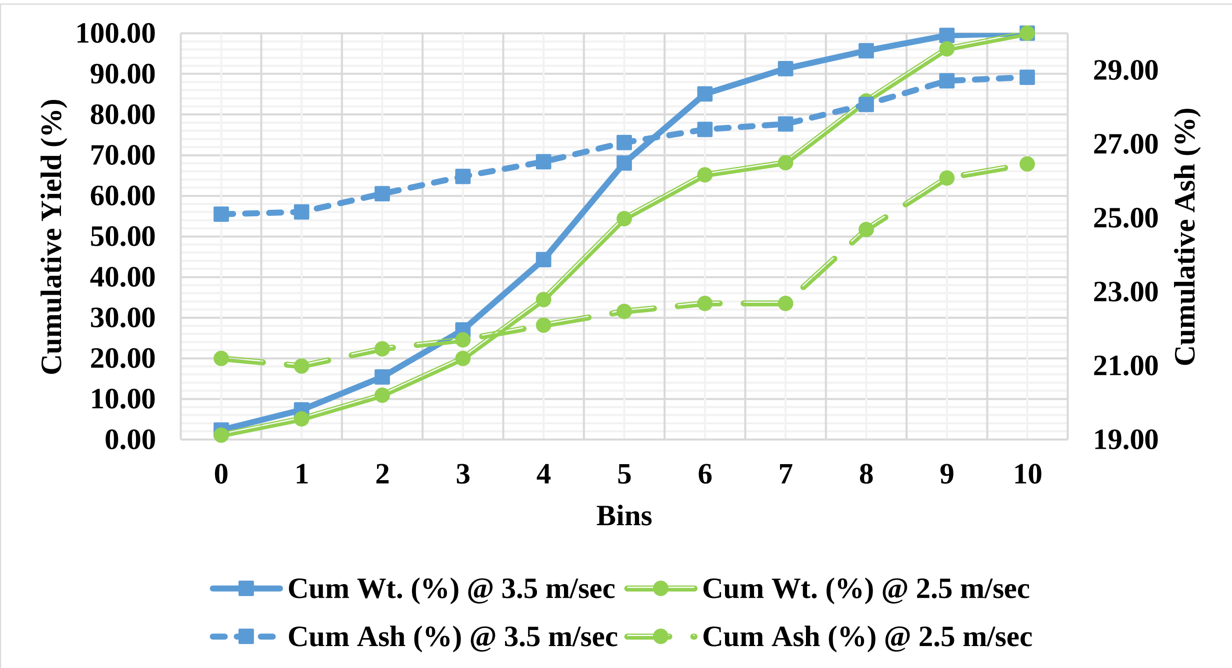

Figure 4.56: Cumulative yield and cumulative ash contents for the (−1.0+0.2 mm) size fraction at different airstream velocities (**coal A, without bins**)

Tables 4.5 and 4.6 show the physico-chemical properties of the feed coal (the (−6.7+3.35 mm) size fraction) and the cleanest coal, respectively, for this study.

Table 4.5: Physico-chemical properties of the feed coal (−6.7+3.35 mm) – air dry basis (adb)

Proximate Analysis (%)	Inherent Moisture		Volatile Matter	Ash Content	Fixed Carbon
	1.99		20.02	37.38	40.61
Calorific Value (MJ/kg)	19.61 (adb)				
Elemental Analysis (%)	Total Carbon 46.60	Hydrogen 2.88	Nitrogen 1.23	Total Sulphur 0.58	Oxygen 10.57

Oxygen: 100 - (Total Carbon + Hydrogen + Nitrogen + Total Sulphur + Ash + Moisture)

Table 4.6: Physico-chemical properties of the cleanest coal – air dry basis (adb)

Proximate Analysis (%)	Inherent Moisture		Volatile Matter	Ash Content	Fixed Carbon
	3.03		29.89	16.73	50.35
Calorific Value (MJ/kg)	26.70 (adb)				
Elemental Analysis (%)	Total Carbon 64.30	Hydrogen 4.20	Nitrogen 1.61	Total Sulphur 0.50	Oxygen 12.14

Oxygen: 100 - (Total Carbon + Hydrogen + Nitrogen + Total Sulphur + Ash + Moisture)

4.4.7. Evaluation of the beneficiation performance of the optimised separator

In this section, the beneficiation performance of the optimised separator was evaluated based on the separation of the (–6.7+3.35 mm), (–3.35+1.0 mm) and (–1.0+0.2 mm) coal A size fractions. The E_p is a widely recognised index in coal preparation that was utilised for this purpose. From Equations 3.19 to 3.29, the E_P values at airstream velocities of 6.0, 5.0 and 4.0 m/sec for the (–6.7+3.35 mm) size fraction were determined. For the (–3.35+1.0 mm) size fraction, the E_p values for 4.2, 3.0 and 2.0 m/sec air velocities were obtained. The same applies to E_p values at 1.0 m/sec and 0.75 m/sec air velocities for the (–1.0+0.2 mm) size fraction. The E_p values for airstreams at 1.7 m/sec and 0.5 m/sec were not determined due to insignificant separation and very low mass yield, respectively.

E_p values of 0.035, 0.095 and 0.16 were obtained at 6.0, 5.0 and 4.0 m/sec air velocities, respectively, for the (–6.7+3.35 mm) fraction (Figure 4.57). For the (–3.35+1.0 mm) coal sample, E_p values of 0.030, 0.099 and 0.125 were achieved for 4.2, 3.0 and 2.0 m/sec air velocities, respectively (Figure 4.58). E_p values of 0.145 and 0.15 were attained at air velocities of 1.0 m/sec and 0.75 m/sec, respectively, for the (–1.0+0.2 mm) coal fraction (Figure 4.59). Thus, the E_p values increase as the airstream velocity decreases. This is due to the separation based on the extrinsic properties of the particles, as shown in Equation 3.8 (buoyant force, drag force and weight), rather than density alone. As the air velocity decreases, there is an increased likelihood of lighter particles with bigger sizes reporting to the reject bins along with the heavier (lower-grade) particles. The beneficiation of the lowest size fraction (–1.0+0.2 mm) (Figure 4.59) was more challenging than that of other coarser sizes. A decreasing particle size fraction may be responsible as the mass becomes very small, as the particle’s density seems to play a minimal role in the separation of this size fraction.

The results show that for the wind-sifter separation process, the E_p value increases as the airstream velocity reduces. This happens because air is a very light separating medium, leading to a low particle-separating ratio, unlike a hydraulic fluid (Ghosh, 2013). However, the E_p values from this process were not as high as other processes that use only air for dry particle separation. For instance, The FGX reportedly gives E_p values ranging between 0.20 and 0.30 (Charan et al., 2016; Jambal et al., 2017), and the air-jig gives a range of 0.16 to 0.30 (Boylu et al., 2015; Chalavadi et al., 2016). The air-table reports a range of 0.18 to 0.65 (Akbari et al., 2017), while the planar air-jet, a novel technique, gives an E_p of 0.2 (Yang et al., 2018). Figures 4.57, 4.58 and 4.59 show the partition curves for (−6.7+3.35 mm), (−3.35+1.0 mm) and (−1.0+0.2 mm) size fractions, respectively. The tables showing the results for the washability studies conducted in this study can be seen in APPENDIX C.

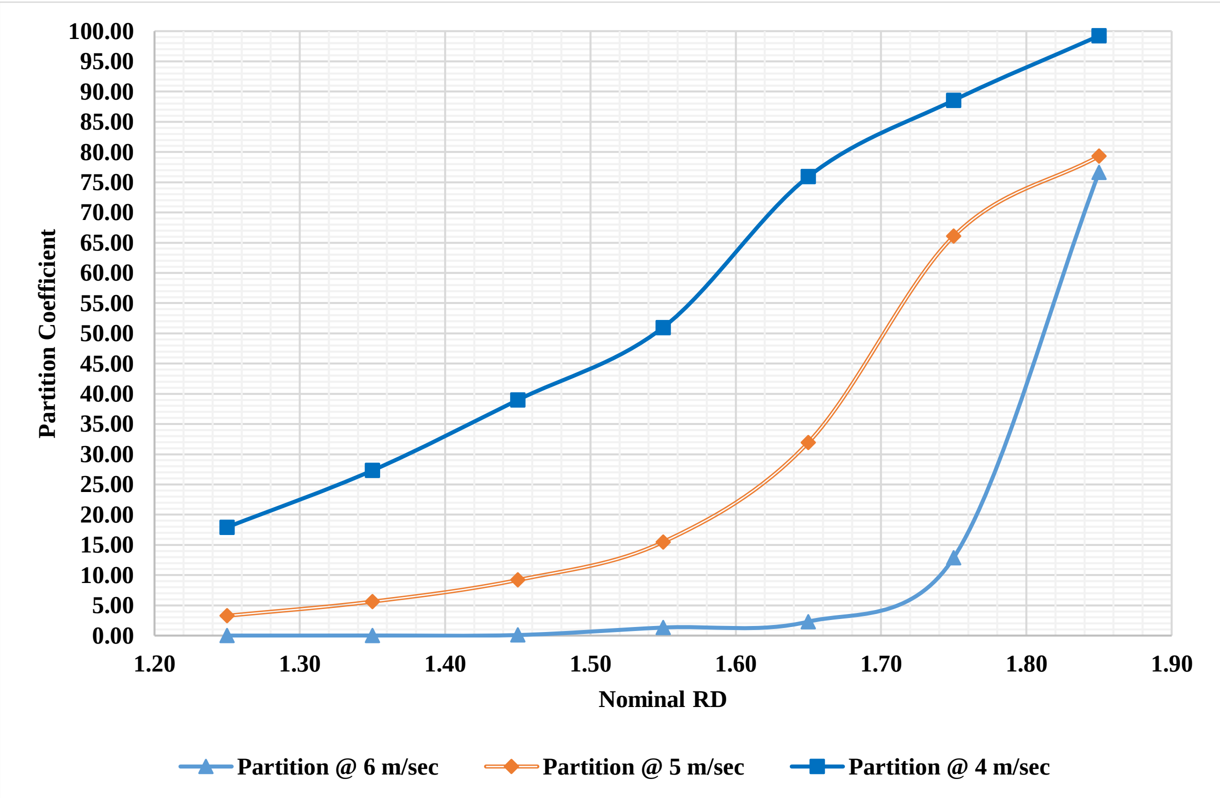

Figure 4.57: Partition curves for the (−6.7+3.35 mm) size fraction

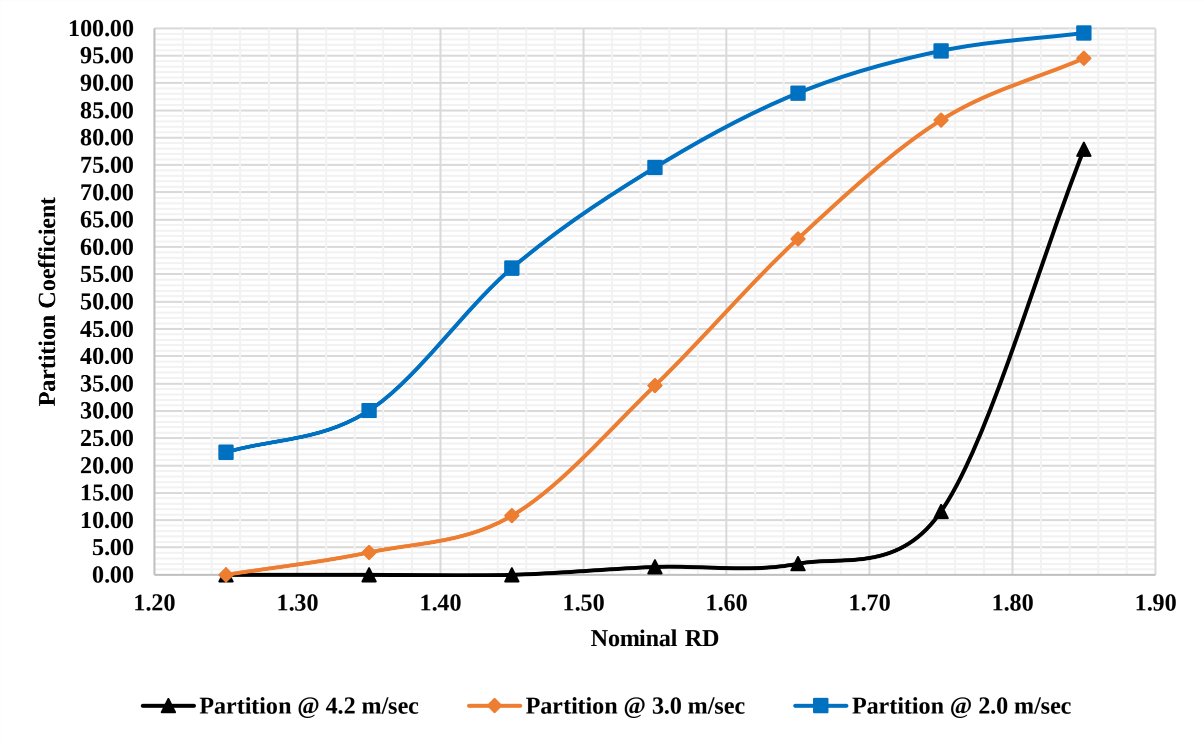

Figure 4.58: Partition curves for the (−3.35+1.0 mm) size fraction

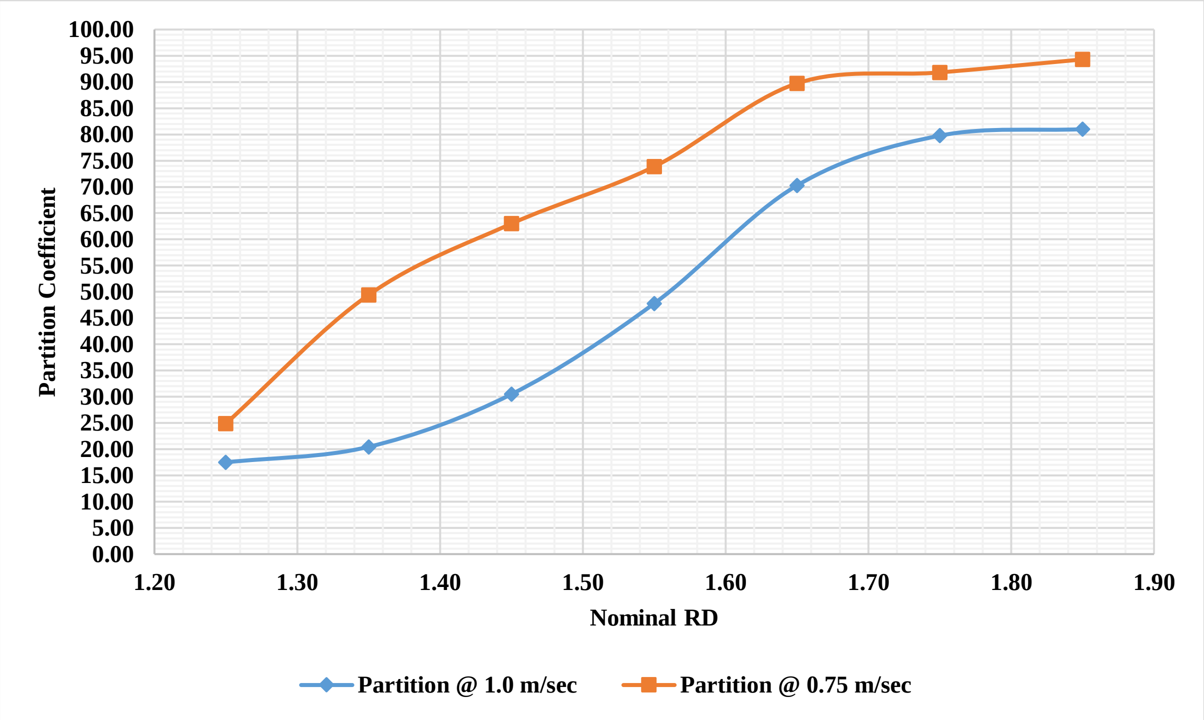

Figure 4.59: Partition curves for the (−1.0+0.2 mm) size fraction

4.4.8. Effect of moisture

The influence of moisture on the separation of particles in the separator was conducted on 500 g of the feed coal A of (−6.7+3.35 mm) and (−3.35+1.0 mm) particle size fraction. The smallest size fraction was not tested due to the mass loss already experienced. A 500 g sample of the two different particle sizes was immersed in water for ten minutes. A portion was taken in plastic and then allowed to dry in a fume hood for 24 hours. Another 500 g sample of the feed coal was also immersed in water and then allowed to dry for 18 hours, 12 hours and six hours. After a set period of drying, the new mass and the amount of moisture in the feed were determined before being fed into the wind-sifter separator. The product and rejects obtained after separation were then recombined (reconstituted), and the mass was recorded. The sample mass lost during separation was determined using this approach. Equation 4.4 was used to determine the new moisture content in the coal immersed in water and dried.

$$\left(\frac{Mass\ of\ Inherent\ moisture\ in\ Dry\ Coal\ (Without\ additional\ moiture) + (New\ mass - Old\ mass)}{New\ Mass}\right) * 100\%$$

(Equation 4.4)

Figures 4.60 and 4.61 show the results of the (−6.7+3.35 mm) (2% inherent moisture air dry basis) and (−3.35+1.0 mm) (2.98% inherent moisture air dry basis) size fractions, respectively.

For the (−6.7+3.35 mm) size fraction dried for 24 hours (2% inherent moisture), the new measured mass was 520 g, resulting in a new moisture content of 5.76%. After being fed into the separator, a 0.25% mass loss (1.28 g lost from 520 g) was experienced. For the sample dried for 18 hours, the new measured mass was 533.31 g, resulting in an inherent moisture content of 8.12% and a 1.03% mass loss (5.49 g lost from 533.31 g). For the sample dried for 12 hours, the new measured mass was 549.24 g, with a moisture content of 10.79%, and approximately 7% mass loss was achieved after separation (38.45 g lost from 549.24 g). At six hours, the new measured mass was 592.81 g, resulting in a moisture content of 17.34%. The separation of this sample in the wind-sifter resulted in a mass loss of about 52.81%. This occurred because some particles were stuck to the paddles/vanes of the rotary hopper valve due to their moisture content. For the (−6.7+3.35) size fraction, the author recommends using coal with at least 8% inherent moisture in the optimised separator.

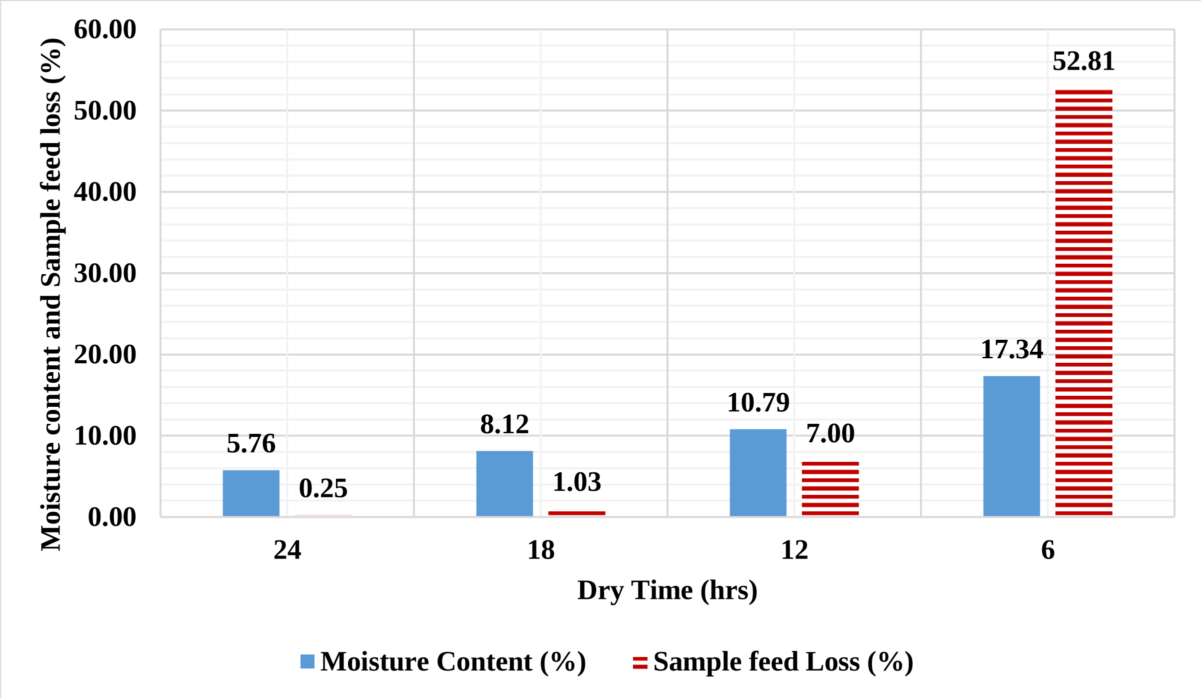

Figure 4.60: Effect of moisture on the (−6.7+3.35 mm) size fraction

For the particle size of (−3.35+1.0 mm) (Figure 4.61) with an inherent moisture content of 2.98%, after 24 hours of drying, the new measured mass was 512.19 g, with a new moisture content of 5.28%. After separation in the wind-sifter, a mass loss of 1.05% was observed. For the sample dried for 18 hours, a new mass of 520.22 g was achieved, with a new moisture content of 6.75% and a mass loss of 3.49% after separation. With the sample dried for 12 hours, a new mass of 534.87 g and a new moisture content of 9.31% were achieved. A mass loss of approximately 21.04% was experienced during separation, which was very significant, leading to the termination of this investigation. For the (−3.35+1.0 mm) size fraction, the author recommends using coal with at least 6% inherent moisture.

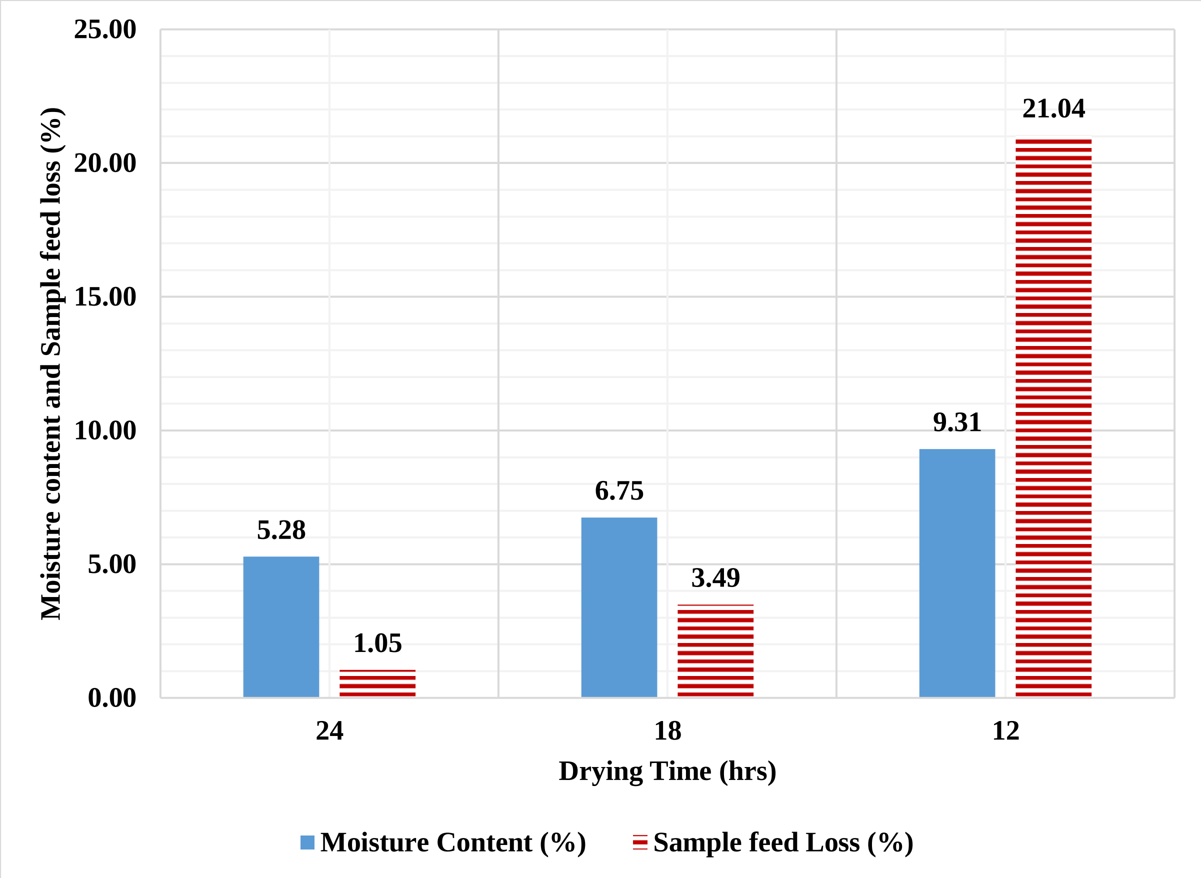

Figure 4.61: Effect of moisture on the (−3.35+1.0 mm) size fraction

4.5. SUMMARY

The newly fabricated and optimised wind-sifter separator was used to upgrade coal A and B coals from the Witbank coalfield at three particle size distributions. Results obtained from this process were compared with the results from the sink and float analysis of the same coal fractions. The results show that the separator could upgrade both coals at the targeted particle size fractions, but it was not as effective as the wet process tested. With the present design, the cleanest coal product achieved was 16.73% ash content from feed coal of 37.38% ash content. This meets the ash content of RB2 coal (Global Coal, 2024) and surpasses the average ESKOM (South African power utility) coal quality for thermal power generation between RB3 and RB 4 (National Coal, 2024a, 2024b; Global Coal , 2024). The results of this test show that the optimised wind-sifter separator can operate with and without bins, proving its suitability for continuous process applications. The results indicate the new design has significantly better sifting effectiveness than the previous separator design (Alade, 2021). It produces higher mass yield products with less sample loss compared to the old/previous design.

CHAPTER 5: CONCLUSION AND RECOMMENDATION

5.1. CONCLUSION

In this study, the wind-sifting principle was used to design and fabricate the optimised version of the initially designed wind-sifter separator. The fabricated separator was then used to beneficiate high-ash coal; coal with ash content ≥ 32% (National Coal, 2024b). The raw coal samples were screened to three particle size fractions and were fed into the newly designed separator for beneficiation. A few modifications were made to the prototype design. One of these includes modifying the air jet angle of the air-inlet section in chamber 1. The angle of 150 degrees vertical in chamber 1 of the prototype was adjusted to 165 degrees in the optimised version. Another modification was the number of collecting bins from seven in the prototype to ten in the optimised version. Yet another modification was the mode of operation; the optimised separator can operate with and without the coal collecting bins by placing the new separator assembly on a designed and fabricated cradle for the assembly. The dimensions of the optimized wind-sifter separator is not included in this thesis because documentations still need to be filed to protect the design for intellectual property.

The experimental study, which includes sink and float analysis, and the dry beneficiation test runs, was carried out to ascertain the present separation capability of this optimised separator. From this study, the following were achieved:

I. It was observed that parameters, such as the airstream velocity, particle size, particle density and particle shape, influenced the separation of particles within the separator.

II. It was also observed that the influence of shape on the particles is most prominent on the coarsest size fraction. This means that as the particle size fraction decreases, so does the influence of shape.

III. From the simulation results, it was predicted that the separator could run with and without the collecting bins effectively.

IV. For each particle size distribution used in this study, the reduction in airstream velocity also decreased the product’s ash content with a corresponding decrease in the yield. This is due to the lower airstream velocities being able to carry the lighter particles (predominantly coal) but not the heavier mineral-rich particles.

V. The ash content of the feed coal influences the results, which was observed from feed coal A’s (of higher ash content) and B’s (of lower ash content) results.

VI. For the (−6.7+3.35 mm) particle size fraction from coal A, the ash content of the clean coal products ranged from 26.97% at the highest air velocity to 20.21% at the lowest velocity. For Coal B of this size fraction, the cumulative ash content of the product ranged from 21.40% to 19.44% for the highest to lowest airstream velocities, respectively.

VII. Comparing both feed coal samples for the (−3.35+1.0 mm) particle size fraction, the ash content of the clean coal products from coal A ranged from 27.29% at the highest air velocity to 20.48% at the lowest velocity. For Coal B of this size fraction, the product's cumulative ash content ranged from 21.40% to 19.44% for the highest and lowest airstream velocities, respectively.

VIII. For the (−1.0+0.2 mm) particle size fraction, the ash content of the clean coal product from coal A ranged from 26.74% at the highest air velocity to 19.59% at the lowest air velocity. For Coal B of this size fraction, the product's cumulative ash content ranged from 23.55% to 20.78% for the highest and lowest airstream velocities, respectively.

IX. The second-stage test was beneficial and may be necessary when beneficiating very high-ash coal. This allows operators to attain a clean coal product that meets customers' requirements.

X. When running the separator without the bins, clean coal products with a cumulative ash content ranging from 22.42% to 19.44% for the (−6.7+3.35 mm) particles, 24.61% to 21.43% for the (−3.35+1.0 mm) particles and 27.54% to 22.51% for the (−1.0+0.2 mm) particles were obtained.

XI. Best separation results were obtained for the coarsest size fraction (−6.7+3.35 mm) in all separation tests.

5.2. RECOMMENDATIONS

The present study has portrayed that the optimised wind-sifter can upgrade two coal samples, denoted in this study as coal A and coal B. Although this present design addressed challenges experienced in the previous design (Alade, 2021), some challenges were still observed. While the optimised design mitigated the sample loss observed in the previous separator (more than 50%), some losses (around 2.25% to 7.06%) were still observed for the finest size fraction. This loss likely results in abrading the fine particles from the rotation of the paddles/vanes. This means particles were further reduced (lower than 0.2 mm, which is the cut-size). To address this, one of the two recommendations can be adopted. First, pass the (−1.0+0.2 mm) particles through a pre-drying section before feeding into the separator. Second, the cut-size for the (−1.0+0.2 mm) should be increased to at least 0.5 mm if the operators want to circumvent the associated cost of drying.

Another challenge, which is the main challenge when running this separator, was that a significant amount (up to 20%) of the feed was elutriated into the hatchet section. This is because the coal particles do not attain their settling velocities quickly enough. This may be because the inlet transition piece section of chamber 2 is too short. This means that the inlet transition piece of this design would contribute little to no particle settling, particularly at a relatively higher velocity and or buoyancy force. This means that only the ***main diffuser section*** is responsible for making the particles attain their settling velocities. It is recommended that the length of the transition piece be increased, as shown in Figure 5.1, to help improve the particles' settling efficiency and attain their settling/terminal velocities faster. The length can be in the range of 175 mm to 200 mm (at the operator's discretion) for this present design, which means a proportional dimension will be factored into a plausible scaling up. Also, in chamber 1, following the logic from Figure 5.1, the lengths of the transition pieces labelled ***A*** and ***B*** in Figure 5.3 can be increased by at most 50 mm. This should be done to facilitate more effective particle elutriation whilst not reducing the dynamic pressure of the airstream. Figures 5.1 and 5.2 show the adjusted inlet diffuser length of chamber 2, while Figure 5.3 shows the transition pieces of chamber 1.

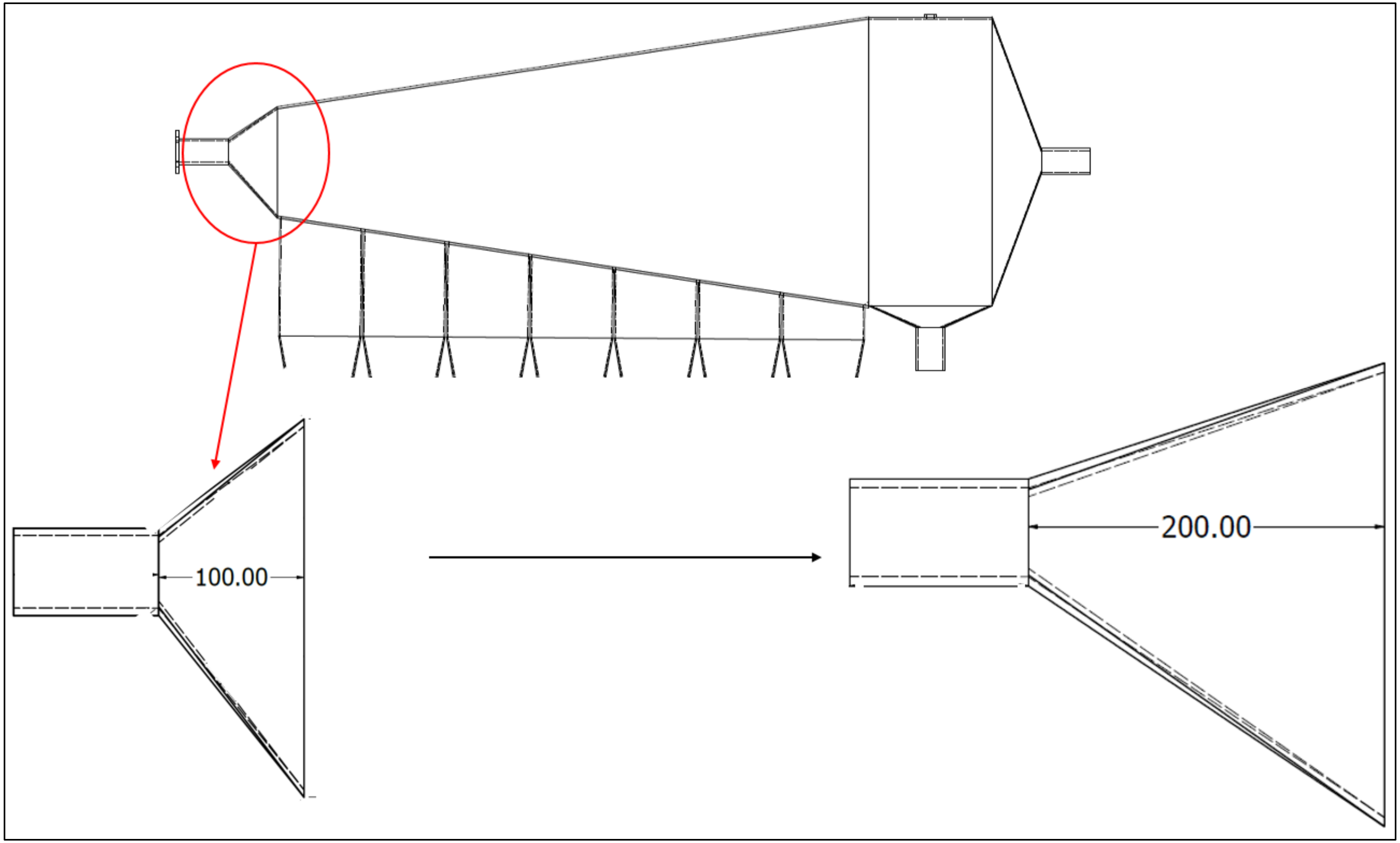

Figure 5.1: Adjustment for the inlet diffuser section of chamber 2 to enhance particle settling

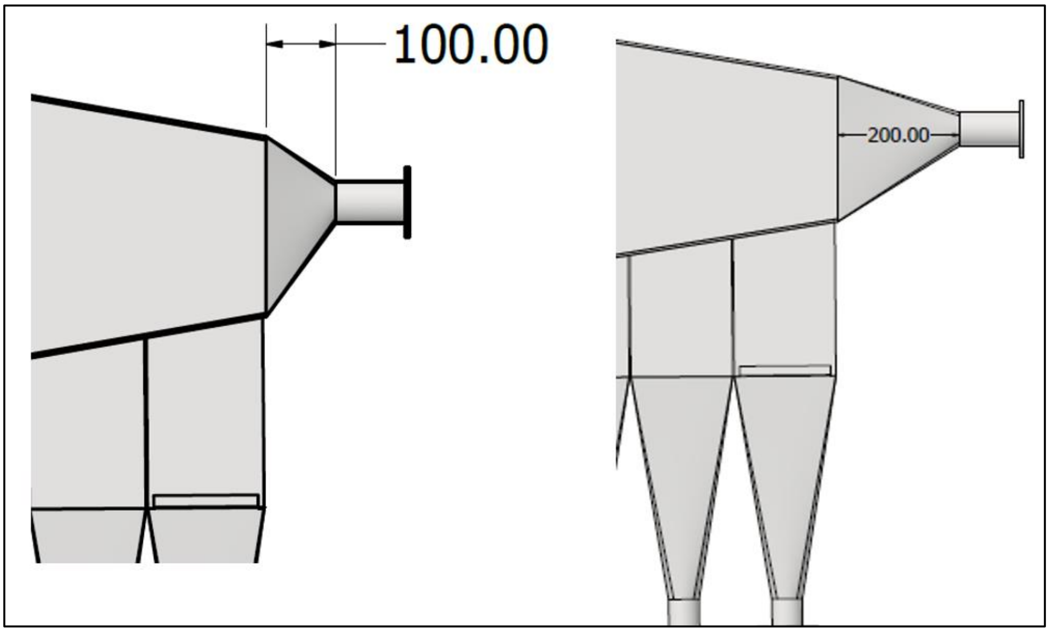

Figure 5.2: Adjusted inlet diffuser section in the chamber 2.

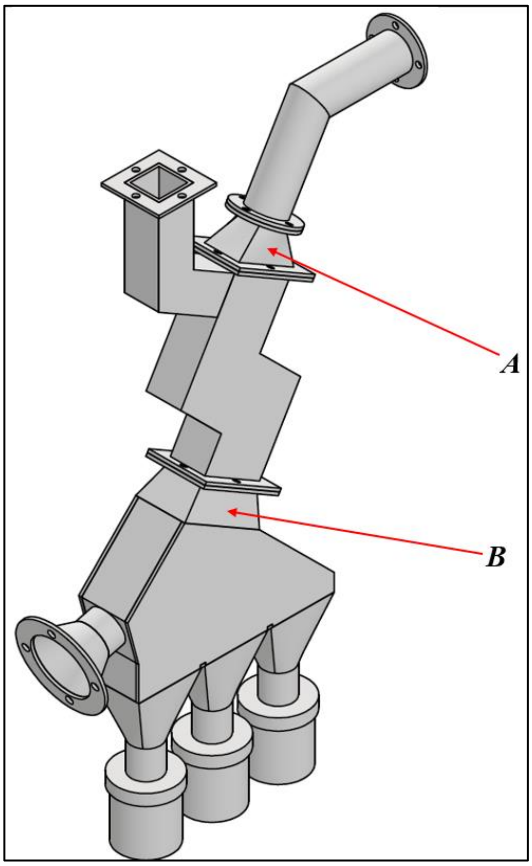

Figure 5.3: Identified transition pieces (A and B) in chamber 1 for the length increment

LIST OF REFERENCES

Adamčík, M., Svěrák, T. & Peciar, P. 2017. Parameters effecting forced vortex formation in blade passageway of dynamic air classifier. *Acta Polytechnica*. 57(5): 304-315. DOI:10.14311/AP.2017.57.0304.

Akbari, H., Ackah, L. & Mohanty, M. 2017. Performance optimization of a new air table and flip-flow screen for fine particle dry separation. *International Journal of Coal Preparation & Utilization*. 40(9): 581-603. DOI:10.1080/19392699.2017.1389727.

Aktaş, Z., Karacan, F. & Olcay, A. 1998. Centrifugal float–sink separation of fine Turkish coals in dense media. *Fuel Processing Technology*. 55(3): 235-250.

Alade, J.J. 2021. Beneficiating high ash coal using wind sifter. MSc. Dissertation. University of the Witwatersrand. https://hdl.handle.net/10539/32946.

Alade, J.J. & Bada, S.O. 2023. Wind-sifting separation: A review. *ACS Omega*. 8(38): 34196-34205. DOI:10.1021/acsomega.3c01087.

Alade, J., Bada, S.O. & Schmitz, W. 2021. Computer-aided design and fabrication of a dry wind-sifter separator. *ACS Omega*. 6(31): 20309-20320. DOI:10.1021/acsomega.1c02192.

AllMineralJig, 2018. Available: https://www.allmineral.com/en/products/alljigr/. [2023 November 19].

Ambrós, W.M., 2020. Jigging: A review of fundamentals and future directions. *Minerals*, *10*(11), p.998.

Azimi, E., Karimipour, S., Rahman, M., Szymanski, J. & Gupta, R. 2013. Evaluation of the performance of air dense medium fluidized bed (ADMFB) for low-ash coal beneficiation. Part 1: Effect of operating conditions. *Energy & Fuels*. 27(10): 5595-5606. DOI:10.1021/ef400456n.

Bada, S.O., Falcon, L.M., Falcon, R. & Du Cann, V.M. 2012. Qualitative analysis of fine coals obtained from triboelectrostatic separation. *Journal of the Southern African Institute of Mining & Metallurgy*. 112(1): 55-62.

Bada, S.O., Tao, D., Honaker, R.Q., Falcon, L.M. & Falcon, R.M.S. 2010a. A study of rotary tribo-electrostatic separation of South African fine coal. *International Journal of Coal Preparation and Utilization*. 30(2-5): 154-172.

Bada, S.O., Tao, D., Honaker, R., Falcon, L. & Falcon, R. 2010b. Parametric study of electrostatic separation of South African fine coal. *Mining Science & Technology (China)*. 20(4): 535-541. DOI:10.1016/S1674-5264(09)60239-8.

Bao, Y., Lin, S. & Weng, L. 2009. Three-dimensional computer aided design of a vertical winnower. *International Conference on Computer and Computing Technologies in Agriculture*. 1497-1503. In *Computer and Computing Technologies in Agriculture II*. Volume 2. CCTA 2008. IFIP Advances in Information and Communication Technology. 294. D. Li, & C. Zhao, Eds. Boston, MA: Springer. DOI:10.1007/978-1-4419-0211-5_79.

Barreiros, F.M., Ferreira, P.J. and Figueiredo, M.M., 1996. Calculating shape factors from particle sizing data. *Particle & particle systems characterization*, *13*(6), pp.368-373.

Behera, S.K., Meena, H., Chakraborty, S. and Meikap, B.C., 2018. Application of response surface methodology (RSM) for optimization of leaching parameters for ash reduction from low-grade coal. *International Journal of Mining Science and Technology*, Vol 28, 621-629.

Benson, J.M. 2012. Safety consideration when handling metal powders. *Journal of the Southern African Institute of Mining & Metallurgy*. 112(7): 563-575.

Blanke, J., Krones AG, 2015. *Zig-zag classifier and method for classifying for separating material to be separated*. U.S. Patent 9,174,242.

Boylu, F., Çinku, K., Çetinel, T., Karakaş, F., Güven, O., KaraağaçlIoğlu, I.E. & Çelik, M.S. 2015. Effect of coal moisture on the treatment of a lignitic coal through a semi-pilot-scale pneumatic stratification jig. *International Journal of Coal Preparation & Utilization*. 35(3): 143-154. DOI:10.1080/19392699.2015.1005743.

BP. 2022. *Statistical review of World Energy 2022*. Available: https://www.bp.com/content/dam/bp/business-sites/en/global/corporate/pdfs/energy-economics/statistical-review/bp-stats-review-2022-full-report.pdf. [2023, August 05]

Bunt, J.R., Neomagus, H.W., Botha, A.A. and Waanders, F.B., 2015. Reactivity study of fine discard coal agglomerates. *Journal of analytical and applied pyrolysis*, *113*, pp.723-728.

Cairncross, B. 2001. An overview of the Permian (Karoo) coal deposits of southern Africa. *Journal of African Earth Sciences*. 33(3-4): 529-562. DOI:10.1016/S0899-5362(01)00088-4.

Campbell, Q.P., Le Roux, M. & Smith, I.G.T. 2015. Water-only laboratory coal fractionation using the reflux classifier. *Minerals Engineering*. 83: 59-63. DOI:10.1016/j.mineng.2015.08.015.

Cappelli, A., Oliva, N. and Cini, E., 2020. Stone milling versus roller milling: A systematic review of the effects on wheat flour quality, dough rheology, and bread characteristics. *Trends in Food Science & Technology*, *97*, pp.147-155.

Ceresiat, L., Grosshans, H. & Papalexandris, M.V. 2019. Powder electrification during pneumatic transport: The role of the particle properties and flow rates. *Journal of Loss Prevention in the Process Industries*. 58: 60-69. DOI:10.1016/j.jlp.2019.01.010.

Çetinkaya, Z. & Bayat, O. 2020. Upgrading low-rank coals (Çan, Çanakkale/Turkey) by float-sink separation in dense media. *Energy Sources, Part A: Recovery, Utilization, & Environmental Effects*. 42(1): 113-120. DOI:10.1080/15567036.2019.1587059.

Chagwedera, K.M. 2017. Cost evaluation of different medium solids for Air Dense Medium Fluidized Bed coal separation. MSc. Dissertation. University of the Witwatersrand.

Chagwedera, K.M., Bada, S.O. & Falcon, R.M.S. 2018. Evaluation of alternative solid media for coal beneficiation using an air dense-medium fluidized bed. *Journal of the Southern African Institute of Mining & Metallurgy*. 118(8): 883-890. DOI:10.17159/2411-9717/2018/v118n8a12.

Chalavadi, G. & Das, A. 2015. Study of the mechanism of fine coal beneficiation in air table. *Fuel*. 154: 207-216. DOI:10.1016/j.fuel.2015.03.063.

Chalavadi, G., Singh, R.K. and Das, A., 2016. Processing of coal fines using air fluidization in an air table. *International Journal of Mineral Processing*, *149*, pp.9-17.

Charan, T.G., Chattopadhyay, U.S., Singh, K.M.P., Kabiraj, S.K. & Haldar, D.D. 2011. Beneficiation of high-ash, Indian non-coking coal by dry jigging. *Mining, Metallurgy & Exploration*. 28(1): 21-23. DOI:10.1007/BF03402320.

Charan, T.G., Riazi M.R. & Gupta, R. 2016. Coal beneficiation. In *Coal Production and Processing Technology*. M.R. Riazi & R. Gupta, Eds. Boca Raton: CRC Press. DOI:10.1201/b19352.

Chen, Q. and Wei, L., 2003. Coal dry beneficiation technology in China: the state-of-the-art. *China Particuology*, *1*(2), pp.52-56.

Cheng, G., Cao, Y., Zhang, C., Jiang, Z., Yu, Y. & Mohanty, M.K. 2020. Application of novel flotation systems to fine coal cleaning. *International Journal of Coal Preparation & Utilization*. 40(1): 24-36. DOI:10.1080/19392699.2018.1476348.

Choung, J., Mak, C. & Xu, Z. 2006. Fine coal beneficiation using an air dense medium fluidized bed. *Coal Preparation*. 26(1): 1-15. DOI: 10.1080/07349340600619345.

Çicek, T. 2008. Dry cleaning of Turkish coal. *Energy Sources, Part A: Recovery, Utilization, & Environmental Effects.* 30(7): 593-605. DOI:10.1080/15459620600826449.

Dave, P.C. 2012. Dry cleaning of coal by a Laboratory Continuous Air Dense Medium Fluidised Bed Separator. MSc. Dissertation. University of Alberta. DOI:10.7939/R3K339.

De Korte, G.J. 2014. Dry processing of coal – Status update. (Report; Csir/Nre/Mnr/Er/20140040B). Coaltech, South Africa.

De Korte, G.J. 2015. Processing low-grade coal to produce high-grade products. *Journal of the Southern African Institute of Mining & Metallurgy*. 115(7): 569-572. DOI:10.17159/2411-9717/2015/v115n7a2.

De la Fuente, T., Bergström, D., González-García, S. & Larsson, S.H. 2018. Life cycle assessment of decentralized mobile production systems for pelletizing logging residues under Nordic conditions. *Journal of Cleaner Production*. 201: 830-841. DOI:10.1016/j.jclepro.2018.08.030.

Department of Mineral Resources and Energy, 2023. *2023 SOUTH AFRICAN ENERGY PRICE REPORT*. Available: https://www.energy.gov.za/files/media/explained/Energy-Price-Report-2023.pdf. [2023, December, 08]

Dong, L., Wang, Z., Zhou, E., Wang, X., Li, G., Fan, X., Zhang, B., Duan, C., Chen, Z., Luo, Z. & Jiang, H. 2019. A novel dry beneficiation process for coal. *International Journal of Coal Preparation & Utilization*. 42(4): 1105-1125. DOI:10.1080/19392699.2019.1692339.

Dong, L., Wang, Z., Zhou, E., Wang, X., Li, G., Fan, X., Zhang, B., Duan, C., Chen, Z., Luo, Z. and Jiang, H., 2022. A novel dry beneficiation process for coal. *International Journal of Coal Preparation and Utilization*, *42*(4), pp.1105-1125.

Duan, C., Yuan, W., Cai, L., Lv, K., Zhao, Y., Zhang, B., Dong, L. & Lv, P. 2015. Characteristics of fine coal beneficiation using a pulsing air dense medium fluidized bed. *Powder Technology*. 283: 286-293. DOI:10.1016/j.powtec.2015.05.033.

Dwari, R.K., Mohanta, S.K., Rout, B., Soni, R.K., Reddy, P.S.R. & Mishra, B.K. 2015. Studies on the effect of electrode plate position and feed temperature on the tribo-electrostatic separation of high ash Indian coking coal. *Advanced Powder Technology*. 26(1): 31-41. DOI:10.1016/j.apt.2014.08.001.

Dwari, R.K. & Rao, K.H. 2007. Dry beneficiation of coal – A review. *Mineral Processing & Extractive Metallurgy Review. An International Journal*. 28(3): 177-234. DOI:10.1080/08827500601141271.

Dwari, R.K. & Rao, K.H. 2009. Fine coal preparation using novel tribo-electrostatic separator. *Minerals Engineering*. 22(2): 119-127. DOI:10.1016/j.mineng.2008.05.009.

Eichert, C., Kernbaum, S. and Solenthaler, C., 2008, March. WEEE treatment by vertical hammer mill–technological results, economic value and ecological implications. In *Proceedings of the 15th CIRP International Conference on Life Cycle Engineering (LCE 2008)* (pp. 17-19).

England, T., Hand, P.E., Michael, D.C., Falcon, L.M. & Yell, A.D. 2002. Rank and types of coal, In Coal preparation in South Africa. 4th Ed. South African Coal Processing Society. 8-13.

EnergyGov 2023. Avalaible: https://www.energy.gov/fecm/improving-competitiveness-coal. [2023, October, 23]

ERGA Global Zigzag Separators. 2022. *Air separator (pneumatic separator) ERGA ZZFlow*. Available: https://rusmagnet.com/catalog/gravity-separators/zig-zag-air-separator/. [2023, June 25].

Ericsson, M. 1991. Minerals and metals production technology: A survey of recent developments. *Resources Policy.* 17(4): 284-300. DOI:10.1016/0301-4207 (91)90014-M.

ESKOM, 2021 Available: https://www.eskom.co.za/wp-content/uploads/2021/08/CO-0007-Coal-in-SA-Rev-16.pdf. [2023, November 24]

Evangelopoulos, P., Sophonrat, N., Jilvero, H., & Yang, W. 2018. Investigation on the low-temperature pyrolysis of automotive shredder residue (ASR) for energy recovery and metal recycling. *Waste Management.* 76*:* 507-515. DOI:10.1016/j.wasman.2018.03.048.

Falcon, R.M.S. 1986. A brief review of the origin, formation and distribution of coal in southern Africa. *Mineral Deposits of Southern Africa*. 2: 1879-1898.

Fan, M., Chen, Q., Zhao, Y. and Luo, Z., 2001. Fine coal (6–1 mm) separation in magnetically stabilized fluidized beds. *International journal of mineral processing*, *63*(4), pp.225-232.

Fan, M., Chen, Q., Zhao, Y., Guan, Z.L.Y. and Li, B., 2002. Magnetically stabilized fluidized beds for fine coal separation. *Powder Technology*, *123*(2-3), pp.208-211.

Fan, M., Chen, Q., Zhao, Y., Tao, D., Luo, Z., Zhang, X., Tao, X. & Yang, G. 2006. Fine coal dry classification and separation. *Mining, Metallurgy & Exploration*. 23(1): 17-21. DOI:10.1007/BF03403330.

Feil, N.F., Sampaio, C.H. & Wotruba, H. 2012. Influence of jig frequency on the separation of coal from the Bonito seam - Santa Catarina, Brazil. *Fuel Processing Technology*. 96: 22-26. DOI:10.1016/j.fuproc.2011.12.010.

Fu, Z., Zhao, Y., Yang, X. & Duan, C. 2017. Spontaneous segregation behavior in a vibrated gas-fluidized bed for fine lignite dry cleaning. *Separation Science & Technology*. 52(12): 2017-2028. DOI:10.1080/01496395.2017.1307226.

Fu, Z., Zhu, J., Barghi, S., Zhao, Y., Luo, Z. & Duan, C. 2019. Dry coal beneficiation by the semi-industrial air dense medium fluidized bed with binary mixtures of magnetite and fine coal particles. *Fuel*. 243: 509-518. DOI:10.1016/j.fuel.2019.01.140.

Future Coal, 2023. *Coal Facts*. Available: https://www.futurecoal.org/coal-facts/. [2023 December, 08].

Galvin, K.P., Callen, A.M. & Spear, S. 2010. Gravity separation of coarse particles using the Reflux Classifier. *Minerals Engineering*. 23(4): 339-349. DOI:10.1016/j.mineng.2009.09.014.

Galvin, K.P., Zhou, J., Sutherland, J.L. and Iveson, S.M., 2020. Enhanced recovery of zircon using a REFLUX™ classifier with an inclined channel spacing of 3 mm. *Minerals Engineering*, *147*, p.106148.

Gericke. 2022. *Centrifugal sifter solutions for bulk solids and powder*. Available: https://www.gerickegroup.com/centrifugal-sifter-gs. [2023, January 29]

Ghosh, T. 2013. Modelling of an Air-based Density Separator. PhD Thesis. University of Kentucky. https://uknowledge.uky.edu/mng_etds/7.

Giani, H., Feil, A., Hornsby, K., Clausen, A. & Pretz, T. 2014. Processing concept for the production of biomass fuel from mixed municipal solid waste. Proceedings of the 2nd International Conference on Sustainable Solid Waste Management. 12-14 June 2014. Athens, Greece.

Global Coal SCoTA, 2024. SCoTA Specifications and Definitions. Available: https://www.globalcoal.com/scota/specifications.cfm. [2024, May 14]

Global Fire Power. 2023a. *Coal production by country (2023)*. Available: https://www.globalfirepower.com/coal-production-by-country.php#google_vignette. [2023, August 06].

Global Fire Power. 2023b. *Coal consumption by country (2023)*. Available: https://www.globalfirepower.com/coal-consumption-by-country.php. [2023, August 06].

Goran, G.K.A., 1951. *Method and apparatus for dividing pulverous material into desired fractions by means of a rotating sifting machine*. U.S. Patent 2,546,068.

Gornet, T.J., Davis, K.R., Starr, T.L. and Mulloy, K.M., 2002. Characterization of selective laser sintering™ materials to determine process stability. In *2002 International Solid Freeform Fabrication Symposium*.

Hacifazlioglu, H. 2018. Production of merchantable coal from low rank lignite coal by using FGX and subsequent IR drying. *International Journal of Coal Preparation & Utilization.* 40(6): 418-425. DOI:10.1080/19392699.2018.1450248.

Hagemeier, T., Glöckner, H., Roloff, C., Thévenin, D. & Tomas, J. 2014. Simulation of multi-stage particle classification in a zigzag apparatus. *Chemical Engineering & Technology*. 37(5): 879-887. DOI:10.1002/ceat.201300670.

Han, C. 1983. Coal cleaning by froth flotation. PhD Thesis. Iowa State University.

Hancox, P.J. & Götz, A.E. 2014. South Africa's coalfields—A 2014 perspective. *International Journal of Coal Geology*. 132: 170-254. DOI:10.1016/j.coal.2014.06.019.

He, J., Zhao, Y., He, Y.Q., Luo, Z. & Duan, C.L. 2013. Separation performance of raw coal from South Africa using the dense gas-solid fluidized bed beneficiation technique. *Journal of the Southern African Institute of Mining & Metallurgy*. 113(7): 01-08.

He, J., Zhao, Y., Huang, G. & Liu, C. 2018. Evaluation of the separation performance of an air dense medium gas-solid fluidized bed for coal cleaning: Effect of the binary dense media. *Advanced Powder Technology*. 29(12): 3265-3273. DOI:10.1016/j.apt.2018.09.008.

He, J., Zhao, Y., Zhao, J., Luo, Z., Duan, C. & He, Y. 2015. Separation performance of fine low-rank coal by vibrated gas–solid fluidized bed for dry coal beneficiation. *Particuology*. 23: 100-108. DOI:10.1016/j.partic.2015.02.006.

He, Y., Xie, W., Zhao, Y., Li, H. & Wang, S. 2017. Triboelectrostatic separation of pulverized fuel of coal power plant based on mineralogical analyses. *International Journal of Mineral Processing*. 166: 7-12. DOI:10.1016/j.minpro.2017.06.005.

Heinrich, M., Metallwerk Bahre KG, 1962. *Centrifugal mill with wind sifter*. U.S. Patent 3,055,597.

Hölzer, A. and Sommerfeld, M., 2008. New simple correlation formula for the drag coefficient of non-spherical particles. *Powder Technology*, *184*(3), pp.361-365.

Honaker, R.Q. 2007. *Coarse dry coal cleaning. Workshop on coal beneficiation & utilization of rejects. Initiatives, policies and practice.* 22-24 August 2007. Ranchi: India. 22-24.

Honaker, R.Q., Saracoglu, M., Thompson, E., Bratton, R., Luttrell, G.H. & Richardson, V. 2008. Upgrading coal using a pneumatic density-based separator. *International Journal of Coal Preparation & Utilization.* 28(1): 51-67. DOI:10.1080/19392690801934054.

Honaker, R.Q., Singh, N. & Govindarajan, B. 2000. Application of dense-medium in an enhanced gravity separator for fine coal cleaning. *Minerals Engineering*. 13(4): 415-427. DOI:10.1016/S0892-6875(00)00023-6.

Hoppe, T., Jaeger, N. and Terry, J. 2000. Safe handling of combustible powders during transportation, charging, discharging and storage. *Journal of Loss Prevention in the Process Industries*. 13(3-5): 253-263. DOI:10.1016/S0950-4230(99)00036-4.

Horsfall, D.W., Zitron, Z. & De Korte, G. 1986. The treatment of ultrafine coal, especially by froth flotation. *Journal of the Southern African Institute of Mining & Metallurgy*. 86(10): 401-407.

Hussain, G. 2013. Presentation on Dense Medium Separation. Available: https://www.slideshare.net/e_gulfam/dense-medium. [2024, May 05].

HSA. 2023. *Healthy, safe and productive lives and enterprises*. Available: https://www.hsa.ie/eng/topics/atex/. [2023, August 03].

IEA South-Africa 2023. South Africa. Available: https://www.iea.org/countries/south-africa. [2023, June 25].

IEA 2022. IEA Coal Market Updates 2022. Available: https://www.iea.org/reports/coal-market-update-july-2022/trade. Available [2023. November 26]

IEA, 2023 IEA Coal Market Updates 2023. Available: https://www.iea.org/reports/coal-market-update-july-2023/trade Available [2023, November 26]

Impact Air Systems. 2021. *Addtech acquires Impact Air Systems and Impact Technical Services*. Available: https://impactairsystems.com/addtech-acquires-impact-air-systems-and-impact-technical-services/ [2022, October 25].

International Atomic Energy Agency 2023. Available: https://www.iaea.org/topics/energy [2023, December 10]

Isaac, K. & Bada, S.O. 2020. The co-combustion performance and reaction kinetics of refuse derived fuels with South African high ash coal. *Heliyon*. 6(1): e03309. DOI:10.1016/j.heliyon.2020.e03309.

Iveson, S.M., Price, A. & Galvin, K.P. 2019. Separation of coal with a top size of up to 6 mm in a full-scale REFLUX™ Classifier. *International Journal of Coal Preparation & Utilization*. 42(3): 694-714. DOI:10.1080/19392699.2019.1646255.

Jaeger, N., 2001. Safety strategy against potential hazards due to the handling of powders in a blending unit. *Journal of Loss Prevention in the Process Industries*, *14*(2), pp.139-151.

Jafarinejad, S., 2016. *Petroleum waste treatment and pollution control*. Butterworth-Heinemann.

Jambal, D., Kim, B.G., Jeon, H.S. & Lee, J.H. 2017. Physical separation using an autogenous medium on coal. *Separation Science & Technology*. 52(5): 958-964. DOI:10.1080/01496395.2016.1254660.

James, P. 1982. Coal: Origins and exploitation. In *The future of coal*. London: Macmillan Press Ltd.

Jang, C., Kahn, N., Langlois, L., Liu, R. & Montanaro, G. 2014. Design of a Winnowing Machine for West African rice farmers. Available: https://escholarship.mcgill.ca/-concern/reports/6t053g21q. [2023, February 28].

Jeffrey, L.S., 2005. Characterization of the coal resources of South Africa. *Journal of the Southern African Institute of Mining & Metallurgy*. 105(2): 95-102.

Jeffrey, R., Falcon, R. & Kinghorn, A. 2014. The benefits and challenges associated with coal in South Africa. *Cornerstone.* 2: 66-70.

Jiao, H.G., Cui, J.Y., Liu, P., Chen, Q.R. & Tie, Z.X. 2009. Experimental study of magnetic property and dry magnetic separation of fine coal. *Journal of China University of Mining & Technology*. 38(1): 131-134.

Kaas, A., Mütze, T. & Peuker, U.A. 2022. Review on zigzag air classifier. *Processes*. 10(4): 764. DOI:10.3390/pr10040764.

Kemutec KEK Centrifugal Sifters, 2016. Available: https://www.kemutec.com/product/centrifugal-sifter/ [2023, February 20].

Killmeyer, R.P., Hucko, R.E. & Jacobsen, P.S. 1992. Centrifugal float-sink testing of fine coal: An interlaboratory test program. *Coal Preparation*. 10(1-4): 107-118. DOI:10.1080/07349349208905196.

Kimmeyer, L. and Schnatz, R., Krupp Polysius AG, 2003. *Method and air separator for classifying charging material reduced in size*. U.S. Patent 6,644,479.

Kopparthi, P., Awasthi, A., Sachinraj, D. & Mukherjee, A.K. 2019. Beneficiation of coal fines using the Reflux™ Classifier. *Minerals Engineering*. 136: 110-119. DOI:10.1016/j.mineng.2019.03.018.

Krauß, G., Kübler, J. & Trentini, E. 2002. Preparation and properties of pressureless infiltrated SiC and AlN particulate reinforced metal ceramic composites based on bronze and iron alloys. *Materials Science & Engineering: A*. 337(1-2): 315-322. DOI:10.1016/S0921-5093(02)00044-8.

Kretzschmar, S. 2010. Dry beneficiation of coal using an air dense-medium fluidised bed separator. MSc dissertation. University of KwaZulu Natal. http://hdl.handle.net/10413/769.

Krüger, B., Mrotzek, A. and Wirtz, S. 2014. Separation of harmful impurities from refuse derived fuels (RDF) by a fluidized bed. *Waste Management*. 34(2): 390-401. DOI:10.1016/j.wasman.2013.10.021.

Kumar, S. & Venugopal, R. 2017. Performance analysis of jig for coal cleaning using 3D response surface methodology. *International Journal of Mining Science and Technology*. 27(2): 333-337. DOI:10.1016/j.ijmst.2017.01.002.

Kumar, S. & Venugopal, R. 2020. Coal cleaning using jig and response surface approach for determination of quality of clean coal. *International Journal of Coal Preparation & Utilization*. 40(2): 107-115. DOI:10.1080/19392699.2017.1346631.

Kuyumcu, H.Z. & Rosenkranz, J. 2009. *Investigation of fluff separation from granulated waste plastics to be used in blast furnace operation*. Available: https://www.diva-portal.org/smash/get/diva2:1011223/FULLTEXT01.pdf. [2023, June 05].

Langner, D.J., 2016. *The dry beneficiation of duff coal in a dense medium fluidised bed* (Doctoral dissertation, North-West University (South Africa), Potchefstroom Campus).

Ling, X., He, Y., Li, G., Tang, X. & Xie, W. 2018. Separation performance of different particle sizes using an industrial FGX dry separator. *International Journal of Coal Preparation & Utilization*. 38(1): 30-39. DOI:10.1080/19392699.2016.1185418.

Lotfi, S., Di Maio, F., Xia, H., Serranti, S., Palmieri, R. & Bonifazi, G. 2015. Assessment of the contaminants level in recycled aggregates and alternative new technologies for contaminants recognition and removal. *EMABM 2015: Proceedings of the 15th Euroseminar on Microscopy Applied to Building Materials.* O. Copuroglu, Ed. 17-19 June 2015. Delft University of Technology, Netherlands. 319-331.

Luijsterburg, B. & Goossens, H. 2014. Assessment of plastic packaging waste: Material origin, methods, properties. *Resources, Conservation & Recycling.* 85: 88-97. DOI:10.1016/j.resconrec.2013.10.010.

Luo, Z., Zhao, Y., Chen, Q., Fan, M. and Tao, X., 2002. Separation characteristics for fine coal of the magnetically fluidized bed. *Fuel Processing Technology*, *79*(1), pp.63-69.

Luo, Z., Fan, M., Zhao, Y., Tao, X., Chen, Q. & Chen, Z. 2008. Density-dependent separation of dry fine coal in a vibrated fluidized bed. *Powder Technology*. 187(2): 119-123. DOI:10.1016/j.powtec.2008.02.001.

Luo, Z.F., Zhu, J.F., Fan, M.M., Zhao, Y.M. & Tao, X.X. 2007. Low density dry coal beneficiation using an air dense medium fluidized bed. *Journal of China University of Mining & Technology*. 17(3): 306-309. DOI:10.1016/S1006-1266(07)60094-7.

Lynch, A.J., Johnson, N.W., Manlapig, E.V. & Thome, C.G. 1981. *Mineral and coal flotation circuits – Their simulation and control*. Netherlands: ETDEWEB.

Ma, G., Bu, X., Xie, G., Peng, Y., Sha, J., Xia, W. and Wu, E., 2018. Comparative study of separation performance of a spiral and dense-medium cyclone on cleaning coal. *International Journal of Coal Preparation and Utilization.* 41(2): 108-116. DOI:10.1080/19392699.2018.1464001.

Maharaj, A., 2014. *Experimental and numerical studies of air preheater leakage* (Doctoral dissertation).

Makokha, A.B., Chikerema, P. and Kiprono, R.J., 2022, June. A Laboratory Scale Investigation Of Dry Coal Beneficiation In An Air Fluidized Bed: Effects Of Particle Size, Shape And Density. In *Proceedings of the Sustainable Research and Innovation Conference* (pp. 257-262).

Mann, H., Roloff, C., Hagemeier, T., Thévenin, D. & Tomas, J. 2017. Model-based experimental data evaluation of separation efficiency of multistage coarse particle classification in a zigzag apparatus. *Powder Technology*. 313: 145-160. DOI:10.1016/j.powtec.2017.03.003.

Mantashe, G. 2022: *Coal colloqiuim*. South African Government. Available: https://www.gov.za/speeches/minister-gwede-mantashe-coal-colloqiuim-1-feb-2022-0000. [2023, February 21]

Meshram, P., Purohit, B.K., Sinha, M.K., Sahu, S.K. & Pandey, B.D. 2015. Demineralization of low grade coal – A review. *Renewable & Sustainable Energy Reviews*. 41: 745-761. DOI:10.1016/j.rser.2014.08.072.

Meyer, E.J. and Craig, I.K., 2014. Coal dense medium separation dynamic and steady-state modelling for process control. *Minerals Engineering, 65*, pp.98-108.

Mielke, C. 2018. Ballistic separators for c&d and landfill mining applications: Technical features of heavy duty ballistic separators. *4th International Symposium on Enhanced Landfill Mining. Proceedings of the Enhanced Landfill Mining*. P.T. Jones & L. Machiels, Eds. 5-6 February 2018. Mechelen, Belgium. 107-112. Available:

https://www.diva-portal.org/smash/get/diva2:1651639/FULLTEXT01.pdf. [2023, January 29].

Mills, S. 2016. *Low quality coals—Key commercial, environmental and plant considerations*. IEA Clean Coal Centre. Available: https://usea.org/sites/default/files/Low%20quality%20coals%20-%20key%20commercial%2C%20environmental%20and%20plant%20considerations%20-ccc270.pdf [2023, November 26].

Millops, 2023. *AMIT 145: Lesson 3 Dense Medium Separation.* Available: https://millops.community.uaf.edu/amit-145/amit-145-lesson-3/. [2023, December 09]

Minerals Council South Africa. 2023. *Coal*. Minerals Council South Africa. Available: www.mineralscouncil.org.za/sa-mining/coal. [2023, August 07].

Mining Africa, 2022. Coal Mining – Supplying Energy to Africa. Available: https://miningafrica.net/natural-resources-africa/coal-mining-in-africa/. [2023, August 07]

Mining Technology. 2023a. *The five largest coal mines in operation in South Africa*. Available: https://www.mining-technology.com/marketdata/five-largest-coal-mines-south-africa/. [2023, August 20].

Mining Technology. 2023b. *Coal production in South Africa and major projects*. Available: https://www.mining-technology.com/data-insights/coal-in-south-africa/. [2023, August 20].

Mutezo, G. and Mulopo, J., 2021. A review of Africa's transition from fossil fuels to renewable energy using circular economy principles. *Renewable and Sustainable Energy Reviews*, Vol 137, 110609.

Napier-Munn, T. 2018. The dense medium cyclone – Past, present and future. *Minerals Engineering.* 116: 107-113. DOI:10.1016/j.mineng.2017.10.002.

National Coal, 2024a. The Difference between RB1, RB2, and RB3 Coal in South Africa. Available: https://www.nationalcoal.co.za/post/difference-between-rb1-rb2-rb3-coal-south-africa. [2024, May 14].

National Coal, 2024b. Understanding Eskom Coal Requirements. Available: https://www.nationalcoal.co.za/post/understanding-eskoms-coal-requirements. [2024, May 14]

Netsch, N., Simons, M., Feil, A., Leibold, H., Richter, F., Slama, J., Yogish, S.P., Greiff, K. and Stapf, D., 2022. Recycling of polystyrene-based external thermal insulation composite systems–Application of combined mechanical and chemical recycling. *Waste management*, *150*, pp.141-150.

Nifuku, M. and Katoh, H., 2003. A study on the static electrification of powders during pneumatic transportation and the ignition of dust cloud. *Powder Technology*, 135-136: 234-242. DOI:10.1016/S0032-5910(03)00163-3.Nishinari, K., Williams, P.A. and Phillips, G.O., 1992. Review of the physico-chemical characteristics and properties of konjac mannan. *Food Hydrocolloids.* 6(2): 199-222. DOI:10.1016/S0268-005X(09)80360-3.

Orem, W.H. and Finkelman, R.B., 2003. *Coal formation and geochemistry* (Vol. 7, p. 407).

Ozmak, M. & Aktas, Z. 2006. Coal froth flotation: Effects of reagent adsorption on the froth structure. *Energy & fuels*. 20(3): 1123-1130. DOI:10.1021/ef0503358.

Patil, D.P. & Parekh, B.K. 2011. Beneficiation of fine coal using the air table. *International Journal of Coal Preparation & Utilization*. 31(3-4): 203-222. DOI:10.1080/19392699.2011.574948.

Paul, S.R. & Bhattacharya, S. 2018. Size by size separation characteristics of a coal cleaning jig. *Transactions of the Indian Institute of Metals*. 71: 1439-1444. DOI:10.1007/s12666-018-1275-2.

Pawlik, M., 2022. Fundamentals of froth flotation. *ChemTexts*, *8*(4), p.19. Available: https://link.springer.com/content/pdf/10.1007/s40828-022-00170-5.pdf. [2023, December, 09]

Pehlken, A., Müller, D.H., 2009. Using information of the separation process of recycling scrap tires for process modelling. *Resources, Conservation and Recycling*, Vol 54, 140–148. doi.org/10.1016/j.resconrec.2009.07.008

Pettinari, M. & Simone, A. 2015. Effect of crumb rubber gradation on a rubberized cold recycled mixture for road pavements. *Materials & Design.* 85: 598-606. DOI:10.1016/j.matdes.2015.06.139.

Polat, M., Polat, H. & Chander, S. 2003. Physical and chemical interactions in coal flotation. *International Journal of Mineral Processing*. 72(1-4): 199-213. DOI:10.1016/S0301-7516(03)00099-1.

Prashant, D., Xu, Z., Szymanshki, J., Gupta, R. & Boddez, J. 2010. Dry cleaning of coal by a laboratory continuous air dense medium fluidized bed separator. Dry Coal Cleaning. *The International Coal Preparation Congress: 2010 Conference Proceedings*. R.Q. Honaker, Ed. Littleton: Society for Mining, Metallurgy & Exploration. 608-616.

Prevost, X.M., 2004, November. SA coal reserves, after the act. In *Presentation at the Fossil Fuel Foundation 10th Southern African Conference on Coal Science and Technology, Sandton, South Africa*.

Ragaert, K., Delva, L. & Van Geem, K. 2017. Mechanical and chemical recycling of solid plastic waste. *Waste Management.* 69: 24-58. DOI:10.1016/j.wasman.2017.07.044.

Rao, K.N. & Vidyadhar, A. 2006. Comparative studies between jigging and HMS for lowering of ash in a coal sample from Assam. *International Seminar on Mineral Processing Technology & Indo-Korean Workshop on Resource Recycling (MPT-2006).* NML Madras Center, Chennai, India. 629-631.

Rautenbach, R., Strydom, C.A., Bunt, J.R., Matjie, R.H., Campbell, Q.P. & Van Alphen, C. 2019. Mineralogical, chemical, and petrographic properties of selected South African power stations' feed coals and their corresponding density separated fractions using float-sink and reflux classification methods. *International Journal of Coal Preparation & Utilization*. 39(8): 421-446. DOI:10.1080/19392699.2018.1533551.

Reddy, Y.H., Purushothaman, K., Sreenivasan, M. & Sivakumar, E.R. 2021. Design and analysis of zigzag classifier in food industry applications. *Journal of Physics: Conference Series.* 2040(1): 012040. International Conference on Physics and Energy 2021 (ICPAE 2021). 24 March 2021, Kancheepuram, India. DOI 10.1088/1742-6596/2040/1/012040.

Redemann, K., Hartge, E.-U. & Werther, J. 2008. Ash management in circulating fluidized bed combustors. *Fuel.* 87(17-18): 3669-3680. DOI:10.1016/j.fuel.2008.07.002.

Reid, I. 2017. *Coal beneficiation*. IEA Clean Coal Centre. International Centre for Sustainable Carbon. Available: https://www.sustainable-carbon.org/report/coal-beneficiation-ccc-278/ . [2023, November 26].

Riazi, M.R. & Gupta, R. Eds. 2015. *Coal production and processing technology*. Boca Raton: CRC Press.

Riazi M. R., Gupta, R., 2016. Coal Beneficiation, in: Coal Production and Processing Technology. Taylor & Francis Group, LLC CRC Press.

Roloff, C., Lukas, E., van Wachem, B. & Thévenin, D. 2019. Particle dynamics investigation by means of shadow imaging inside an air separator. *Chemical Engineering Science*. 195: 312-324. DOI:10.1016/j.ces.2018.09.020.

Rumpf, H. and Leschonski, K., 1979. *Method of an apparatus for sifting particulate material in a cross-current*. U.S. Patent 4,132,634.

Rusmagnet, 2022. Available: https://rusmagnet.com/catalog/gravity-separators/erga-ds-densimetric-table. [2022, September 05]

Sahu, A.K., Biswal, S.K. and Parida, A., 2009. Development of air dense medium fluidized bed technology for dry beneficiation of coal–A review. *International Journal of Coal Preparation and Utilization*, *29*(4), pp.216-241.

Sahu, A.K., Tripathy, A., Biswal, S.K. and Parida, A., 2011. Stability study of an air dense medium fluidized bed separator for beneficiation of high-ash Indian coal. *International Journal of Coal Preparation and Utilization*, *31*(3-4), pp.127-148.

Sahu AK, Tripathy A, Biswal SK. Study on particle dynamics in different cross sectional shapes of air dense medium fluidized bed separator. Fuel 2013; 111: 472–7.

Sampaio, C.H., Aliaga, W., Pacheco, E.T., Petter, E. and Wotruba, H., 2008. Coal beneficiation of Candiota mine by dry jigging. *Fuel Processing Technology*, *89*(2), pp.198-202.

Santos, S.M., Tambourgi, E.B., Fernandes, F.A.N., Moraes Júnior, D. & Moraes, M.S. 2011. Dilute-phase pneumatic conveying of polystyrene particles: pressure drop curve and particle distribution over the pipe cross-section. *Brazilian Journal of Chemical Engineering*. 28(1): 81-88. DOI:10.1590/S0104-66322011000100010.

Scholtz, J., Du Plessis, K., Roche, R., Cresswell, M., Toerin, L., Voges, J., Reddy, D., De Korte, J., Craddock, M., Lok, G., McMillian, K., Buthelezi, V., Darley, P., Jacobs, Jakes, Campbell, Q., Jacobs, Jayson, 2015. Section2: Geology, in: Coal Preparation in Southern Africa. p. 17.

Schulz & Berger. 2014a. Available. https://www.youtube.com/watch?v=4G-3jSWgy2I. [2022, September 14].

Schulz & Berger. 2014b. Available: https://www.schulz-berger.com/media/pages/produkte/windsichter/2783218338-1597936937/schulz-berger-broschuere_dt.pdf. [2023, August 27]

Shanmugam, B.K., Vardhan, H., Raj, M.G., Kaza, M. and Sah, R., 2022. Evaluation of a new vibrating screen for dry screening fine coal with different moisture contents. *International Journal of Coal Preparation and Utilization*, *42*(3), pp.752-761.

Shapiro, M. & Galperin, V. 2005. Air classification of solid particles: A review. *Chemical Engineering & Processing: Process Intensification*. 44(2): 279-285. DOI:10.1016/j.cep.2004.02.022.

Shi, C., Cheng, G. & Wang, S. 2019. Optimization of coal washery tailings by flotation process. *Energies*. 12(20): 3956. DOI:10.3390/en12203956.

Song, S., Zhao, Y., Luo, Z. & Tang, L. 2012a. Motion behavior of particles in air-solid magnetically stabilized fluidized beds for separation. *International Journal of Mining Science & Technology*. 22(5): 725-729.

Song, S.L., Zhao, Y.M., Jia, Z.F., Tang, L.G. & Yang, X.L. 2012b. Fine coal particles separation by air solid magnetic fluidization. *Journal of China Coal Society*. 37(9): 1586-1590.

Soong, Y., Link, T.A., Schoffstall, M.R., Gray, M.L., Fauth, D.J., Knoer, J.P., Jones, J.R. & Gamwo, I.K. 2001. Dry beneficiation of Slovakian coal. *Fuel Processing Technology*. 72(3): 185-198. DOI:10.1016/S0378-3820(01)00187-4.

Stebbins, A.H. 1932. Air classifier. U.S. Patent No. 1,861,248. Available: https://patentimages.storage.googleapis.com/d7/9d/bf/e8286c018d2249/US1861248.pdf. [2022, November 22].

Steiling, W., Almeida, J.F., Vandecasteele, H.A., Gilpin, S., Kawamoto, T., O'Keeffe, L., Pappa, G., Rettinger, K., Rothe, H. and Bowden, A.M., 2018. Principles for the safety evaluation of cosmetic powders. *Toxicology letters*, *297*, pp.8-18.

Suresh, P.D., Kumar, V., Sripriya, R., Chakraborty, S. & Meikap, B.C. 2010. Performance characteristics of pilot plant dense media hydrocyclone for beneficiation of coal and 3-D CFD simulation. *Chemical Engineering Science*. 65(16): 4661-4671. DOI:10.1016/j.ces.2010.05.006.

Taole, R.E.L., 2015. *The impact of coal quality and technical operating conditions on the efficiency of a spreader stoker boiler* (Doctoral dissertation).

Terblanche, A.N. 2013. Dry beneficiation of fine coal using a fluidized dense medium bed. MSc. Dissertation. North-West University, Potchefstroom. http://hdl.handle.net/10394/15607.

Trennso Technik. 2018. *Recycling plants, screening technology, separating tables, wind sifters, dosing and conveying technology*. Available: https://www.tst.de/en/. [2023, November 27].

Tripathy, A., Panda, L., Sahoo, A.K., Biswal, S.K., Dwari, R.K. & Sahu, A.K. 2016. Statistical optimization study of jigging process on beneficiation of fine size high ash Indian non-coking coal. *Advanced Powder Technology*. 27(4): 1219-1224. DOI:10.1016/j.apt.2016.04.006.

Walton, O., Dreyer, C. & Riedel, E. 2015. U.S. Patent No: US 9,073,088 B2. Centrifugal size-separation sieve for granular materials. Available:

https://ntrs.nasa.gov/api/citations/20150014982/downloads/20150014982.pdf. [2022, December 29].

Wang, Y., Luo, Z., Huang, G., Ren, B. 2016. Effect of agitation on the characteristics of air dense medium fluidization. *International Journal of Mining Science & Technology*. 26(3): 383-387. DOI:10.1016/j.ijmst.2016.02.003.

Wang, G., Bai, X., Wu, C., Li, W., Liu, K. and Kiani, A., 2018. Recent advances in the beneficiation of ultrafine coal particles. *Fuel Processing Technology*, Vol 178, 104-125.

Wagner, J. N., Malumbazo, N., Falcon, R.M.S., 2018. Section1: Coalfields of South-Africa, in: Southern African Coals and Carbons. p. 13 – 15.

Williams, O.S.A., Daley, P., Perkins, J., Martinez-Mendoza, K.L., Guerrero-Perrez, J., Mazabuel, L.M.S., Saavedra, E.A.G., Trujillo, M., Barraza-Burgos, J., Barajas, M. and Romero, M.H., 2022. Upgrading of Low-Grade Colombian Coals via Low-Cost and Sustainable Calcium Nitrate Dense Media Separation. *ACS omega*, *7*(4), pp.3348-3358.

Wills, B.A. & Napier-Munn, T.J. 2006. An introduction to the practical aspects of ore treatment and mineral recovery. *Wills' Mineral Processing Technology*. Elsevier Science and Technolgy Books.

Woollacott, L.C., 2018. On the size dependence of the King stratification index. *Minerals Engineering*, *124*, pp.86-97.

Woollacott, L.C. and Silwamba, M., 2016. An experimental study of size segregation in a batch jig. *Minerals Engineering*, *94*, pp.41-50.

Xin-xi, Z., Dai-yong, D., Bing, T., Jin-song, W., Feng, D., Hai-sheng, L. & Rui-xin, M. 2009. Research on the triboelectrostatic separation of minerals from coal. *Procedia Earth and Planetary Science*. 1(1): 845-850. DOI:10.1016/j.proeps.2009.09.132.

Yang, X.L., Zhao, Y.M., Luo, Z.F., Chen, Z.Q., Song, S.L. & Duan, C.L. 2013a. Energy transfer mechanism of vibro-fludization and its separation for fine coal. *Journal of China University of Mining & Technology*. 42(2): 266-270.

Yang, X., Zhao, Y., Luo, Z., Song, S., Duan, C. & Dong, L. 2013b. Fine coal dry cleaning using a vibrated gas-fluidized bed. *Fuel Processing Technology*. 106: 338-343. DOI:10.1016/j.fuproc.2012.08.019.Yang, X., Zhao, Y., Zhou, E., Luo, Z., Fu, Z., Dong, L. and Jiang, H., 2015a. Kinematic properties and beneficiation performance of fine coal in a continuous vibrated gas-fluidized bed separator. *Fuel*, *162*, pp.281-287.

Yang, X., Wang, S., Zhang, Y., Zhao, Y. & Luo, Z. 2018. Dry beneficiation of fine coal using planar air jets. *Powder Technology*. 323: 518-524. DOI:10.1016/j.powtec.2017.10.042.

Yu, X., Luo, Z., Yang, X., Jiang, H., Zhou, E., Zhang, B. & Dong, L. 2016. Oil shale separation using a novel combined dry beneficiation process. *Fuel*. 180: 148-156. DOI:10.1016/j.fuel.2016.04.036.

Zhang, B., Akbari, H., Yang, F., Mohanty, M.K. & Hirschi, J. 2011. Performance optimization of the FGX dry separator for cleaning high-sulfur coal. *International Journal of Coal Preparation & Utilization*. 31(3-4): 161-186. DOI:10.1080/19392699.2011.574943.

Zhang, B., Zhao, Y., Luo, Z., Song, S., Li, G. & Sheng, C. 2014a. Utilizing an air-dense medium fluidized bed dry separating system for preparing a low-ash coal. *International Journal of Coal Preparation & Utilization*. 34(6): 285-295. DOI:10.1080/19392699.2014.880695

Zhang, L., Xia, X. & Zhang, J. 2014b. Improving energy efficiency of cyclone circuits in coal beneficiation plants by pump-storage systems. *Applied Energy*. 119: 306-313. DOI:10.1016/j.apenergy.2014.01.031.

Zhang, Z., Yan, G., Zhu, G., Zhao, P., Ma, Z. & Zhang, B. 2020. Using microwave pretreatment to improve the high-gradient magnetic-separation desulfurization of pulverized coal before combustion. *Fuel*. 274: 117826. DOI:10.1016/j.fuel.2020.117826.

Zhao, Y., Fu, Z., Yang, X., Luo, Z., Duan, C., Song, S. & Cai, L. 2015. Fine coal dry cleaning using an air dense medium fluidized bed with improved magnetite medium. *Procedia Engineering*. 102: 1133-1141. DOI:10.1016/j.proeng.2015.01.236.

Zhao, Y., Li, G., Luo, Z., Zhang, B., Dong, L., Liang, C. & Duan, C. 2017. Industrial application of a modularized dry-coal-beneficiation technique based on a novel air dense medium fluidized bed. *International Journal of Coal Preparation & Utilization*. 37(1): 44-57. DOI:10.1080/19392699.2015.1125344.

Zhao, Y., Yang, X., Luo, Z., Duan, C. & Song, S. 2014. Progress in developments of dry coal beneficiation. *International Journal of Coal Science & Technology*. 1: 103-112. DOI:10.1007/s40789-014-0014-5.

Zhenfu, L. & Qingru, C., 2001. Dry beneficiation technology of coal with an air dense-medium fluidized bed. *International Journal of Mineral Processing*. 63(3): 167-175. DOI:10.1016/S0301-7516(01)00049-7.

Zhou, S., Garbett, E.S. and Boucher, R.F., 1996. Gravity-enhanced magnetic (HGMS) coal cleaning. *Industrial & engineering chemistry research*, *35*(11), pp.4257-4263.

APPENDIX A: DESIGN OF THE OPTIMISED WIND-SIFTER SEPARATOR FROM AUTODESK INVENTOR SOFTWARE.

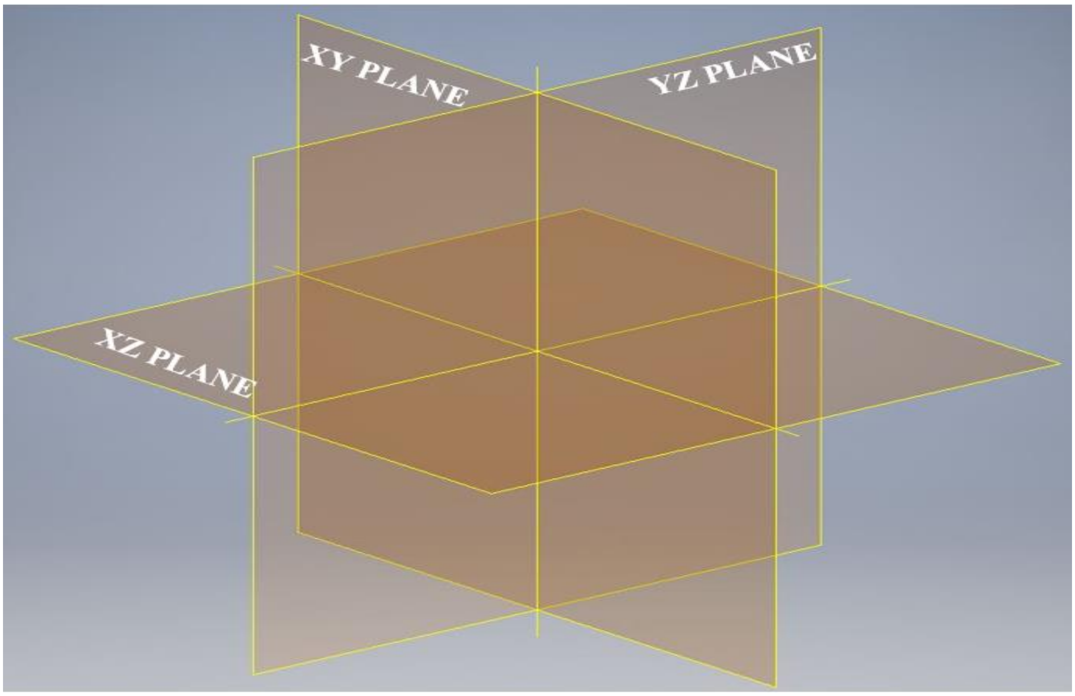

Figure A.1: The three-dimensional Cartesian planes when starting a new drawing

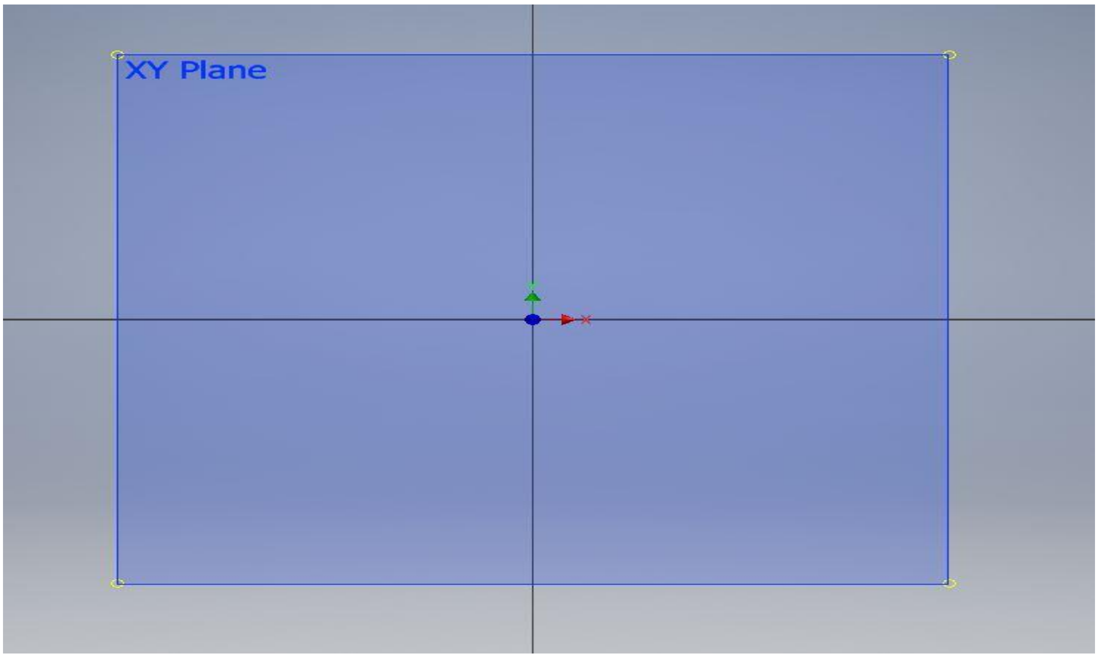

Figure A.2: XY plane selected to draw the first chamber

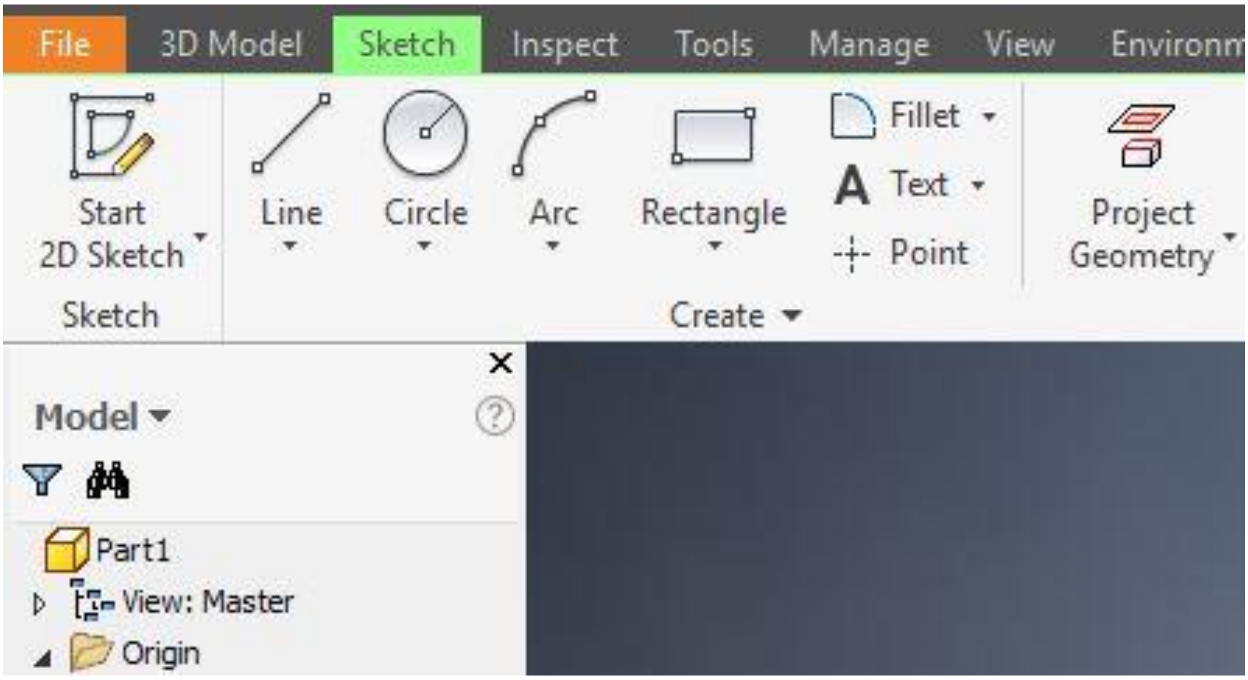

Figure A.3: Selecting the “Sketch” tab and then “Circle” to draw the first circle

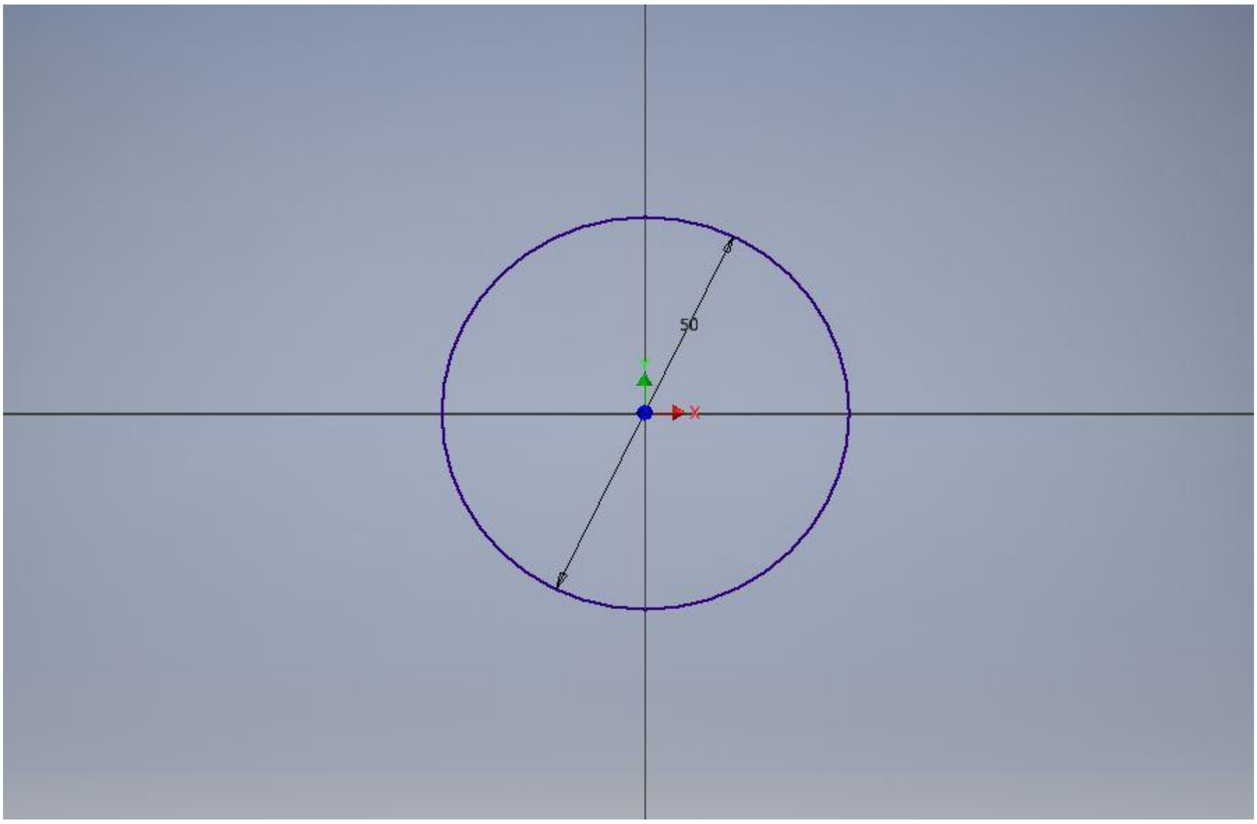

Figure A.4: The first circle of 50 mm in dimension, representing the outlet of the first chamber 1 drawn on the XY plane.

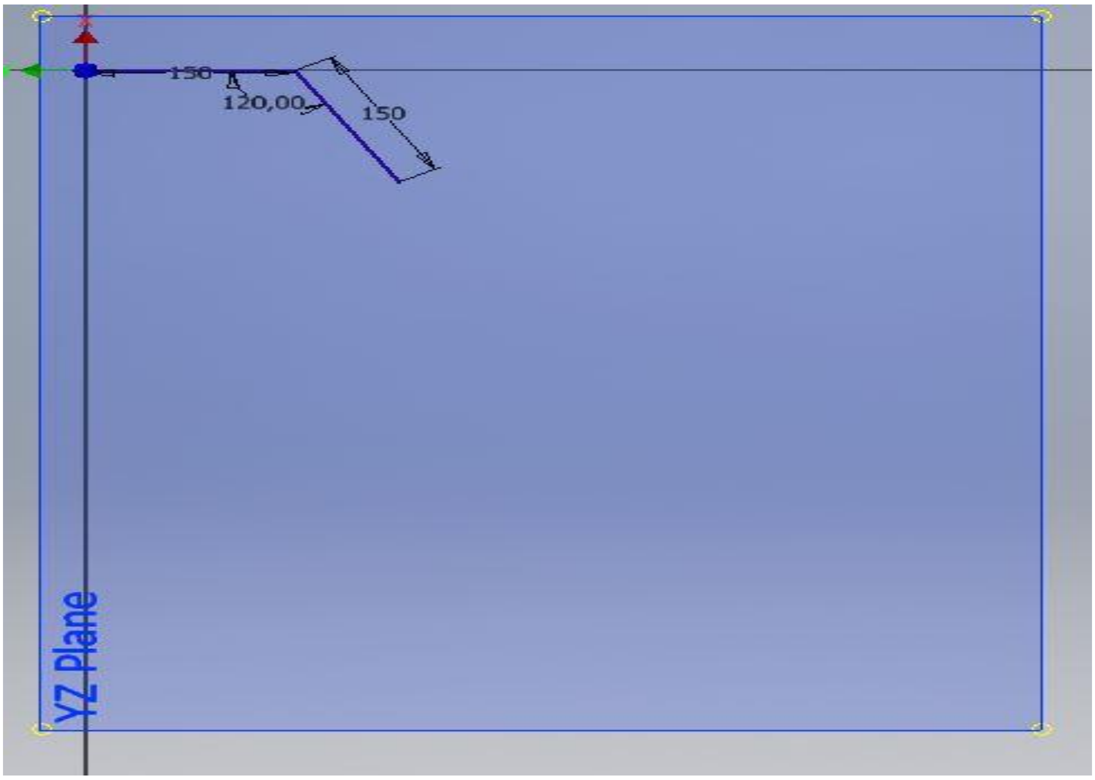

Figure A.5: lines drawn on the YZ plane to represent the outlet pipe.

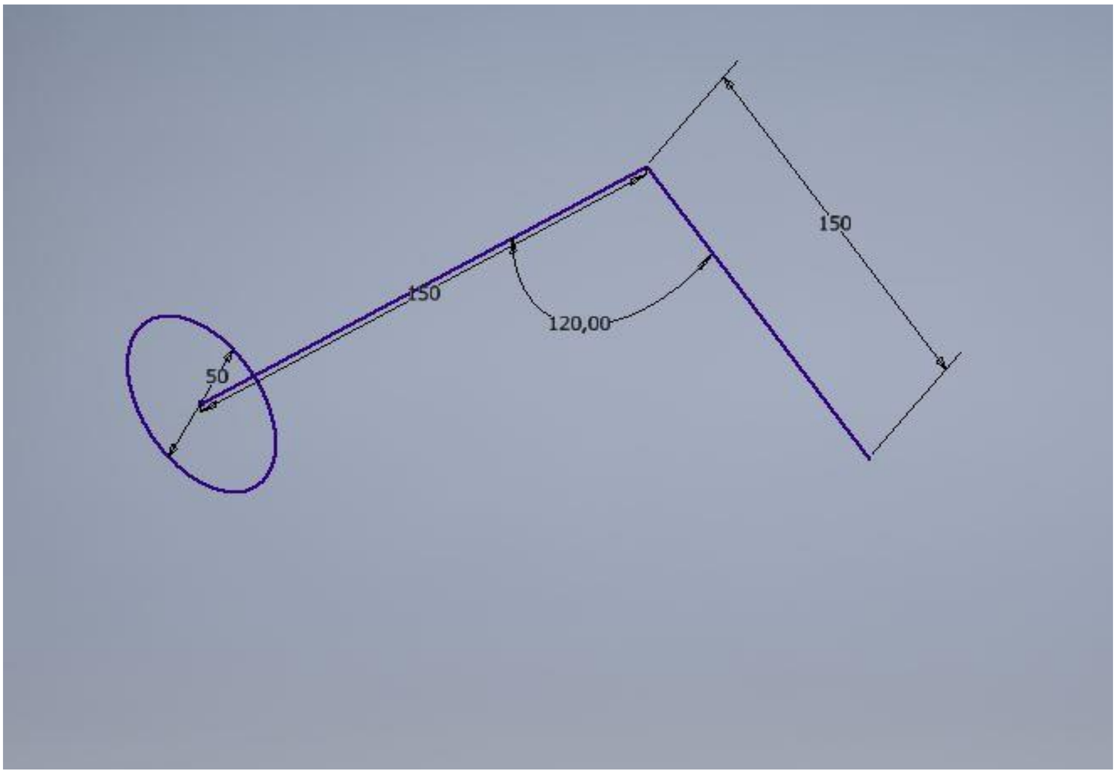

Figure A.6: The circle and the line drawn to create the outlet pipe of chamber 1

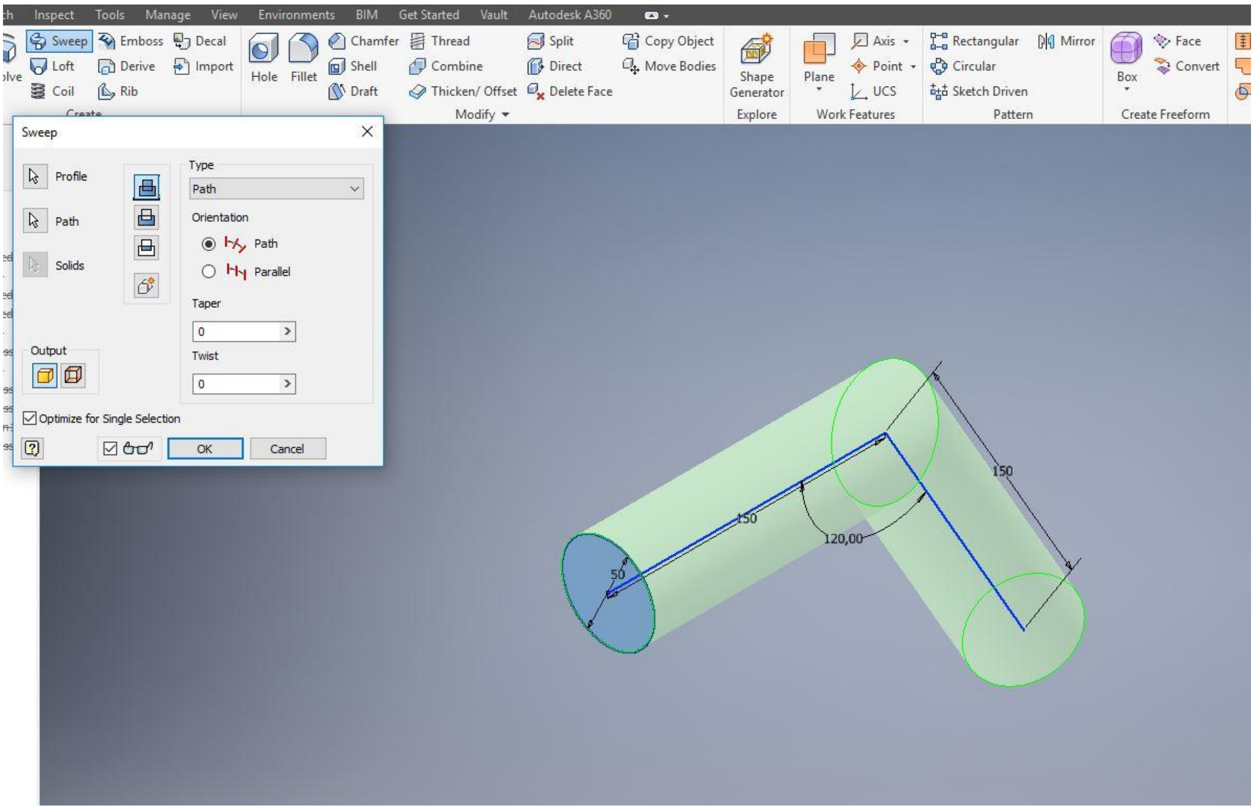

Figure A.7: Creating the outlet of the first chamber using the “Sweep” tool

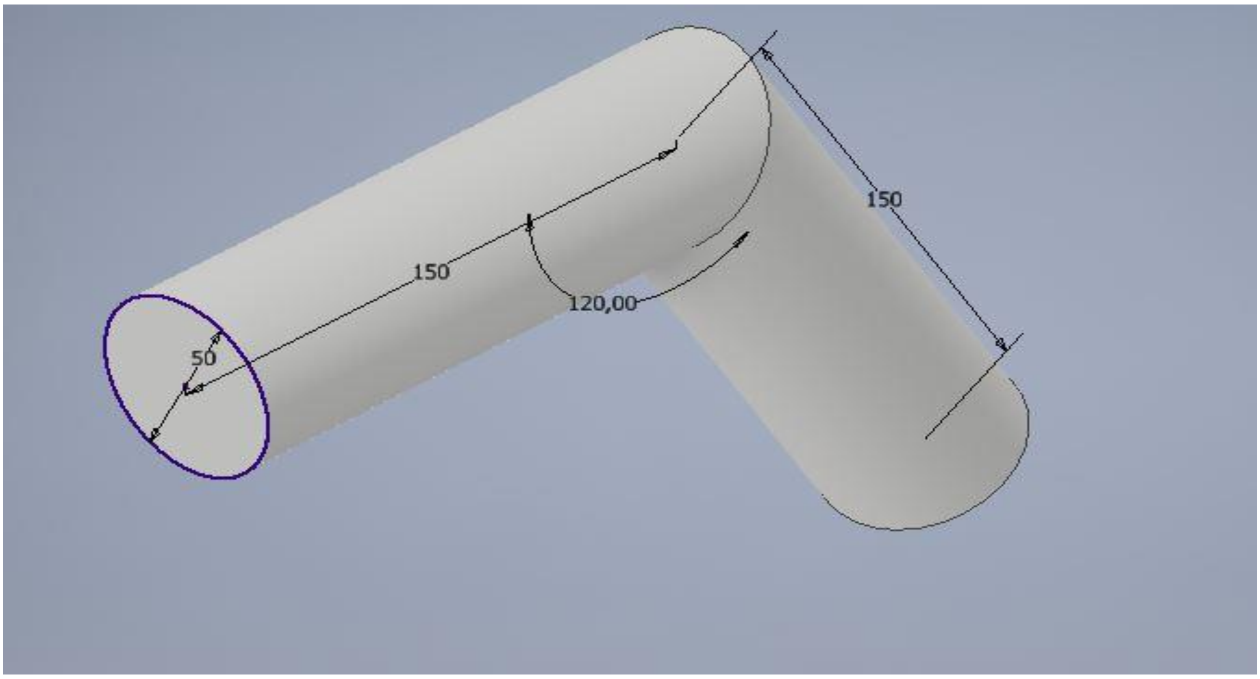

Figure A.8: Outlet pipe created

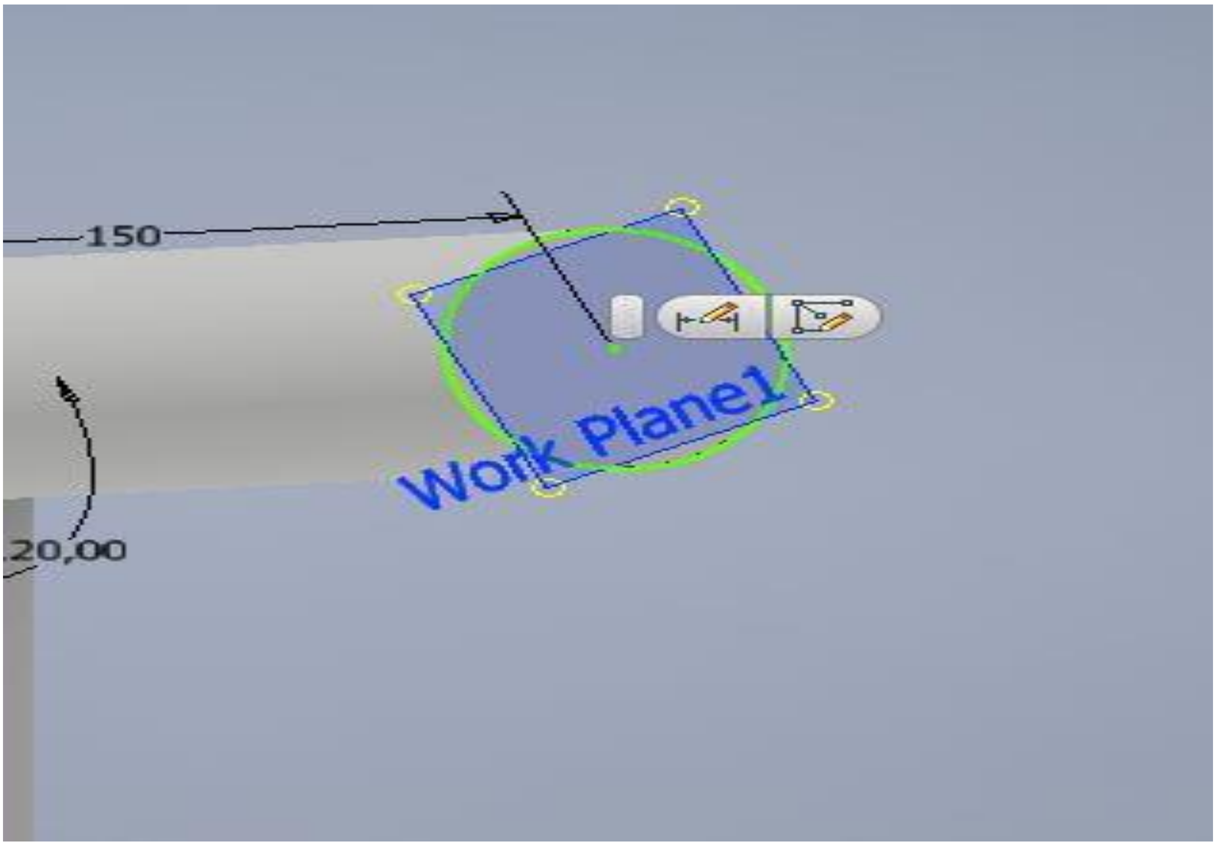

Figure A.9: Base part of the Chamber 1-outlet pipe is lifted to draw the design transition piece.

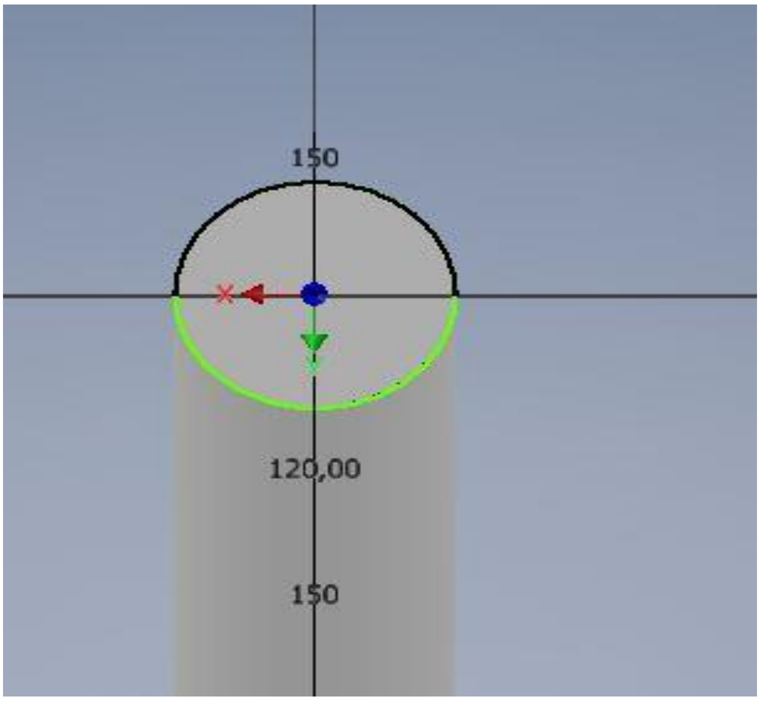

Figure A.10: Circle drawn and the base of the Outlet Pipe

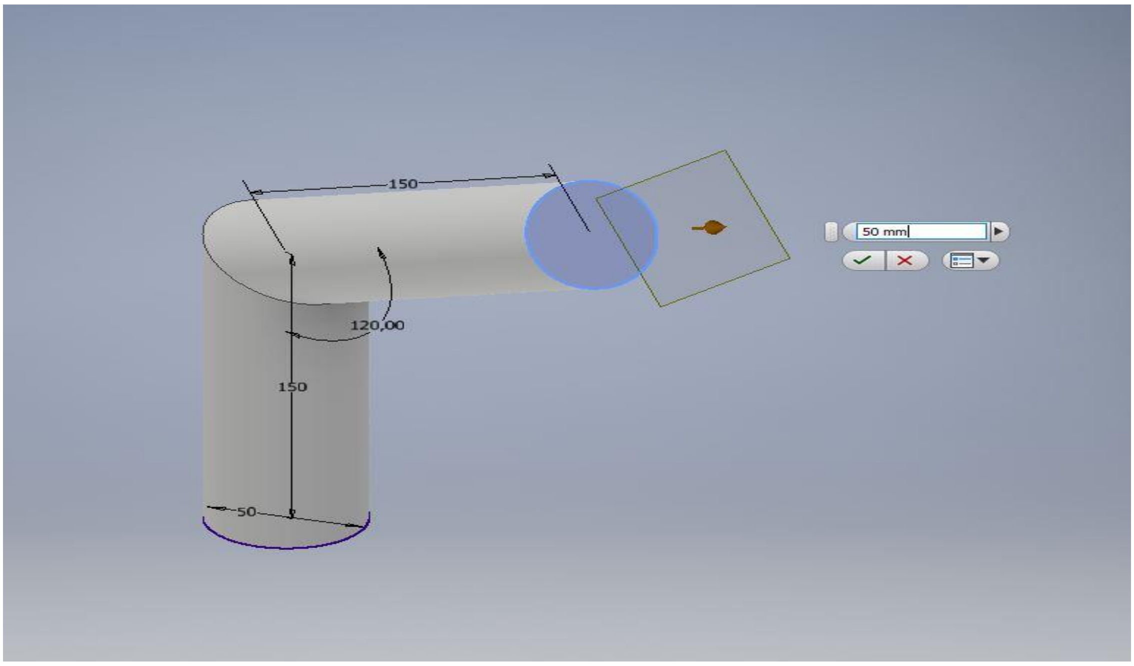

Figure A.11: Another work plane to draw the base part of the transition piece

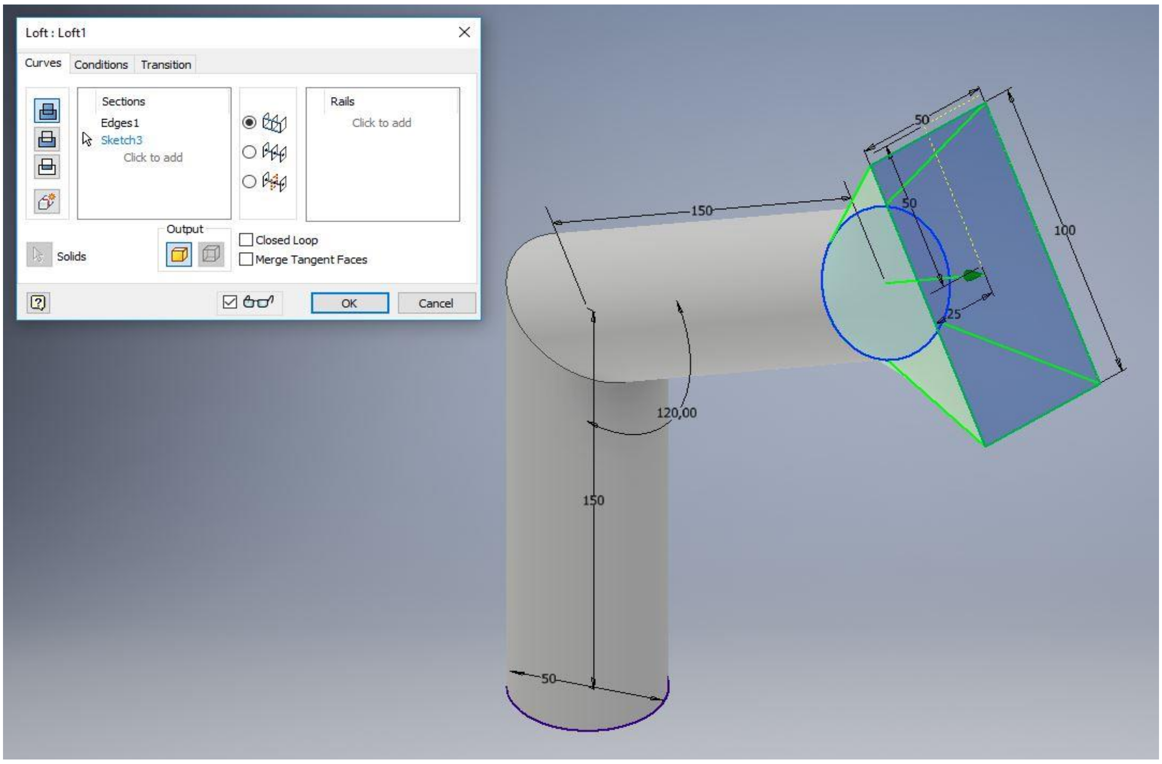

Figure A.12: The first nozzle-transition piece designed using the “Loft” tool.

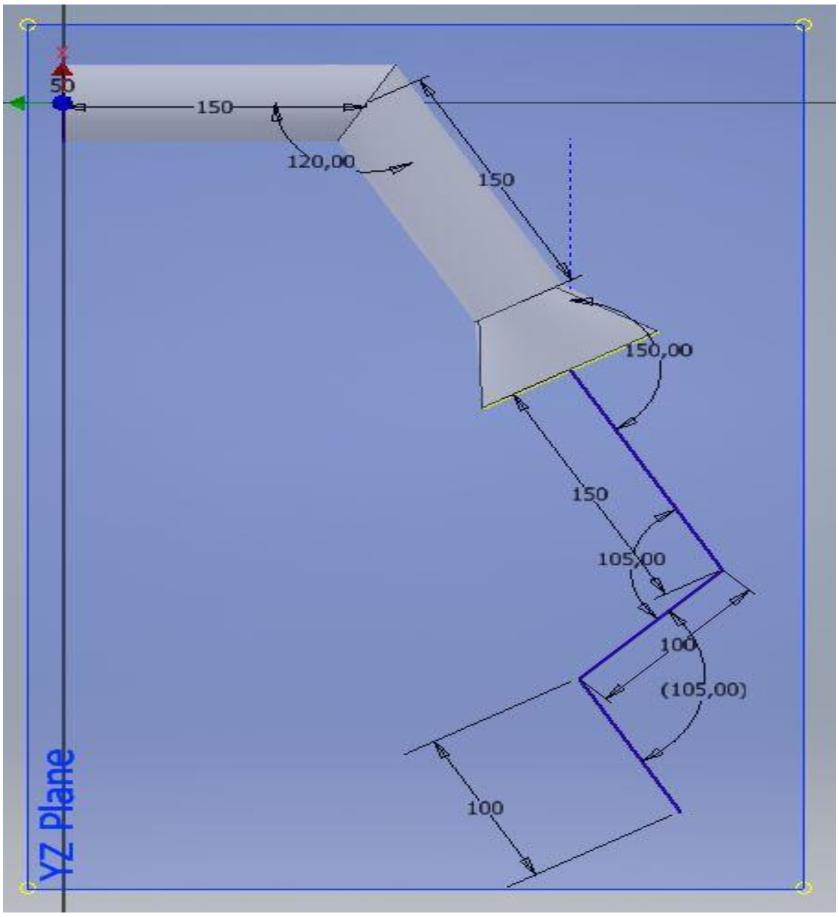

Figure A.13: Line drawn to create the zigzag section

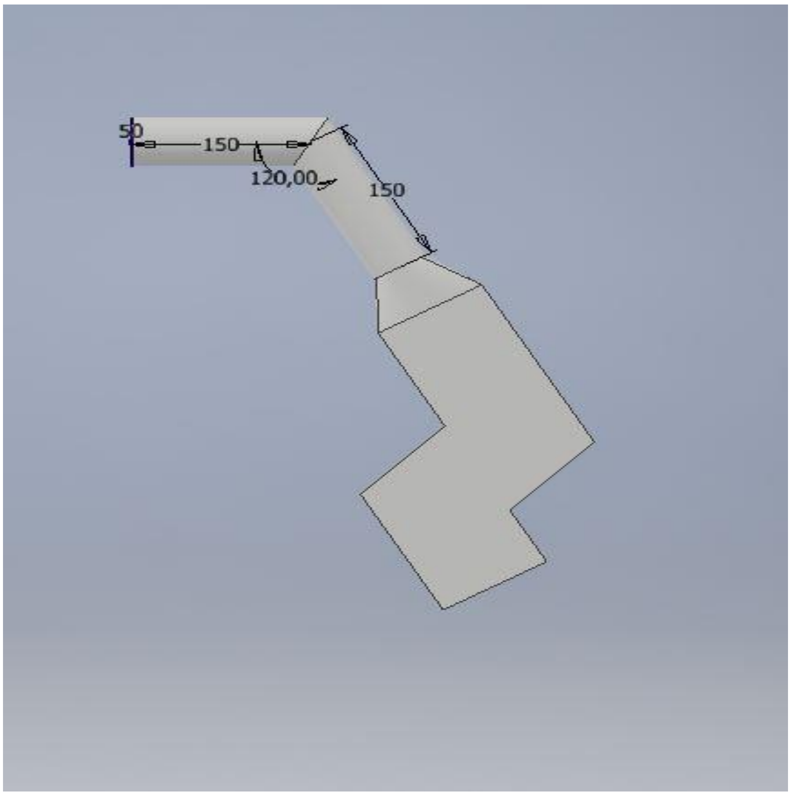

Figure A.14: The zigzag section once the sweep is completed

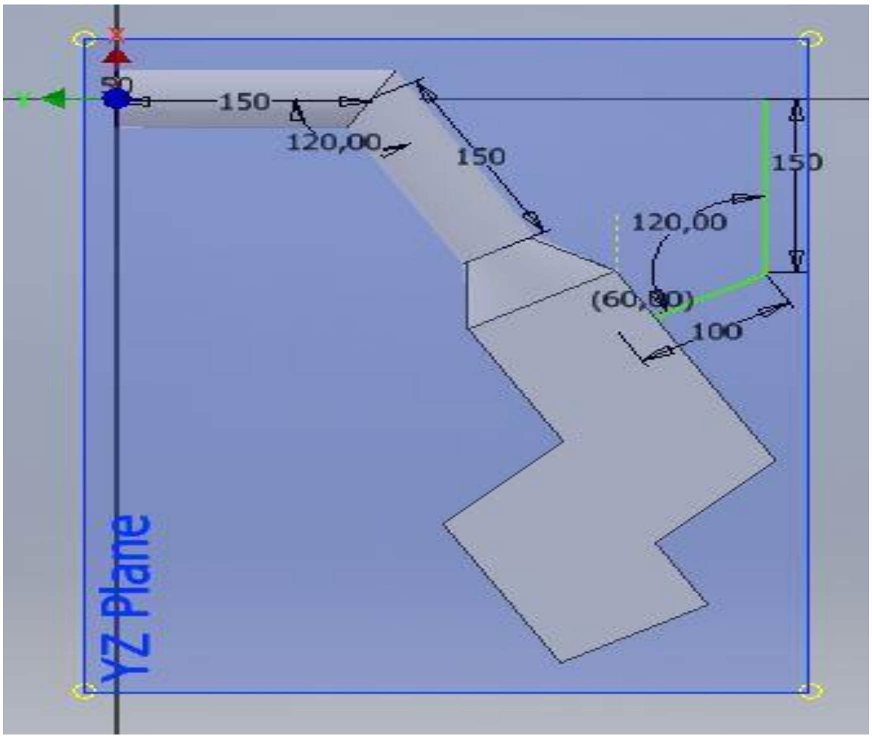

Figure A.15: Line for the raw coal-feed inlet

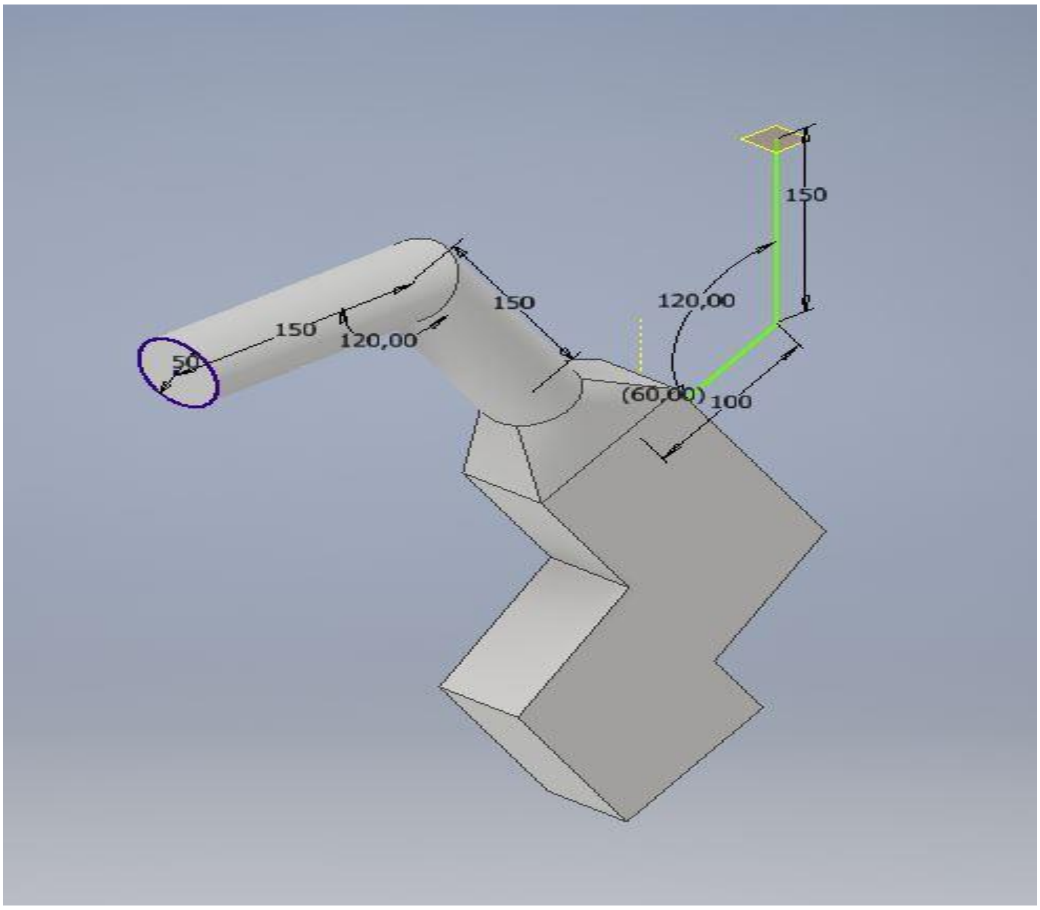

Figure A.16: Customized work-plane to draw for the raw coal inlet

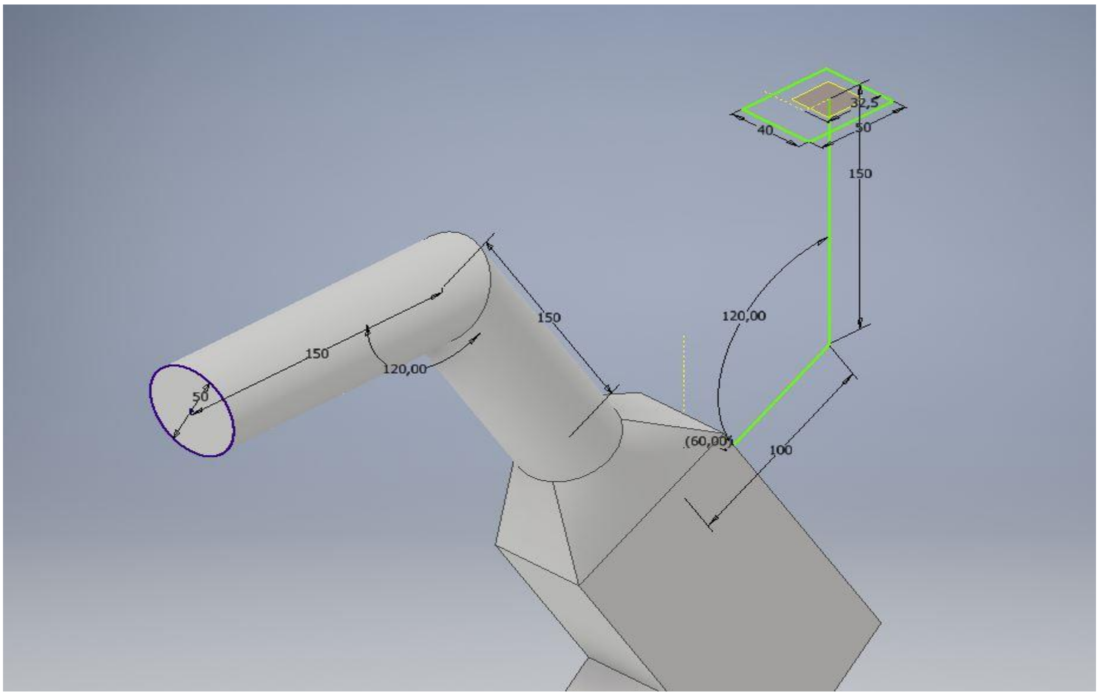

Figure A.17: Square drawn on a work plane to serve as raw coal inlet

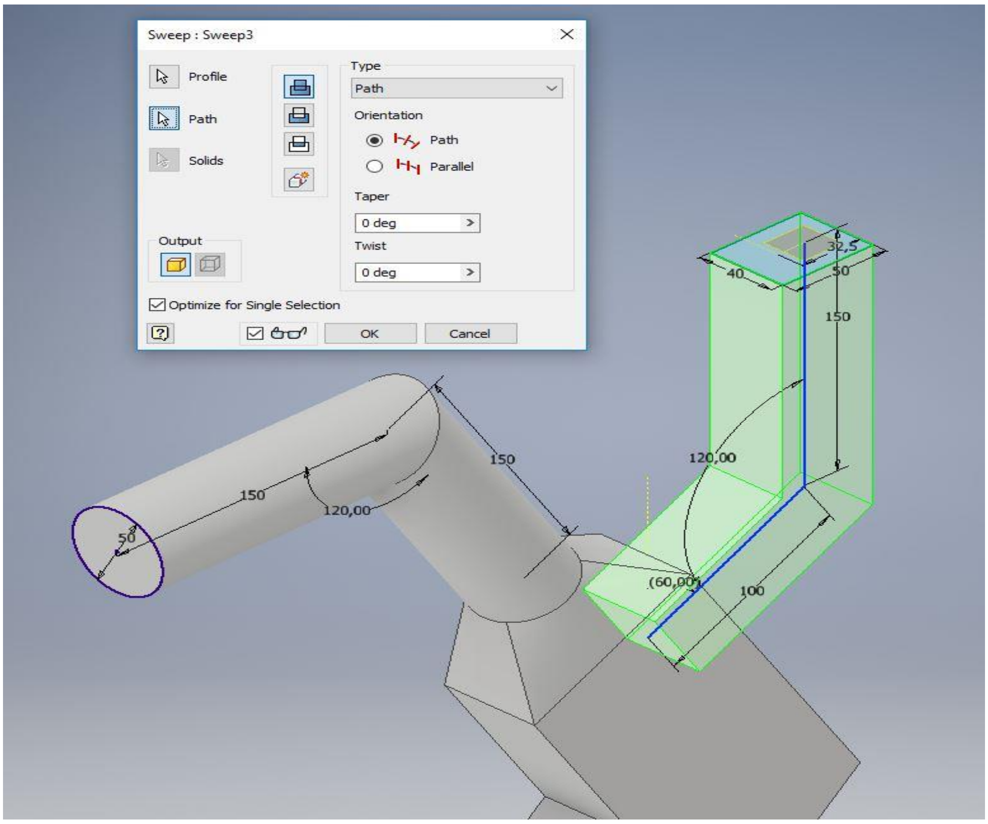

Figure A.18: The Design of the inlet pipe for the coal feed using the “Sweep” tool.

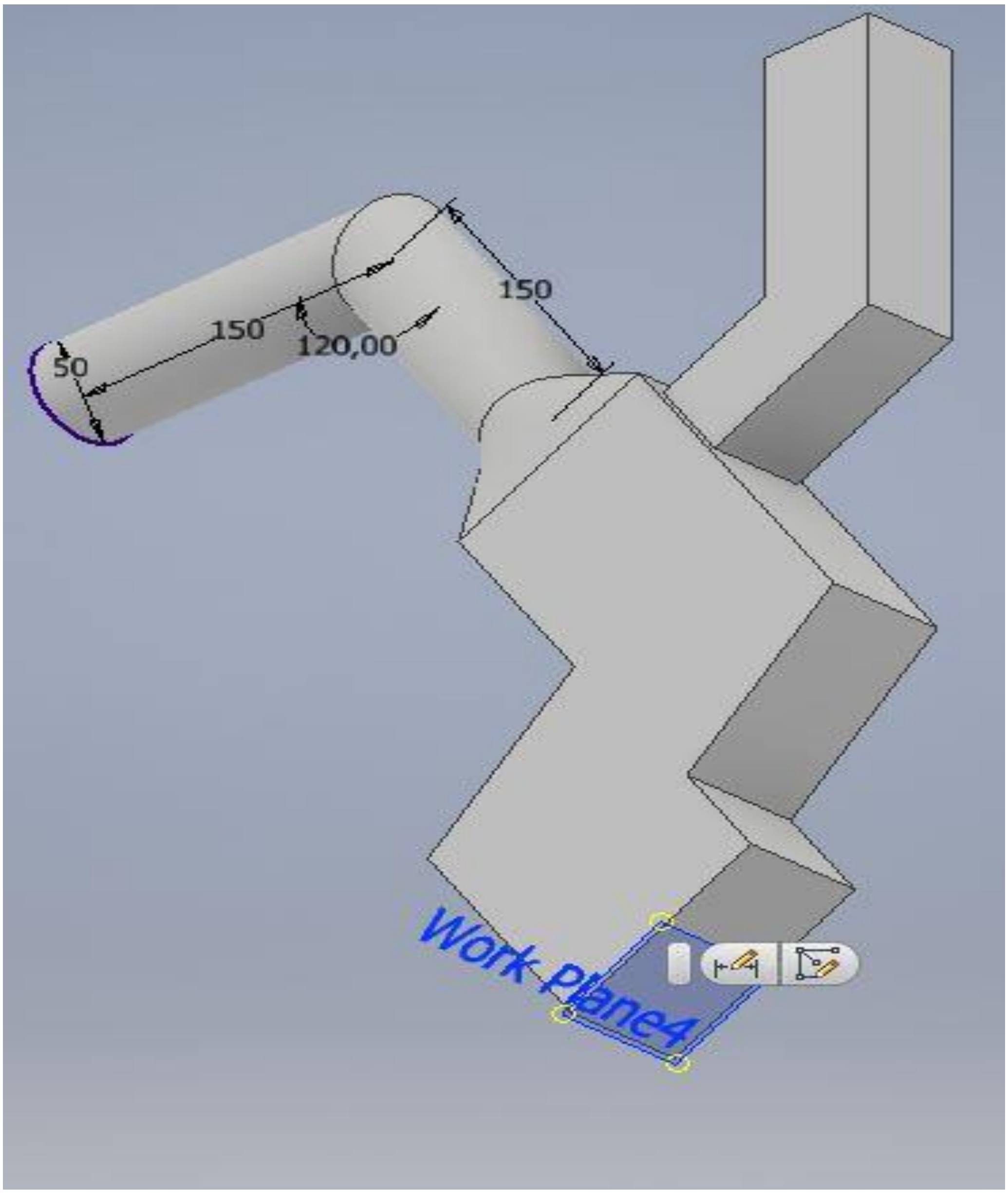

Figure A.19: Work plane to create the second nozzle-transition piece

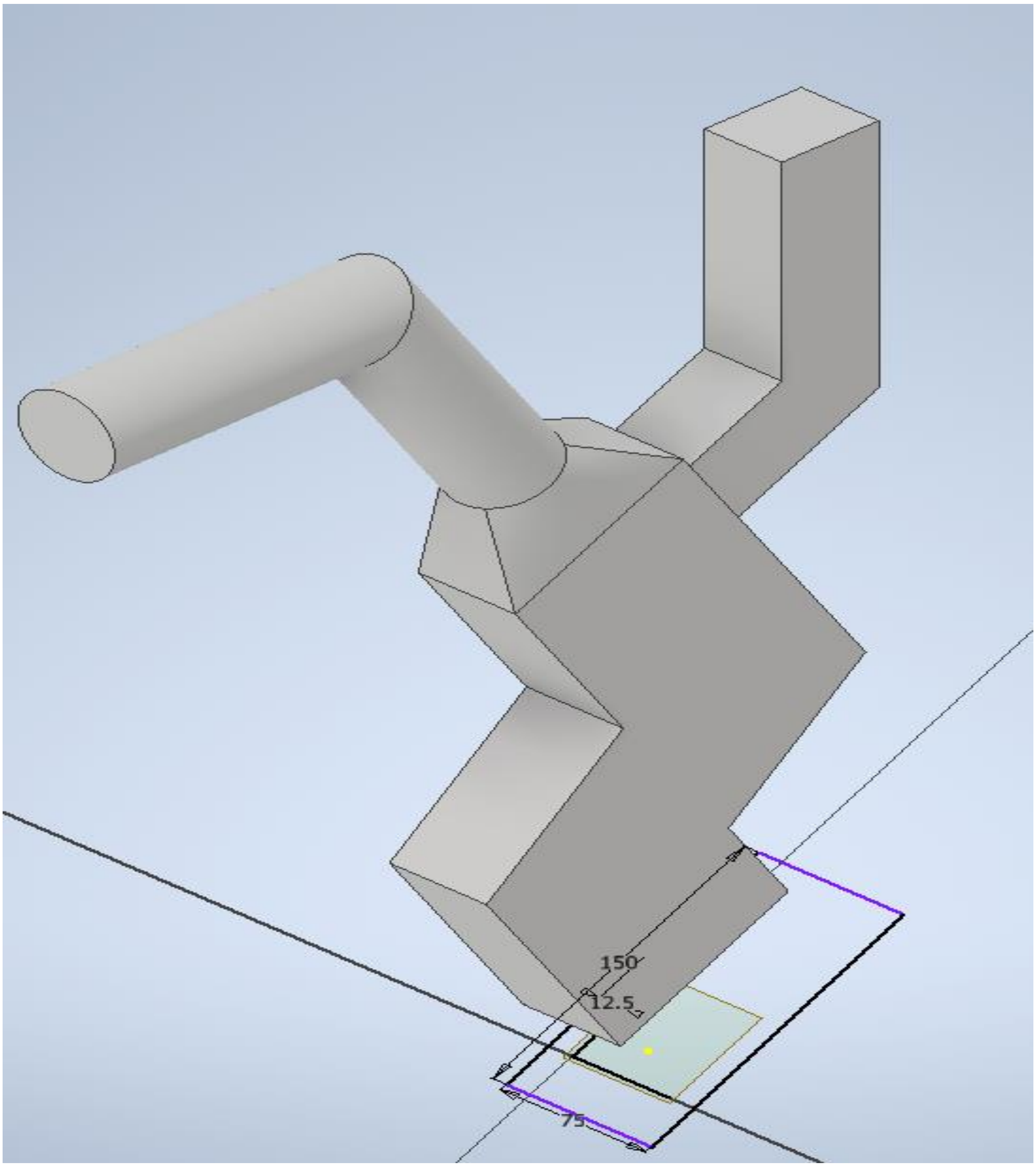

Figure A.20: The second part of the second nozzle for chamber 1

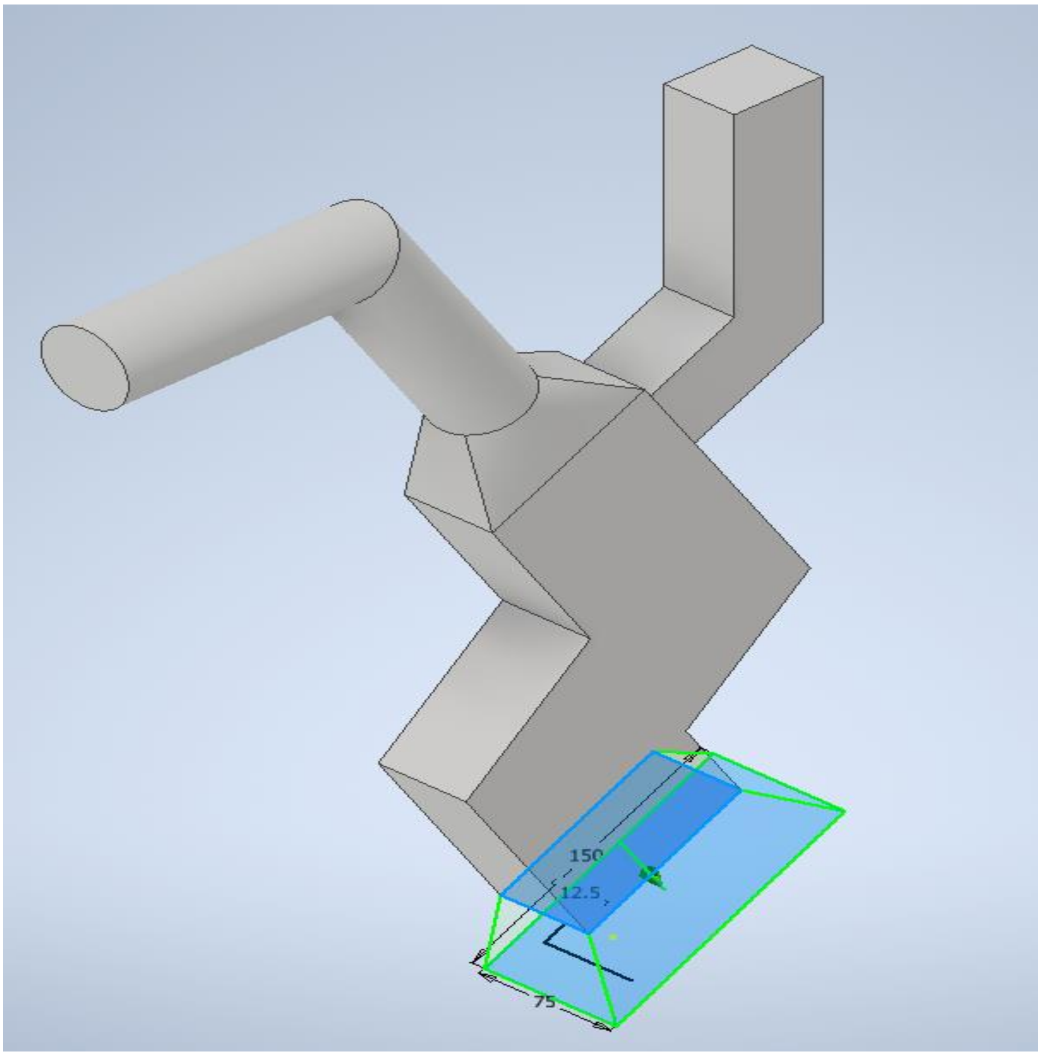

Figure A.21: Second loft completed for the second nozzle transition piece

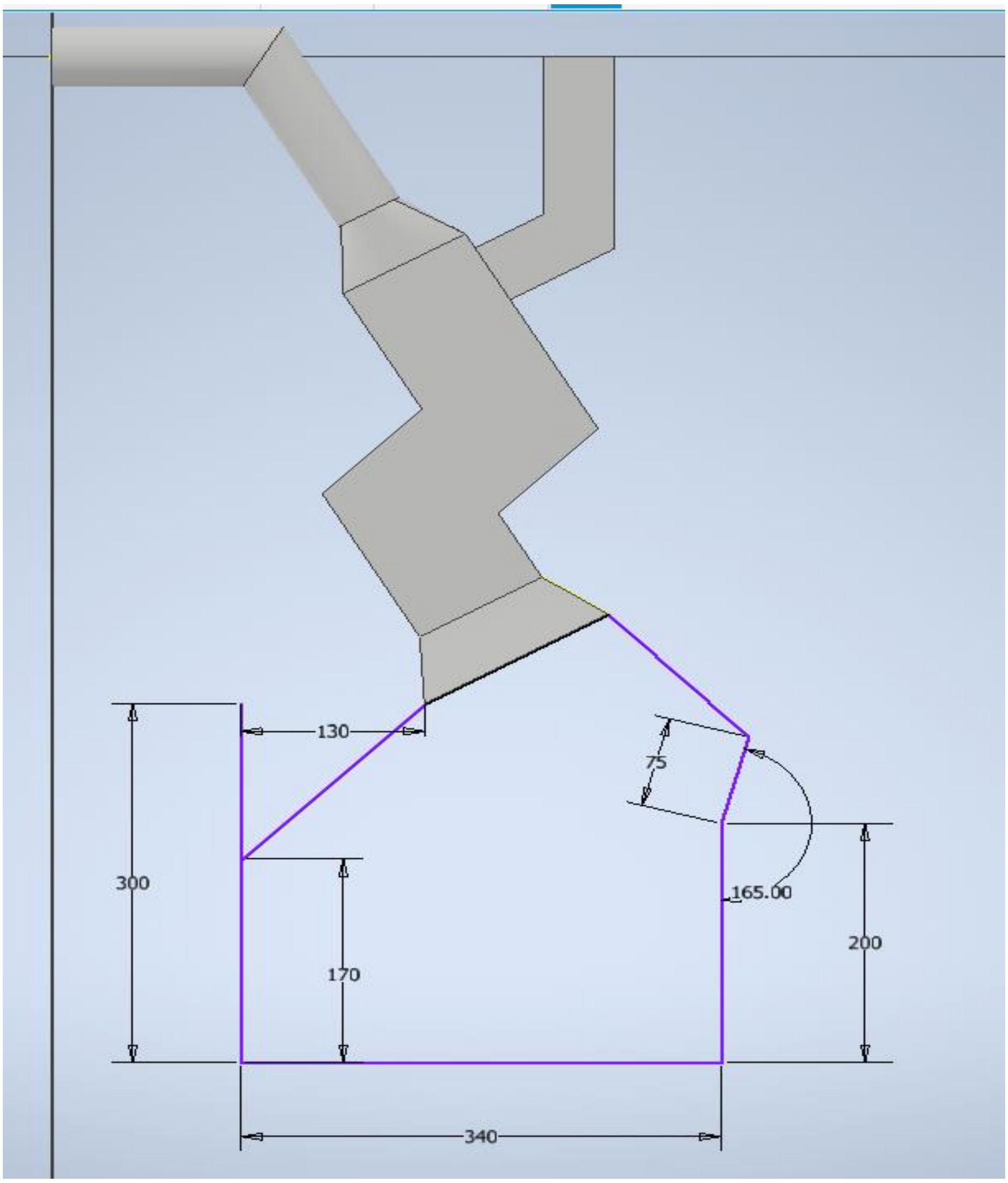

Figure A.22: The line for the bin compartment of chamber 1

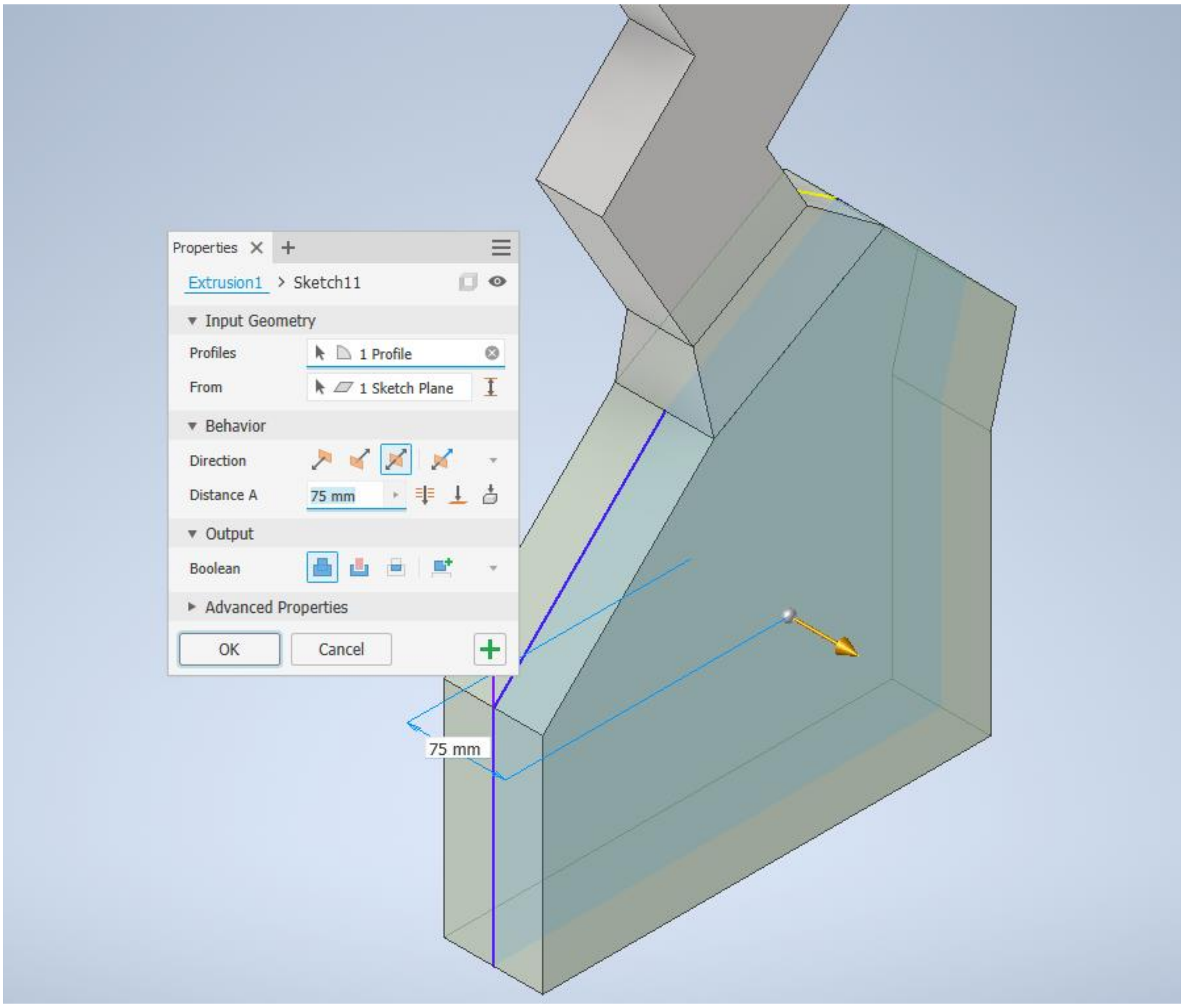

Figure A.23: The bin compartment for chamber 1 using "Extrusion" tool

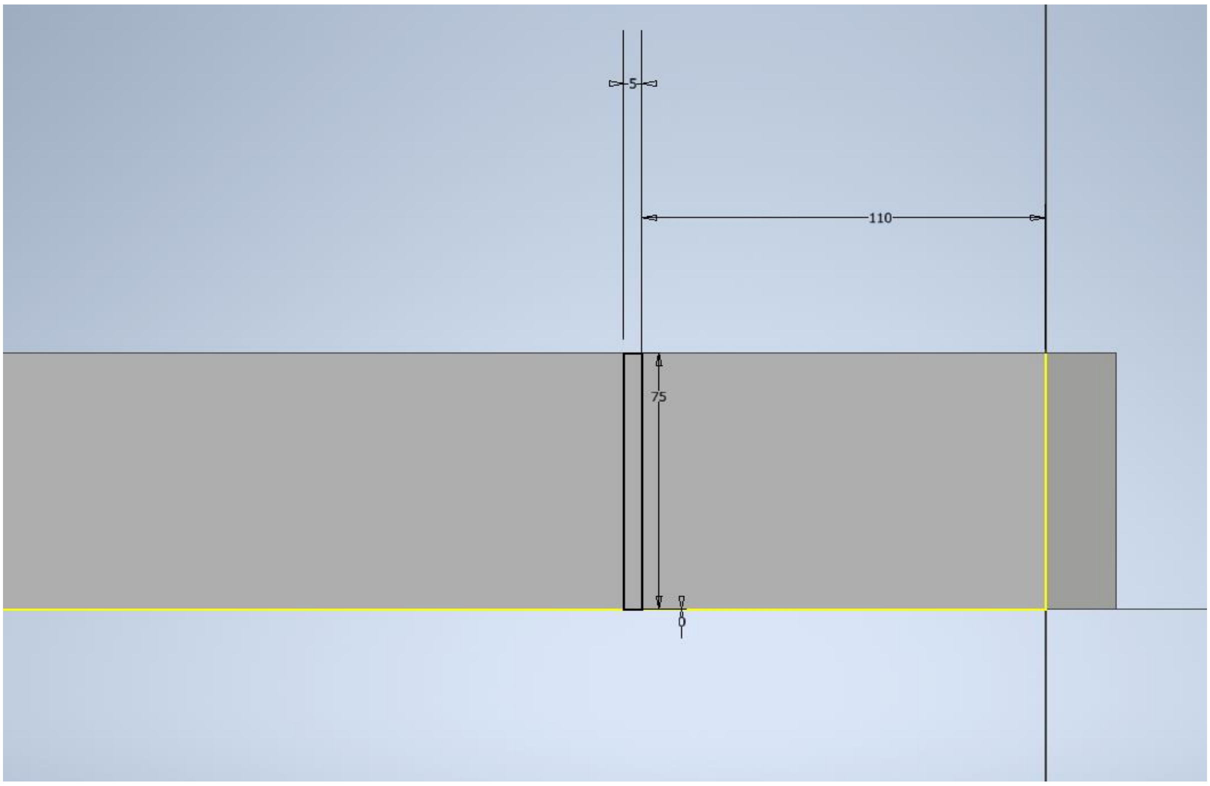

Figure A. 24: The Drawing of the bin compartment at the base of the first chamber (Upside down view of the Chamber 1)

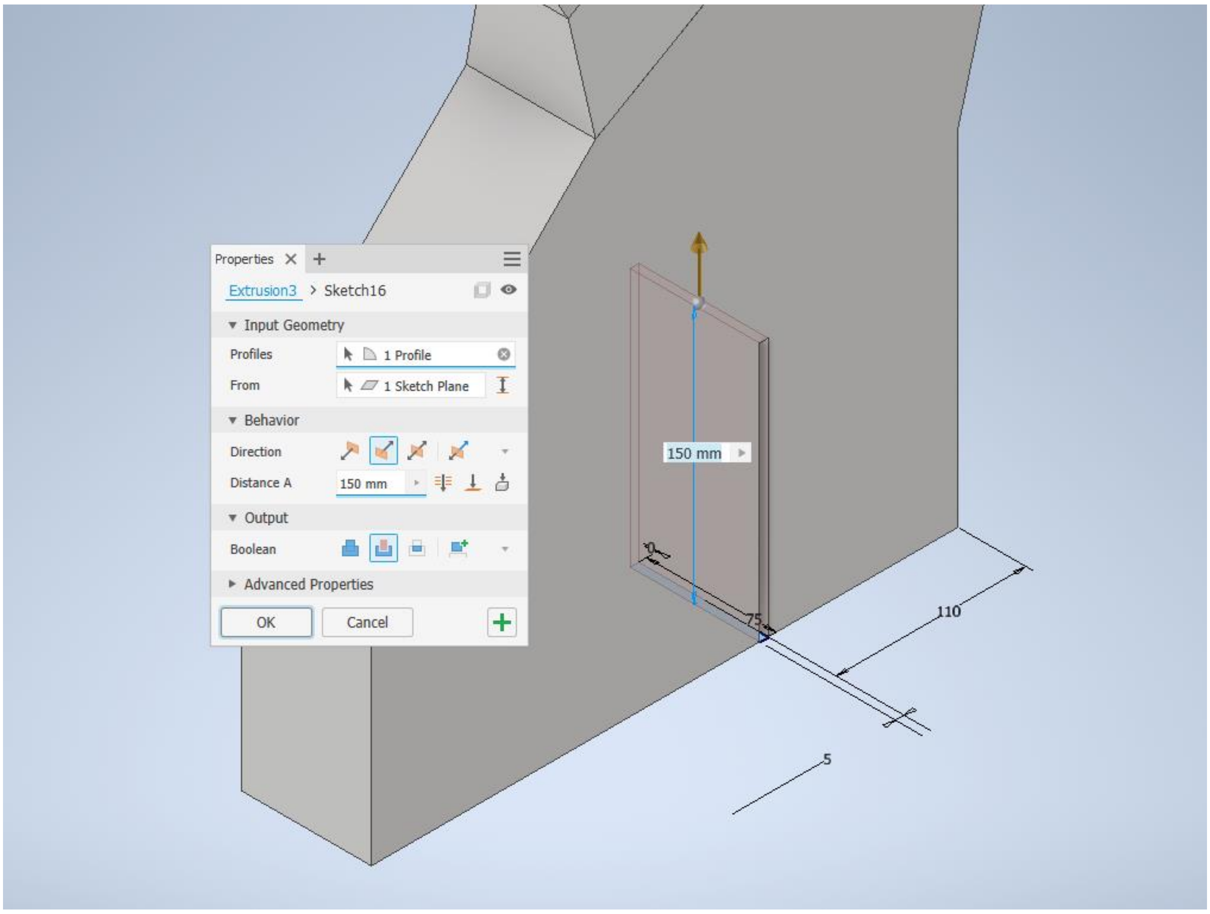

Figure A.25: Extruding the drawn line inwards

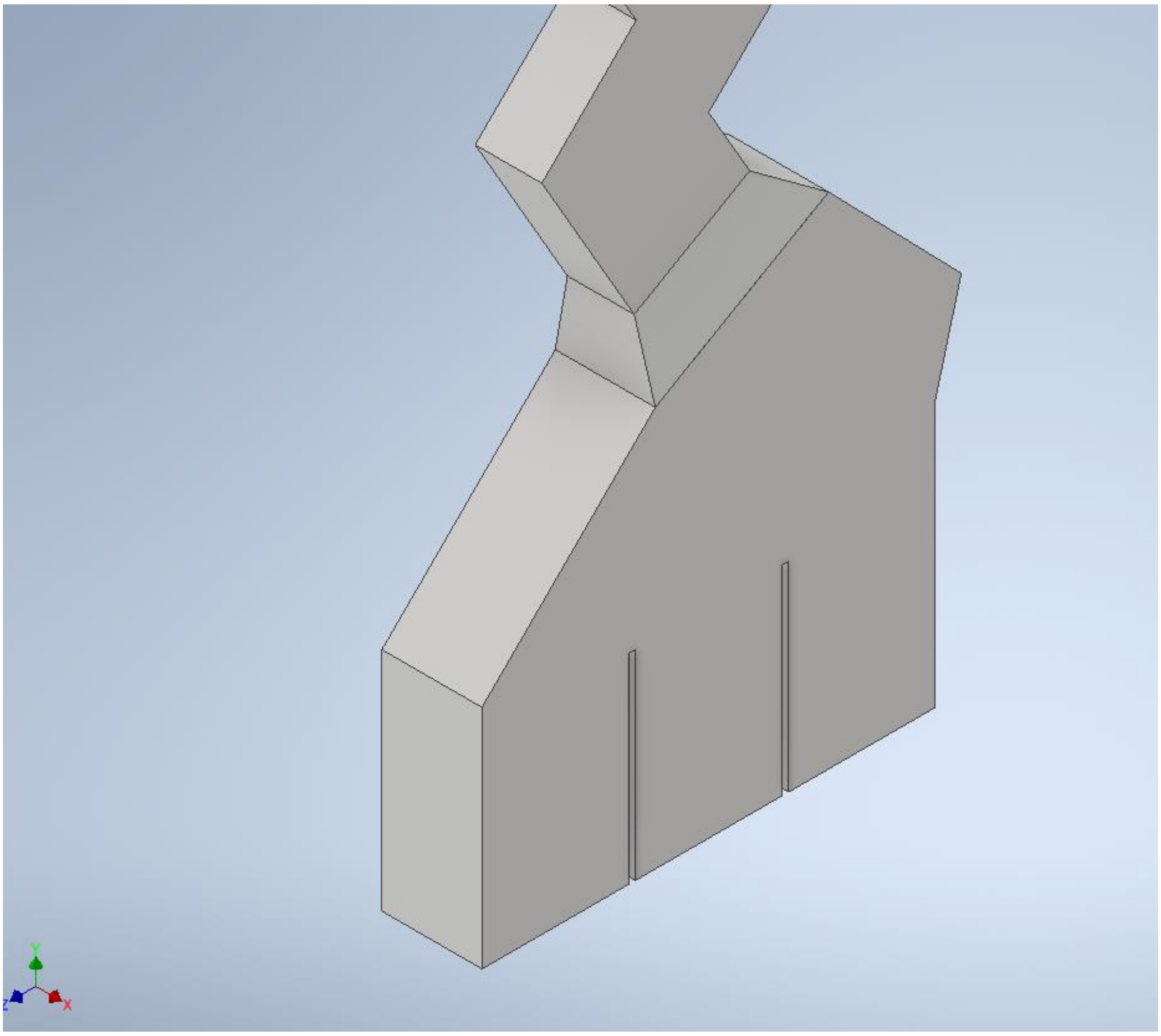

Figure A.26: Creating the remaining bin section using the “Repeated Rectangular Pattern” tool

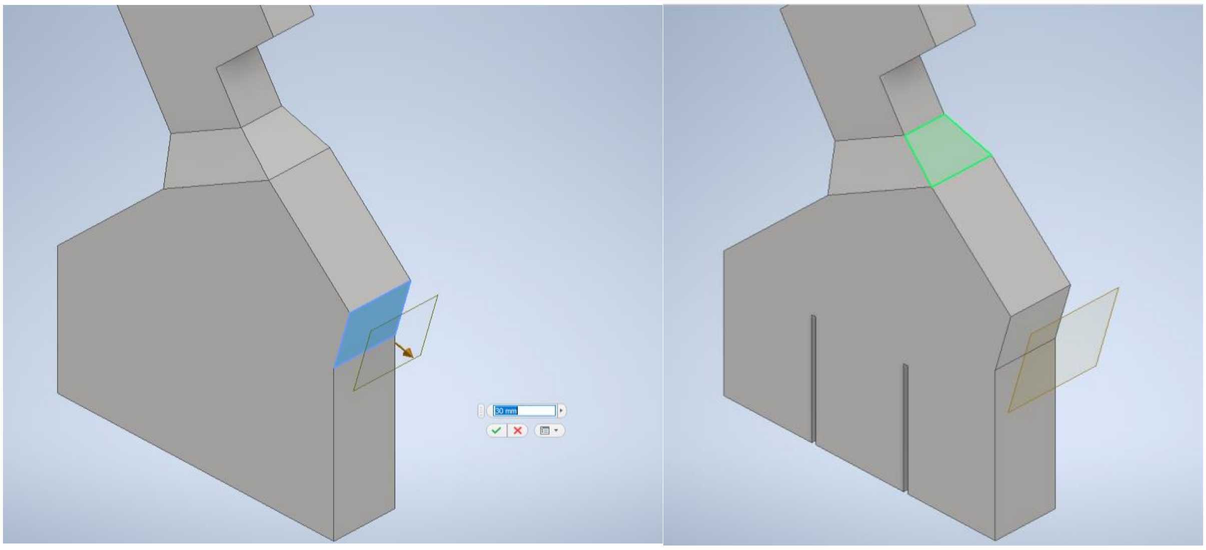

Figure A. 27: Work plane for the designing of the inner section

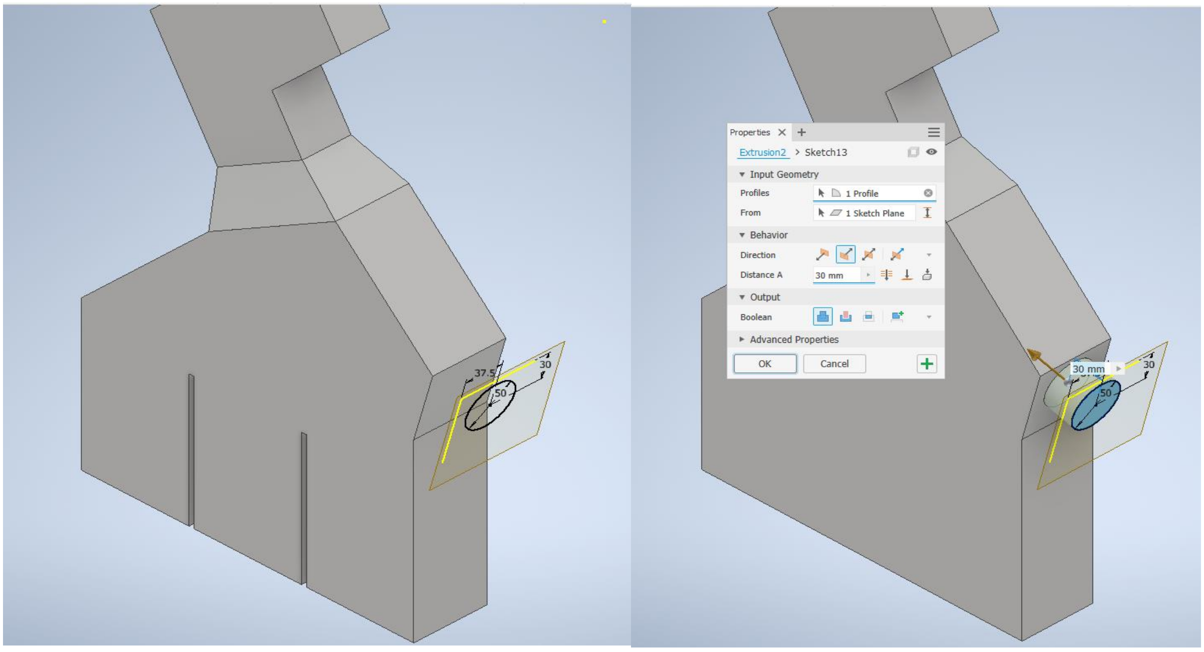

Figure A.28: Drawing and Extruding the Circle for part of the inlet section

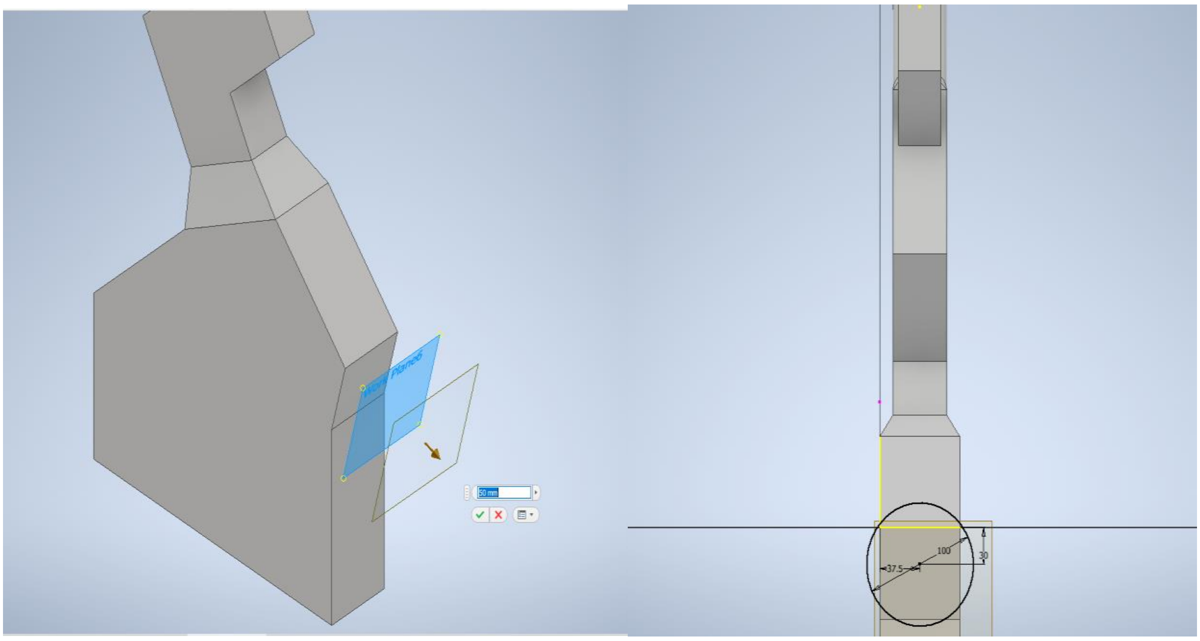

Figure A.29: Drawing and Extruding the Circle for part of the Nozzle section

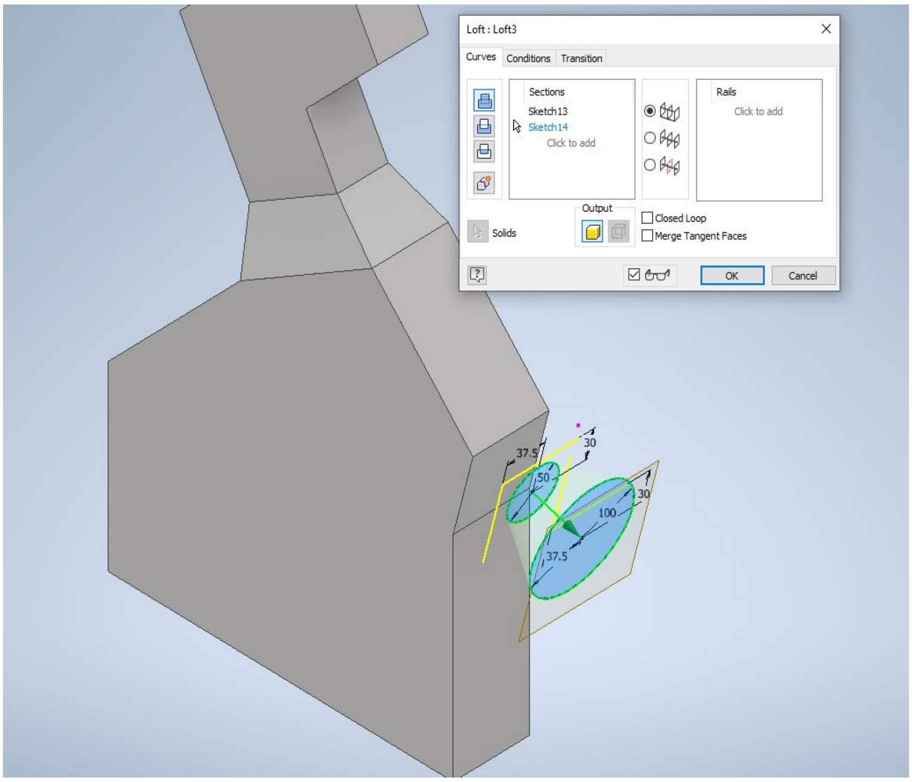

Figure A.30: Using the Loft tool for the Nozzle section

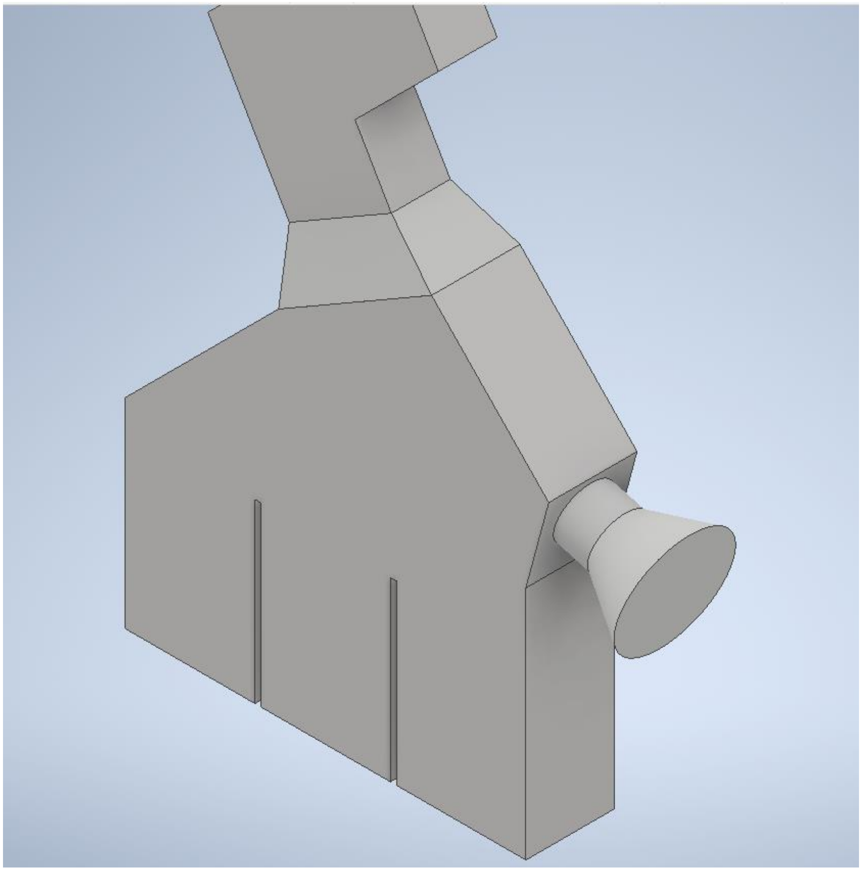
Figure A.31: Designed Air-inlet and Nozzle section

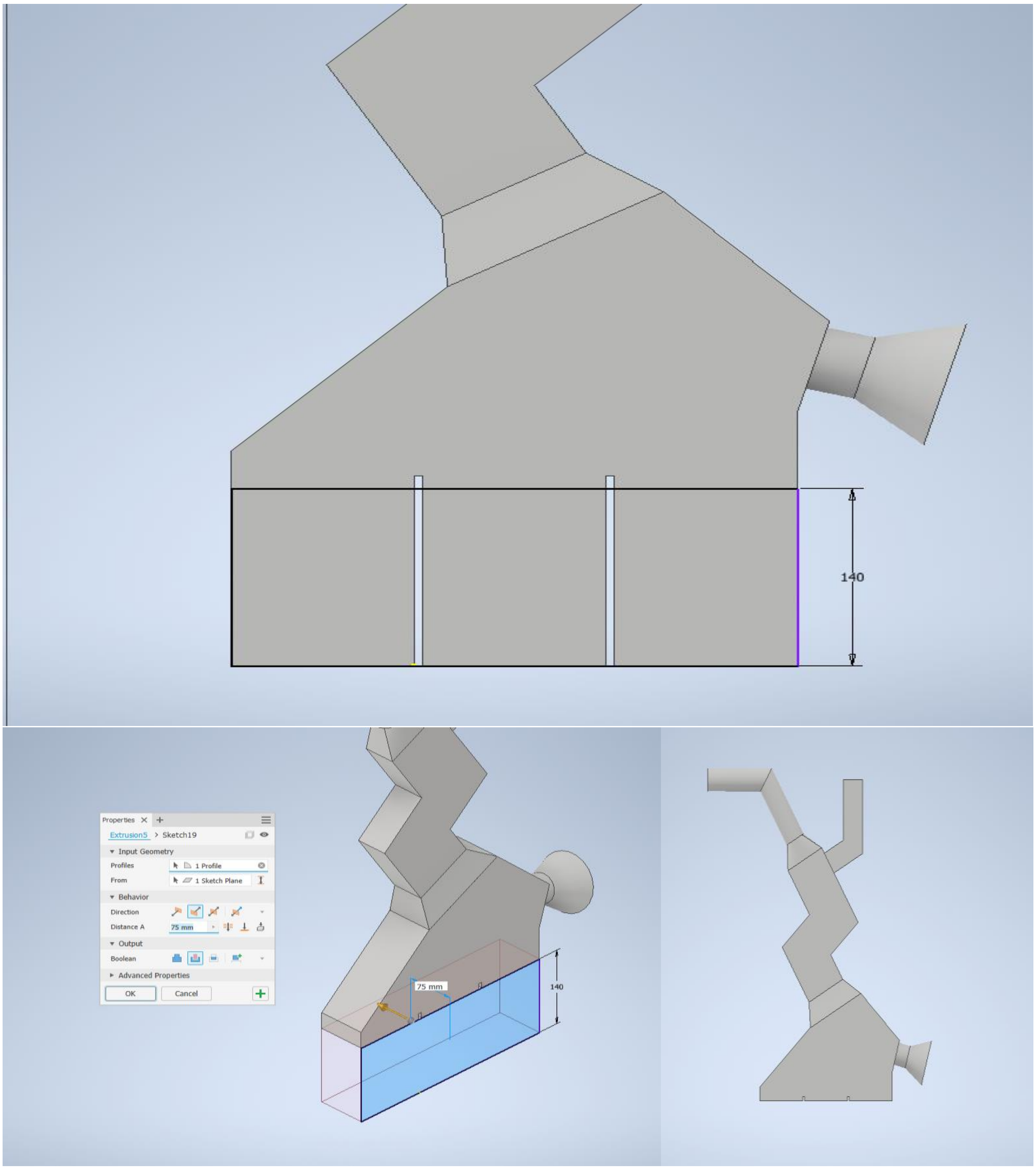

Figure A.32: Drawing a section to cut the base part away to join the collecting bins section.

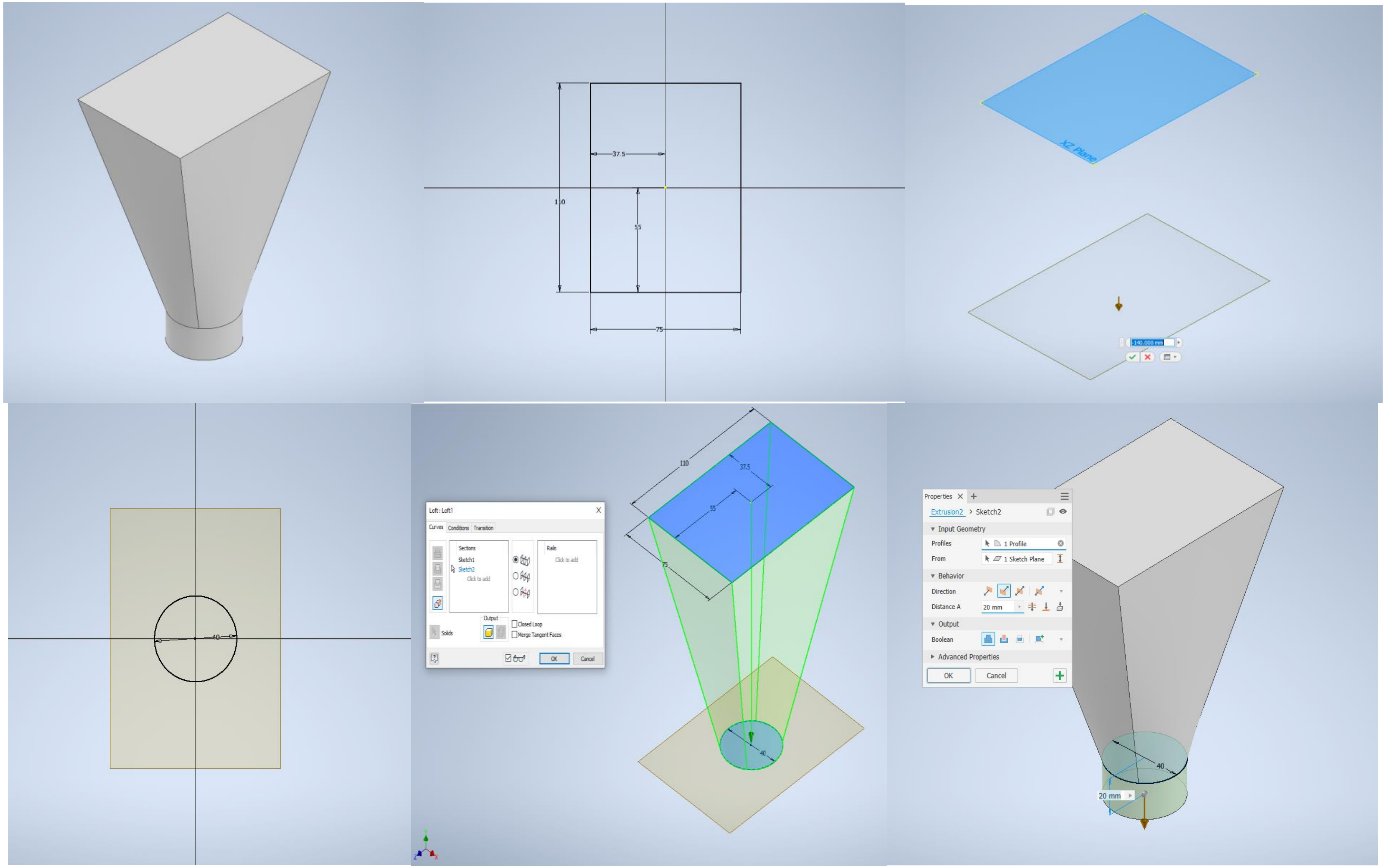

Figure A.33: Designing chute section of the collecting bins section for Chamber 1 using the “Loft” and “Extrude” tools.

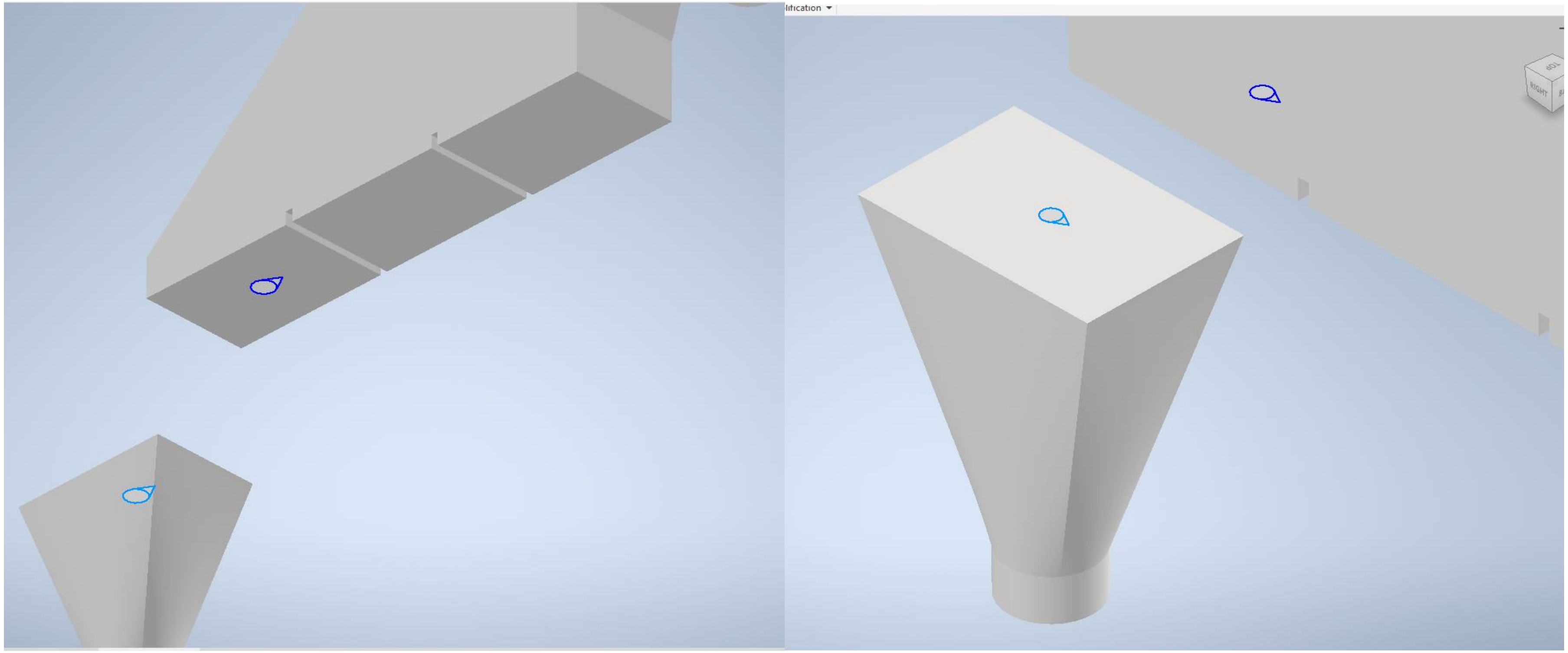

Figure A.34: Using the joint tool to connect the chute

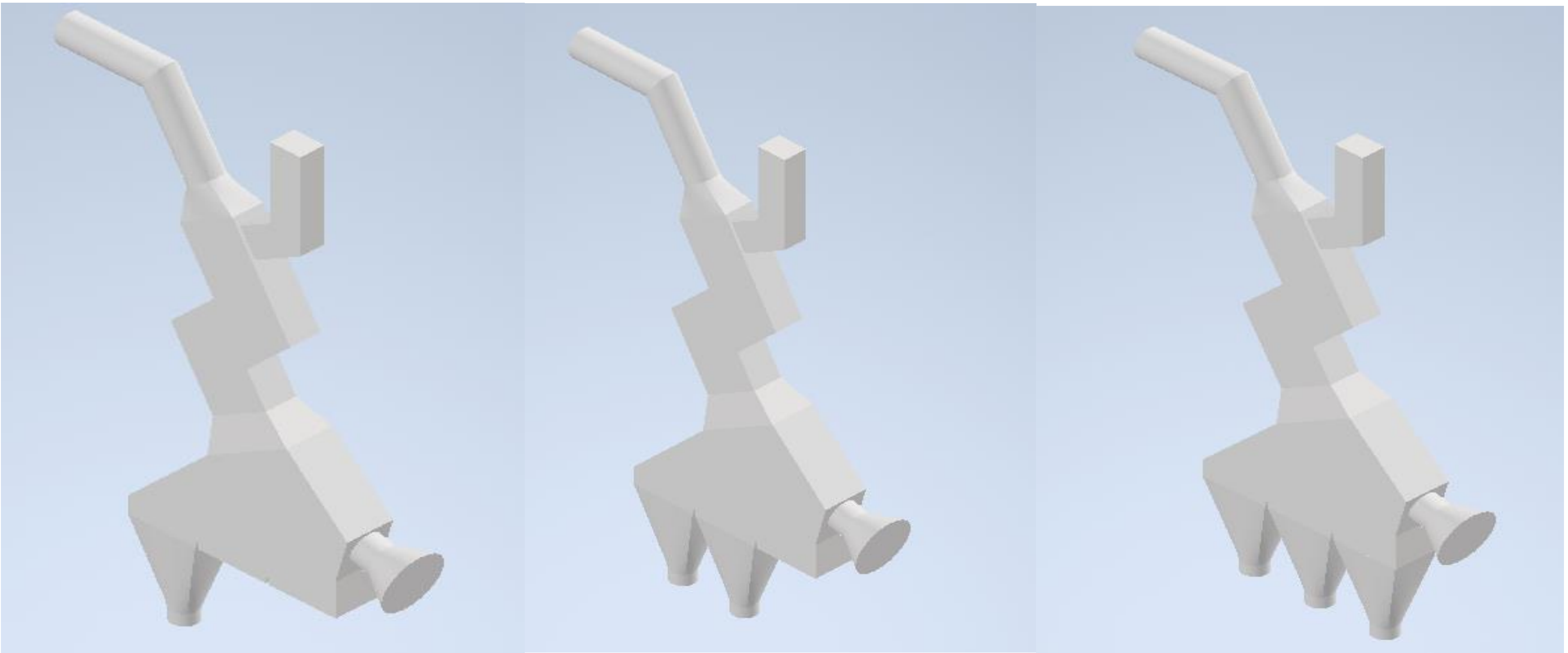

Figure A.35: Using the joint tool to connect the chute to the upper section of chamber 1

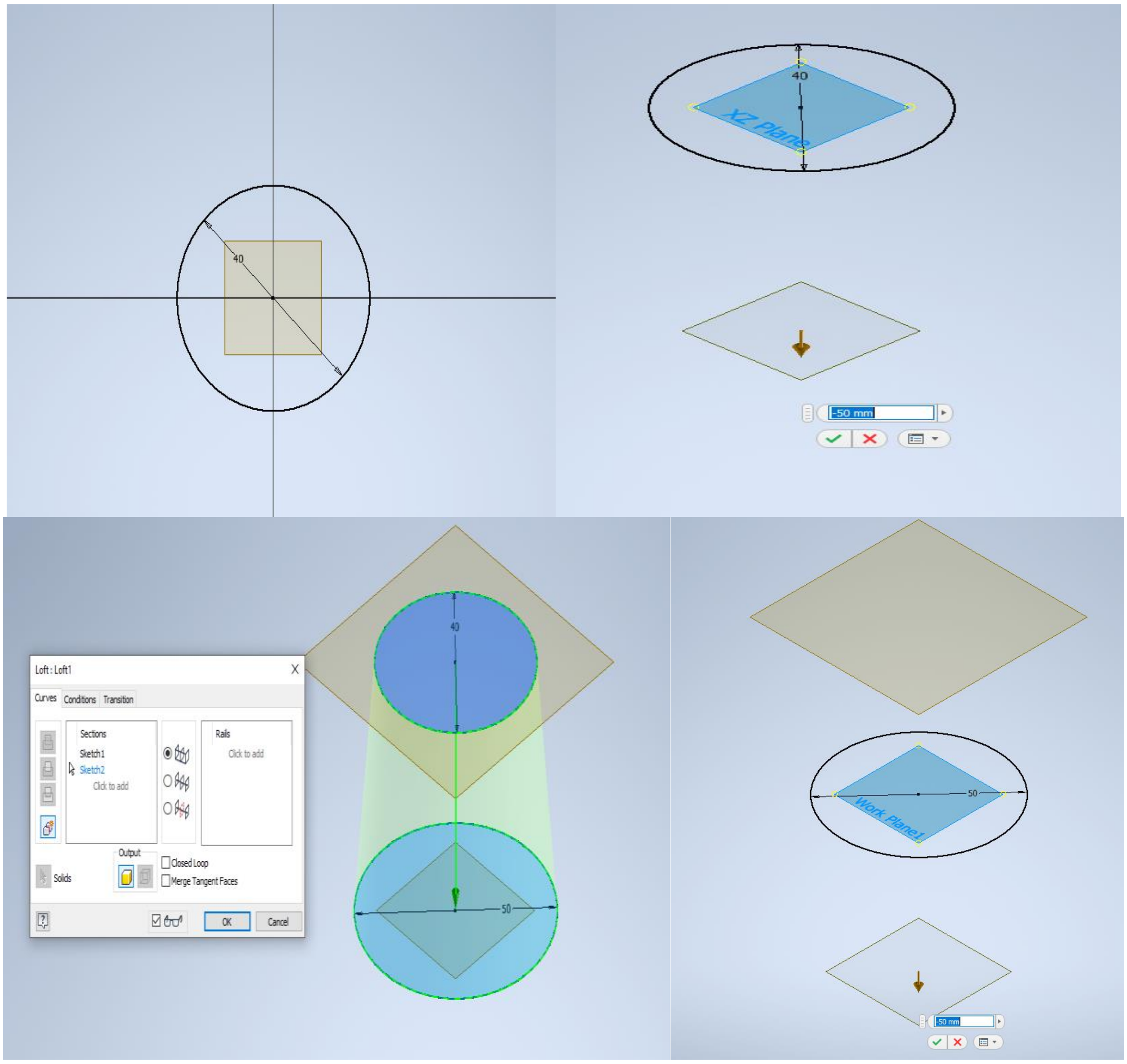

Figure A.36: Drawing the collecting bins

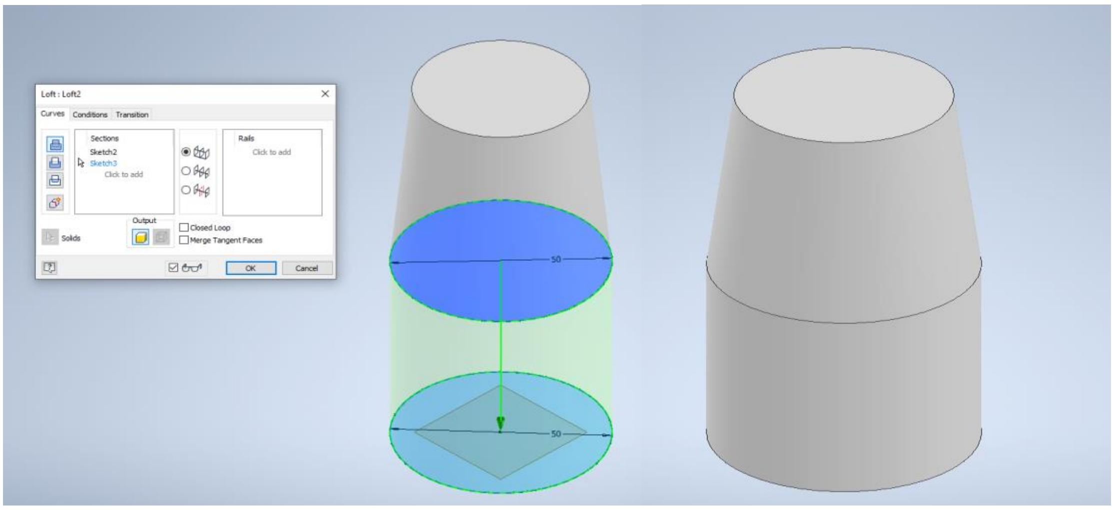

Figure A. 37: Completing the collecting bins

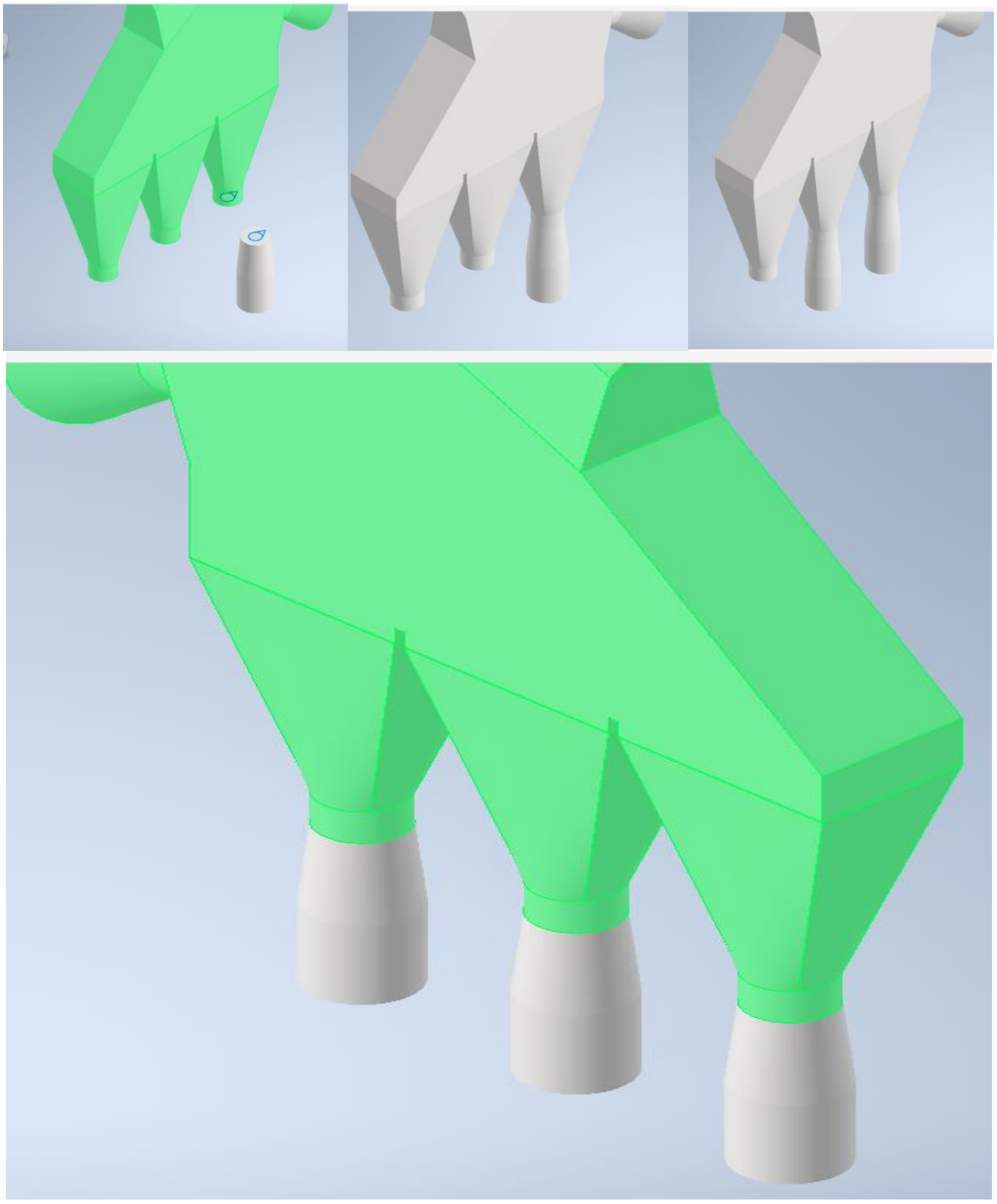

Figure A.38: Joining the collecting bins to the chamber 1

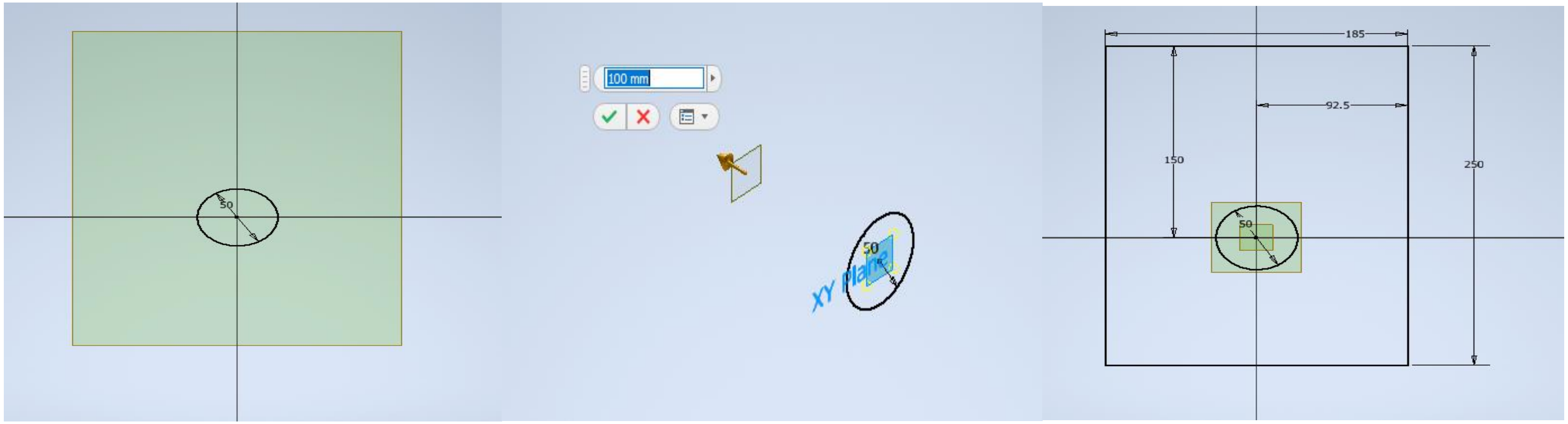

Figure A.39: Drawing of the Inlet diffuser-transition piece of the second chamber

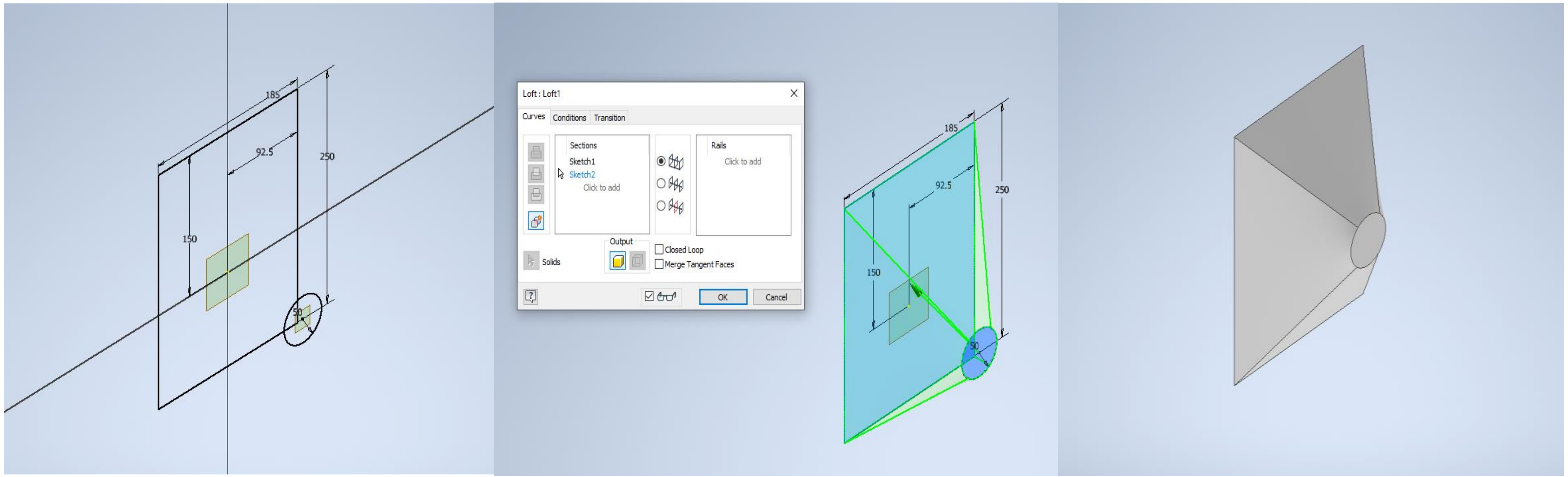

Figure A.40: Completing the Inlet diffuser-transition piece of the second chamber using the loft tool.

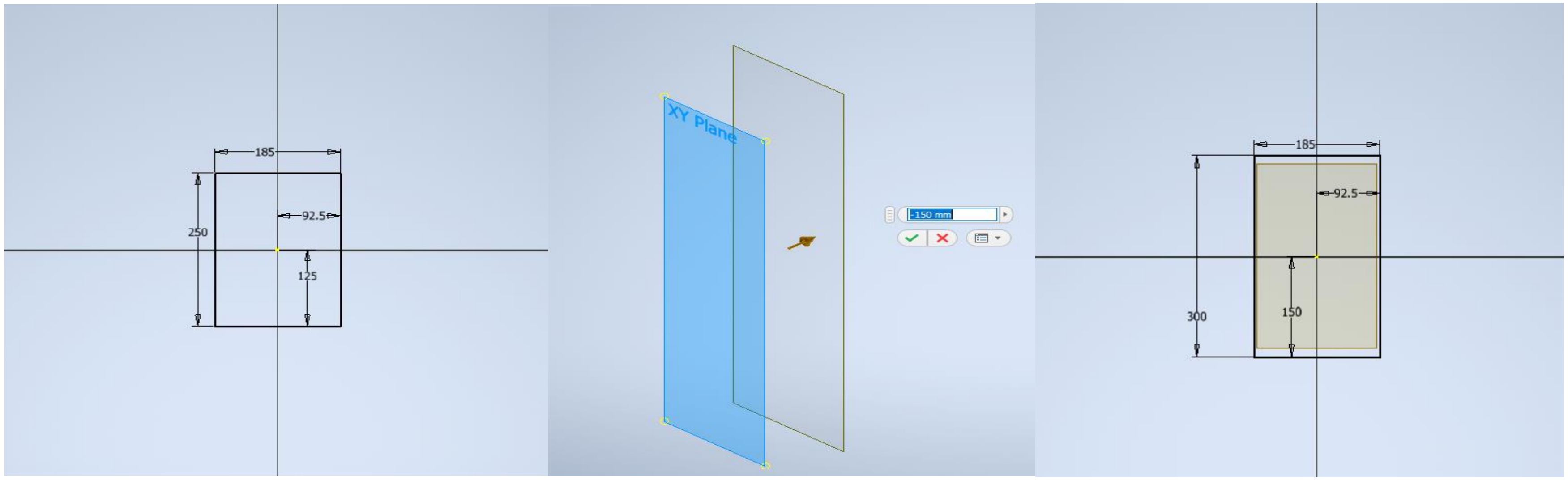

Figure A.41: Drawing the upper section of the Main Diffuser Section of the chamber 2 (a).

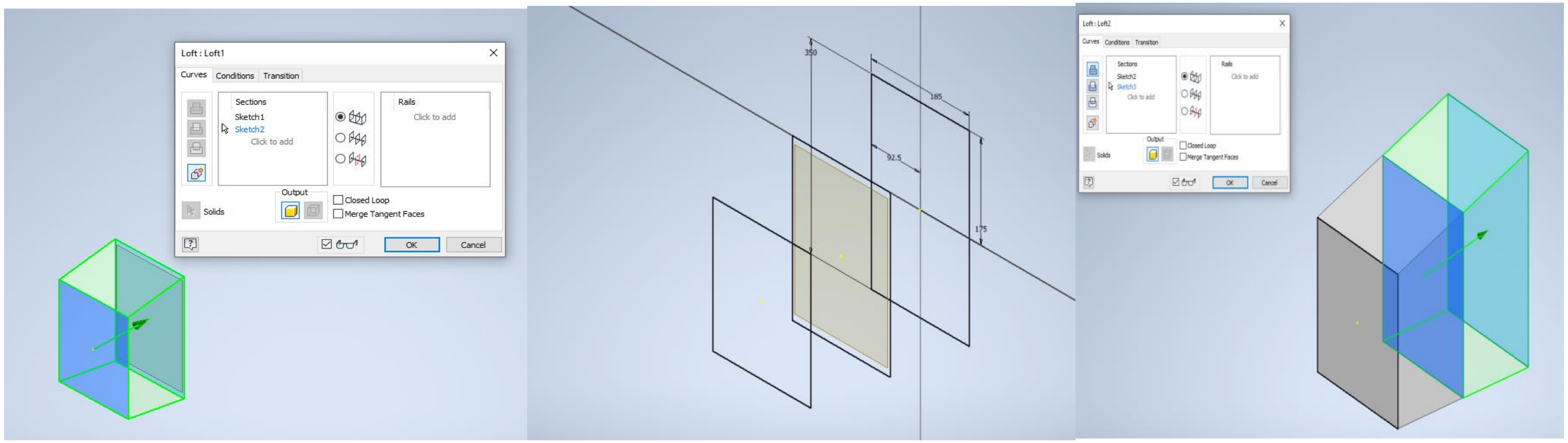

Figure A.42: Drawing the upper section of the Main Diffuser Section of the chamber 2 (b).

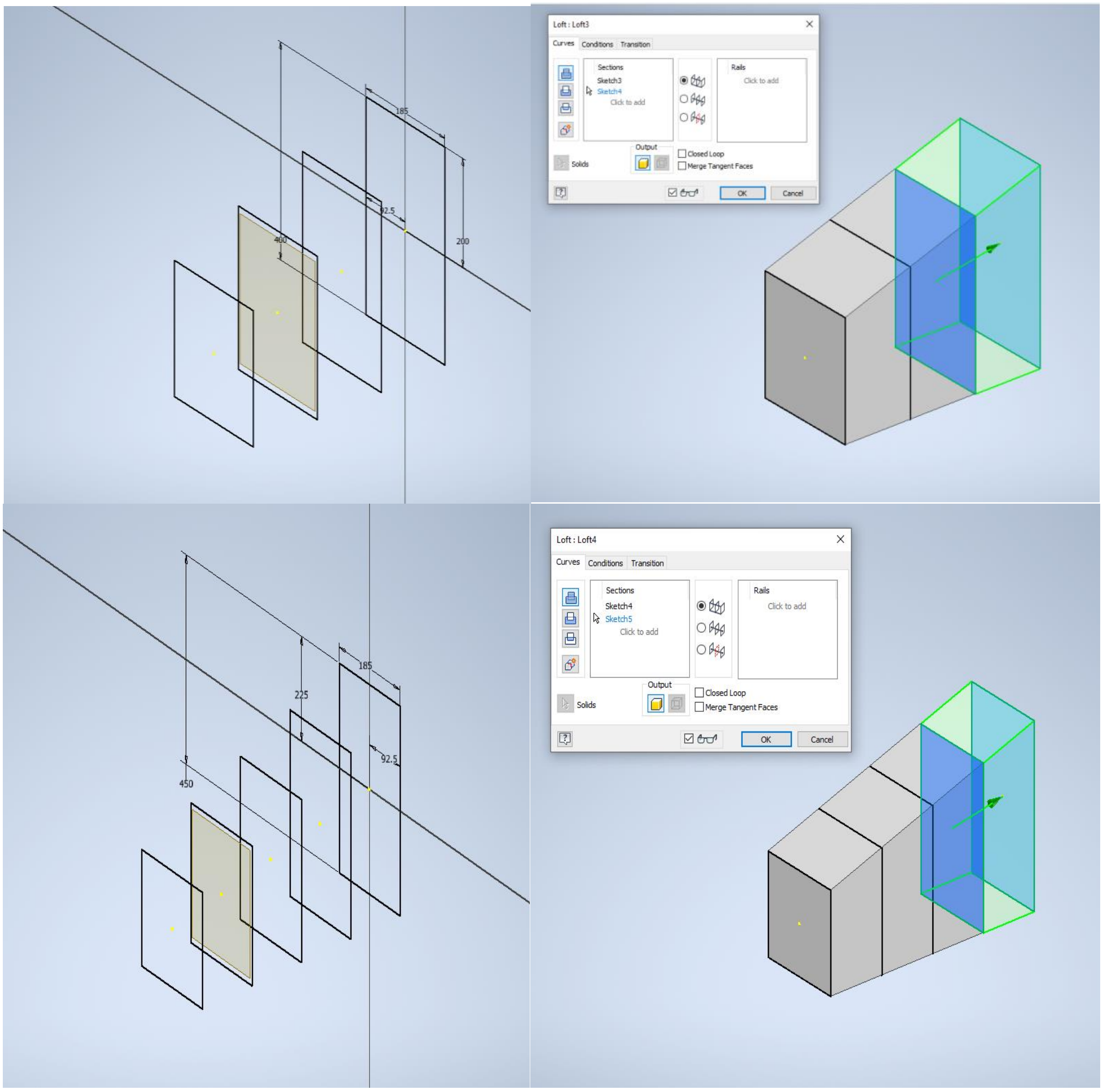

Figure A.43: Drawing the upper section of the Main Diffuser Section of the chamber 2 (c).

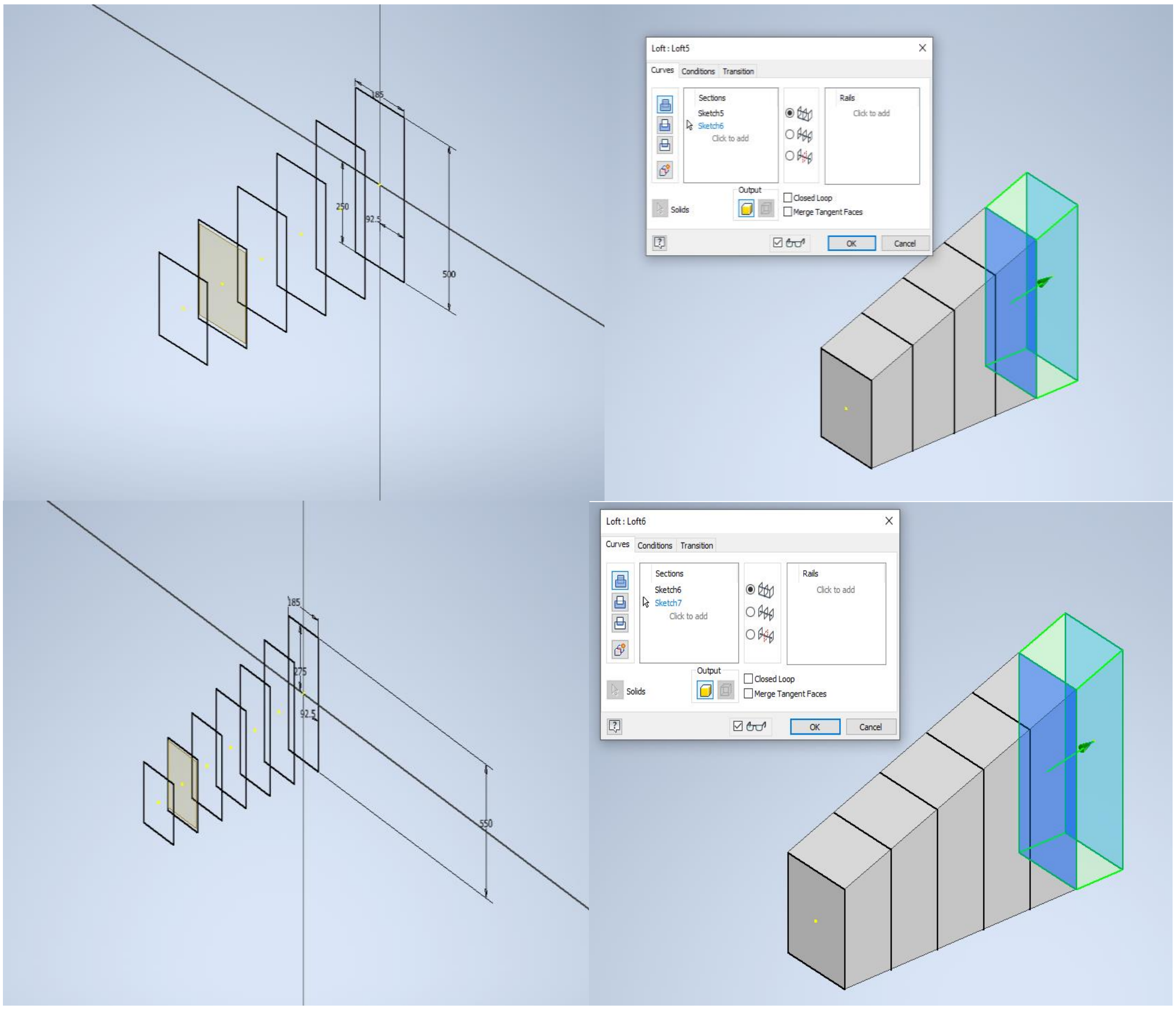

Figure A.44: Drawing the upper section of the Main Diffuser Section of the chamber 2 (d).

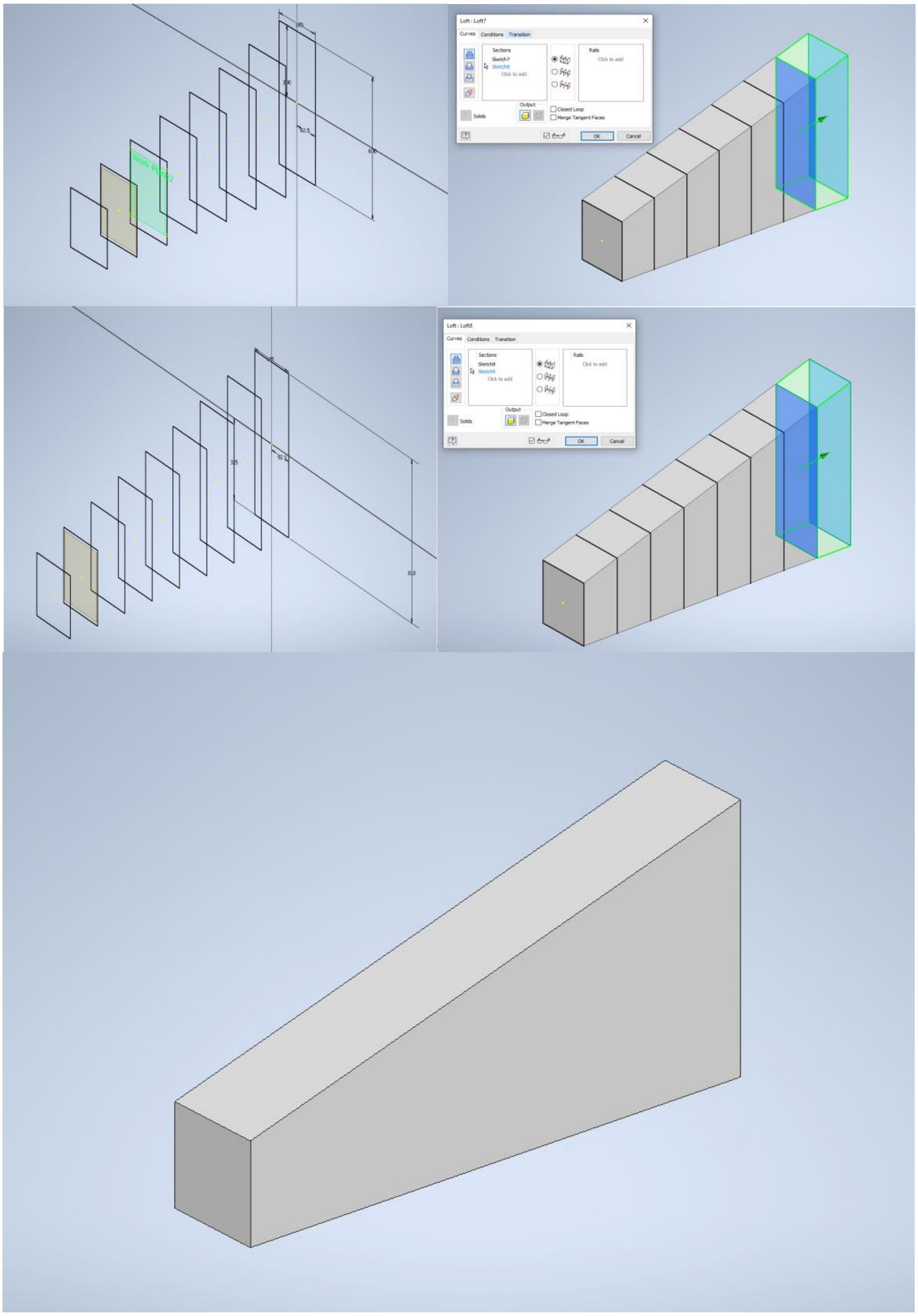

Figure A.45: Drawing and completing the upper section of the Main Diffuser of the chamber 2 (e).

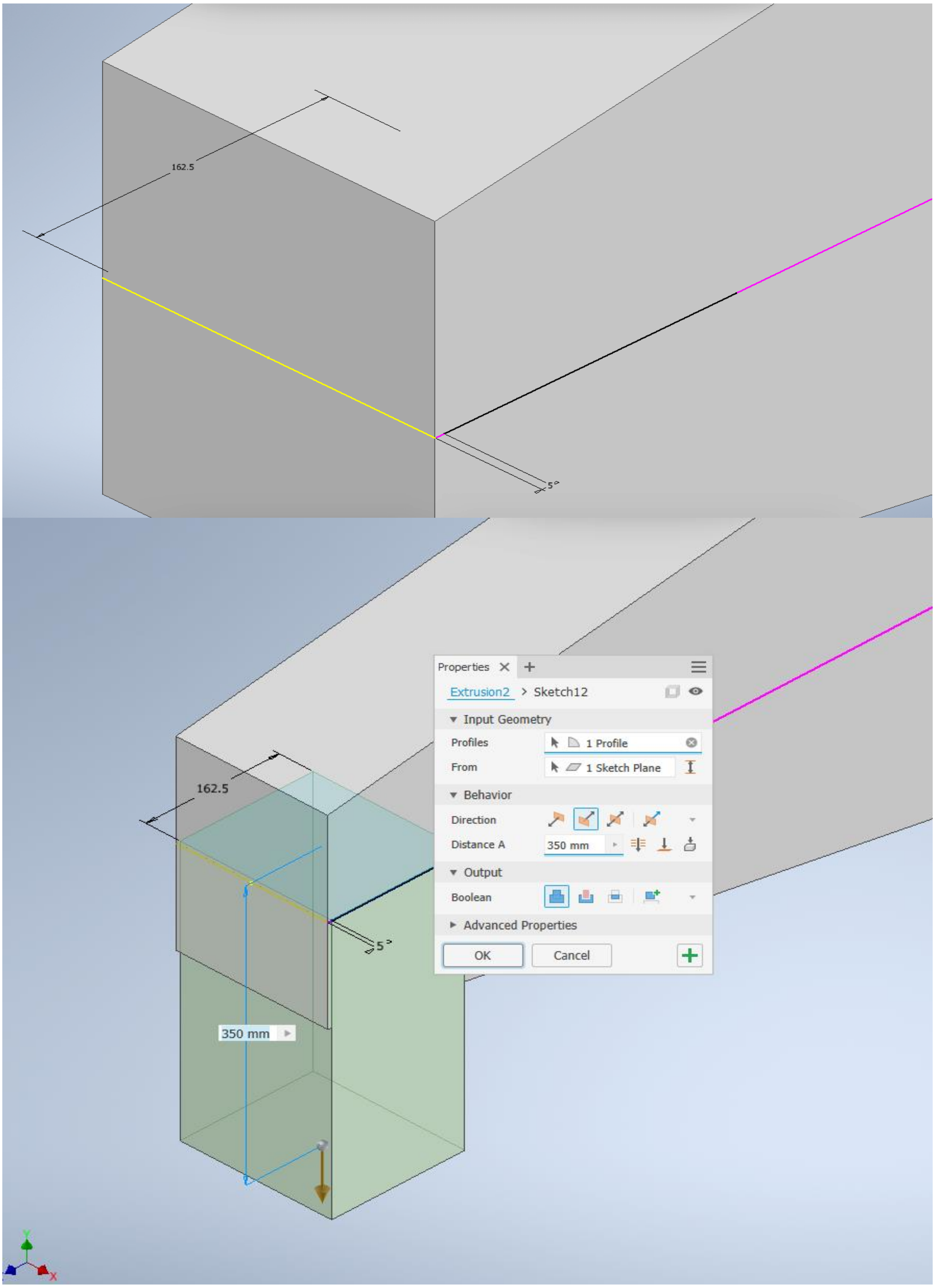

Figure A.46: drawing the pipes of the second chamber Extrusion of the pipe for the collection bin of the second chamber

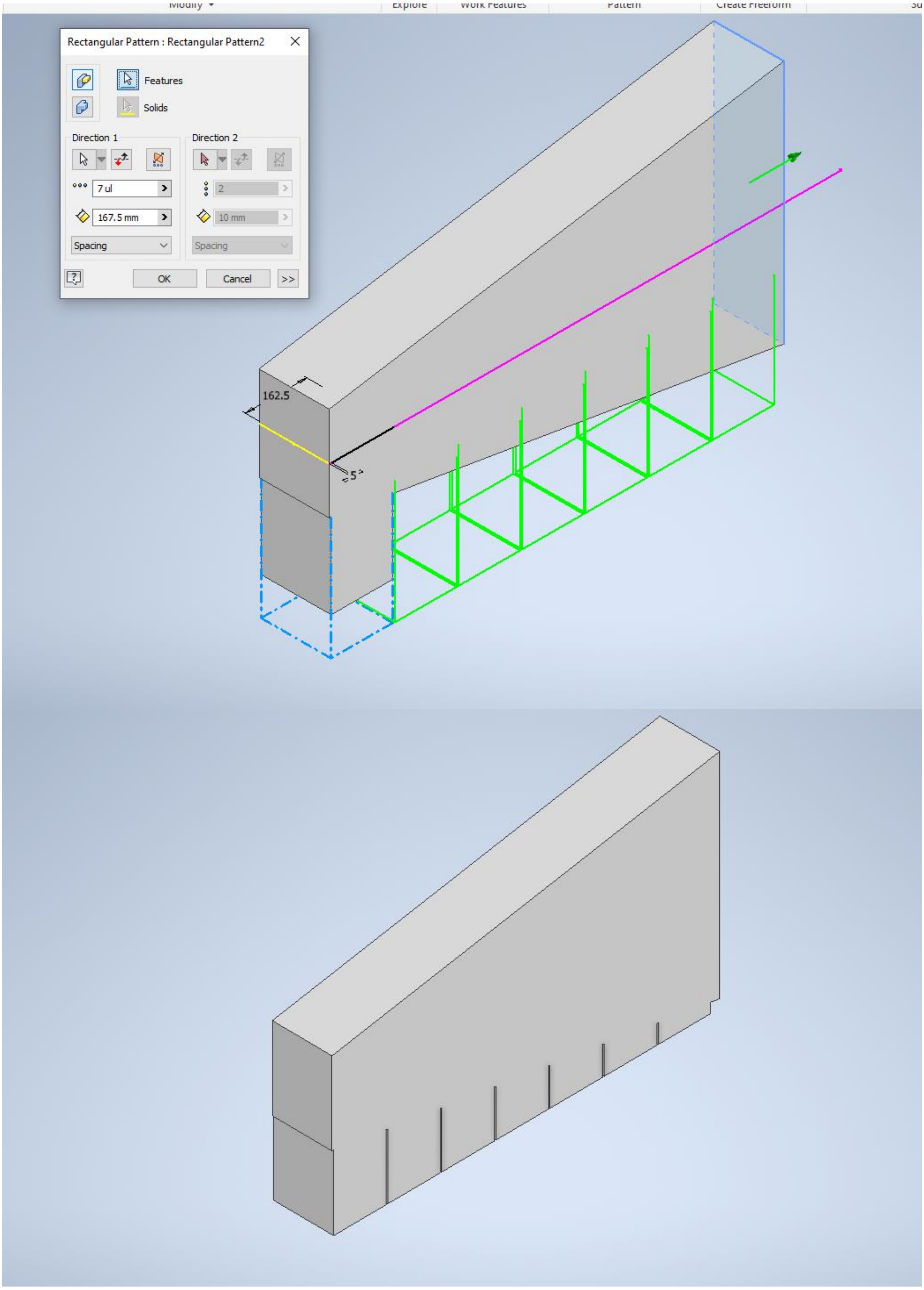

Figure A.47: Using "Repeated Pattern" tool to design the remaining pipes for the collection bins of the chamber 2

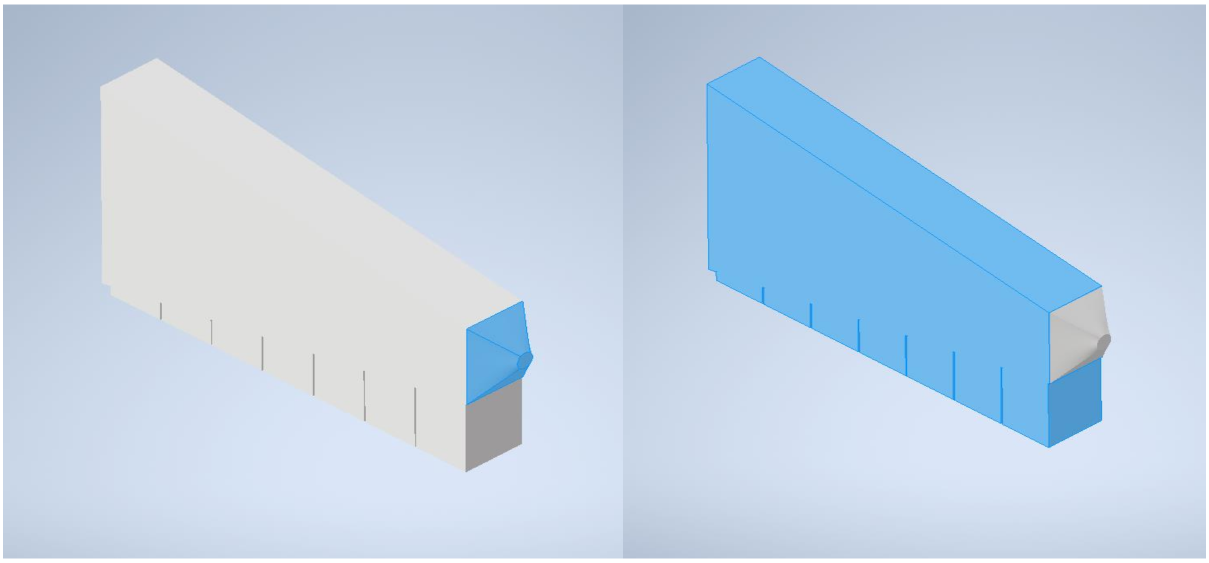

Figure A.48: Assembling the Inlet diffuser-transition piece and the main diffuser section

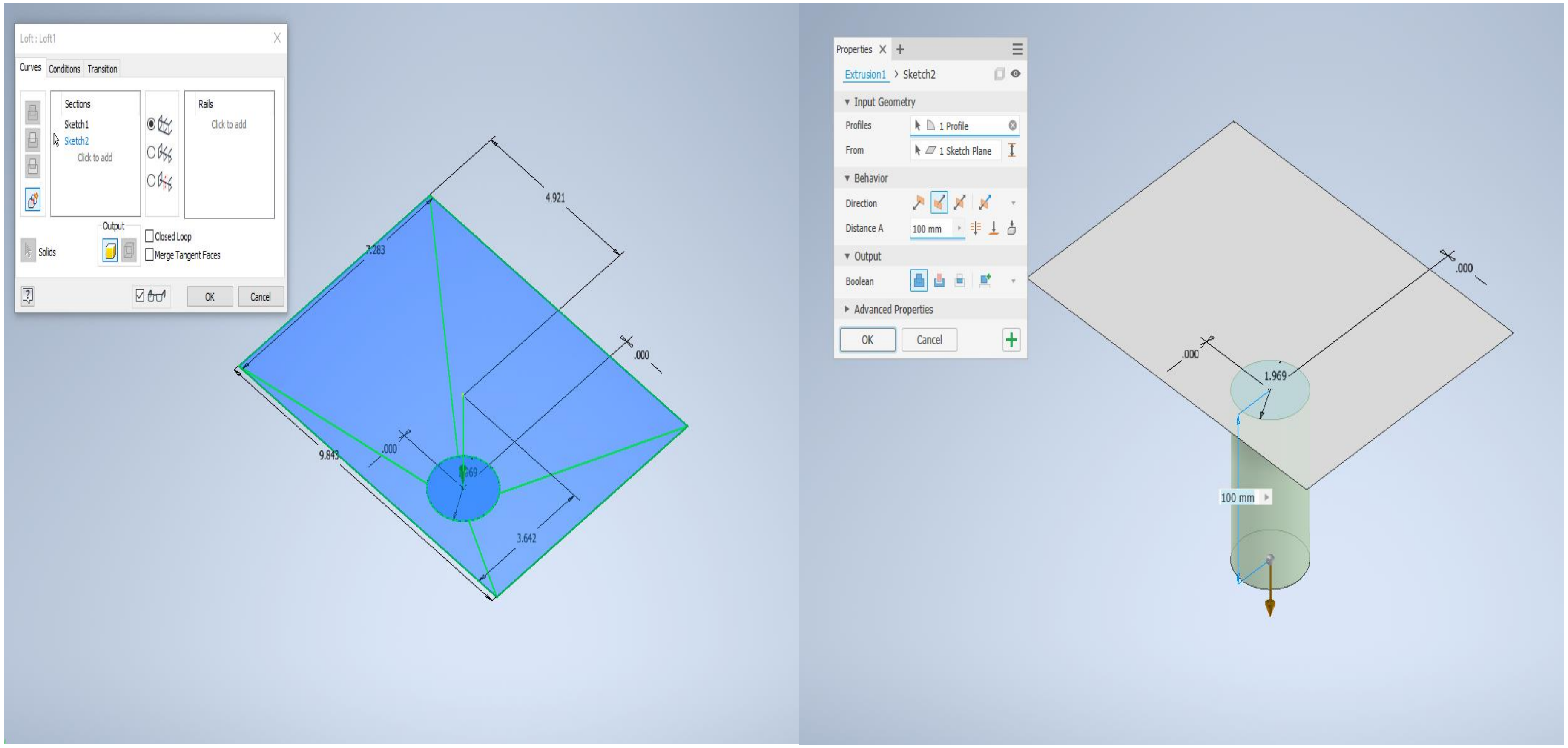

Figure A.49: Drawing the base of the Hatchet Section

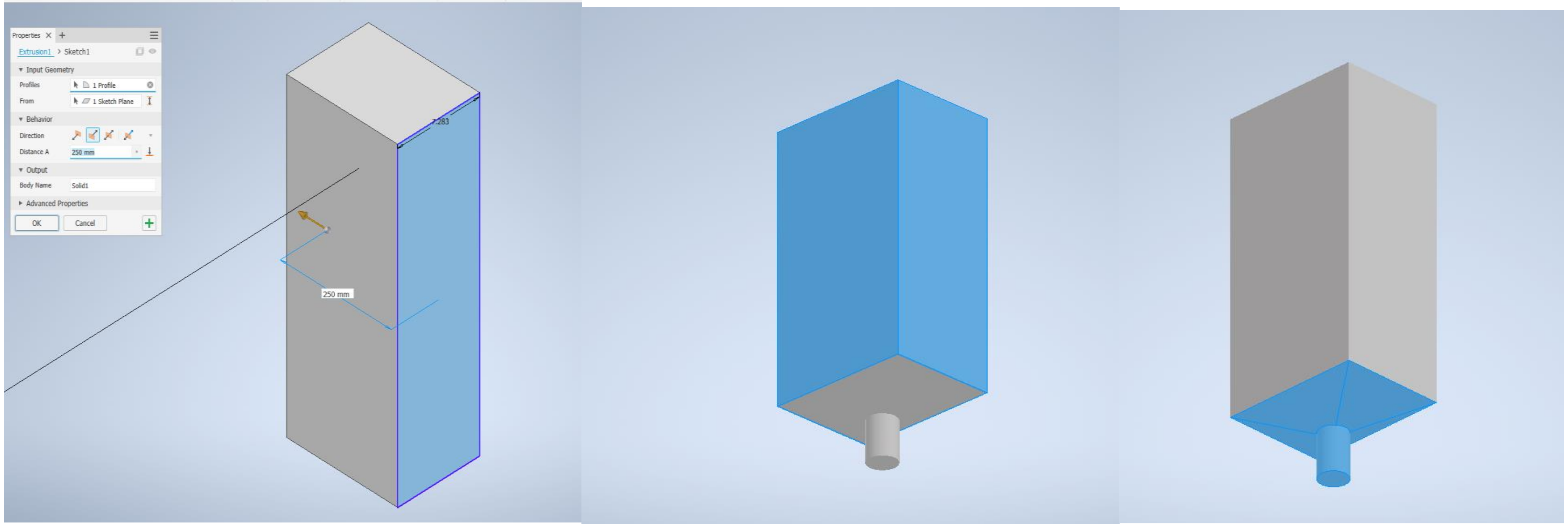

Figure A. 50: Drawing the Upper part of the Hatchet Section

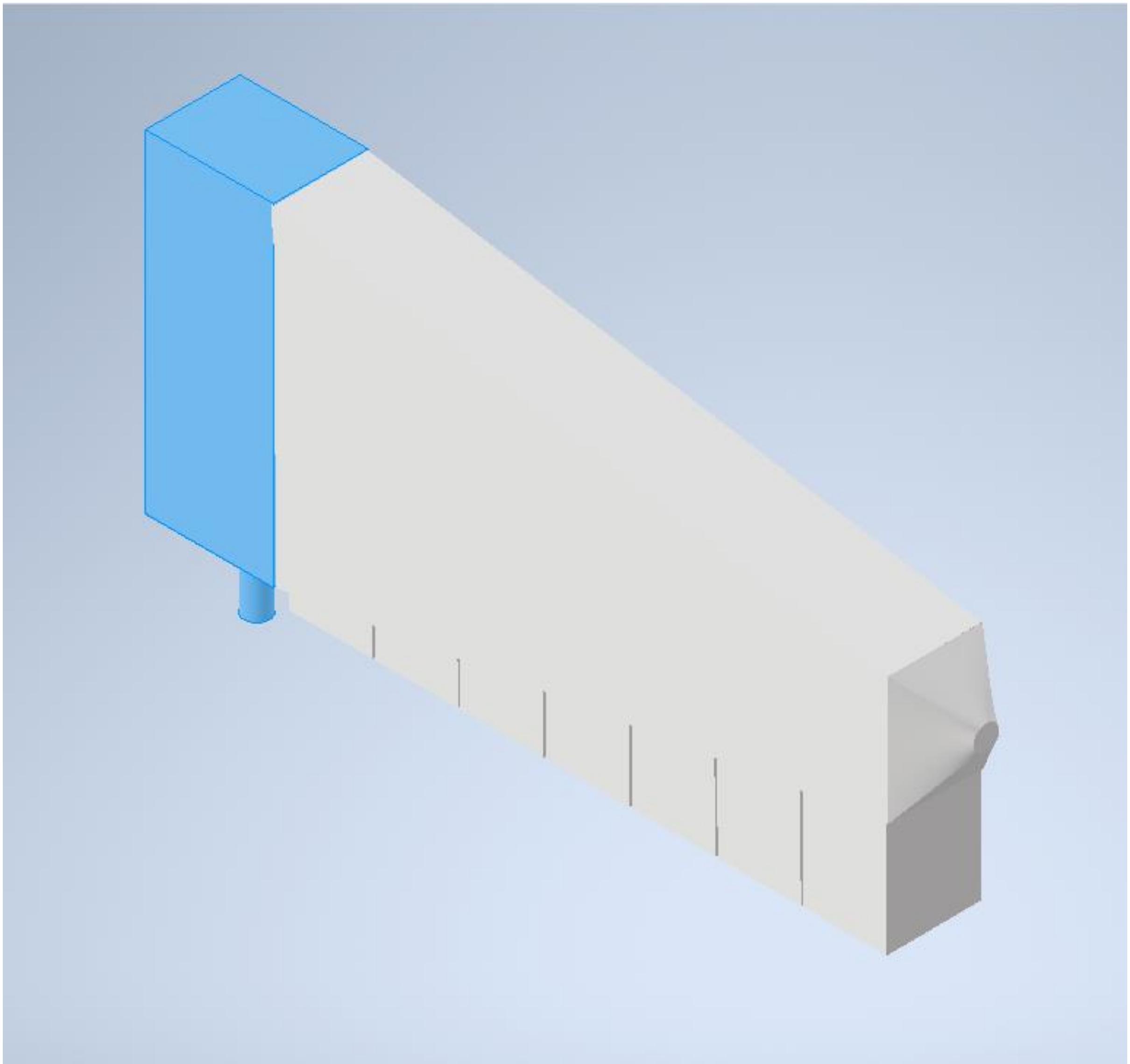

Figure A.51: Joining the Hatchet to the diffuser section thus far.

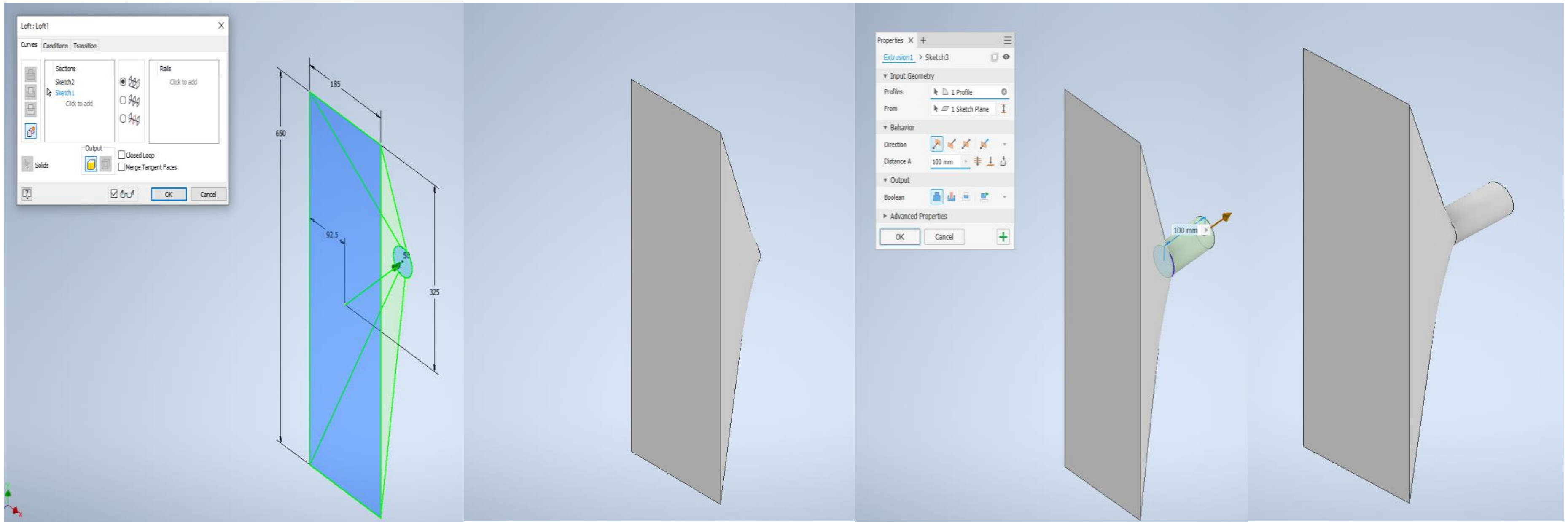

Figure A.52: Drawing the Outlet diffuser part first with the “Loft” and then the “Extrude” tools.

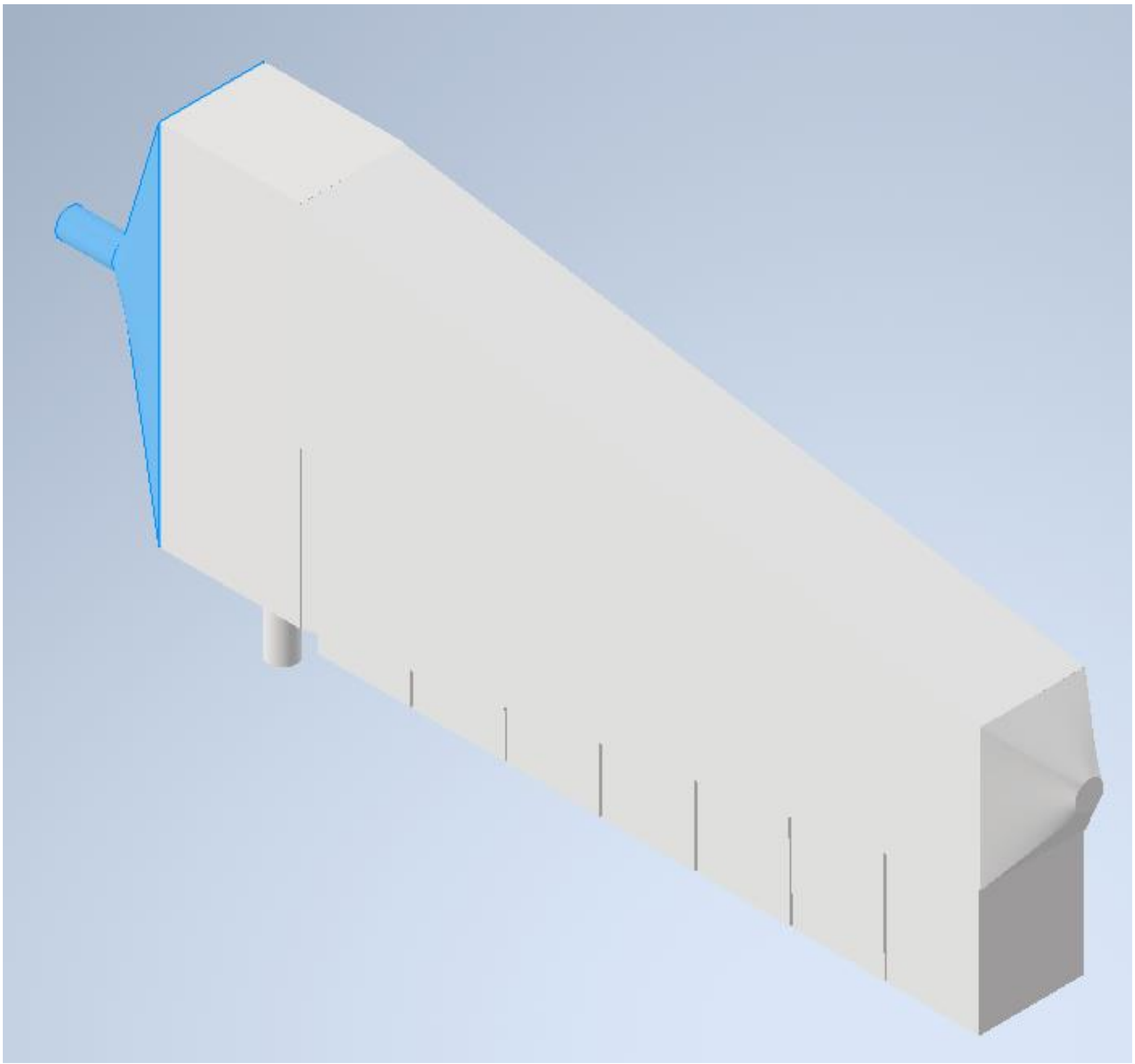
Figure A.53: Joining the Outlet part section to the diffuser section thus far.

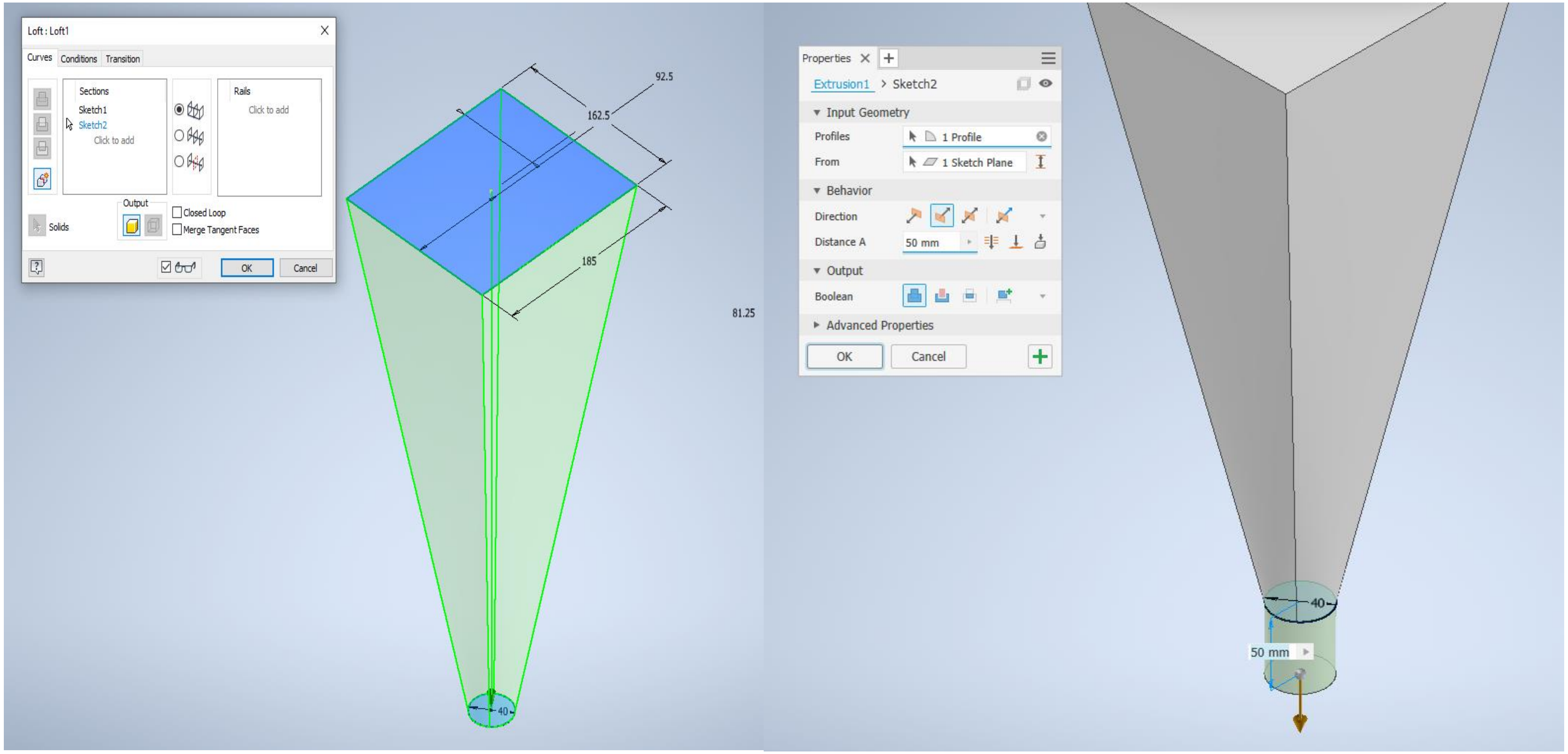

Figure A.54: Designing chute section of the collecting bins section for Chamber 2 using the “Loft” and “Extrude” tools.

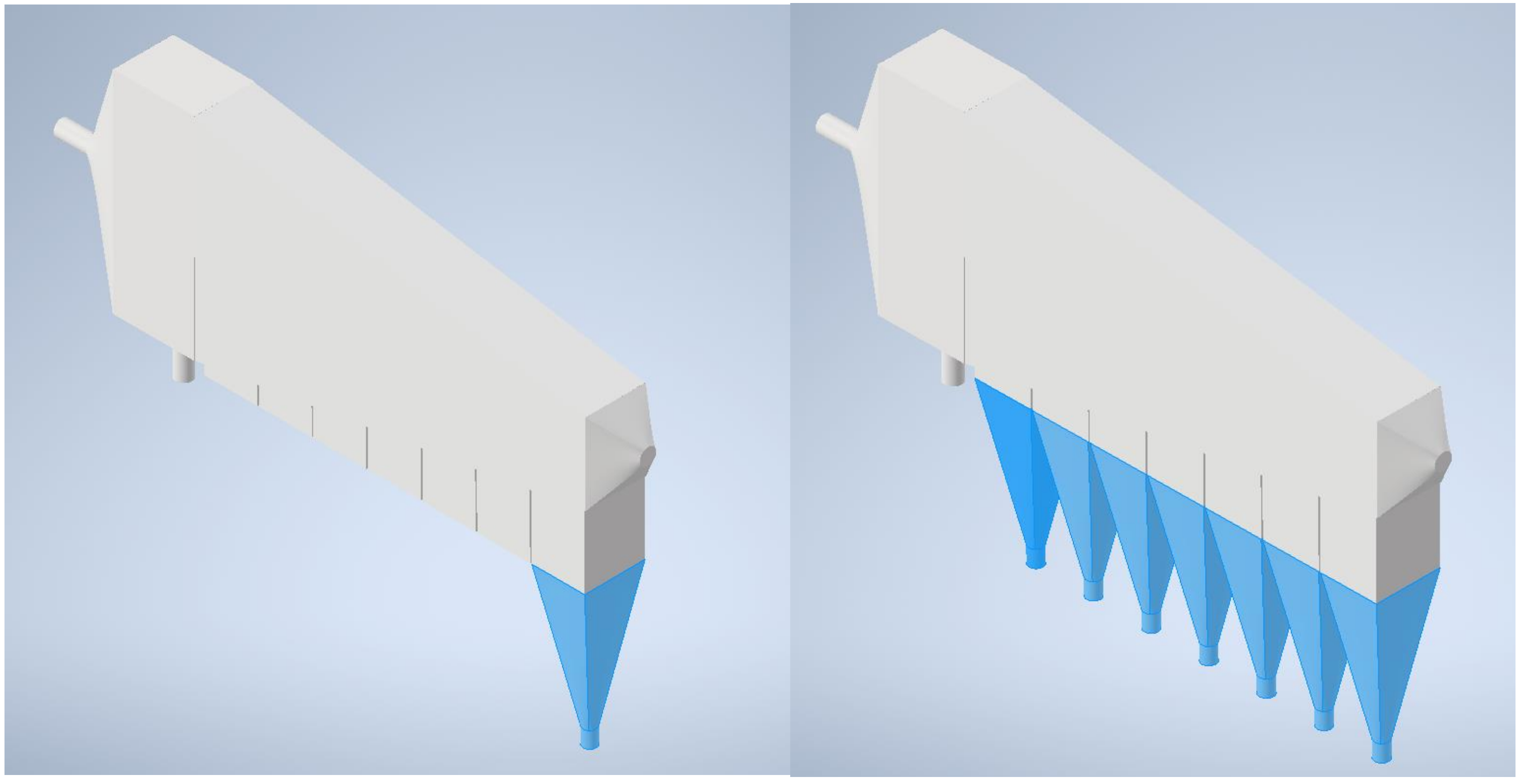

Figure A.55: Joining all the chutes using the joint tool to connect them to complete the chamber 2 without the collecting bins.

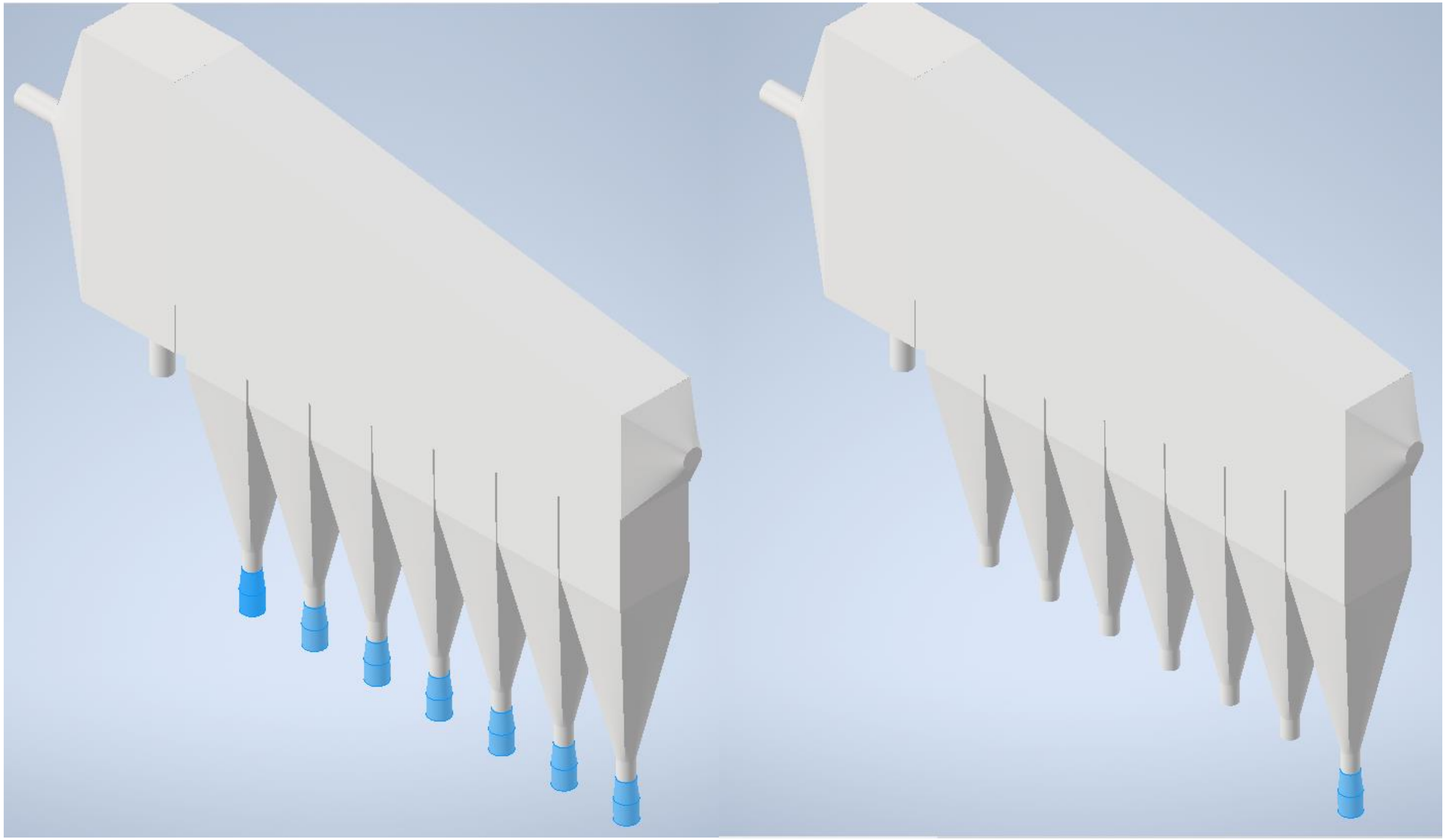

Figure A.56: Joining all the bins using the joint tool to connect them to complete the chamber 2 with the collecting bins.

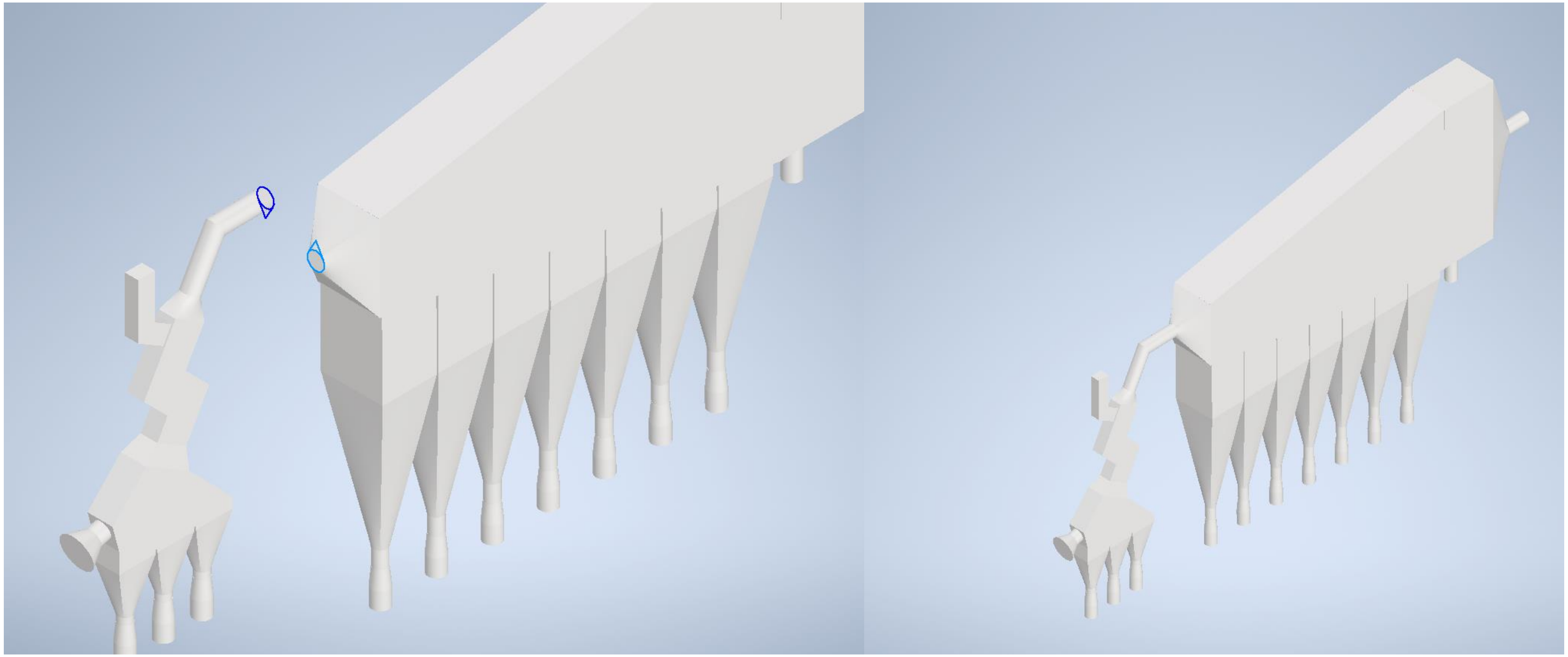

Figure A. 57: Joining the chamber 1 to the chamber 2 for the full fluid-body of the separator assembly.

APPENDIX B: PARTICLE TRACKS FOR – 3.35+1 mm AND – 1+0.2 mm SIMULATION TESTS.

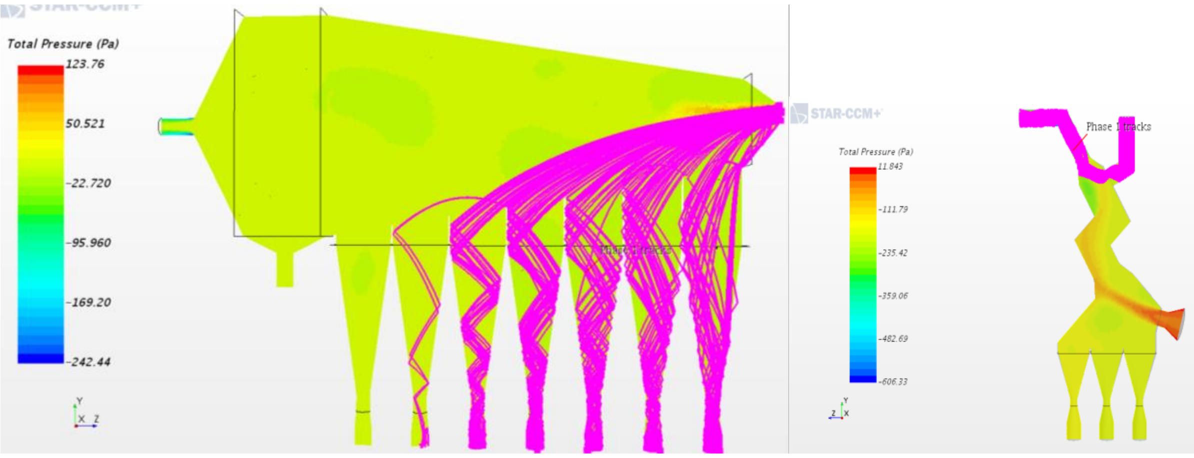

Figure B.1: Particle tracks for – 3.35+1 mm at 1.3 RD in both chambers at 4.2 m/sec (with bins)

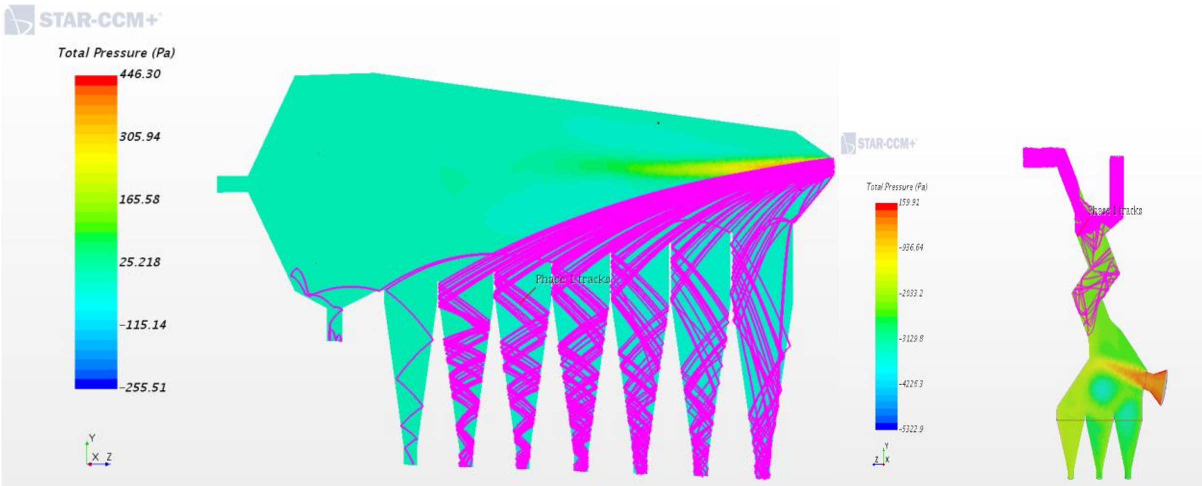

Figure B.2: Particle tracks for – 3.35+1 mm at 1.3 RD in both chambers at 7 m/sec (without bins)

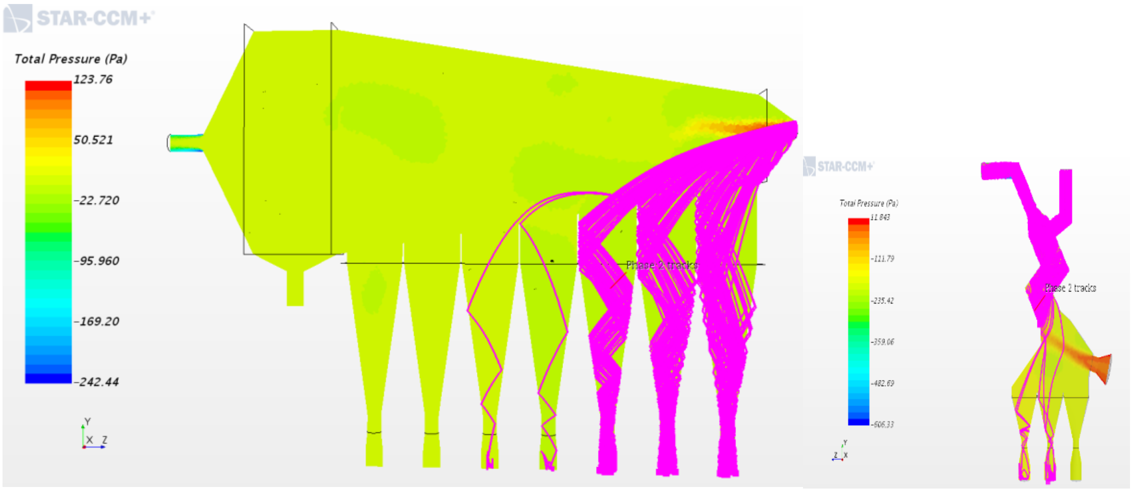

Figure B.3: Particle tracks for – 3.35+1 mm at 1.4 RD in both chambers at 4.2 m/sec (with bins)

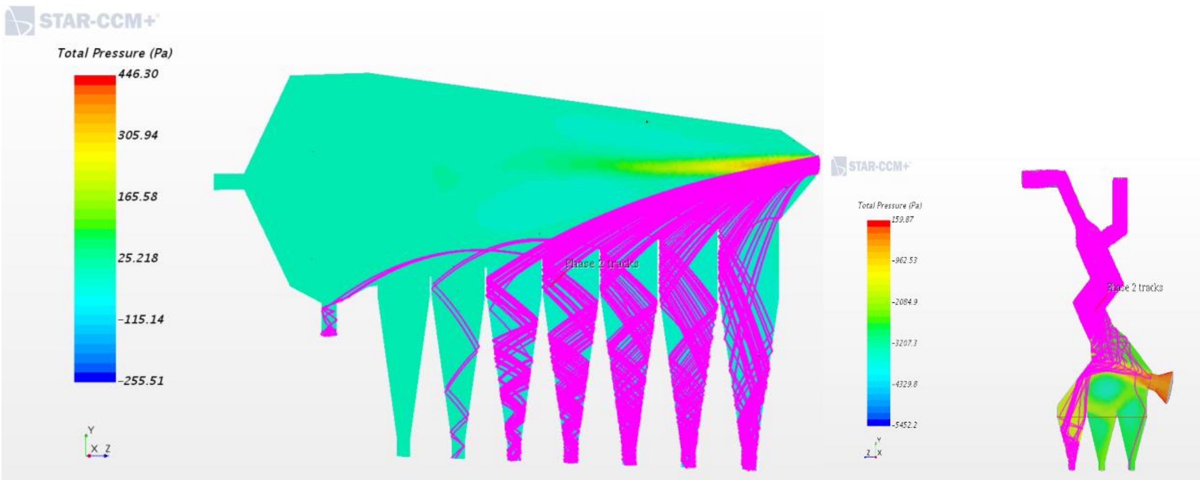

Figure B.4: Particle tracks for – 3.35+1 mm at 1.4 RD in both chambers at 7 m/sec (without bins)

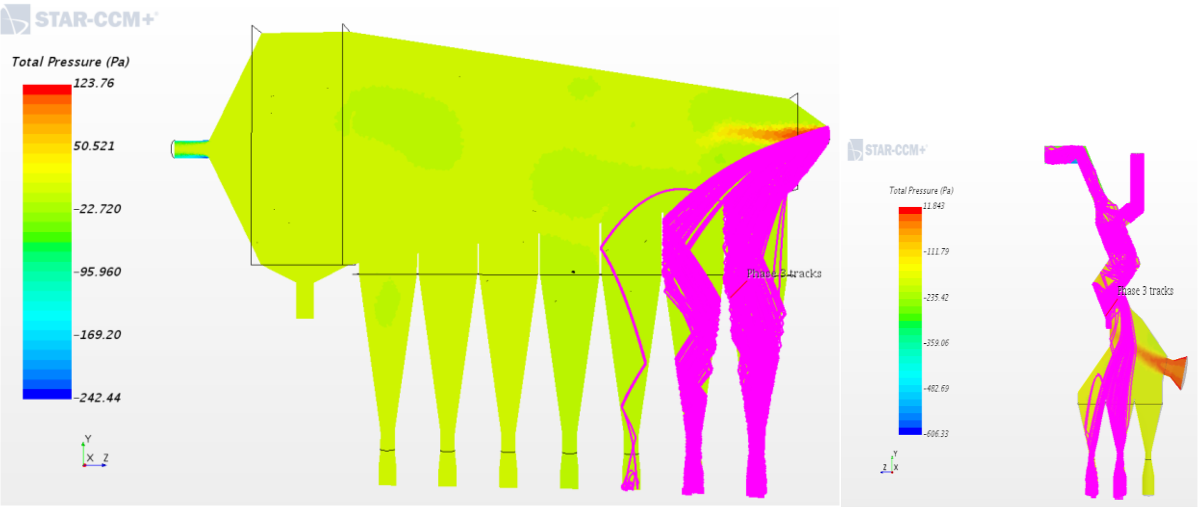

Figure B.5: Particle tracks for – 3.35+1 mm at 1.5 RD in both chambers at 4.2 m/sec (with bins)

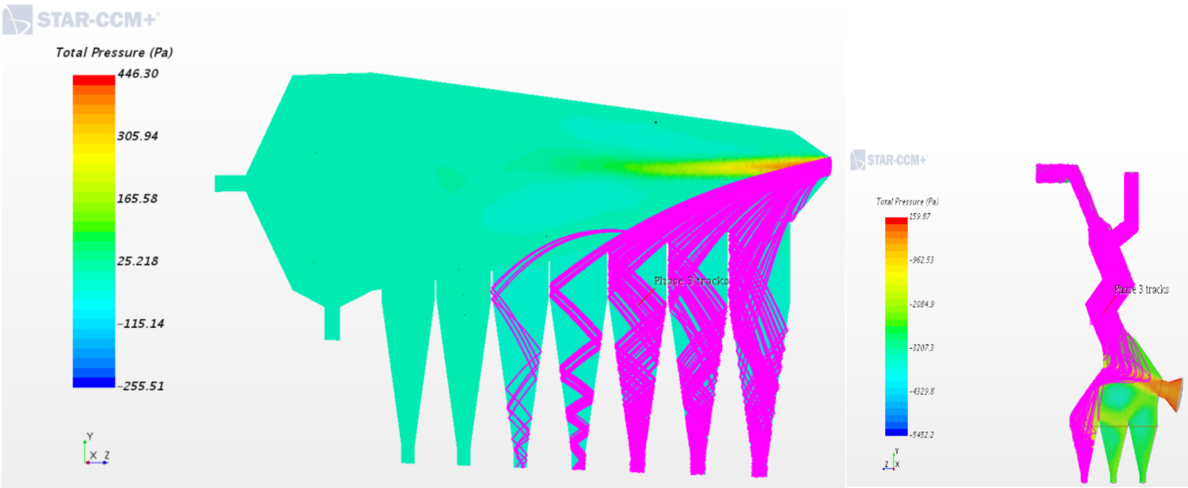

Figure B.6: Particle tracks for – 3.35+1 mm at 1.5 RD in both chambers at 7 m/sec (without bins)

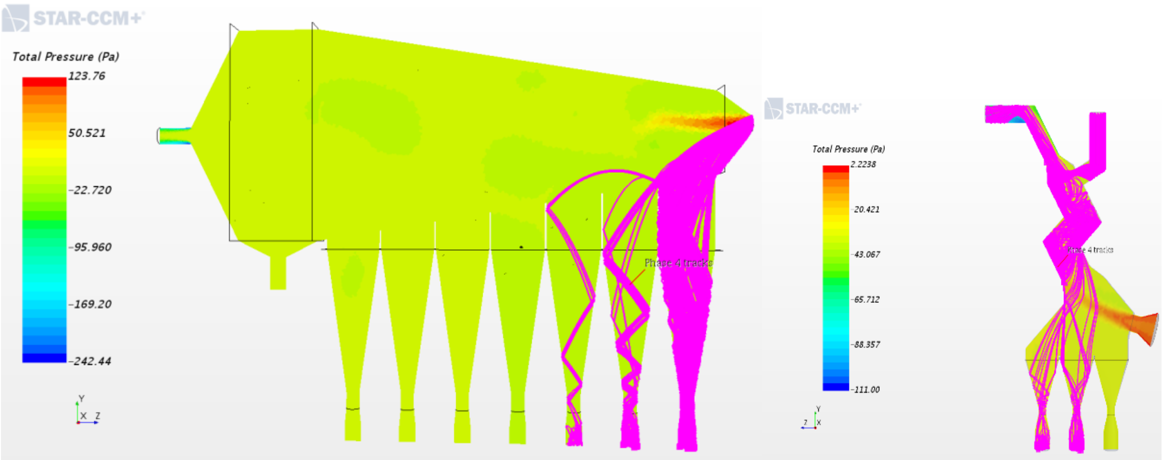

Figure B.7: Particle tracks for – 3.35+1 mm at 1.6 RD in both chambers at 4.2 m/sec (with bins)

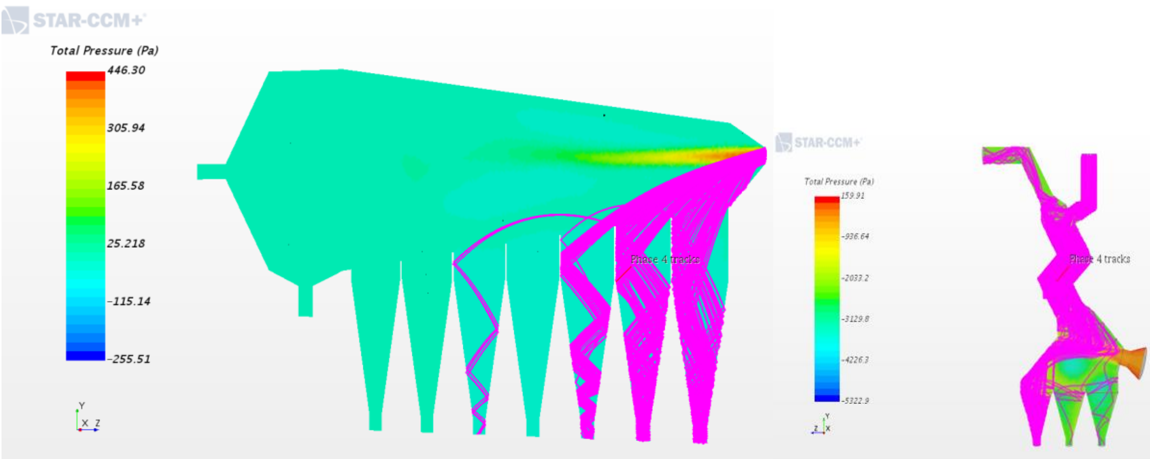

Figure B.8: Particle tracks for – 3.35+1 mm at 1.6 RD in both chambers at 7 m/sec (without bins)

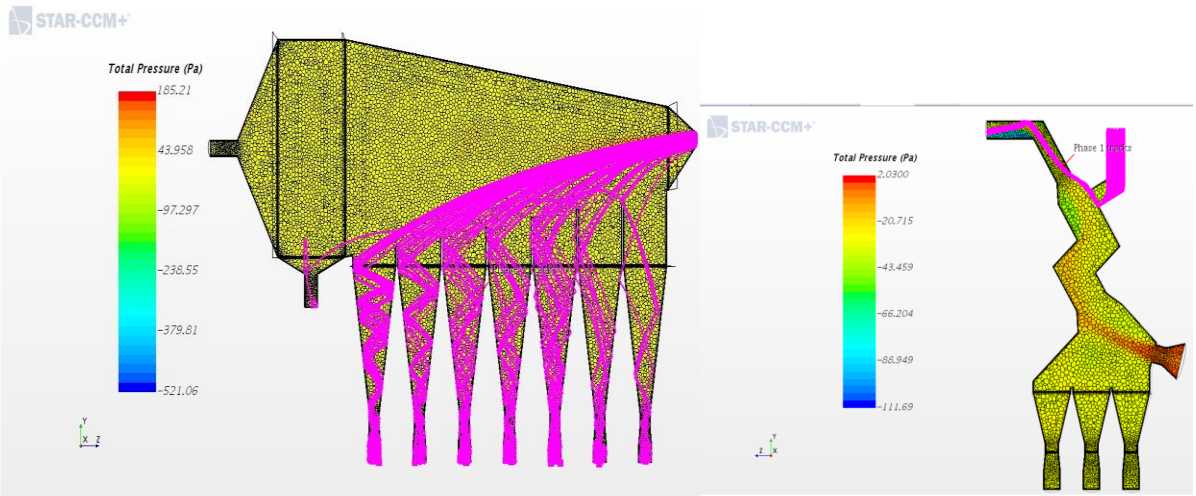

Figure B.9: Particle tracks for – 1+0.2 mm at 1.3 RD in both chambers at 1.7 m/sec (with bins)

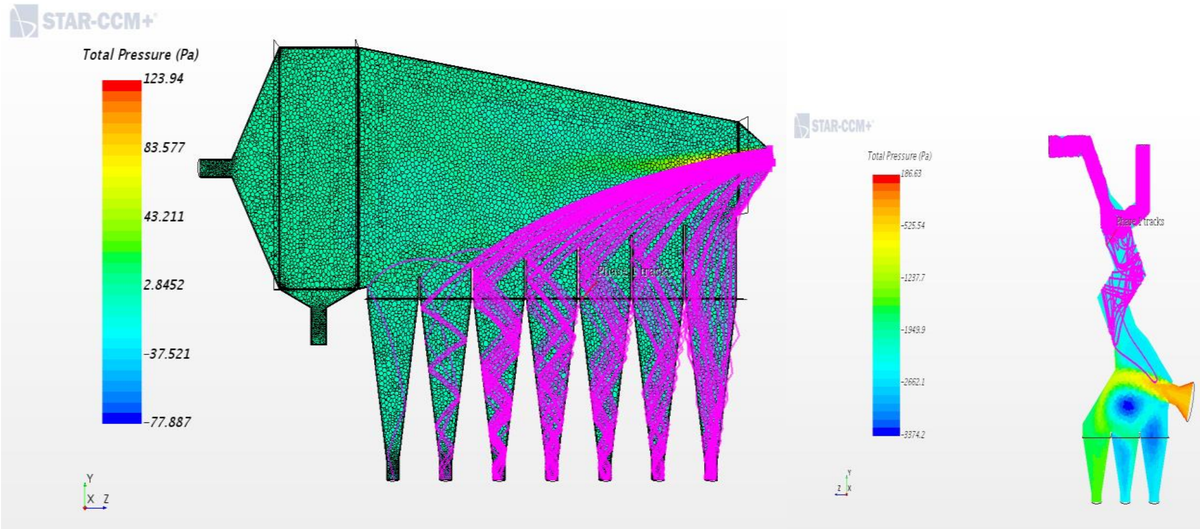

Figure B.10: Particle tracks for – 1+0.2 mm at 1.3 RD in both chambers at 3.5 m/sec (without bins)

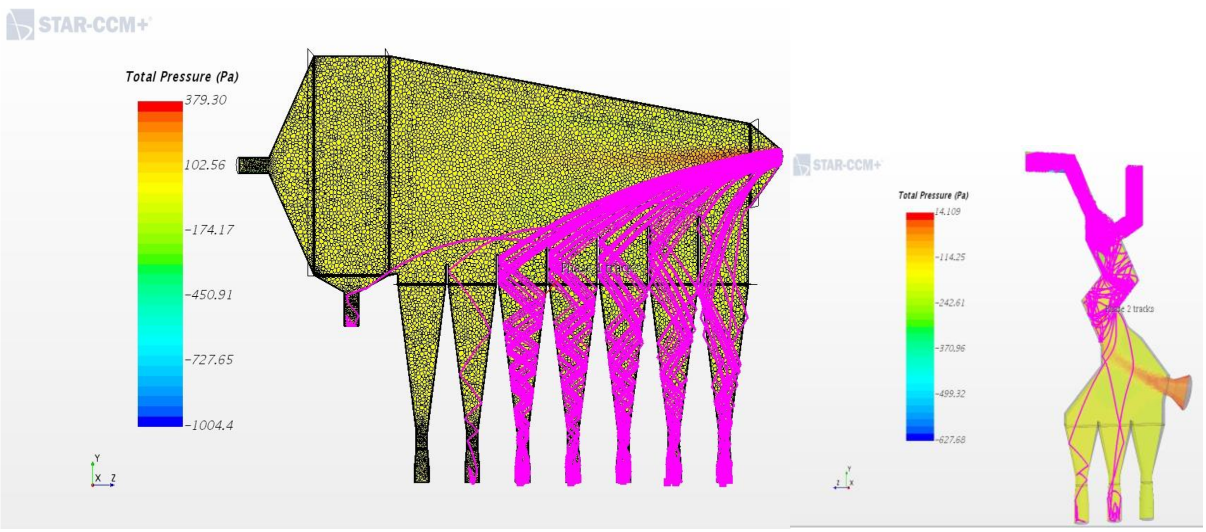

Figure B.11: Particle tracks for – 1+0.2 mm at 1.4 RD in both chambers at 1.7 m/sec (with bins)

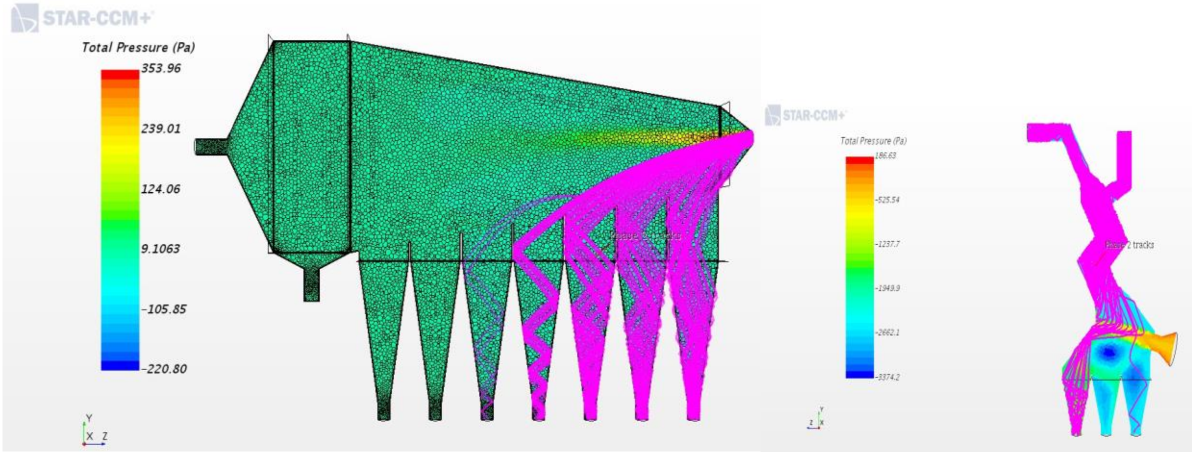

Figure B.12: Particle tracks for – 1+0.2 mm at 1.4 RD in both chambers at 3.5 m/sec (without bins)

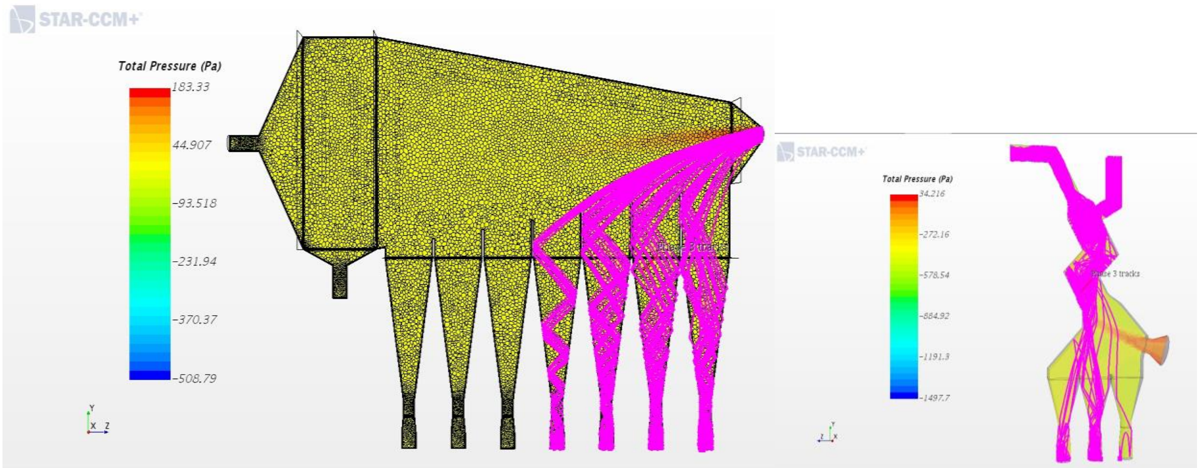

Figure B.13: Particle tracks for – 1+0.2 mm at 1.5 RD in both chambers at 1.7 m/sec (with bins)

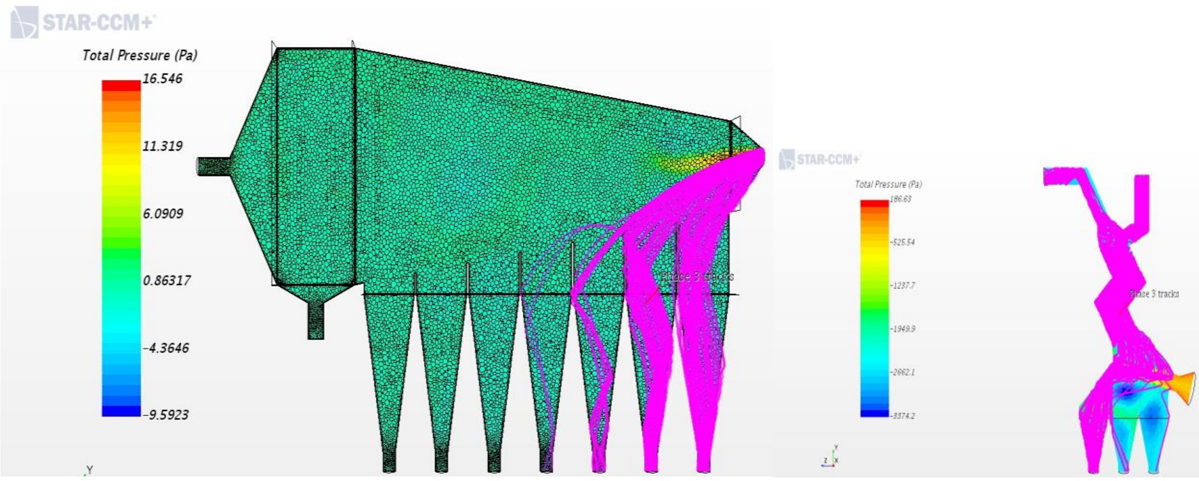

Figure B.14: Particle tracks for – 1+0.2 mm at 1.5 RD in both chambers at 3.5 m/sec (without bins)

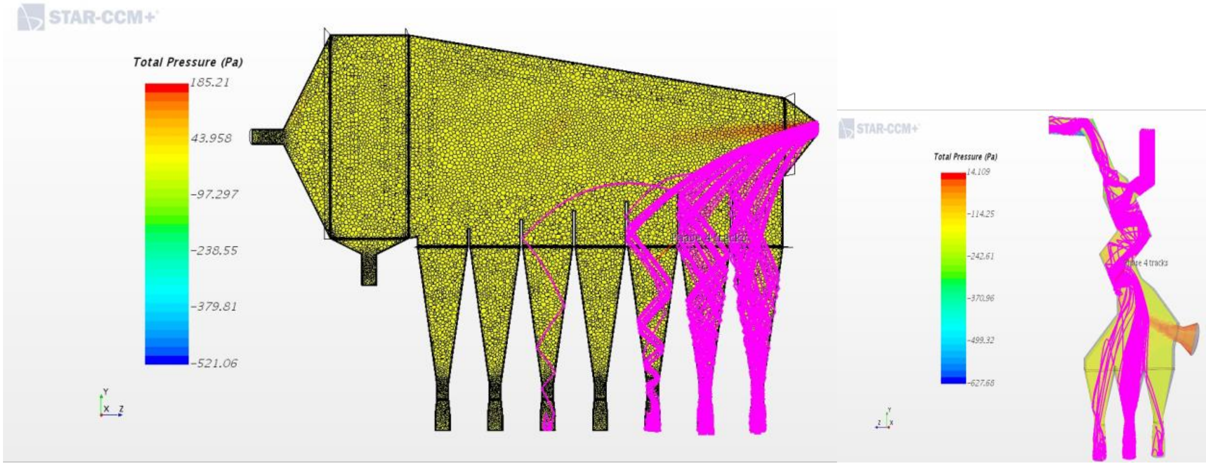

Figure B. 15: Particle tracks for – 1+0.2 mm at 1.6RD in both chambers at 1.7 m/sec (with bins)

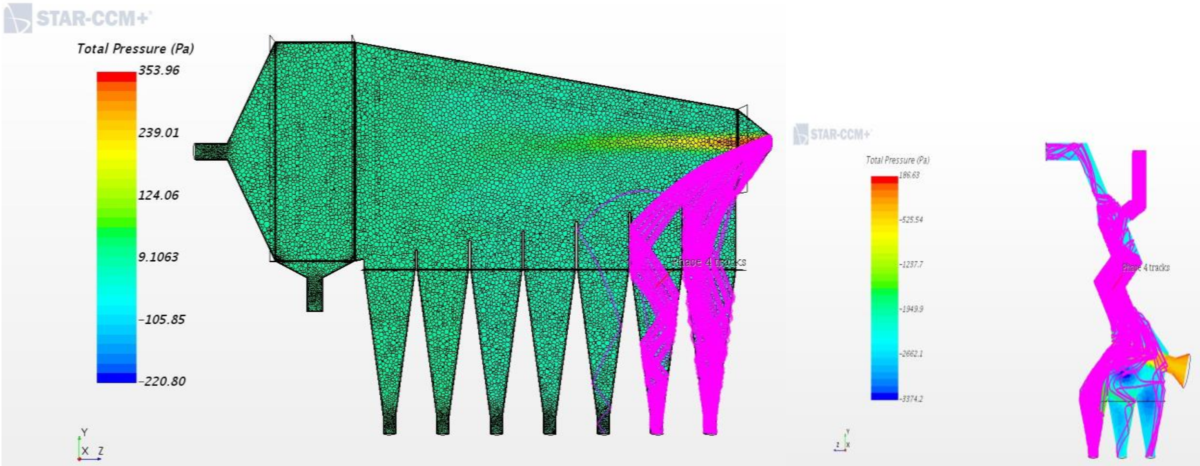

Figure B.16: Particle tracks for – 1+0.2 mm at 1.6 RD in both chambers at 3.5 m/sec (without bins)

APPENDIX C: WASHABILITY DATA OF ALL THREE PARTICLE SIZE FRACTION FOR FLOAT AND SINK ANALYSIS AND DRY BENEFICIATION PROCESS

Table C.1: Float and sink test result for – 6 7+3.35 mm size fraction of the feed Coal A

Relative Density	Mass (Wt) g	Fractional Yield (Wt) %	Cum. Wt (%)	Ash content (%)	Cum Ash content (%)	Combustible Recovery (%)	Ash rejection (%)	Separation Efficiency (%)
1.3	26.89	5.40	5.40	5.89	5.89	8.11	99.15	7.26
1.4	80.67	16.20	21.60	8.74	8.03	31.72	95.36	27.08
1.5	93.71	18.82	40.41	16.65	12.04	56.76	86.98	43.74
1.6	40.48	8.13	48.54	24.67	14.16	66.54	81.61	48.16
1.7	32.55	6.54	55.08	30.45	16.09	73.80	76.29	50.09
1.8	24	4.82	59.90	37.48	17.81	78.61	71.46	50.07
1.9	199.72	40.10	100.00	66.60	37.38	100.00	0.00	0.00
Total	498.02	100.00		37.38				

Table C.2: Float and sink test result for – 3.35+1 mm size fraction of the feed Coal A

Relative Density	Mass (Wt) g	Fractional Yield (Wt) %	Cum. Yield %	Ash content	Cum Ash content (%)	Combustible Recovery (%)	Ash rejection (%)	Separation Efficiency (%)
1.3	30.71	6.48	6.48	5.55	5.55	8.89	98.84	7.73
1.4	90.67	19.14	25.62	8.47	7.73	34.31	93.63	27.94
1.5	89.31	18.85	44.47	15.11	10.86	57.53	84.48	42.01
1.6	60.84	12.84	57.31	22.40	13.44	72.00	75.23	47.23
1.7	40	8.44	65.75	29.80	15.54	80.60	67.14	47.74
1.8	27.29	5.76	71.51	37.70	17.33	85.81	60.16	45.97
1.9	135	28.49	100.00	65.68	31.11	100.00	0.00	0.00
Total	473.82	100.00		31.11				

Table C.3: Float and sink test result for – 1+0.2 mm size fraction of the feed Coal A

Relative Density	Mass (Wt) g	Fractional Yield (Wt) %	Cum. Wt (%)	Ash content (%)	Cum Ash content (%)	Combustible Recovery (%)	Ash rejection (%)	Separation Efficiency (%)
1.3	43.96	8.81	8.81	4.29	4.29	11.92	98.71	10.63
1.4	99.46	19.93	28.74	7.82	6.74	37.91	93.39	31.30
1.5	88.72	17.78	46.51	14.45	9.69	59.42	84.62	44.04
1.6	69.90	14.01	60.52	22.56	12.66	74.76	73.84	48.59
1.7	35.66	7.15	67.67	29.24	14.42	81.91	66.70	48.61
1.8	28.27	5.66	73.33	37.44	16.19	86.92	59.46	46.38
1.9	133.10	26.67	100.00	65.32	29.30	100.00	0.00	0.00
Total	499.07	100.00		29.30				

Table C.4: Float and sink test result for – 6.7+3.35 mm size fraction of the feed Coal B

Relative Density	Mass (Wt) g	Fractional Yield (Wt) %	Cum. Wt (%)	Ash content (%)	Cum Ash content (%)	Combustible Recovery (%)	Ash rejection (%)	Separation Efficiency (%)
1.3	24.00	4.81	4.81	5.83	5.83	6.18	98.95	5.13
1.4	109.34	21.94	26.75	10.85	9.95	32.84	90.02	22.86
1.5	135.00	27.08	53.83	13.56	11.76	64.76	76.23	40.99
1.6	89.98	18.05	71.89	21.10	14.11	84.18	61.94	46.12
1.7	24.02	4.82	76.71	31.40	15.20	88.68	56.26	44.95
1.8	23.51	4.72	81.42	38.24	16.53	92.66	49.50	42.15
1.9	92.60	18.58	100.00	71.00	26.65	100.00	0.00	0.00
Total	498.45	100.00		26.65				

Table C. 5: Float and sink test result for – 3.35+1 mm size fraction of the feed Coal B

Relative Density	Mass (Wt) g	Fractional Yield (Wt) %	Cum. Wt (%)	Ash content (%)	Cum Ash content (%)	Combustible Recovery (%)	Ash rejection (%)	Separation Efficiency (%)
1.3	33.69	6.77	6.77	5.43	5.43	8.75	98.63	7.38
1.4	106.19	21.35	28.13	11.74	10.22	34.49	89.27	23.76
1.5	91.31	18.36	46.49	15.89	12.46	55.58	78.37	33.95
1.6	128.00	25.74	72.23	24.76	16.84	82.03	54.58	36.61
1.7	33.10	6.66	78.88	35.27	18.40	87.91	45.81	33.73
1.8	19.33	3.89	82.77	38.50	19.34	91.18	40.22	31.40
1.9	85.69	17.23	100.00	62.52	26.78	100.00	0.00	0.00
Total	497.31	100.00		26.78				

Table C.6: Float and sink test result for – 1+0.2 mm size fraction of the feed Coal B

Relative Density	Mass (Wt) g	Fractional Yield (Wt) %	Cum. Wt (%)	Ash content (%)	Cum Ash content (%)	Combustible Recovery (%)	Ash rejection (%)	Separation Efficiency (%)
1.3	29.41	5.88	5.88	4.13	4.13	7.46	99.00	6.46
1.4	78.00	15.60	21.49	8.31	7.17	26.37	93.68	20.04
1.5	119.75	23.96	45.45	13.75	10.64	53.68	80.15	33.83
1.6	105.39	21.08	66.53	21.99	14.23	75.42	61.10	36.52
1.7	33.05	6.61	73.14	28.73	15.55	81.65	53.30	34.95
1.8	56.07	11.22	84.36	35.04	18.14	91.28	37.15	28.44
1.9	78.17	15.64	100.00	57.84	24.35	100.00	0.00	0.00
Total	499.84	100.00		24.35				

Table C.7: Wind sifter separation result for – 6.7+3.35 mm size fraction at 6.0 m/sec Coal A with Bins

Bin number	Mass (Wt) g	Fractional Yield (Wt) %	Cum. Wt (%)	Ash content (%)	Cum Ash content (%)	Combustible Recovery (%)	Ash rejection (%)	Separation Efficiency (%)
0	121.59	24.60	24.60	26.99	26.99	26.83	79.92	6.75
1	70.26	14.21	38.81	25.93	26.60	42.56	68.78	11.34
2	53.53	10.83	49.64	26.38	26.55	54.47	60.14	14.61
3	43.97	8.89	58.53	26.70	26.58	64.21	52.96	17.16
4	42.92	8.68	67.21	27.62	26.71	73.59	45.71	19.30
5	30.72	6.21	73.43	28.62	26.87	80.22	40.33	20.55
6	15.17	3.07	76.49	28.50	26.94	83.50	37.68	21.18
7	4.46	0.90	77.40	29.94	26.97	84.44	36.87	21.31
8	37.42	7.57	84.97	49.44	28.97	90.16	25.55	15.71
9	69.47	14.05	99.02	56.18	32.84	99.36	1.67	1.03
10	4.85	0.98	100.00	56.41	33.07	100.00	0.00	0.00
Total	494.36	100.00		33.07				

Table C.8: Wind-sifter separation result for – 6.7+3.35 mm size fraction at 5.0 m/sec Coal A with Bins

Bin number	Mass (Wt) g	Fractional Yield (Wt) %	Cum. Wt (%)	Ash content (%)	Cum Ash content (%)	Combustible Recovery (%)	Ash rejection (%)	Separation Efficiency (%)
0	89.52	17.96	17.96	23.98	23.98	21.26	87.96	9.22
1	44.72	8.97	26.93	23.86	23.94	31.89	81.98	13.87
2	41.37	8.30	35.23	24.03	23.96	41.71	76.41	18.12
3	39.63	7.95	43.18	25.91	24.32	50.88	70.65	21.53
4	40.30	8.08	51.26	25.31	24.48	60.29	64.93	25.21
5	32.78	6.58	57.84	26.94	24.76	67.77	59.98	27.74
6	17.07	3.42	61.27	25.54	24.80	71.74	57.53	29.27
7	6.60	1.32	62.59	26.50	24.84	73.25	56.55	29.80
8	58.39	11.71	74.30	49.44	28.71	82.47	40.36	22.84
9	116.88	23.45	97.75	56.18	35.30	98.47	3.55	2.02
10	11.21	2.25	100.00	56.41	35.78	100.00	0.00	0.00
Total	498.47	100.00		35.78				

Table C.9: Wind-sifter test separation for – 6.7+3.35 mm size fraction at 4.0 m/sec Coal A with Bins

Bin number	Mass (Wt) g	Fractional Yield (Wt) %	Cum. Wt (%)	Ash content (%)	Cum Ash content (%)	Combustible Recovery (%)	Ash rejection (%)	Separation Efficiency (%)
0	27.28	5.47	5.47	19.79	19.79	6.06	97.01	3.07
1	15.58	3.12	8.59	20.89	20.19	9.48	93.73	3.21
2	21.58	4.32	12.91	20.17	20.18	14.25	90.58	4.83
3	25.12	5.03	17.95	20.19	20.19	19.80	86.90	6.71
4	27.46	5.50	23.45	20.69	20.30	25.84	82.79	8.63
5	17.30	3.47	26.92	20.08	20.27	29.67	80.27	9.94
6	15.80	3.17	30.09	20.05	20.25	33.17	77.98	11.14
7	5.40	1.08	31.17	19.09	20.21	34.38	77.23	11.61
8	62.22	12.47	43.64	27.41	22.27	46.89	64.87	11.77
9	240.00	48.10	91.74	31.09	26.89	92.71	10.82	3.53
10	41.24	8.26	100.00	36.21	27.66	100.00	0.00	0.00
Total	498.98	100.00		27.66				

Table C.10: Wind-sifter separation result for – 3.35+1 mm size fraction at 4.2 m/sec Coal A with Bins

Bin number	Mass (Wt) g	Fractional Yield (Wt) %	Cum. Wt (%)	Ash content (%)	Cum Ash content (%)	Combustible Recovery (%)	Ash rejection (%)	Separation Efficiency (%)
0	102.67	20.76	20.76	25.39	25.39	22.40	82.91	5.31
1	71.36	14.43	35.19	26.70	25.93	37.70	70.42	8.11
2	66.89	13.53	48.72	27.86	26.46	51.81	58.20	10.00
3	50.01	10.11	58.83	28.25	26.77	62.30	48.93	11.23
4	43.07	8.71	67.54	28.71	27.02	71.28	40.83	12.10
5	40.41	8.17	75.72	28.07	27.13	79.78	33.39	13.17
6	30.23	6.11	81.83	28.94	27.27	86.06	27.65	13.71
7	7.70	1.56	83.39	28.14	27.29	87.68	26.23	13.91
8	37.52	7.59	90.97	46.78	28.91	93.52	14.72	8.24
9	40.59	8.21	99.18	50.14	30.67	99.43	1.38	0.81
10	4.04	0.82	100.00	52.09	30.84	100.00	0.00	0.00
Total	494.49	100.00		30.84				

Table C.11: Wind-sifter separation result for – 3.35+1 mm size fraction at 3.0 m/sec Coal A with Bins

Bin number	Mass (Wt) g	Fractional Yield (Wt.) %	Cum. Wt. (%)	Ash content (%)	Cum Ash content (%)	Combustible Recovery (%)	Ash rejection (%)	Separation Efficiency (%)
0	93.39	19.20	19.20	23.43	23.43	20.80	84.64	5.44
1	41.00	8.43	27.63	23.48	23.45	29.92	77.89	7.81
2	44.92	9.24	36.87	23.06	23.35	39.97	70.62	10.59
3	45.72	9.40	46.27	24.01	23.48	50.08	62.91	12.99
4	45.11	9.28	55.55	25.51	23.82	59.85	54.83	14.69
5	42.00	8.64	64.19	25.34	24.03	68.97	47.36	16.34
6	26.31	5.41	69.60	25.04	24.10	74.71	42.74	17.45
7	9.91	2.04	71.63	24.35	24.11	76.89	41.05	17.94
8	45.07	9.27	80.90	37.63	25.66	85.06	29.14	14.21
9	82.07	16.88	97.78	44.92	28.98	98.21	3.27	1.48
10	10.81	2.22	100.00	43.09	29.30	100.00	0.00	0.00
Total	486.31	100.00		29.30				

Table C.12: Wind-sifter separation result for – 3.35+1 mm size fraction at 2.0 m/sec Coal A with Bins

Bin number	Mass (Wt) g	Fractional Yield (Wt.) %	Cum. Wt. (%)	Ash content (%)	Cum Ash content (%)	Combustible Recovery (%)	Ash rejection (%)	Separation Efficiency (%)
0	17.91	3.59	3.59	19.49	19.49	4.07	97.58	1.64
1	11.62	2.33	5.92	20.13	19.74	6.69	95.95	2.64
2	15.95	3.20	9.13	20.48	20.00	10.27	93.68	3.95
3	21.91	4.40	13.52	20.48	20.16	15.18	90.57	5.75
4	28.24	5.67	19.19	20.57	20.28	21.51	86.53	8.05
5	27.02	5.42	24.61	20.90	20.42	27.54	82.61	10.15
6	16.59	3.33	27.94	20.63	20.44	31.26	80.24	11.49
7	4.76	0.96	28.89	21.76	20.48	32.31	79.52	11.82
8	83.56	16.77	45.66	26.47	22.68	49.65	64.16	13.80
9	246.39	49.44	95.09	33.91	28.52	95.59	6.14	1.73
10	24.45	4.91	100.00	36.14	28.89	100.00	0.00	0.00
Total	498.40	100.00		28.89				

Table C.13: Wind-sifter separation result for – 1+0.2 mm size fraction at 1.7 m/sec Coal A with Bins

Bin number	Mass (Wt) g	Fractional Yield (Wt) %	Cum. Wt (%)	Ash content (%)	Cum Ash content (%)	Combustible Recovery (%)	Ash rejection (%)	Separation Efficiency (%)
0	15.87	3.44	3.44	26.97	26.97	3.47	96.62	0.09
1	30.22	6.55	10.00	26.43	26.62	10.12	90.32	0.44
2	38.26	8.30	18.29	26.10	26.38	18.58	82.45	1.02
3	73.00	15.83	34.13	27.21	26.77	34.47	66.78	1.25
4	89.19	19.34	53.47	25.00	26.13	54.48	49.19	3.67
5	120.00	26.03	79.50	27.00	26.41	80.68	23.64	4.32
6	56.90	12.34	91.84	28.00	26.63	92.94	11.07	4.01
7	18.07	3.92	95.76	29.31	26.74	96.76	6.89	3.65
8	10.63	2.31	98.06	41.01	27.07	98.64	3.46	2.09
9	7.92	1.72	99.78	48.86	27.45	99.85	0.40	0.25
10	1.02	0.22	100.00	50.12	27.50	100.00	0.00	0.00
Total	461.08	100.00		27.50				

Table C. 14: Wind-sifter separation result for –1+0.2 mm size fraction at 1.0 m/sec Coal A with Bins

Bin number	Mass (Wt) g	Fractional Yield (Wt) %	Cum. Wt (%)	Ash content (%)	Cum Ash content (%)	Combustible Recovery (%)	Ash rejection (%)	Separation Efficiency (%)
0	1.21	0.25	0.25	21.67	21.67	0.28	99.83	0.11
1	1.81	0.37	0.62	22.61	22.23	0.70	99.56	0.26
2	7.27	1.49	2.11	24.03	23.50	2.34	98.41	0.75
3	15.47	3.17	5.27	24.50	24.10	5.81	95.93	1.74
4	27.63	5.65	10.92	24.94	24.54	11.98	91.41	3.39
5	57.07	11.68	22.60	25.30	24.93	24.66	81.94	6.59
6	69.08	14.13	36.73	25.59	25.18	39.94	70.34	10.28
7	26.40	5.40	42.13	25.49	25.22	45.79	65.93	11.72
8	66.00	13.50	55.64	32.09	26.89	59.12	52.04	11.15
9	207.40	42.43	98.07	36.54	31.07	98.25	2.33	0.58
10	9.43	1.93	100.00	37.66	31.19	100.00	0.00	0.00
Total	488.77	100.00		31.19				

Table C.15: Wind-sifter separation result for – 1+0.2 mm size fraction at 0.75 m/sec Coal A with Bins

Bin number	Mass (Wt) g	Fractional Yield (Wt) %	Cum. Wt (%)	Ash content (%)	Cum Ash content (%)	Combustible Recovery (%)	Ash rejection (%)	Separation Efficiency (%)
0	0.00	0.00	0.00	0.00	0.00	0.00	-	0.00
1	0.00	0.00	0.00	0.00	0.00	0.00	-	0.00
2	0.00	0.00	0.00	0.00	0.00	0.00	-	0.00
3	0.00	0.00	0.00	0.00	0.00	0.00	-	0.00
4	4.00	0.86	0.86	19.32	19.32	0.97	99.41	0.38
5	15.21	3.27	4.13	19.56	19.51	4.63	97.14	1.77
6	60.23	12.96	17.10	19.92	19.82	19.09	87.98	7.06
7	28.11	6.05	23.14	21.06	20.14	25.74	83.46	9.19
8	85.49	18.40	41.54	26.10	22.78	44.67	66.42	11.09
9	270.00	58.10	99.64	31.99	28.15	99.69	0.47	0.16
10	1.65	0.36	100.00	37.22	28.18	100.00	0.00	0.00
Total	464.69	100.00		28.18				

Table C.16: Wind-sifter separation result for – 1+0.2 mm size fraction at 0.5 m/sec Coal A with Bins

Bin number	Mass (Wt) g	Fractional Yield (Wt) %	Cum. Wt (%)	Ash content (%)	Cum Ash content (%)	Combustible Recovery (%)	Ash rejection %	Separation Efficiency (%)
0	0.00	0.00	0.00	0.00	0.00	0.00	-	0.00
1	0.00	0.00	0.00	0.00	0.00	0.00	-	0.00
2	0.00	0.00	0.00	0.00	0.00	0.00	-	0.00
3	0.00	0.00	0.00	0.00	0.00	0.00	-	0.00
4	0.00	0.00	0.00	0.00	0.00	0.00	-	0.00
5	0.00	0.00	0.00	0.00	0.00	0.00	-	0.00
6	25.00	5.10	5.10	18.90	18.90	5.93	96.80	2.73
7	45.00	9.19	14.29	19.98	19.59	16.46	90.72	7.17
8	99.30	20.27	34.57	26.02	23.36	37.94	73.23	11.17
9	291.00	59.41	93.98	33.18	29.57	94.79	7.89	2.68
10	29.48	6.02	100.00	39.55	30.17	100.00	0.00	0.00
Total	489.78	100.00		30.17				

Table C.17: Wind-sifter separation result for – 6.7+3.35 mm size fraction at 5.0 m/sec Coal B with Bins

Bin number	Mass (Wt) g	Fractional Yield (Wt) %	Cum. Wt (%)	Ash content (%)	Cum Ash content (%)	Combustible Recovery (%)	Ash rejection (%)	Separation Efficiency (%)
0	53.29	10.65	10.65	20.74	20.74	11.93	92.45	4.39
1	42.22	8.44	19.08	20.99	20.85	21.36	86.40	7.76
2	28.78	5.75	24.84	21.12	20.91	27.77	82.25	10.02
3	31.91	6.38	31.21	21.33	21.00	34.86	77.60	12.47
4	31.28	6.25	37.46	21.54	21.09	41.80	73.00	14.80
5	24.21	4.84	42.30	22.52	21.25	47.09	69.28	16.38
6	12.37	2.47	44.77	22.57	21.32	49.80	67.38	17.18
7	4.60	0.92	45.69	24.97	21.40	50.78	66.59	17.37
8	76.10	15.21	60.90	25.13	22.33	66.87	53.53	20.40
9	173.08	34.58	95.48	40.90	29.06	95.77	5.20	0.97
10	22.60	4.52	100.00	33.70	29.27	100.00	0.00	0.00
Total	500.45	100.00		29.27				

Table C.18: Wind-sifter separation result for – 6.7+3.35 mm size fraction at 4.0 m/sec Coal B with Bins

Bin number	Mass (Wt) g	Fractional Yield (Wt) %	Cum. Wt (%)	Ash content (%)	Cum Ash content (%)	Combustible Recovery (%)	Ash rejection (%)	Separation Efficiency (%)
0	27.28	5.45	5.45	18.90	18.90	6.16	96.34	2.50
1	15.58	3.11	8.57	19.71	19.19	9.64	94.16	3.80
2	21.58	4.31	12.88	17.38	18.59	14.60	91.50	6.10
3	25.12	5.02	17.91	20.93	19.24	20.13	87.77	7.90
4	27.46	5.49	23.40	19.91	19.40	26.25	83.89	10.14
5	17.30	3.46	26.85	19.25	19.38	30.14	81.53	11.67
6	11.80	2.36	29.21	20.16	19.44	32.76	79.84	12.60
7	6.40	1.28	30.49	22.09	19.55	34.15	78.83	12.98
8	62.22	12.44	42.93	21.45	20.10	47.75	69.36	17.12
9	242.20	48.42	91.36	35.26	28.14	91.40	8.75	0.15
10	43.24	8.64	100.00	28.53	28.17	100.00	0.00	0.00
Total	500.18	100.00		28.17				

Table C.19: Wind-sifter separation result for – 3.35+1 mm size fraction at 3.0 m/sec Coal B with Bins

Bin number	Mass (Wt) g	Fractional Yield (Wt) %	Cum. Wt (%)	Ash content (%)	Cum Ash content (%)	Combustible Recovery (%)	Ash rejection (%)	Separation Efficiency (%)
0	71.00	14.22	14.22	21.20	21.20	14.69	87.29	1.98
1	31.90	6.39	20.60	21.21	21.20	21.28	81.58	2.87
2	37.95	7.60	28.20	21.95	21.40	29.06	74.55	3.61
3	44.38	8.89	37.09	22.15	21.58	38.13	66.25	4.38
4	45.48	9.11	46.20	22.18	21.70	47.42	57.74	5.16
5	35.74	7.16	53.35	22.23	21.77	54.71	51.03	5.75
6	23.66	4.74	58.09	22.63	21.84	59.52	46.51	6.03
7	10.64	2.13	60.22	22.67	21.87	61.68	44.48	6.15
8	66.55	13.33	73.55	26.27	22.67	74.56	29.72	4.28
9	120.00	24.03	97.57	26.31	23.56	97.77	3.07	0.84
10	12.12	2.43	100.00	29.97	23.72	100.00	0.00	0.00
Total	499.42	100.00		23.72				

Table C.20: Wind-sifter separation result for – 3.35+1 mm size fraction at 2.0 m/sec Coal B with Bins

Bin number	Mass (Wt) g	Fractional Yield (Wt) %	Cum. Wt (%)	Ash content (%)	Cum Ash content (%)	Combustible Recovery (%)	Ash rejection (%)	Separation Efficiency (%)
0	19.15	3.84	3.84	18.60	18.60	4.14	97.10	1.23
1	14.28	2.86	6.70	18.66	18.63	7.22	94.92	2.15
2	17.87	3.58	10.28	19.05	18.77	11.06	92.15	3.21
3	20.30	4.07	14.34	19.13	18.87	15.42	88.98	4.40
4	21.34	4.27	18.62	19.21	18.95	20.00	85.64	5.64
5	20.30	4.07	22.68	19.29	19.01	24.35	82.45	6.80
6	19.29	3.86	26.55	19.46	19.08	28.48	79.39	7.86
7	6.36	1.27	27.82	19.70	19.11	29.83	78.36	8.20
8	65.32	13.08	40.90	23.45	20.50	43.11	65.87	8.98
9	272.01	54.48	95.39	27.33	24.40	95.60	5.26	0.86
10	23.04	4.61	100.00	28.01	24.57	100.00	0.00	0.00
Total	499.26	100.00		24.57				

Table C.21: Wind-sifter separation result for – 1+0.2 mm size fraction at 1.0 m/sec Coal B with Bins

Bin number	Mass (Wt) g	Fractional Yield (Wt) %	Cum. Wt (%)	Ash content (%)	Cum Ash content (%)	Combustible Recovery (%)	Ash rejection (%)	Separation Efficiency (%)
0		0.00	0.00	0.00	0.00	0.00	-	0.00
1	1.44	0.31	0.31	21.20	21.20	0.33	99.76	0.09
2	5.41	1.15	1.46	21.86	21.72	1.57	98.83	0.40
3	11.20	2.39	3.85	21.90	21.83	4.13	96.91	1.04
4	21.25	4.53	8.38	23.48	22.72	8.89	93.00	1.89
5	45.56	9.71	18.09	23.50	23.14	19.09	84.61	3.71
6	53.05	11.31	29.39	23.86	23.42	30.92	74.70	5.61
7	15.71	3.35	32.74	24.67	23.55	34.38	71.66	6.04
8	54.81	11.68	44.42	27.70	24.64	45.98	59.76	5.74
9	256.25	54.61	99.03	29.21	27.16	99.08	1.11	0.20
10	4.55	0.97	100.00	31.19	27.20	100.00	0.00	0.00
Total	469.24	100.00		27.20				

Table C.22: Wind-sifter separation result for – 1+0.2 mm size fraction at 0.75 m/sec Coal B with Bins

Bin number	Mass (Wt) g	Fractional Yield (Wt) %	Cum. Wt (%)	Ash content (%)	Cum Ash content (%)	Combustible Recovery (%)	Ash rejection (%)	Separation Efficiency (%)
0	0.00	0.00	0.00	0.00	0.00	0.00	-	0.00
1	0.00	0.00	0.00	0.00	0.00	0.00	-	0.00
2	0.00	0.00	0.00	0.00	0.00	0.00	-	0.00
3	0.00	0.00	0.00	0.00	0.00	0.00	-	0.00
4	6.80	1.46	1.46	19.00	19.00	1.60	98.94	0.54
5	21.91	4.71	6.17	19.23	19.18	6.75	95.49	2.24
6	75.60	16.24	22.40	20.00	19.77	24.35	83.10	7.45
7	32.20	6.92	29.32	24.06	20.78	31.47	76.75	8.22
8	59.39	12.76	42.07	24.90	22.03	44.45	64.63	9.08
9	266.00	57.13	99.20	29.21	26.17	99.26	0.95	0.21
10	3.71	0.80	100.00	31.19	26.21	100.00	0.00	0.00
Total	465.60	100.00		26.21				

Table C.23: 2nd stage Result of – 6.7+3.35 mm at 5.0 m/sec airstream velocity (Product feed).

Bin number	Mass (Wt) g	Fractional Yield (Wt) %	Cum. Wt (%)	Ash content (%)	Cum Ash content (%)	Combustible Recovery (%)	Ash rejection (%)	Separation Efficiency (%)
0	65.70	23.63	23.63	21.42	21.42	24.27	78.45	2.71
1	35.98	12.94	36.57	21.37	21.40	37.57	66.67	4.24
2	32.39	11.65	48.22	21.78	21.49	49.48	55.87	5.34
3	29.16	10.49	58.71	21.95	21.58	60.18	46.06	6.24
4	25.50	9.17	67.88	22.03	21.64	69.52	37.46	6.98
5	18.94	6.81	74.70	22.44	21.71	76.43	30.95	7.38
6	11.18	4.02	78.71	22.50	21.75	80.50	27.10	7.60
7	2.96	1.07	79.78	24.36	21.79	81.55	25.99	7.54
8	19.03	6.84	86.62	28.41	22.31	87.95	17.71	5.67
9	32.95	11.85	98.48	30.44	23.29	98.73	2.35	1.08
10	4.24	1.52	100.00	36.21	23.48	100.00	0.00	0.00
Total	278.01	100.00		23.48				

Table C.24: 2nd stage Result of – 6.7+3.35 mm at 5.0 m/sec airstream velocity (Discard feed).

Bin number	Mass (Wt) g	Fractional Yield (Wt) %	Cum. Wt (%)	Ash content (%)	Cum Ash content (%)	Combustible Recovery (%)	Ash rejection (%)	Separation Efficiency (%)
0	13.13	6.17	6.17	22.94	22.94	8.18	96.62	4.80
1	8.59	4.04	10.21	28.70	25.22	13.13	93.85	6.98
2	6.41	3.01	13.22	30.07	26.32	16.75	91.68	8.44
3	10.23	4.81	18.03	30.68	27.49	22.49	88.16	10.65
4	8.00	3.76	21.79	26.29	27.28	27.25	85.80	13.05
5	9.29	4.37	26.16	32.04	28.07	32.36	82.46	14.81
6	4.94	2.32	28.48	26.60	27.95	35.29	80.98	16.27
7	1.09	0.51	28.99	38.60	28.14	35.83	80.51	16.34
8	37.56	17.66	46.65	40.41	32.79	53.93	63.46	17.39
9	93.61	44.01	90.66	49.65	40.97	92.04	11.25	3.29
10	19.86	9.34	100.00	50.43	41.86	100.00	0.00	0.00
Total	212.70	100.00		41.86				

Table C.25: 2nd stage Result of –6.7+3.35 mm at 4.0 m/sec airstream velocity (Product feed).

Bin number	Mass (Wt) g	Fractional Yield (Wt) %	Cum. Wt (%)	Ash content (%)	Cum Ash content (%)	Combustible Recovery (%)	Ash rejection (%)	Separation Efficiency (%)
0	19.04	11.17	11.17	18.90	18.90	11.25	91.47	2.72
1	11.84	6.94	18.11	17.75	18.46	18.35	82.87	1.22
2	11.87	6.96	25.07	18.34	18.43	25.41	76.33	1.75
3	14.88	8.73	33.80	18.09	18.34	34.30	68.24	2.54
4	13.40	7.86	41.66	19.18	18.50	42.19	60.52	2.71
5	10.44	6.12	47.78	19.90	18.68	48.28	54.28	2.56
6	6.52	3.82	51.61	16.27	18.50	52.26	51.09	3.35
7	2.21	1.30	52.90	17.96	18.49	53.58	49.90	3.48
8	30.30	17.77	70.67	20.18	18.91	71.21	31.53	2.74
9	43.83	25.71	96.38	20.46	19.32	96.62	4.58	1.20
10	6.17	3.62	100.00	24.73	19.52	100.00	0.00	0.00
Total	170.50	100.00		19.52				

Table C.26: 2nd stage Result of – 6.7+3.35 mm at 4.0 m/sec airstream velocity (Discard feed).

Bin number	Mass (Wt) g	Fractional Yield (Wt) %	Cum. Wt (%)	Ash content (%)	Cum Ash content (%)	Combustible Recovery (%)	Ash rejection (%)	Separation Efficiency (%)
0	0.66	0.20	0.20	18.55	18.55	0.26	99.91	0.17
1	0.54	0.16	0.37	18.58	18.56	0.47	99.82	0.29
2	0.56	0.17	0.54	16.21	17.81	0.70	99.74	0.44
3	1.3	0.40	0.93	18.52	18.11	1.21	99.55	0.76
4	1.39	0.42	1.35	19.26	18.47	1.76	99.33	1.09
5	1.54	0.47	1.82	18.50	18.48	2.37	99.10	1.46
6	1.13	0.34	2.17	20.21	18.75	2.80	98.91	1.71
7	0.19	0.06	2.22	21.21	18.82	2.88	98.88	1.75
8	39.75	12.09	14.31	24.30	23.45	17.46	90.98	8.44
9	254.68	77.47	91.78	39.49	36.99	92.13	8.81	0.94
10	27.02	8.22	100.00	39.91	37.23	100.00	0.00	0.00
Total	328.76	100.00		37.23				

Table C.27: 2nd stage Result of – 3.35+1 mm at 3.0 m/sec airstream velocity (Product feed).

Bin number	Mass (Wt) g	Fractional Yield (Wt) %	Cum. Wt (%)	Ash content (%)	Cum Ash content (%)	Combustible Recovery (%)	Ash rejection (%)	Separation Efficiency (%)
0	63.84	21.73	21.73	19.49	19.49	22.55	81.09	3.65
1	31.81	10.83	32.57	20.89	19.96	33.59	71.00	4.59
2	31.80	10.83	43.39	21.17	20.26	44.59	60.77	5.36
3	36.16	12.31	55.70	21.44	20.52	57.06	48.99	6.05
4	35.55	12.10	67.81	22.69	20.91	69.12	36.73	5.85
5	28.96	9.86	77.67	22.08	21.06	79.02	27.02	6.04
6	17.90	6.09	83.76	20.35	21.00	85.27	21.48	6.76
7	6.68	2.27	86.03	16.35	20.88	87.73	19.82	7.55
8	16.46	5.60	91.64	28.41	21.34	92.90	12.72	5.62
9	20.81	7.08	98.72	33.70	22.23	98.95	2.06	1.01
10	3.75	1.28	100.00	36.21	22.41	100.00	0.00	0.00
Total	293.72	100.00		22.41				

Table C. 28: 2nd stage Result of – 3.35+1 mm at 3.0 m/sec airstream velocity (Discard feed).

Bin number	Mass (Wt) g	Fractional Yield (Wt) %	Cum. Wt (%)	Ash content (%)	Cum Ash content (%)	Combustible Recovery (%)	Ash rejection (%)	Separation Efficiency (%)
0	7.15	3.60	3.60	26.66	26.66	4.00	97.18	1.19
1	4.34	2.18	5.78	28.28	27.27	6.38	95.37	1.75
2	5.65	2.84	8.63	25.05	26.54	9.61	93.28	2.89
3	7.84	3.95	12.57	27.00	26.68	13.98	90.15	4.13
4	9.05	4.55	17.13	27.18	26.82	19.01	86.51	5.52
5	8.41	4.23	21.36	27.06	26.86	23.69	83.15	6.84
6	5.05	2.54	23.90	23.27	26.48	26.65	81.41	8.06
7	1.61	0.81	24.71	33.69	26.72	27.46	80.61	8.07
8	37.84	19.04	43.76	31.70	28.89	47.19	62.89	10.07
9	91.18	45.89	89.64	37.26	33.17	90.84	12.68	3.52
10	20.58	10.36	100.00	41.70	34.06	100.00	0.00	0.00
Total	198.69	100.00		34.06				

Table C. 29: 2nd stage Result of – 3.35+1 mm at 2.0 m/sec airstream velocity (Product feed).

Bin number	Mass (Wt) g	Fractional Yield (Wt) %	Cum. Wt (%)	Ash content (%)	Cum Ash content (%)	Combustible Recovery (%)	Ash rejection (%)	Separation Efficiency (%)
0	15.40	10.71	10.71	19.06	19.06	10.84	89.84	0.68
1	9.61	6.68	17.39	19.43	19.20	17.58	83.38	0.96
2	13.59	9.45	26.84	19.40	19.27	27.11	74.25	1.36
3	19.46	13.53	40.36	19.45	19.33	40.75	61.15	1.90
4	23.28	16.18	56.55	20.16	19.57	56.92	44.91	1.83
5	21.36	14.85	71.40	20.43	19.75	71.70	29.81	1.51
6	12.38	8.61	80.01	19.64	19.74	80.36	21.39	1.75
7	3.79	2.63	82.64	21.21	19.78	82.95	18.61	1.56
8	10.02	6.97	89.61	21.41	19.91	89.81	11.18	0.99
9	12.61	8.77	98.37	21.22	20.03	98.45	1.92	0.37
10	2.34	1.63	100.00	23.75	20.09	100.00	0.00	0.00
Total	143.84	100.00		20.09				

Table C.30: 2nd stage Result of – 3.35+1 mm at 2.0 m/sec airstream velocity (Discard feed).

Bin number	Mass (Wt) g	Fractional Yield (Wt) %	Cum. Wt (%)	Ash content (%)	Cum Ash content (%)	Combustible Recovery (%)	Ash rejection (%)	Separation Efficiency (%)
0	0.67	0.19	0.19	23.17	23.17	0.20	99.85	0.05
1	1.19	0.34	0.53	23.70	23.51	0.56	99.56	0.12
2	1.57	0.44	0.97	23.52	23.51	1.03	99.20	0.23
3	2.20	0.62	1.59	24.03	23.72	1.69	98.67	0.36
4	3.67	1.04	2.63	22.13	23.09	2.82	97.86	0.67
5	3.95	1.12	3.74	22.66	22.96	4.02	96.96	0.98
6	2.38	0.67	4.41	22.09	22.83	4.75	96.44	1.19
7	0.86	0.24	4.66	24.06	22.89	5.01	96.23	1.24
8	60.47	17.07	21.73	24.90	24.47	22.89	81.21	4.10
9	256.50	72.42	94.15	29.21	28.12	94.39	6.45	0.83
10	20.71	5.85	100.00	31.19	28.30	100.00	0.00	0.00
Total	354.17	100.00		28.30				

Table C.31: Wind-sifter separation result for – 6.7+3.35 mm size fraction at 10.5 m/sec without Bins

Bin number	Mass (Wt) g	Fractional Yield (Wt) %	Cum. Wt (%)	Ash content (%)	Cum Ash content (%)	Combustible Recovery (%)	Ash rejection (%)	Separation Efficiency (%)
0	35.00	7.05	7.05	19.19	19.19	7.77	94.92	2.69
1	20.54	4.14	11.19	19.56	19.33	12.30	91.88	4.18
2	28.69	5.78	16.97	20.98	19.89	18.53	87.32	5.85
3	35.72	7.20	24.17	21.61	20.40	26.22	81.48	7.70
4	41.32	8.33	32.49	20.05	20.31	35.29	75.21	10.51
5	48.00	9.67	42.17	23.78	21.11	45.34	66.58	11.92
6	57.00	11.48	53.65	24.57	21.85	57.15	55.98	13.13
7	23.72	4.78	58.43	28.82	22.42	61.78	50.81	12.59
8	60.00	12.09	70.52	32.15	24.09	72.96	36.21	9.17
9	72.32	14.57	85.09	30.15	25.13	86.83	19.71	6.55
10	74.00	14.91	100.00	35.21	26.63	100.00	0.00	0.00
Total	496.31	100.00		26.63				

Table C. 32: Wind-sifter separation test result for – 6.7+3.35 mm size fraction at 9 m/sec without Bins

Bin number	Mass (Wt) g	Fractional Yield (Wt) %	Cum. Wt (%)	Ash content (%)	Cum Ash content (%)	Combustible Recovery (%)	Ash rejection (%)	Separation Efficiency (%)
0	13.44	2.69	2.69	16.87	16.87	2.99	98.19	1.17
1	10.12	2.03	4.72	21.35	18.79	5.11	96.46	1.58
2	14.10	2.82	7.54	16.73	18.02	8.25	94.57	2.83
3	22.44	4.50	12.04	19.78	18.68	13.07	91.03	4.09
4	35.70	7.15	19.19	18.50	18.61	20.84	85.75	6.59
5	35.50	7.11	26.30	20.48	19.12	28.39	79.94	8.33
6	41.62	8.34	34.64	20.00	19.33	37.29	73.28	10.58
7	11.28	2.26	36.90	21.15	19.44	39.67	71.37	11.05
8	116.91	23.42	60.32	28.92	23.12	61.89	44.35	6.24
9	107.03	21.44	81.77	26.87	24.10	82.81	21.36	4.17
10	91.01	18.23	100.00	29.36	25.06	100.00	0.00	0.00

Table C.33: Wind sifter separation test result for – 3.35+1 mm size fraction at 7 m/sec without Bins

Bin number	Mass (Wt) g	Fractional Yield (Wt) %	Cum. Wt (%)	Ash content (%)	Cum Ash content (%)	Combustible Recovery	Ash rejection (%)	Separation Efficiency (%)
0	21.30	4.26	4.26	20.52	20.52	4.65	96.79	1.44
1	17.10	3.42	7.68	21.59	21.00	8.34	94.08	2.42
2	29.67	5.94	13.62	22.91	21.83	14.63	89.09	3.71
3	39.84	7.97	21.59	23.26	22.36	23.03	82.28	5.31
4	65.18	13.04	34.62	23.85	22.92	36.68	70.86	7.54
5	71.64	14.33	48.95	24.83	23.48	51.48	57.79	9.28
6	51.16	10.23	59.19	24.77	23.70	62.06	48.49	10.55
7	17.40	3.48	62.67	24.61	23.75	65.67	45.34	11.01
8	77.99	15.60	78.27	32.24	25.44	80.19	26.87	7.07
9	52.55	10.51	88.78	33.57	26.41	89.79	13.91	3.71
10	56.08	11.22	100.00	33.78	27.23	100.00	0.00	0.00
Total	499.91	100.00		27.23				

Table C.34: Wind sifter separation test result for – 3.35+1 mm size fraction at 5 m/sec without Bins

Bin number	Mass (Wt) g	Fractional Yield (Wt) %	Cum. Wt (%)	Ash content (%)	Cum Ash content (%)	Combustible Recovery (%)	Ash rejection (%)	Separation Efficiency (%)
0	2.09	0.42	0.42	18.78	18.78	0.47	99.71	0.18
1	3.86	0.78	1.20	20.46	19.87	1.32	99.13	0.45
2	7.59	1.53	2.73	19.15	19.47	3.02	98.05	1.07
3	13.11	2.64	5.37	19.61	19.54	5.94	96.15	2.09
4	25.04	5.04	10.41	20.89	20.19	11.42	92.29	3.70
5	43.13	8.69	19.09	21.28	20.69	20.82	85.50	6.32
6	36.11	7.27	26.37	21.43	20.89	28.67	79.78	8.45
7	12.88	2.59	28.96	21.43	20.94	31.47	77.74	9.21
8	71.00	14.30	43.26	23.45	21.77	46.51	65.43	11.95
9	108.80	21.91	65.17	28.00	23.86	68.20	42.92	11.11
10	172.96	34.83	100.00	33.57	27.24	100.00	0.00	0.00

Table C.35: Wind sifter separation test result for – 1+0.2 mm size fraction at 3.5 m/sec without Bins

Bin number	Mass (Wt) g	Fractional Yield (Wt) %	Cum. Wt (%)	Ash content (%)	Cum Ash content (%)	Combustible Recovery (%)	Ash rejection (%)	Separation Efficiency (%)
0	10.97	2.33	2.33	25.10	25.10	2.45	97.97	0.42
1	23.25	4.94	7.27	25.19	25.16	7.65	93.65	1.29
2	38.26	8.13	15.41	26.10	25.66	16.09	86.28	2.37
3	54.56	11.60	27.01	26.74	26.12	28.03	75.51	3.54
4	81.15	17.25	44.26	27.15	26.52	45.68	59.26	4.94
5	112.19	23.85	68.11	28.00	27.04	69.80	36.08	5.88
6	79.96	17.00	85.11	28.82	27.40	86.80	19.07	5.87
7	29.03	6.17	91.28	29.51	27.54	92.91	12.75	5.66
8	20.63	4.39	95.67	39.17	28.07	96.66	6.79	3.45
9	17.87	3.80	99.46	44.87	28.71	99.60	0.87	0.47
10	2.52	0.54	100.00	46.82	28.81	100.00	0.00	0.00
Total	470.39	100.00		28.81				

Table C.36: Wind sifter separation test result for – 1+0.2 mm size fraction at 2.5 m/sec without Bins

Bin number	Mass (Wt) g	Fractional Yield (Wt) %	Cum. Wt (%)	Ash content (%)	Cum Ash content (%)	Combustible Recovery (%)	Ash rejection (%)	Separation Efficiency (%)
0	5.12	1.10	1.10	21.20	21.20	1.18	99.12	0.30
1	18.45	3.96	5.06	20.93	20.99	5.43	95.99	1.42
2	27.45	5.89	10.95	21.87	21.46	11.69	91.12	2.81
3	41.98	9.01	19.95	21.99	21.70	21.24	83.64	4.88
4	67.51	14.48	34.44	22.65	22.10	36.48	71.24	7.72
5	93.11	19.98	54.41	23.12	22.47	57.36	53.78	11.15
6	50.00	10.73	65.14	23.81	22.69	68.48	44.13	12.61
7	14.08	3.02	68.16	22.52	22.69	71.66	41.56	13.22
8	70.71	15.17	83.33	33.67	24.69	85.35	22.26	7.60
9	60.00	12.87	96.21	35.10	26.08	96.71	5.18	1.89
10	17.68	3.79	100.00	36.14	26.46	100.00	0.00	0.00
Total	466.09	100.00		26.46				

Table C.37: Partition curves – 6.7+3.35 mm size fraction at 6.0 m/sec

Specific gravity fraction	Floats analysis (wt %)	Sinks analysis (wt %)	Floats % of feed	Sinks % of feed	Reconstituted feed (%)	Nominal RD	Partition coefficient
<1.30	7.84	0.00	5.54	0.00	5.54	1.25	0.00
1.30-1.40	25.26	0.00	17.84	0.00	17.84	1.35	0.00
1.40-1.50	25.85	0.00	18.26	0.00	18.26	1.45	0.00
1.50-1.60	11.35	0.00	8.02	0.00	8.02	1.55	0.00
1.60-1.70	9.46	0.00	6.68	0.00	6.68	1.65	0.00
1.70-1.80	7.81	1.95	5.52	0.57	6.09	1.75	9.40
>1.80	12.43	98.05	8.78	28.79	37.57	1.85	76.64
							D_{50} =1.81
Total	100.00	100.00	70.63	29.37	100.00	E_p = 0.035	

Table C.38: Partition curves – 6.7+3.35 mm size fraction at 5.0 m/sec

Specific gravity fraction	Floats analysis (wt%)	Sinks analysis (wt %)	Floats % of feed	Sinks % of feed	Reconstituted feed (%)	Nominal RD	Partition coefficient
<1.30	10.05	0.48	5.85	0.20	6.05	1.25	3.29
1.30-1.40	26.73	2.22	15.57	0.93	16.50	1.35	5.62
1.40-1.50	24.34	3.44	14.18	1.44	15.62	1.45	9.20
1.50-1.60	14.59	3.73	8.50	1.56	10.06	1.55	15.48
1.60-1.70	6.58	4.31	3.83	1.80	5.63	1.65	31.96
1.70-1.80	3.40	9.25	1.98	3.86	5.84	1.75	66.08
>1.80	14.31	76.57	8.34	31.96	40.30	1.85	79.31
							D_{50} = 1.62
Total	100.00	100.00	58.25	41.75	100.00	E_p = 0.95	

Table C.39: Partition curves – 6.7+3.35 mm size fraction at 4.0 m/sec

Specific gravity fraction	Floats analysis (wt%)	Sinks analysis (wt %)	Floats % of feed	Sinks % of feed	Reconstituted feed (%)	Nominal RD	Partition coefficient
<1.30	13.92	1.64	4.88	1.07	5.95	1.25	17.93
1.30-1.40	28.75	5.83	10.08	3.79	13.87	1.35	27.32
1.40-1.50	26.23	9.05	9.20	5.87	15.07	1.45	38.98
1.50-1.60	25.24	14.17	8.85	9.20	18.05	1.55	50.97
1.60-1.70	3.65	6.21	1.28	4.04	5.31	1.65	75.94
1.70-1.80	1.37	5.74	0.48	3.73	4.21	1.75	88.56
>1.80	0.84	57.35	0.29	37.24	37.54	1.85	99.22
							D_{50} = 1.33
Total	100.00	100.00	35.06	64.94	100.00	E_p = 0.16	

Table C.40: Partition curves – 3.35+1 mm size fraction at 4.2 m/sec

Specific gravity fraction	Floats analysis (wt%)	Sinks analysis (wt %)	Floats % of feed	Sinks % of feed	Reconstituted feed (%)	Nominal RD	Partition coefficient
<1.30	8.47	0.00	6.59	0.00	6.59	1.25	0.00
1.30-1.40	24.44	0.00	19.04	0.00	19.04	1.35	0.00
1.40-1.50	23.71	0.00	18.47	0.00	18.47	1.45	0.00
1.50-1.60	16.73	0.85	13.03	0.19	13.22	1.55	1.43
1.60-1.70	12.36	0.90	9.63	0.20	9.83	1.65	2.02
1.70-1.80	6.61	3.05	5.15	0.67	5.83	1.75	11.57
>1.80	7.68	95.20	5.98	21.04	27.02	1.85	77.87
							D_{50} = 1.81
Total	100.00	100.00	77.90	22.10	100.00	E_p = 0.030	

Table C.41: Partition curves – 3.35+1 mm size fraction at 3.0 m/sec

Specific gravity fraction	Floats analysis (wt%)	Sinks analysis (wt %)	Floats % of feed	Sinks % of feed	Reconstituted feed (%)	Nominal RD	Partition coefficient
<1.30	12.90	0.00	7.40	0.00	7.40	1.25	0.00
1.30-1.40	33.07	1.90	18.98	0.81	19.79	1.35	4.09
1.40-1.50	30.85	5.04	17.71	2.15	19.86	1.45	10.82
1.50-1.60	14.28	10.19	8.20	4.34	12.54	1.55	34.63
1.60-1.70	4.48	9.64	2.57	4.11	6.68	1.65	61.50
1.70-1.80	1.78	11.89	1.02	5.07	6.09	1.75	83.20
>1.80	2.64	61.33	1.51	26.13	27.64	1.85	94.53
							D_{50} = 1.51
Total	100.00	100.00	57.39	42.61	100.00	E_p = 0.099	

Table C.42: Partition curves – 3.35+1 mm size fraction at 2.0 m/sec

Specific gravity fraction	Floats analysis (wt%)	Sinks analysis (wt %)	Floats % of feed	Sinks % of feed	Reconstituted feed (%)	Nominal RD	Partition coefficient
<1.30	16.74	2.13	5.12	1.48	6.59	1.25	22.41
1.30-1.40	39.82	7.53	12.17	5.23	17.40	1.35	30.05
1.40-1.50	27.00	15.22	8.25	10.57	18.82	1.45	56.14
1.50-1.60	12.62	16.25	3.86	11.28	15.14	1.55	74.53
1.60-1.70	2.23	7.31	0.68	5.07	5.76	1.65	88.16
1.70-1.80	0.79	9.49	0.24	6.59	6.83	1.75	96.45
>1.80	0.80	42.07	0.24	29.21	29.46	1.85	99.17
							D_{50} = 1.43
Total	100.00	100.00	30.57	69.43	100.00	E_p = 0.125	

Table C. 43: Partition curves – 1+0.2 mm size fraction at 1.0 m/sec

Specific gravity fraction	Floats analysis (wt%)	Sinks analysis (wt %)	Floats % of feed	Sinks % of feed	Reconstituted feed (%)	Nominal RD	Partition coefficient
<1.30	13.18	2.90	6.71	1.42	8.14	1.25	17.49
1.30-1.40	33.34	8.95	16.99	4.39	21.38	1.35	20.54
1.40-1.50	21.63	9.85	11.02	4.83	15.85	1.45	30.48
1.50-1.60	15.22	14.46	7.75	7.09	14.85	1.55	47.77
1.60-1.70	4.59	11.26	2.34	5.52	7.86	1.65	70.27
1.70-1.80	2.17	8.87	1.10	4.35	5.46	1.75	79.77
>1.80	9.87	43.71	5.03	21.44	26.47	1.85	81.01
							D_{50} = 1.56
Total	100.00	100.00	50.94	49.06	100.00	E_p = 0.145	

Table C. 44: Partition curves – 1+0.2 mm size fraction at 0.75 m/sec

Specific gravity fraction	Floats analysis (wt%)	Sinks analysis (wt %)	Floats % of feed	Sinks % of feed	Reconstituted feed (%)	Nominal RD	Partition coefficient
<1.30	23.03	3.08	6.61	2.19	8.81	1.25	24.89
1.30-1.40	31.01	12.20	8.91	8.70	17.60	1.35	49.41
1.40-1.50	22.81	15.64	6.55	11.15	17.70	1.45	62.99
1.50-1.60	13.33	15.18	3.83	10.82	14.65	1.55	73.87
1.60-1.70	2.68	9.44	0.77	6.73	7.50	1.65	89.74
1.70-1.80	1.49	6.73	0.43	4.80	5.23	1.75	91.82
>1.80	5.66	37.73	1.62	26.89	28.52	1.85	94.30
							D_{50} = 1.35
Total	100.00	100.00	28.72	71.28	100.00	E_p = 0.15	